

**Influence of basin physiography on the
evolution and sedimentation from flows
transitional between turbidity current and
debris flow.**

Sarah Joy Desiderata Southern

Submitted in accordance with the requirements for the degree of
Doctor of Philosophy

The University of Leeds
School of Earth and Environment

The candidate confirms that the work submitted is her own, except where work which has formed part of jointly-authored publications has been included. The contribution of the candidate and the other authors to this work has been explicitly indicated below. The candidate confirms that appropriate credit has been given within the thesis where reference has been made to the work of others.

A version of Chapter 3 is intended for submission to the *Journal of Sedimentary Research* under the title “Transitional flow deposits: character, distribution and significance in the Maastrichtian Springar Formation, NWVøring Basin, Norwegian Sea” with the following order of authors: Southern, S.J., Kane, I.A., Warchoř, M., Porten, K.W. and McCaffrey, W.D. Collection, processing and interpretation of subsurface core and associated subsurface data, writing and production of figures and graphs were the work of the candidate, except where stated in the text. KWP advised SJS on point counting methods for the collection of compositional and grain size data from thin sections. IK and MW proposed the broader concepts which underlie and helped shape the research. All co-authors provided feedback on provisional drafts of the manuscript. From this research, sedimentological descriptions, interpretations and the distribution of bed types documented were used as contributions in a second jointly authored manuscript intended for submission to *Marine and Petroleum Geology* under the title “Depositional reservoir quality of deep-marine sandstones: a sedimentological process-based approach – an examples from the Springar Formation, NWVøring Basin, Norwegian Sea” with the following order of authors: Porten, K.W., Kane, I.A., Warchoř, M. & Southern, S.J.

Data from Chapter 4 and 5 is that of the candidate except for the sedimentological log from Mam Tor which was originally collected by Davis (2012) who identified the three palaeoflow zones within the succession here. However, the candidate calibrated this log with her own facies and bed classification schemes. In the field the candidate reassessed this log in terms of applying these revised facies and bed type classifications, collecting new palaeoflow data and identifying depositional packages. The candidate was also responsible for setting the scope of the work within the broader research program, data processing, interpretation, writing and the production of figures and graphs. Discussions with IK, WDM and NPM helped to shape ideas which underlie the research.

A version of Chapter 6 was accepted for publication in *Sedimentary Geology* (11th March, 2015) under the title “Influence of flow containment and substrate entrainment upon sandy hybrid event beds containing a co-genetic mud-clast-rich division” with the following order of authors: Southern, S.J., Patacci, M., Felletti, F. and McCaffrey, W.D. Field data, collected over two field seasons in Italy, was collected by the candidate, MP and FF. MP constructed the basin scale correlation of the sections logged by SJS, MP and FF. The candidate set the scientific scope of the work within the broader research program, processed and interpreted data, produced figures and graphs and wrote the text, except where stated. Co-authors provided feedback on provisional drafts of the manuscript.

This copy has been supplied on the understanding that it is copyright material and that no quotation from the thesis may be published without proper acknowledgement. The right of Sarah Joy Desiderata Southern to be identified as Author of this work has been asserted by her in accordance with the Copyright, Designs and Patents Act 1988.

© 2015 The University of Leeds and Sarah Joy Desiderata Southern.

Acknowledgements

First and foremost I am grateful for my supervisors, Bill McCaffrey, Ian Kane and Nigel Mountney, the project has evolved somewhat since initial conception, and I'd like to thank them for allowing it to do so. Bill is thanked for his unfailing encouragement, his critical nature, the opportunities he has provided, and mostly for just being there. Ian, the remote supervisor, the same goes to you, thanks for the time invested in me, for the times I bombarded you with emails and for the occasional fishing trip in Bergen. Nigel is thanked for his continued enthusiasm - I'm sure what were essentially discussions about muddy sandstone were thrilling at times.

Thanks to the team at Statoil (Ian Kane, Michal Warchoř and Kristin Porten), I thoroughly enjoyed my time in Bergen. Kristin is thanked for her advice during the point counting of thin sections. I am grateful for the assistance of Marco Patacci and Fabrizio Felletti whilst working on the Castagnola Basin. Hope Cement Works are thanked for allowing access to the Mam Tor Sandstone exposure in the Hope Quarry. Many thanks go to the various people I've discussed things all deep-water sedimentology with over the years; Esther Sumner, David Hodgson, Jaco Baas, Joris Eggenhuisen and Hans Nelson, and notably Chris Stevenson, our discussions were a continued source of motivation.

To my Huddersfield "family", notably Andy McCarthy and Jon Byles, I am grateful for the thesis-free home you provided outside of Leeds. Thanks to the many people who have made my time at Leeds so enjoyable, particularly those from Level 7 (Steve Banham, Luke Faggetter for the "write-up gin and tonics", Tom Fletcher, Lyndsey Fox, Robbie Jones, Andy Parsons for enforced days off and adventures, Jess Ross, Rachael Spraggs and Alan Wood), there was never a dull moment. Laura Gregory, thanks for being such a good cook and for putting a roof over my head towards the end. The biggest of thanks goes to Hollie Romain, for your support, proof-reading services, and for our antics in and outside the office - we plan the best geolidays.

A final thanks goes to my family for their encouragement despite my continued avoidance of a "proper" job, whatever that may be.

Abstract

Hybrid event beds (HEBs) containing matrix (clay)-poor and overlying matrix-rich sandstone facies are increasingly recognised in deep-water systems and differ significantly from facies traditionally associated with sediment gravity flow deposition. HEBs are thought to reflect deposition from flows whose turbulence became increasingly suppressed due to the enrichment of cohesive clay within the flow. Conceptual and experimental work has stressed either the longitudinal or vertical redistribution of cohesive clay material within flows; resulting end-member models tend to envisage the development of discrete rheological zones along the flow vs. the progressive rheological evolution of the whole flow. HEBs are largely documented in the distal, unconfined regions of deep-water systems with only a few studies having considered their development in association with confining sea-floor topography. Prior to this work, no case studies existed from fully contained (ponded) basins.

This work presents case studies of HEB-prone deep-water systems from unconfined (intra-Springar Sandstone, Norwegian Sea), confined (Mam Tor Sandstone and Shale Grit, N England) and contained (Costa Grande Member, NW Italy) basins. Principal findings are: 1) Hybrid-flow development is complex in that a flow may become increasingly clay-rich and turbulence-suppressed in hindward regions whilst headward regions remain non-cohesive, and undergo downstream turbulence-enhancement driven by declining sediment concentration, 2) Styles of HEB suggest that flows can be characterised by both longitudinal and vertical redistribution of cohesive material, indicating that current models for hybrid flow are not mutually exclusive. 3) In confined or contained settings, HEBs are not always laterally-restricted or systematically variable in their depositional character with respect to confining topography as documented in previous studies. Thus, in topographically complex settings, confinement is not always the trigger mechanism for hybrid-flow development; prior development may occur in relatively distal confined settings where a greater flow run-out distance, and thus time for other mechanisms promoting flow transformation to operate, is achieved. 4) In contained settings complex patterns of flow expansion and confinement are interpreted to; a) prevent the development of slope-localised HEBs; and b) promote the development of relatively sandy HEBs.

Table of Contents

Acknowledgments	iii
Abstract	iv
Table of Contents	v
List of Figures	x
List of Tables	xiv
Abbreviations	xiv
Chapter 1 – Thesis rationale and structure	1
1.1 – Introduction.....	1
1.2 – Aims and objectives.....	2
1.3 – Thesis structure.....	4
Chapter 2 – Deep-water sediment gravity flows - an overview	6
2.1 – Introduction.....	6
2.2 – Flow behaviour.....	6
2.2.1 – Cohesive debris flows.....	6
2.2.2 – Non-cohesive turbidity currents.....	8
2.3 – Flow processes.....	10
2.3.1 – Flow capacity and competence.....	12
2.3.2 – Flow non-uniformity.....	12
2.3.3 – Flow unsteadiness.....	12
2.3.4 – Spatial variation and temporal evolution of flow character.....	14
2.3.5 – Interactions with sea-floor topography.....	16
2.4 – Hybrid event beds - Introduction and adopted terminology.....	20
2.5 – Hybrid event bed - depositional character.....	22
2.5.1 – Vertical bed character.....	22
2.5.2 – Long length-scale facies tracts.....	24
2.5.3 – Short length-scale facies tracts.....	26
2.6 – Hybrid event bed - distribution.....	26

2.7 – Hybrid flow development.....	28
2.7.1 – Turbulence enhancement.....	28
2.7.2 – Turbulence suppression.....	28
2.8 – Styles of flow transformation associated with hybrid event bed development.....	30
2.8.1 – Transformation of an initial relatively cohesive non-turbulent flow.....	30
2.8.1.1 – Dilution of flow.....	30
2.8.1.2 – Deceleration of a low coherency debris flow.....	32
2.8.2 – Transformation of an initial relatively non-cohesive turbulent flow.....	32
2.8.2.1 – Entrainment of muddy substrate.....	32
2.8.2.2 – Hydraulic (longitudinal) segregation.....	34
2.8.2.3 – Flow deceleration.....	34
2.9 – Other mechanisms emplacing HEB-like deposits.....	36
2.9.1 – Liquefaction.....	36
2.9.2 – Modification by succeeding flow events.....	37
2.9.3 – Failure of a heterogeneous source area.....	38
2.9.4 – Failure of a heterogeneous source area.....	38
2.9.5 – Intra-bed flow processes.....	38
2.10 – Hybrid event beds and sea-floor topography.....	39

Chapter 3 – Hybrid event beds dominated by transitional facies types: character, distribution and significance in the Maastrichtian Springar Fm. NWVøring Basin, Norwegian Sea.....43

3.1 – Introduction.....	43
3.2 – Geological setting.....	45
3.3 – Data and methods.....	48
3.4 – Results.....	48
3.4.1 – Key bed types of the intra-Springar sandstone.....	48
3.4.1.1 – Bed Type A.....	48
3.4.1.2 – Bed Type B.....	52
3.4.1.3 – Bed Type C and D.....	54
3.4.1.4 – Bed Type E.....	59
3.4.2 – Well summaries.....	60
3.4.2.1 – Well 1.....	60
3.4.2.2 – Well 2.....	62
3.4.2.3 – Well 3.....	62
3.4.2.4 – Well 4.....	62
3.4.2.5 – Well 5.....	64
3.4.3 – Bed type-distribution.....	64

3.4.3.1 – Downstream bed-type distributions.....	64
3.4.3.2 – Stratigraphic bed-type distributions.....	64
3.4.4 – Spatial facies trends within HEBs.....	65
3.4.4.1 – Downstream facies trends.....	65
3.4.4.2 – Downstream variation in HEB bed base facies.....	66
3.4.4.3 – Stratigraphic facies trends.....	70
3.5 – Discussion.....	70
3.5.1 – Hybrid flow development and sedimentary facies tracts.....	70
3.5.1.1 – Insights from vertical facies arrangement within HEBs.....	70
3.5.1.2 – Insights from spatial bed type distributions and facies trends.....	71
3.5.2 – Comparison to other HEB studies.....	73
3.5.2.1 – Origin of relatively matrix-poor sandstone at bed bases.....	73
3.5.2.2 – Expanded thickness of banded sandstones.....	75
3.5.2.3 – Bed-top stratified sandstones.....	76
3.5.3 – Interaction with sea-floor topography.....	76
3.5.4 – Influence of system evolution upon HEB distributions and proportions.....	78
3.6 – Conclusions.....	78

Chapter 4 – Influence of confining topography upon hybrid event bed character and distribution in a confined basin setting: insights from the Edale Basin, Carboniferous, U.K.....80

4.1 – Introduction.....	80
4.2 – Geological setting.....	83
4.2.1 – Regional geological framework.....	83
4.2.2 – Stratigraphy.....	84
4.3 – Data and methods.....	85
4.4 – Facies and deposit types of the Mam Tor Sandstones and Shale Grit Formation.....	85
4.4.1 – Type A and B beds (FA-1A).....	85
4.4.2 – Type C, D and E beds (FA-1B).....	95
4.4.3 – Type F and G beds (FA-2).....	97
4.5 – Depositional character and distribution with respect to the confining basin margin.....	99
4.5.1 – Strata upstream and distant from the confining basin margin.....	99
4.5.1.1 – Wicken and Ashop river sections.....	99
4.5.2 – Localities adjacent to the downstream confining basin margin.....	100
4.5.2.1 – Mam Tor.....	100
4.5.2.2 – Hope Quarry.....	104
4.6 – Discussion.....	118
4.6.1 – Origin of FA-1 deposits.....	118

4.6.1.1 – Failure from the confining basin margin.....	118
4.6.1.2 – Substrate deformation and delamination.....	119
4.6.1.3 – Confinement-driven flow transformation.....	119
4.6.2 – Influence of the proximity of confining topography upon HEB character and distribution.....	122
4.6.2.1 – Proximally-confined flow.....	123
4.6.2.2 – Distally-confined flow.....	123
4.6.2.3 – Unconfined flow.....	123
4.7 – Conclusions.....	126

Chapter 5 – Character and occurrence of deposits from flows transitional between fully turbulent and fully cohesive flow behaviours: insights from the deep-water infill of the Edale Basin, Carboniferous, UK..... 128

5.1 – Introduction.....	128
5.2 – Data and methods.....	129
5.3 – Studied localities.....	130
5.3.1 – Hope Quarry, Mam Tor and Back Tor.....	130
5.3.1.1 – Mam Tor.....	131
5.3.1.2 – Hope Quarry (HQ).....	132
5.3.1.3 – Back Tor.....	132
5.3.1.4 – Wicken & Ashop.....	134
5.3.1.5 – Alport Castles.....	134
5.3.1.6 – Locality interpretations.....	137
5.4 – Discussion.....	138
5.4.1 – Evolution of basin infill and implications for the character and distribution of matrix-rich bed types.....	138
5.4.1.1 – System evolution and distribution of matrix-rich deposits.....	139
5.4.1.2 – Small-scale evolution and distribution of matrix-rich deposits.....	140
5.4.2 – Implications for models describing types of hybrid and transitional flow.....	142
5.5 – Conclusions.....	145

Chapter 6 – Influence of flow containment and substrate entrainment upon sandy hybrid event beds: insights from the Castagnola Basin, Miocene, NW, Italy..... 147

6.1 – Introduction.....	147
6.2 – Geological background.....	148
6.3 – Data and methods.....	150
6.4 – Results.....	151
6.4.1 – Bed types of the Costa Grande Member.....	151

6.4.1.1 – Type A.....	151
6.4.1.2 – Type B.....	157
6.4.1.3 – Type C.....	158
6.4.1.4 – Type D.....	162
6.4.2 – Evolution of palaeoflow associated with a confining basin margin.....	165
6.4.3 – Spatial variation of depositional character with respect to a downstream confining basin margin.....	167
6.5 – Discussion.....	168
6.5.1 – Gravity-current confinement and containment within the Castagnola Basin.....	168
6.5.2 – Origin of mud-clast-rich divisions within Type C beds.....	170
6.5.2.1 – Gravity-flow-driven substrate modification.....	170
6.5.2.2 – Interaction of gravity flows with a confining basin margin.....	171
6.5.2.3 – Entrainment and transport of substrate-derived mud clasts.....	172
6.5.3 – Influence of flow containment upon the character and distribution of sandy HEBs in confined deep-water systems.....	176
6.5.3.1 – Processes of flow confinement and containment.....	178
6.6 – Conclusions.....	178
Chapter 7 – Discussion, conclusions and further work.....	180
7.1 – Introduction.....	180
7.2 – The character and evolution of flows emplacing HEBs.....	180
7.2.1 – Clay content of the upper “linked debrite” in matrix-poor HEBs.....	180
7.2.2 – Development of stratification in the lower part of HEBs.....	181
7.2.3 – Downstream variation of facies in the lower part of HEBs.....	181
7.2.4 – Clay content of facies in the lower part of HEBs.....	183
7.2.5 – Position and proportion of banded sandstone facies.....	184
7.3 – Influence of basin physiography upon flows emplacing HEBs.....	186
7.4 – Applications to the hydrocarbon industry - reservoir quality and prediction.....	189
7.5 – Main conclusions.....	190
7.6 – Future work.....	192
References.....	195
Appendix.....	217

List of Figures

Figure 2.1.	Block model illustrating the range of deep-water sedimentation processes. From Stow & Mayall (2000).....	7
Figure 2.2.	Examples of the spectrum of sediment gravity flows and grain-support mechanisms. Each represents a given point along a continuum of flow characters. Modified from Middleton & Hampton (1976).....	7
Figure 2.3.	Vertical profiles of downstream velocity for turbulent and laminar flow from Mulder & Alexander (2001).....	9
Figure 2.4	Examples of the characteristics of debrites deposited from debris flows.....	9
Figure 2.5	Experimental examples of variation in debris flow strength arising from relative concentrations of cohesive material within the flow. Modified from Marr et al. (2001).....	9
Figure 2.6	The Lowe sequence and its hypothetical variation downstream into the Bouma Sequence due to flow dilution during run-out. Modified from Allen (1985) and Lowe (1982).....	11
Figure 2.7	A) Schematic diagram of spatial variation in flow velocity at a given instant in time (flow non-uniformity). B) Schematic diagram of temporal velocity variation in flow passing a fixed point in space. Modified from Kneller (1995).....	11
Figure 2.8	Morphology of a turbidity current; divided into head, body and tail, with typical velocity, concentration and grain size data for these regions. From Baas et al. (2005) from Baas et al. (2005).....	13
Figure 2.9	Schematic illustrating the typical vertical distribution of velocity, sediment concentration and sediment type within a turbidity current. Modified from Kneller & McCaffrey (1996) and Haughton et al. (2003).....	13
Figure 2.10	Diagram illustrating transformation of velocity structure of a given flow during run-out downstream and associated velocity profiles experienced at relatively proximal and distal points along this flow pathway. Modified from Kneller & McCaffrey (2003).....	13
Figure 2.11	Examples of potential flow transformations that can occur during downstream flow run-out. Modified from Fisher (1983).....	15
Figure 2.12	General trends of flow transformation during run-out downstream. A) Traditional facies tract for which the SGF underwent increasing dilution and became increasingly turbulent distally. B) Emerging flow transformation trends whereby flow may become turbulence suppressed and cohesive distally. Modified from Haughton et al. (2003).....	15
Figure 2.13	Schematic block model illustrating the influence of sea-floor topography upon shelf, slope and basin floor depositional systems. A) From Prather et al. (1998); B & C) from Mayall et al. (2010).....	17
Figure 2.14	Schematic matrix illustrating scenarios of sediment gravity-flow interaction with sea-floor topography with varying degrees of flow stratification and obstacle height. Modified from Kneller & McCaffrey (1999).....	18
Figure 2.15	Classification of sediment gravity flows, and the deep-water systems they emplace, based upon flow interaction with various styles of sea-floor topography.....	18
Figure 2.16	Examples of deposits emplaced by gravity flows which interacted with confining sea-floor topography.....	19
Figure 2.17	A) Idealised hybrid event bed (modified from Haughton et al., 2009) with interpretation compiled from Haughton et al. (2009) and Baas et al. (2011). B) Examples of variations in HEB depositional character (from Talling, 2013).....	21
Figure 2.18	Schematic models illustrating documented change in the vertical rheological structure of experimental turbulent, transitional and quasi-laminar flow as clay concentration is increased. Modified from Bass et al. (2009).....	23
Figure 2.19	The effect of clay and flow deceleration (timing and rate) upon the depositional character of experimental beds deposited from variably clay-rich, turbulence-suppressed flows. Modified from Sumner et al. (2009).....	23

Figure 2.20.	Summary of long length-scale variations documented in HEBs.....	25
Figure 2.21.	Documented geographical distribution of HEBs in deep-water systems.....	27
Figure 2.22.	Documented stratigraphic distribution of HEBs in deep-water systems.....	27
Figure 2.23.	Schematic illustrating flow transformations associated with changes in the turbulence and cohesive characteristics of the flow as driven by changes in sediment concentration, proportion of cohesive materials or flow velocity.....	29
Figure 2.24.	Emplacement of co-genetic matrix-rich and matrix-poor sandstone due to partial dilution of an initial cohesive debris flow into relatively dilute turbulent flow. Modified from Talling et al. (2004).....	31
Figure 2.25.	Emplacement of co-genetic matrix-rich and matrix-poor sandstone due to deceleration and sand settling from clay-rich flow. Modified from Talling et al. (2004).....	31
Figure 2.26.	Emplacement of co-genetic matrix-rich and matrix-poor sandstone due to entrainment of muddy substrate. Modified from Haughton et al. (2003).....	33
Figure 2.27.	Emplacement of co-genetic matrix-rich and matrix-poor sandstone due to hydraulic fractionation (redistribution) of low-settling velocity particles (e.g., mud & silt, mud clasts and carbonaceous fragments) towards the rear of the flow.(sensu Haughton et al.2009).....	33
Figure 2.28.	Deposition of co-genetic matrix-rich and matrix-poor sandstone due to deceleration of clay-rich turbulent flow. Modified from Talling et al. (2004).....	35
Figure 2.29.	Processes that can result in deposits with a pseudo-HEB depositional character, in which constituent facies were not deposited together from a single flow event as occurring in HEBs.....	35
Figure 2.30.	Deposition of co-genetic matrix-rich and matrix-poor sandstone due to failure of a heterogeneous source in which the sand-rich (non-cohesive) component consistently outruns the mud-rich (cohesive) component of flow. Modified from Haughton et al. (2003).....	37
Figure 2.31.	Deposition of co-genetic matrix-rich and matrix-poor sandstone due to gravity flow-triggered destabilisation of local confining slopes. Modified from McCaffrey & Kneller (2001).....	37
Figure 2.32.	Summary of published examples of HEB depositional character and distribution in relation to downstream and laterally confining slopes. Modified from Barker et al. (2008) and Patacci et al. (2014).....	39
Figure 3.1.	Stratigraphy and location map for the Cretaceous Vøring Basin, Norwegian Sea, with the locations of Wells 1 to 5 described in this study.....	43
Figure 3.2.	Diagram summarising the characteristics of Wells 1 to 5 and the sub-divisions of the Maastrichtian, intra-Springar Sandstone.....	44
Figure 3.3.	Graphic sedimentary logs of cored sections from Wells 1 to 5.....	47
Figure 3.4.	Core and thin-section photographs of facies present within the studied cored intervals of the intra-Springar Sandstone.....	50-52
Figure 3.5.	Descriptions and process interpretations for event beds of the intra-Springar sandstone.....	53
Figure 3.6.	Average facies proportions of total event bed thickness (A) and facies probability (B) within bed types B, C and D.....	54
Figure 3.7.	Petrological, textural, porosity and permeability characteristics of a Type C bed.....	56
Figure 3.8.	Petrological, textural, porosity and permeability characteristics of a Type D bed.....	57
Figure 3.9.	Palaeogeography and depositional model for the Maastrichtian intra-Springar Sandstone.....	61
Figure 3.10.	Photographs of distinct composite deposits found in Well 2.....	61
Figure 3.11.	Frequency and distribution of key bed types across the lower sandy body of the intra-Springar Sandstone (Wells 2 to 5).....	63
Figure 3.12.	Graphs illustrating the probability and average proportion of facies within beds for both Type C and D beds at Wells 3 to 5 (lower sand body of the intra-Springar Sandstone).....	66
Figure 3.13.	Graphic logs of beds from Wells 3 and 4 showing variations of the facies proportion within beds.....	67

Figure 3.14.	Graphs illustrating the probability and average proportion of facies at the base of bed Type C and D at Wells 3 to 5 (lower sand body of the intra-Springar Sandstone).....	68
Figure 3.15.	Graphic log illustrating vertical facies and bed type trends occurring in the lower sandstone body of the intra-Springar Sandstone.....	69
Figure 3.16.	Process model for the spatio-temporal evolution of flow emplacing transitional flow deposits observed in the lower sand body of the intra-Springar sandstone.....	72
Figure 3.17.	Diagram illustrating how the proportion and distribution of HEBs can vary in HEB-prone systems depending upon relative rates of system progradation and retreat.....	77
Figure 4.1.	Regional location, stratigraphy and geological map for the Carboniferous Edale Basin, N England.....	81
Figure 4.2	Photo demonstrating the nature of the downstream confining basin margin and deep-water silliclastic basin fill.....	82
Figure 4.3	Key characteristics and interpretations of facies found in the Mam Tor Sandstones and Shale Grit Formation.....	86
Figure 4.4.	Bed types of the Mam Tor Sandstones and Shale Grit Formation arranged according to bed thickness and grain size.....	90
Figure 4.5.	Characteristics of matrix-rich mud-clast-rich deposits (Type A beds).....	91
Figure 4.6.	Characteristics of matrix-rich mud-clast-rich deposits (Type B beds).....	92
Figure 4.7.	Characteristics of matrix-rich, relatively mud-clast-poor deposits (Type C, D and E beds).....	96
Figure 4.8.	Characteristics of matrix-poor deposits (Type F and G beds).....	97
Figure 4.9.	Sedimentary logs of upstream exposures of the Mam Tor Sandstones from the Ashop and Wicken river-cut sections.....	98
Figure 4.10.	Sedimentary log of the Mam Tor Sandstone succession exposed at Mam Tor, illustrating palaeoflow zones and smaller-scale depositional packages.....	101
Figure 4.11.	A) Stratigraphic subdivision of the Mam Tor succession into 3 palaeoflow divisions separated from each other by mudstone-dominated successions. B) Illustration of palaeoflow zonation resulting from changes in the lobe position and interaction with the confining basin margin.....	103
Figure 4.12.	Location map and fence diagram indication the location and orientation of exposures of the Mam Tor Sandstone in quarried faces at Hope Quarry.....	105
Figure 4.13.	Composite stratigraphic succession collated from correlated exposures of the lower Mam Tor Sandstones, Hope Quarry.....	106
Figure 4.14.	Examples of marine fauna from a fossiliferous marine band found near the boundary between the Edale Shales and overlying Mam Tor Sandstones, Hope Quarry.....	107
Figure 4.15.	Examples of bimodal palaeoflow trends indicated by sole structures on the bases of beds, Hope Quarry.....	107
Figure 4.16.	Correlation panels of sedimentary logs collected from the Mam Tor Sandstones at Hope Quarry.....	109
Figure 4.17.	Transects of individual beds summarising variations in depositional character with respect to palaeoflow direction or increasing proximity towards the downstream confining basin margin.....	113
Figure 4.18.	Orientation of mud-clast axes and fold noses collected from the mud-clast-rich division of two HEBs exposed at Hope Quarry.....	116
Figure 4.19.	Examples of rare composite deposits with chaotic sandwiched divisions found in the Mam Tor Sandstones.....	120
Figure 4.20.	Schematic illustrating how interpretation of a one-dimensional succession as a composite deposit or HEB has implications for reservoir connectivity, hydrocarbon fluid flow and volumes of net sand.....	120
Figure 4.21.	Schematic block model illustrating the effect of flow run-out distance, as determined by basin physiography, exerts upon flow transformation processes and the distribution of HEB in basin infill successions.....	124

Figure 4.22.	Schematic model illustrating how temporal variations in the position or presence of confining topography, and subsequent flow run-out distance, may affect the stratigraphic distribution of HEBs within a basin infill succession.....	125
Figure 5.1.	Distribution of studied localities with respect to the downstream confining basin margin (Derbyshire Massif).....	130
Figure 5.2.	Sedimentary log of the Shale Grit Formation succession exposed at Back Tor.....	133
Figure 5.3.	Photographs, logs and correlation of strata from the Shale Grit Formation, Alport Castles.....	135
Figure 5.4.	Photographs of facies and key characteristics associated with incision surfaces in the Shale Grit Formation, Alport Castles.....	136
Figure 5.5.	Conceptual model illustrating flow processes which account for the deposition of matrix-poor or matrix-richer sandstone beneath co-genetic mud-clast-rich divisions (Type A and B beds, respectively).....	143
Figure 6.1.	Stratigraphic column, regional cross section, and location map of the Castagnola Basin with the distribution of logged sections and palaeoflow indicated. Stratigraphic column after Andreoni et al. (1981), cross section after Di Giulio & Galbiati (1993), and location map modified from Felletti (2002a). Correlation of logged sections through the tabular strata of the c. 250 m study interval in the Costa Grande Member.....	148
Figure 6.2.	Summaries of Types A to D beds recognised within the studied interval of the Costa Grande Member.....	152
Figure 6.3.	Palaeoflow data collected from different palaeoflow indicators found within the study interval.....	154
Figure 6.4.	Graph depicting maximum grain size versus bed thickness.....	154
Figure 6.5.	Key characteristics of the different styles of mud-clast distribution observed within deposits of the Costa Grande Member.....	155
Figure 6.6.	Short-scale transect of a typical Type B bed (Bed 215) which exhibits minimal variation in depositional character over short length-scales.....	158
Figure 6.7.	Basin-scale transects of individual bed types across the studied interval of the Costa Grande Member.....	159
Figure 6.8.	Rare example of a lateral transition from a Type B to Type C bed character within Bed 212...	161
Figure 6.9.	Basin-scale correlation of beds illustrating how dramatic changes in Type C bed character can arise from changes in the abundance and size of mud-clasts.....	161
Figure 6.10.	Short length-scale transect through a Type C bed at Location IV illustrating how the thickness of the co-genetic mud-clast-rich division, and the mud-clast abundance and size within, is highly variable over short length-scales.....	163
Figure 6.11.	Truncated laminations and alternating facies observed within Type D beds.....	164
Figure 6.12.	Diagram illustrating the stratigraphic change in palaeoflow direction arising from basin floor aggradation near an inclined basin margin sensu Kneller and McCaffrey, (1999). Block model modified from Felletti et al. (2002).....	165
Figure 6.13.	Characteristics which discount various mechanisms for the development of HEB-like sandstone deposits containing a distinct mud-clast-rich division.....	169
Figure 6.14.	Contrasting flow dynamics and depositional trends between confined contained (CC) settings and confined uncontained (CU) settings.....	175
Figure 7.1.	Variations in HEB depositional character and inferred variations in flow character based on insights gained from the presented case studies.....	179
Figure 7.2.	Schematic summarising: 1) the potential range of boundary controls upon hybrid flow development and evolution; and 2) near-bed flow character and transformations suggested to account for the character and distribution of HEBs in the presented case studies.....	182

Figure 7.3. Summary of the effects that various styles of basin physiography (unconfined, confined and contained) can exert upon flows emplacing HEBs, and the subsequent character and distribution of HEBs..... 187

Figure 7.4. Diagram integrating findings from the presented research with those from previous studies to demonstrate how flow interaction with topography, and subsequent flow non-uniformity, affects flow transformation and HEB distribution..... 188

List of Tables

Table 3.1. Dataset summary.....43

Table 3.2. Description and process interpretation of facies present in the intra-Springar Sandstone.....49

Abbreviations

CC	- Confined, contained
CU	- Confined, uncontained
HEB	- Hybrid event bed
HQ	- Hope Quarry
LS	- Lower sand (of the intra-Springar Sandstone)
MCR	- Mud-clast-rich
MS	- Middle sand (of the intra-Springar Sandstone)
MTS	- Mam Tor Sandstones
SGF	- Sediment gravity flow
TFD	- Transitional flow deposit
US	- Upper sand (of the intra-Springar Sandstone)
UU	- Unconfined, uncontained

Chapter 3 facies

Sma	- Matrix-poor, non-stratified sandstone.
Ss	- Stratified/laminated sandstone
Sws	- Weakly stratified sandstone
Sb	- Banded sandstone
Smu	- Matrix-rich, non-stratified sandstone
Srw	- Reworked sandstone
St	- Tractional lag sandstone
Rb	- Remobilised strata
Mm	- Mudstone

Chapter 4 & 5 facies

CS-U	- Matrix-poor, non-stratified sandstone.
CS-L(c/p)	- Matrix-poor laminated sandstone (current ripple- or planar lamination)
BA	- Banded sandstone
AS-U	- Matrix-rich non-stratified sandstone
AS-La	- Matrix-rich laminated sandstone
HAS-Cla	- Highly matrix-rich, mud-clast-rich sandstone
MCB	- Mud-clast-breccia
MD	- Mud-dominated packages with thin, fine-grained sand laminae and beds
M	- Mudstone

Chapter I. – Thesis rationale and structure

This chapter outlines the motivation for the thesis and the presented case studies by; 1) framing the topic of the thesis – the nature of hybrid event beds deposited from flows transitional between fully turbulent and fully cohesive behaviour – within the field of sub-aqueous particulate gravity currents; 2) outlining the specific research objectives of the thesis; and 3) explaining the structure of the thesis.

1.1 Introduction

Sub-aqueous sediment gravity flows represent some of the most important agents of sediment transport on Earth (Elmore et al., 1979; Masson et al., 1993; Piper et al., 1999), yet arguably they are amongst the least well understood. Gaps in our understanding largely arise from the scarcity of direct observations from these relatively inaccessible, infrequent and destructive phenomena (Heezen & Erwing, 1952; Piper et al., 1999; Khripounoff et al., 2003; Xu et al., 2004). Accordingly, inferences regarding the range of behaviour of such flows have largely been derived from studies of the deposits they emplace, both modern and ancient (Bouma 1962; Lowe, 1982; Kneller & McCaffrey, 2003; Haughton et al., 2003, 2009), experimental studies (Hampton, 1975; Al Ja'Aidi et al., 2004; McCaffrey et al., 2003; Baas et al., 2005 2009, 2011; Sumner et al., 2009) and numerical modelling (Mulder et al., 1997; Imran et al., 1999; Janocko et al., 2013).

Sediment gravity flows have traditionally been classified on the basis of rheology, with flows largely subdivided into: 1) cohesive, laminar, (non-Newtonian) debris flows, in which particles are largely supported by the cohesive strength arising from high concentrations of clay; or 2) non-cohesive, fluidal (Newtonian) flows in which particles are largely (though not exclusively) supported by fluid turbulence. However, many subaqueous deposits do not appear to have been laid down by such simple end-member flow types; instead, they appear to have been deposited from flows that were either characterised by some intermediate flow rheology or by flows exhibiting spatio-temporal variations in rheology. Such deposits can contain variably matrix (clay)-rich sandstone facies recording deposition from both non-cohesive and relatively more cohesive flow during a single flow event (see Talling, 2013 and references therein). Collectively, these deposits – termed hybrid event beds (HEB) herein – are thought to record the influence of high proportions of cohesive clay upon flow structure during downstream run-out; such fine grained material may have been present in the initial flow or incorporated into the flow following entrainment of mud-rich substrate on the sea floor.

A broad range of HEB deposit types and occurrences are being documented as the number of case studies increases. However, our current understanding of the character (i.e. structure and evolution) of flows emplacing HEBs, and the boundary controls upon their development, is still not sufficiently comprehensive to account for the observed spectrum of HEBs deposits. Experimental studies have demonstrated the nature of rheology, and its vertical distribution, within variably clay-rich open-channel flows (Baas et al., 2003, 2009; Sumner et al., 2009). However, understanding of the longitudinal distribution of zones of differing rheology that can arise in these flow types remains conceptual (Haughton et al., 2003, 2009; Kane & Pontén, 2012) and less constrained.

When present, HEBs are typically documented in the distal and marginal parts of deep-water systems, commonly where systems are unconfined and largely unaffected by local confining sea-floor topography (Haughton et al. 2003, 2009; Amy & Talling, 2006; Hodgson, 2009; Kane & Pontén, 2012). In many systems, however, particulate gravity currents are affected by obverse slopes, either in "confined and uncontained" scenarios, in which the configuration of sea-floor topography still permits downstream run-out of flows, or in "confined and contained" scenarios, in which fully enclosed bathymetry completely traps the flow. Despite the recognition of the importance of confined or contained systems as hydrocarbon reservoirs, relatively few studies have documented the character and distribution of HEBs, and associated flow processes, with respect to confining sea-floor topography (Barker et al., 2008; Patacci et al., 2014). Barker et al. (2008) and Patacci et al. (2014) documented the preferential occurrence of HEBs locally adjacent to confining slopes, where they exhibited systematic variation in depositional character towards their pinch-out and onlap onto the confining slope. Such observations have implications for the distribution of facies, and thus reservoir quality, in onlap settings where the potential for the development of stratigraphic traps can make attractive hydrocarbon prospects. However, it remains to be established whether such patterns are ubiquitous, and whether the type of topography (contained vs. confined) affects flow and facies development.

1.2 Aim and Objectives

The aim of this thesis is to document the character and distribution of HEBs on a variety of scales in deep-water systems which were variably affected by confining sea-floor topography and to assess the principal controls upon their development. To achieve this, one detailed subsurface study and two field studies were carried out with the following objectives:

- To use field and core data to demonstrate the range of facies types and relative proportions, and inferred flow processes, that can occur in HEBs, and further, to use

documented downstream facies trends to infer the complex spatio-temporal evolution of the depositing flow.

- To document the spatial (geographic and stratigraphic) distribution of HEBs, and associated relatively matrix-poor turbidites, in three deep-water systems affected by discrete basin physiography (i.e. unconfined, confined yet uncontained, and both confined and contained deep-water systems).
- Construct lateral correlations of individual HEBs to document their character and distribution with respect to increasing proximity to a downstream confining counter-slope onto which they onlap. In order to investigate potential differences arising from confining or containing basin physiography. This task was carried out for both a confined deep-water system (Chapter 4) and a confined, contained deep-water system (Chapter 6).

The findings of the studies are novel and contributed to the field of research by providing broader insight into a number of themes. Specifically, they:

- expand our generic understanding of the range and complexity of flows emplacing HEBs.
- evaluate the influence that confining topography may exert upon local flow transformation and the development of HEBs as noted by Barker et al. (2008) and Patacci et al. (2014). A key uncertainty prior to this work was whether HEBs are always localised adjacent to counter slopes in confined or contained settings. Further, what are the possible controls upon variation in the pattern of HEB occurrence?
- assess to what extent confining and containing styles of basin physiography affect processes associated with the character and distribution of HEBs and thus the distribution of reservoir heterogeneity in topographically-complex deep-water systems.
- contribute to the reconciliation of current terminology. How do conceptual models for rheologically, longitudinally segregated hybrid flow (*sensu* Haughton et al., 2003, 2009) compare with observations from experimental clay-rich, turbulence-suppressed flows which are prone to developing vertical rheological heterogeneity (Baas et al., 2009, 2011; Sumner et al., 2009). Can flow processes, and related flow characters, associated with these models co-occur within a single gravity flow during its downstream run-out? Thus, what is the potential range in flow character within the larger spectrum of flow types that exhibit downstream flow transformations due to clay-enrichment?

1.3 Thesis structure

This thesis presents the findings of subsurface and outcrop case studies; the principal chapters have been written in manuscript form to permit straightforward submission to journals. The data presented consider a variety of scales from that of the individual bed to that of the larger depositional system. Results from these case studies are discussed in terms of the generic insight they offer into HEB deposits and the flows that emplace them.

Chapter 2 provides the background to the study by summarising pertinent literature regarding gravity-flow dynamics, classification, evolution and their interaction with topographic features on the sea floor with particular focus on hybrid flows and hybrid event beds.

Chapter 3 presents detailed facies descriptions of subsurface core data from the Cretaceous Vøring Basin, Norwegian Sea, which document the character and spatial distribution (geographic and stratigraphic) of HEBs in a mud-rich, unconfined deep-water system which was relatively unaffected by sea-floor topography. Observations provide new insights into the evolution of gravity-flow dynamics during long-distance flow run-out in unconfined settings, and highlight the complexity of discrete flow transformations occurring internally within the larger-scale flow. Controls on the large-scale distribution of HEB, and thus reservoir quality distribution, are discussed. A version of this Chapter has been submitted for publication in *Sedimentology*. Work from this case study also forms a contribution to Porten et al. "Depositional reservoir quality of deep-marine sandstones: a sedimentological process-based approach – an example from the Springar Formation, NW. Vøring Basin, Norwegian Sea" which has been submitted to *Sedimentology*.

Chapter 4 provides detailed descriptions of facies and bed types within a mixed (sand-mud) deep-water system from the Central Pennine Basin, Carboniferous, N England. HEBs are discussed in terms of their character, distribution and origin with respect to a downstream confining basin margin onto which the deep-water succession onlapped. Findings provide insight into the influence that the relative proximity of confining topography along the flow path, and thus timing of flow confinement, can have upon gravity-flow transformation and resulting HEB character and distribution within basin fill successions. Such insight is of importance regarding the prediction of reservoir quality distribution in subsurface systems developed in topographically complex settings.

Chapter 5 expands upon the case study presented in Chapter 4 by documenting stratigraphic variations in HEB character and distribution in the wider context of system evolution and basin infill. Findings suggest that HEB characteristics can be linked to variations in the incision of muddy substrate, which occur over a range of time scales. However, a number of other

controlling factors also appear to determine the stratigraphic depositional trends expressed on the basin floor (e.g. lobe switching or local confinement).

Chapter 6 describes lateral correlations of individual beds across the Miocene Castagnola Basin, NW Italy. In addition to allowing further investigation of HEB character and distribution with respect to downstream confinement, as in Chapter 4, this study is novel in providing an opportunity to study HEBs in a deep-water system where basin physiography resulted in containment (ponding) of flows in addition to flow confinement. Gravity flows are discussed in terms of their resulting dynamics in light of this combined confinement and containment. A version of this chapter has been published in *Sedimentary Geology* (Southern et al., 2015).

Chapter 7 integrates the findings of the individual case studies and discusses their generic implications with respect to hybrid flow development, evolution and deposition in variably topographically complex settings. The chapter concludes with suggestions for future research.

Chapter 2. Deep-water sediment gravity flows; an overview

2.1 Introduction

This chapter summarises previous outcrop, experimental and numerical studies concerning gravity flow dynamics, classification and transformation, as well as studies documenting gravity-flow interaction with basin-floor topography, in order to provide the necessary background for this study. The chapter concludes with a review of deposits containing co-genetic matrix-rich sandstones in terms of their character, distribution and potential origins and a consideration of the likely controls upon their development, as well as their significance within deep-water depositional systems.

Deep-water depositional environments receive sediment from shelf and slope failures, or directly via cross-shelf transport, surface current transport or river discharge; pelagic and hemipelagic sedimentation may also occur (Fig. 2.1; Einsele, 1996; Stow & Mayall 2000). Subaqueous sediment gravity-driven flows (SGFs) are amongst the most frequent and volumetrically significant re-sedimentation events in deep-water settings (Normark et al., 1993). These complex phenomena may exhibit a spectrum of flow behaviours, due to differing combinations of grain-support mechanisms, largely determined by sediment composition and concentration, and thus flow rheology (Fig. 2.2; Bouma, 1962; Middleton & Hampton, 1976; Lowe, 1982, 1988). Heterogeneity in such flow character can be expressed as spatial heterogeneity across different flow regions at any instant in time, and/or spatio-temporally as the flow structure transforms *en-masse* or within discrete regions during flow run-out downstream. Thus, it is better to characterise discrete zones of similar character within a flow, whether they co-occur during any one instant of flow, or whether they succeed one another temporally during flow run-out, rather than to attempt to characterise an entire flow event according to one process.

2.2 Flow behaviour

SGFs have traditionally been considered in terms of two end-member rheologies: plastic or fluidal, depending upon their sediment composition (i.e. proportion of cohesive material) and sediment concentration, which jointly determine the mechanism(s) of grain support and flow rheology (Fig. 2.2, Middleton & Hampton, 1976; Mulder & Alexander, 2001).

2.2.1 Cohesive debris flows

Traditionally, the term debris flow has been used to refer to plastic flows characterised by high proportions of cohesive material, which provides a yield strength grain support, suppresses fluid turbulence and prevents differential-grain settling (Hampton, 1975; Middleton & Hampton, 1976; Marr et al., 2001; Mulder & Alexander, 2001) (Fig. 2.2). Debris flows largely move as

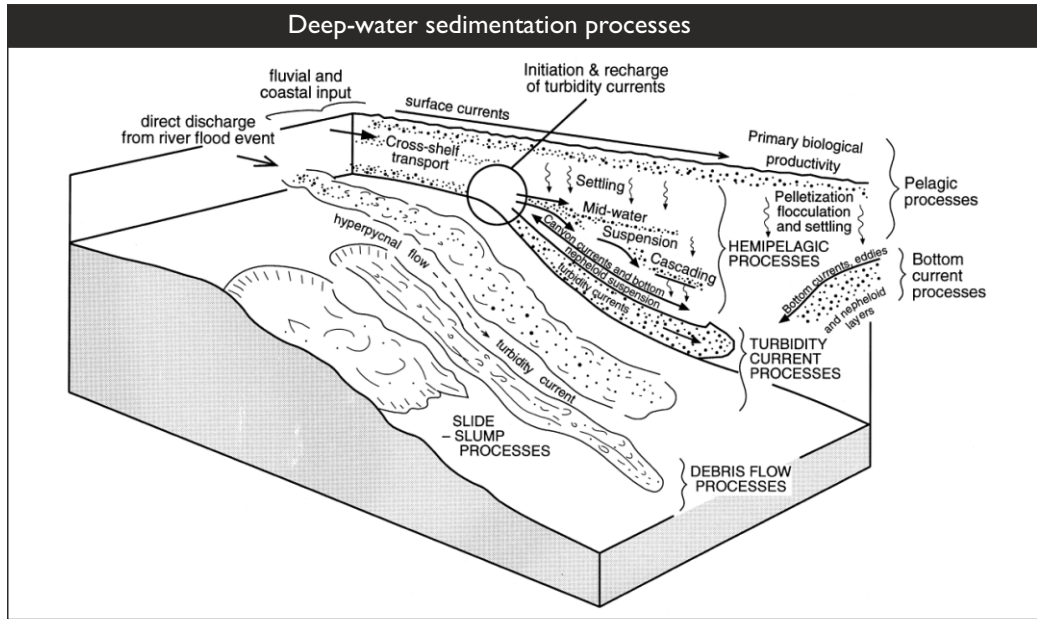


Figure 2.1. Block model illustrating the range of deep-water sedimentation processes. From Stow & Mayall (2000).

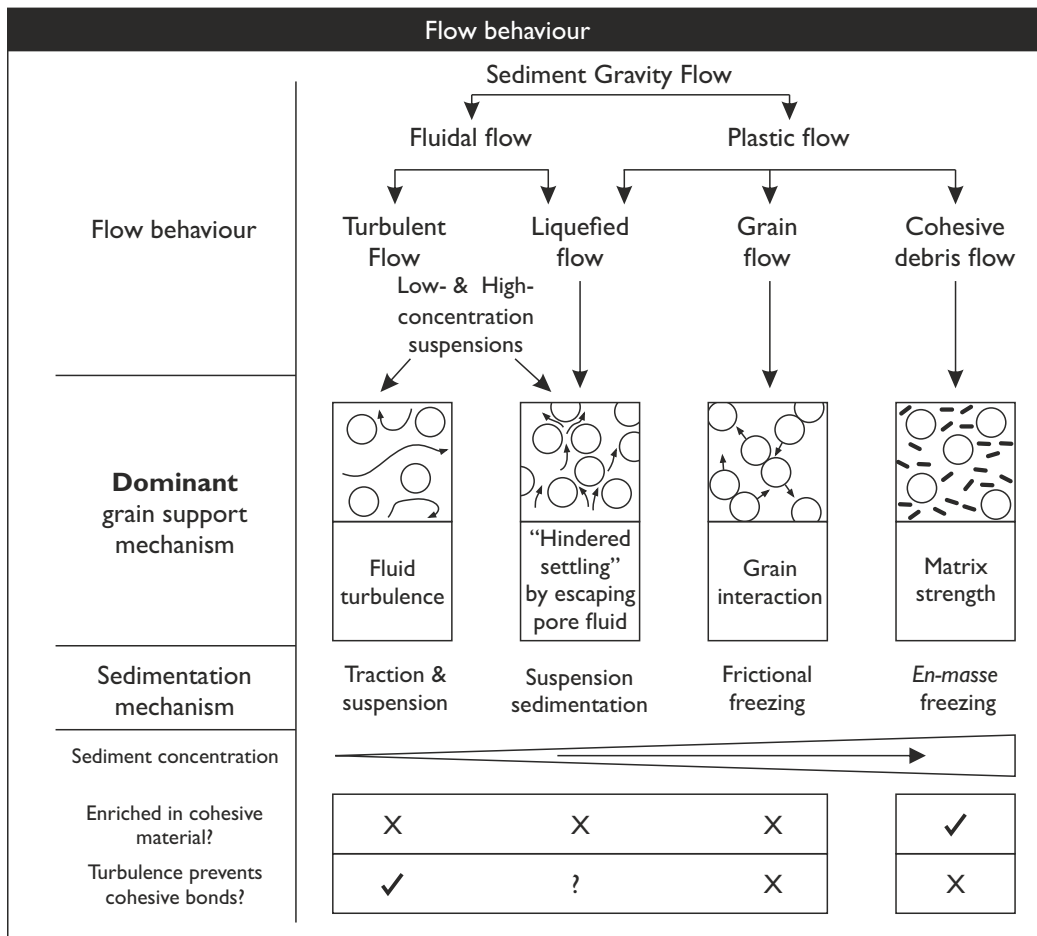


Figure 2.2. Examples of the spectrum of sediment gravity flow behaviour as determined by their sediment composition and sediment concentration and associated dominant grain-support mechanism. Note that each is part of a continuum of flow behaviour and that multiple grain-support mechanism may characterise a region of flow. Furthermore, SGFs are highly complex phenomena in terms of spatial and temporal variations in these characteristics and thus may exhibit multiple flow behaviour during a single sediment gravity flow event. Modified from Middleton & Hampton (1976).

laminar flows above a basal shear zone, where the velocity gradient and shear stresses are higher (Fig. 2.3; Johnson, 1970; Hampton, 1972, 1975; Carter, 1975; Marr et al., 2001; Iverson et al., 2010). Once flow yield-strength is no longer exceeded by shear stresses, deposition occurs via *en-masse* freezing to emplace debrite deposits (Carter, 1975; Mohrig et al., 1998). Owing to their high yield strength, debrites often terminate abruptly, are often localised to their source (i.e. the continental slope or local sea-floor topography, Hampton, 1972), may exhibit a frond like geometry in plan view, and may exhibit an irregular, mounded bed top from which transported clasts may protrude (Fig. 2.4; Middleton & Hampton, 1976; Pickering et al., 1989; Twichell et al., 1995; Schwab et al., 1996). Debrites are typically matrix (clay)-rich and clast-rich, poorly sorted deposits, largely devoid of internal stratification (Middleton & Hampton, 1973; Embley, 1976; Naylor, 1980; Mohrig et al., 1998). Clasts are supported both by matrix strength and by a matrix-buoyancy effect; they may be abundant and their size can vary greatly (Moscardelli et al., 2006; Moscardelli & Wood, 2008; Talling et al., 2010; Jackson & Johnson 2009). Mudstone clasts, or rafts, can be very large owing to their positive buoyancy in typical debris flow sediment-water mixtures (Flemings et al., 2006; Talling et al., 2010).

Experimental studies have demonstrated how variations in the proportion of cohesive material and bulk sediment drive variation in the magnitude of the flow's yield strength (i.e., flow coherency *sensu* Marr et al., 2001), and thus flow character of clay-rich flows.

Low-coherency debris flows are characterized by lower proportions of cohesive material, lower bulk sediment and a lower magnitude of yield strength (Marr et al., 2001; Sumner et al., 2009). Compared to higher coherency debris flows, low coherency debris flows may: 1) lack sufficient yield strength to support the entire sand fraction or mud clasts within the flow (Marr et al., 2001; Amy & Talling, 2006; Talling et al., 2007a, 2012a; Sumner et al., 2009); and 2) achieve relatively greater flow run-out distances owing to their lower yield strength (Talling et al., 2012a; Talling, 2013).

2.2.2 Non-cohesive turbidity currents

Traditionally, the term turbidity current has been used to refer to SGFs thought to be turbulent suspensions in which sediment is suspended via fluid turbulence (Fig. 2.2; Bagnold, 1966; Sander, 1965; Middleton & Hampton, 1973; Lowe, 1982). However defining a SGF by grain-support mechanism is problematic (see Mulder et al., 1997; Kneller & Buckee, 2000) as the character and grain-support mechanism in such natural phenomena is unclear, owing to the difficulties associated with direct monitoring of the character of naturally occurring flows and inferring flow character from their deposits. Further, these flow characteristics may vary spatially and temporally within a flow event due to variations in velocity, turbulence and sediment concentration (Smith, 1955; Sinclair, 1962; Kuenen & Menard, 1952; Middleton & Southard, 1984; Allen, 1991; Garcia, 1994; Mulder et al., 1997; Postma et al., 1998; Kneller and

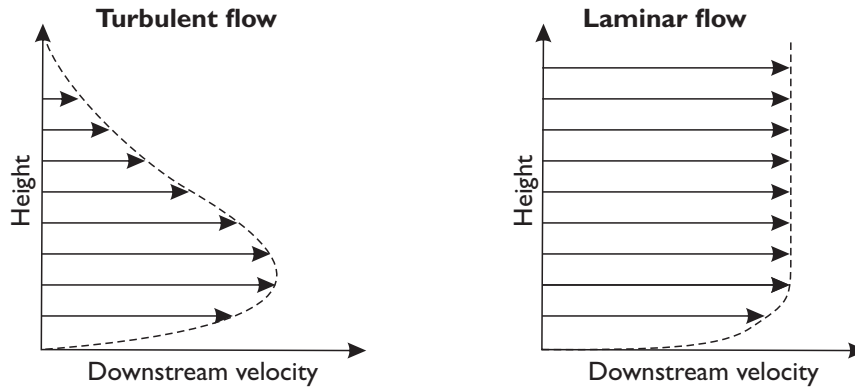


Figure 2.3. Vertical profiles of downstream velocity for turbulent and laminar flow from Mulder & Alexander (2001).

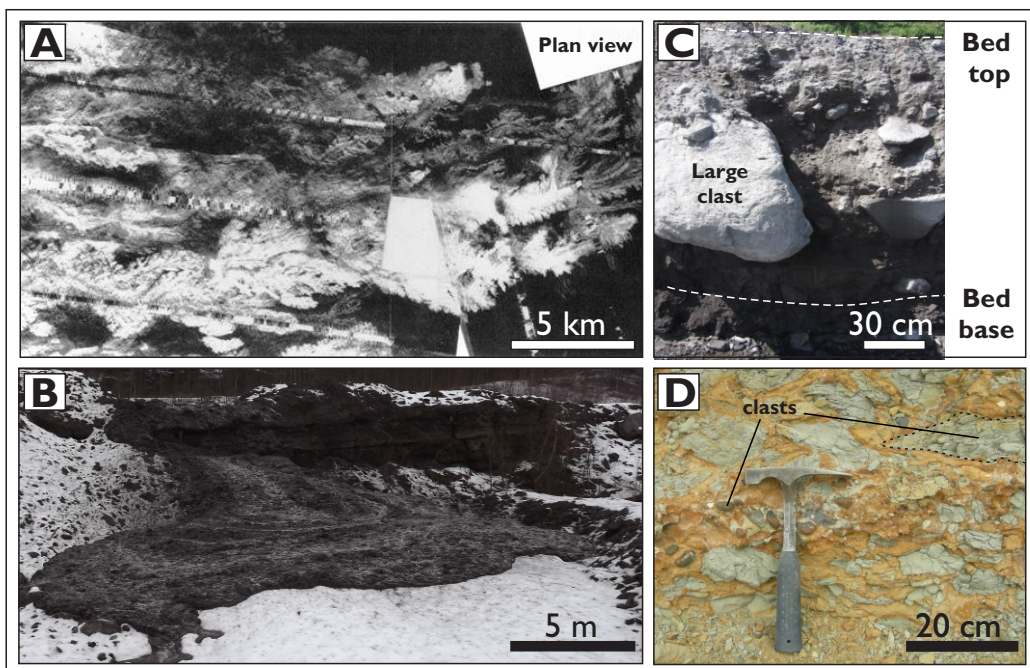


Figure 2.4. Examples of debrisites deposited from debris flows. **A)** Sub-aqueous debrisite with a frond-like geometry, Modern Mississippi Fan (Schwabb et al., 1996). **B)** Modern sub-aerial debrisite with compression ridges upon its surface. **C)** Modern sub-aerial debrisite supporting poorly sorted clasts, Semeru, Indonesia. **D)** Sub-aqueous debrisite, with sub-angular to sub-rounded, poorly sorted clasts, Rosario Formation, California.

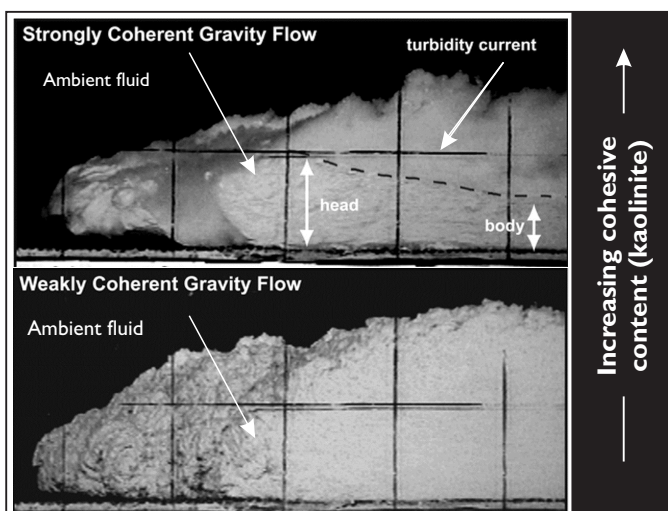


Figure 2.5. Head regions of experimental gravity flows with differing coherence (yield strength) owing to their contrast in concentration of cohesive material (kaolinite). Stronger coherence (higher yield strength) flows resist dilution and mixing with the ambient fluid due to higher proportions of cohesive material. Modified from Marr et al. (2001).

Buckee, 2000, McCaffrey et al., 2003). Herein, the term turbidity current builds on the definition of suspension currents provided by Kneller and Buckee (2000) who defined such flows as “fluidal mixtures of suspended sediment and water” in which “suspension of grains above the bed may involve grain-support mechanisms other than fluid turbulence”. As such, turbidity currents are fluidal, non-cohesive sediment-water mixtures which may exhibit turbulent (disturbed by eddies) or laminar-like, yet non-cohesive, behaviour depending upon the local sediment concentration and associated dominant grain-support mechanism(s). Such varying turbulence in non-cohesive flows is expressed in their resulting deposits (i.e. high- and low-density turbidites *sensu* Lowe, 1982; Bouma, 1962). The term turbulent suspension is included with the turbidity current definition but is more specific in that it is reserved for dilute suspensions in which fluid turbulence is thought to have been the dominant grain-support mechanism and have influenced depositional character. Bagnold (1962, 1966) suggested a sediment volume below 9%, however this will be variable depending upon flow characteristics such as velocity and sediment composition (i.e. Baas & Best, 2002).

Deposition from a turbidity current is most commonly considered to commence when shear velocity decreases (spatially or temporally) below the suspension threshold of the coarsest grains in the flow, with aggradation of the bed capturing any spatio-temporal changes that occur in the character of the flow (i.e. sediment size, composition, concentration, and thus grain-support mechanism and flow rheology) passing the depositional point (Kneller & Branney; 1995; Kneller & McCaffrey, 2003; McCaffrey et al., 2003). As such, turbidites are often normally graded in terms of grain size (Bouma, 1962; Kuenen, 1966). Bouma (1962) proposed an idealised turbidite bed sequence, characterised by normal grading and a distinct vertical succession of sedimentary structures and was inferred to be deposited by a single, waning, dilute surge-type turbidity current (Fig. 2.6). Recognising that different sedimentary structures occurred in coarser grained deposits, Lowe (1982) proposed that additional divisions could be added to the base of the Bouma Sequence; these additional divisions were interpreted as recording relatively more proximal flow with higher near-bed sediment concentration and sediment fall-out rate in a fluidal, weakly turbulent flow (high-density turbidity current) compared to more downstream flow emplacing the Bouma Sequence (low-density turbidity current).

2.3 Flow processes

Deep-water depositional systems may be extremely complex, nevertheless, with a basic understanding of the mechanisms of gravity currents, it is possible to gain insight into such systems and their deposits. Several key variables which are important to consider in subsequent chapters are discussed below: 1) flow capacity and competence; 2) flow non-uniformity; 3) flow unsteadiness; 4) flow structure; 5) flow transformation; and 6) flow interac-

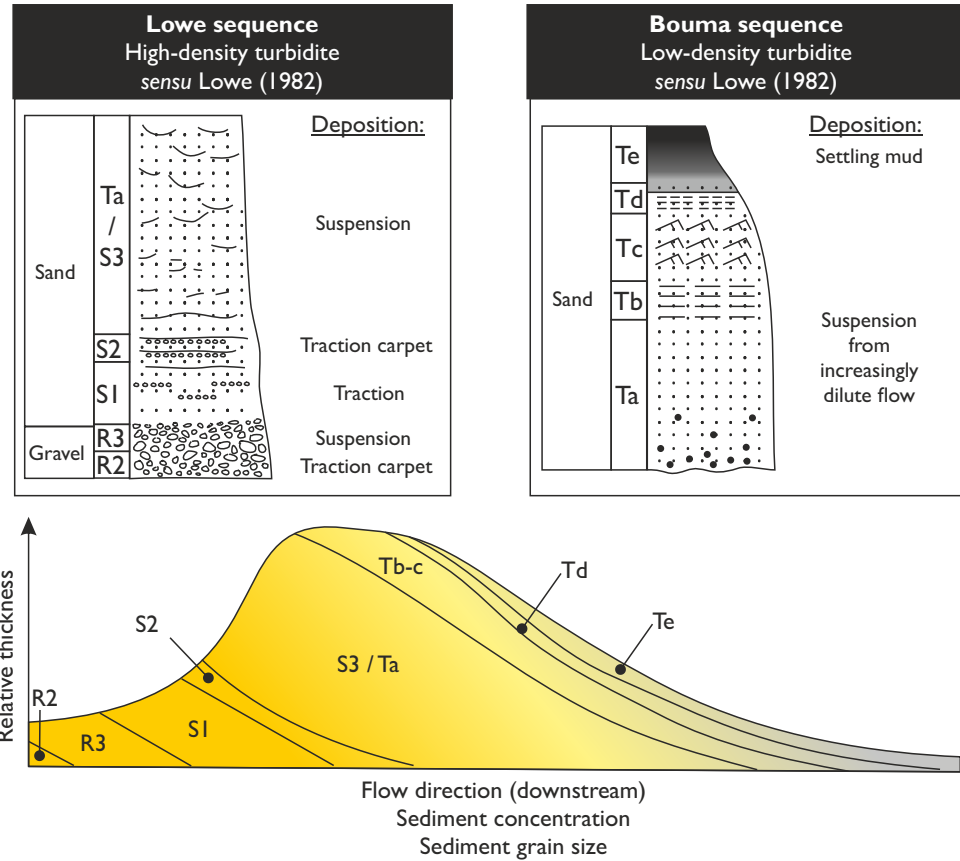


Figure 2.6. Downstream variation from coarser grained high-density turbidite to finer grained low-density turbidite within a surge like turbidity current deposit due to downstream reduction of flow concentration and sediment grain size. Note the overlap between the Ta and S3 division of the Bouma and Lowe sequence, respectively. Modified from Allen (1985) and Lowe (1982).

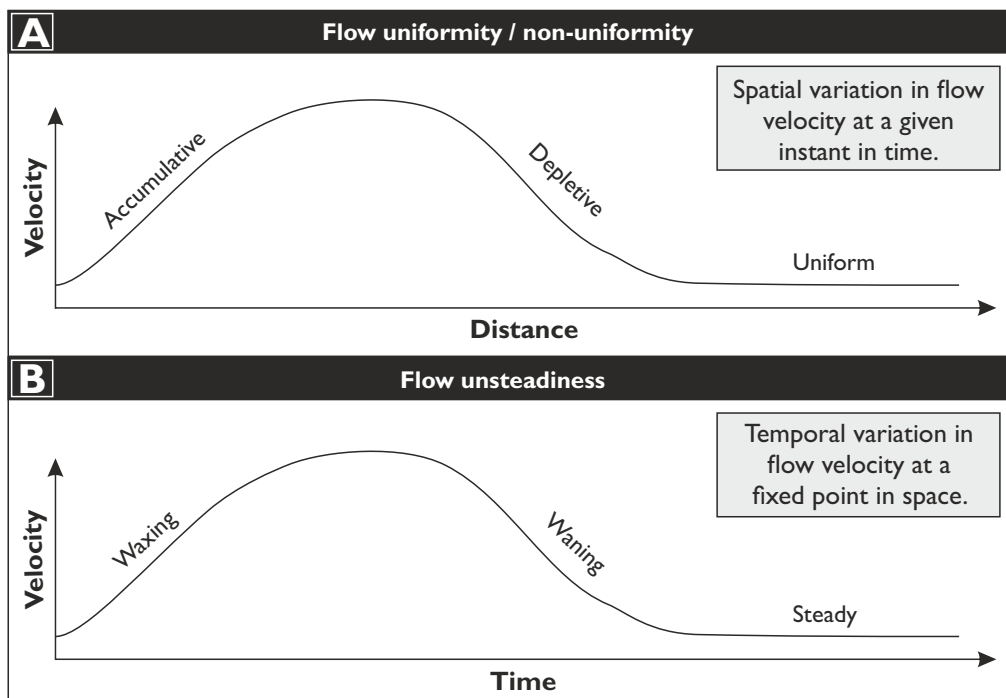


Figure 2.7. A) Schematic diagram of spatial variation in flow velocity at a given instant in time (flow non-uniformity). **B)** Schematic diagram of temporal velocity variation in flow passing a fixed point in space. Modified from Kneller (1995).

tion with sea-floor topography.

2.3.1 Flow capacity and competence

Flow capacity refers to the mass per unit volume of sediment which is supported within non-cohesive flow and is related to fluid discharge and turbulence intensity (Hiscott, 1994a; Kneller & McCaffrey, 2003; Dorrell et al. 2013). Deposition occurs when the flow capacity drops below that of the flow concentration whereas erosion occurs when flow capacity exceeds flow concentration (Kneller, 1995). Competence refers to the ability of non-cohesive flows to carry grains of a specific settling velocity, as determined by their density, size and shape, and the shear velocity of the flow (Kneller & McCaffrey, 1999). Flow capacity and competence concepts may break down as the proportion of cohesive clay and flow coherency (*sensu* Marr et al., 2001) increases such that particles are instead supported by matrix-strength.

2.3.2 Flow non-uniformity

Uniform flows are those whose mean velocity does not vary spatially, whereas non-uniform flows (*sensu* Kneller, 1995) are those which exhibit spatial variation in flow velocity when observed at an instant in time (i.e. instantaneous flow structure) due to changes in flow constriction or substrate gradient (Fig. 2.7a; Kneller 1995; Kneller and Branney 1995). As such, depletive flow (flow which is slower downstream) may occur at the base of slope (Kneller, 1995; McCaffrey & Kneller, 2004), upstream of topographic obstacles (Kneller et al., 1999) and where flow exits a constriction such as that associated with channels or between salt-topography (Davis et al., 2009; Wynn et al., 2002a; Terlaky & Arnott, 2014). Many spatial facies variations observed in deep-water settings, particularly those in topographically complex settings (Kneller et al., 1991; Kneller, 1995; Barker et al., 2008; Patacci et al., 2014), are expected to arise from processes associated with flow non-uniformity.

2.3.3 Flow unsteadiness

Flow unsteadiness describes the temporal variation in flow velocity as observed from a fixed point along the flow pathway (Allen, 1985; Kneller & Branney, 1995; Kneller, 1995) (Fig. 2.7b). Where flow passing this point becomes progressively faster or slower it is termed waxing flow or waning flow, respectively (Kneller, 1995). Waxing flow is capable of producing inverse grading, however it is most likely to be recorded in proximal regions as zones of faster travelling flow are thought to eventually advance towards the front of the flow during downstream run-out (Kneller & McCaffrey, 2003). Waning flow is more significant distally and emplaces deposits whose vertical profile of grain size and sedimentary structures record waning of successive portions of the flow as it passes the depositional point (Bouma, 1962; Lowe, 1982).

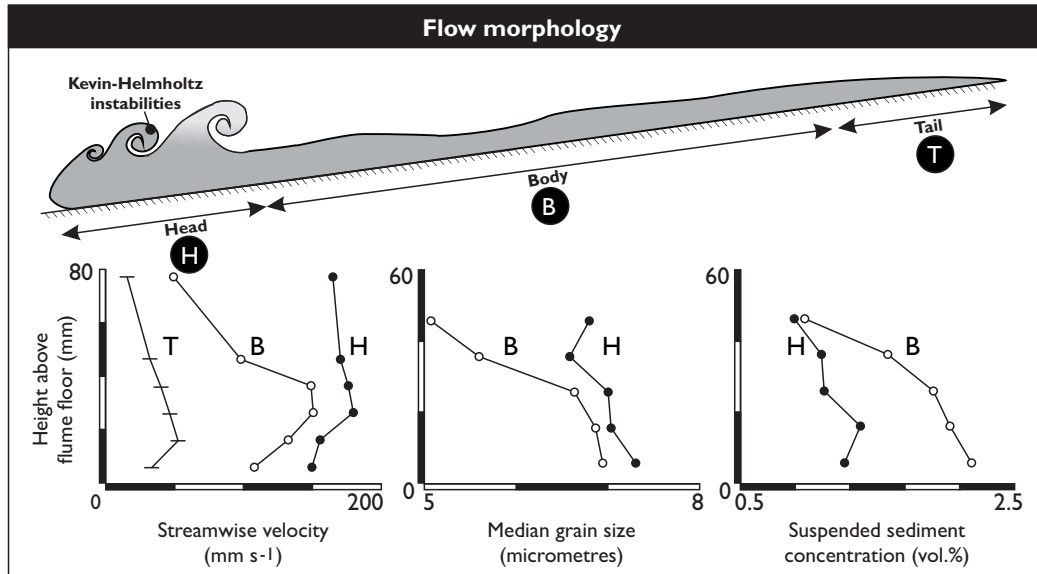


Figure 2.8. Morphology of a turbidity current; divided into head, body and tail, with typical velocity, concentration and grain size data for these regions. Vertical flow stratification (velocity, grain size and concentration) is most pronounced in the flow body. Velocity, concentration and grain size from Baas et al. (2005).

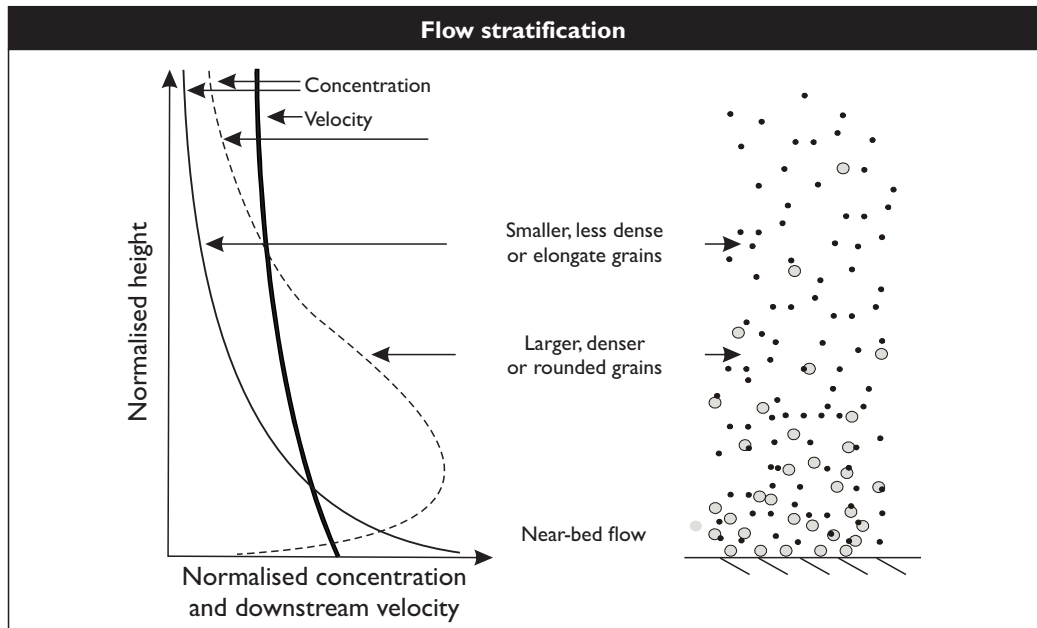


Figure 2.9. Schematic illustrating the typical vertical distribution of velocity, sediment concentration and sediment type within a turbidity current. Vertical flow stratification arises due to grain size, density and shape with higher settling velocity particles concentrated in near-bed flow whilst lower settling velocity particles are more evenly distributed vertically. Modified from Kneller & McCaffrey (1996) and Haughton et al. (2003).

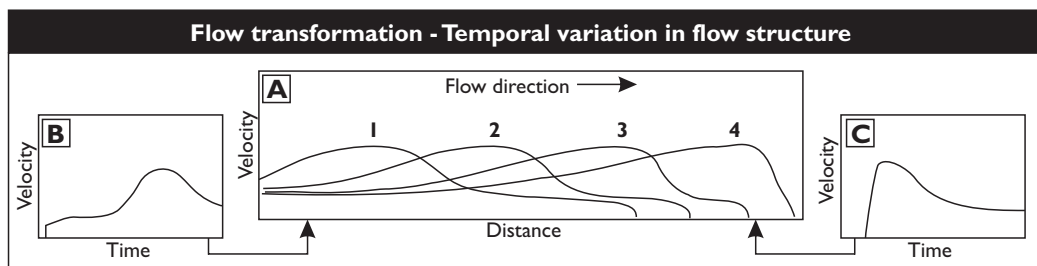


Figure 2.10. **A)** Longitudinal velocity structure at four different times within a flow illustrating the progression of a surge towards the front of the current with time. **B)** Time series of flow velocity in a proximal position (waxing then waning flow). **C)** Time series of flow velocity in a distal position (waning flow only). From Kneller & McCaffrey, (2003). Variation in velocity structure drives modification of the structure of sediment concentration and associated grain-support mechanism(s) and thus that of flow behaviour.

2.3.4 Spatial variation and temporal evolution of flow character

Experimental and theoretical work has shown how turbidity currents can develop instantaneous structure (longitudinally or vertically) in terms of velocity, turbulence, sediment concentration and grain size, and associated flow rheology (Figs 2.8, 2.9; Kuenen & Menard, 1952; Middleton & Southard, 1984; Allen, 1991; Middleton, 1993; Garcia, 1994; Altinaker et al., 1996; Hand, 1997; Kneller et al., 1997; Parsons & Garcia, 1998; Kneller & McCaffrey, 1999; Kneller & Buckee 2000; Peakall et al., 2000; Choux & Druit, 2002; McCaffrey et al., 2003; Choux et al., 2004; Baas et al., 2005). For example, particles with relatively higher settling velocities (e.g., larger or denser grains) tend to concentrate in near-bed flow, whereas particles with relatively lower settling velocities tend to be more evenly distributed through the flow height, resulting in vertical flow stratification in terms of sediment concentration (density stratification), grain size, composition and rheology (Fig. 2.9; Rouse, 1939; Middleton & Southard, 1984; Stacey & Bowen, 1988; Zeng et al., 1991; Garcia, 1994; Kneller & McCaffrey, 1995, 1999; Kneller & Buckee, 2000; Buckee et al., 2001). The action of vertical gradients in horizontal velocity upon such density and grain size stratification can result in the hydraulic segregation and redistribution of lower-settling velocity particles (e.g. smaller, less dense or elongate particles) longitudinally towards the rear of the flow (Stacey & Bowen, 1988; Garcia & Parker, 1993; Garcia, 1994; Altinaker et al., 1996; Kneller & Buckee, 2000). Flows may further self-organise during downstream run-out as faster travelling regions of the flow advance headwards until equilibrium with the surrounding flow, thus flow structure undergoes a spatio-temporal transformation in terms of velocity, turbulence and sediment concentration, size and composition (Fig. 2.10; McCaffrey et al., 2003). The term flow transformation refers to such temporal variation in flow characteristics (i.e. grain size, concentration, velocity, turbulence and rheology) and the instantaneous flow structure during downstream run-out (Fig. 2.10, 2.11). Study of sub-aerial pyroclastic flows and flume tank experiments with particulate gravity flows have provided insight into the range of flow transformations affecting SGFs (Fig. 2.3, 2.11; Kuenen, 1952; Middleton, 1967, 1970; Hampton, 1972; Middleton & Hampton, 1973; Fisher, 1983; Marr et al., 2001; Branney & Kokelaar, 2002; Mohrig & Marr, 2003; Baas et al., 2009, 2011, Sumner et al., 2009).

Models attempting to predict the depositional record of SGF evolution during downstream run-out, termed facies tracts, have traditionally been dominated by a downstream trend of increasing flow dilution, driven by mixing with the ambient fluid and sediment deposition, accompanied with an increase in turbulence intensity and downstream reduction in sediment concentration and grain size (Fig. 2.12a; Bouma, 1962; Walker, 1967, 1978; ; Hampton, 1972; Piper et al., 1985; Lowe, 1982, 1988; Allen, 1991; Stow et al., 1996; Mutti, 1992). A range of mechanisms are now recognised which are thought to result in downstream

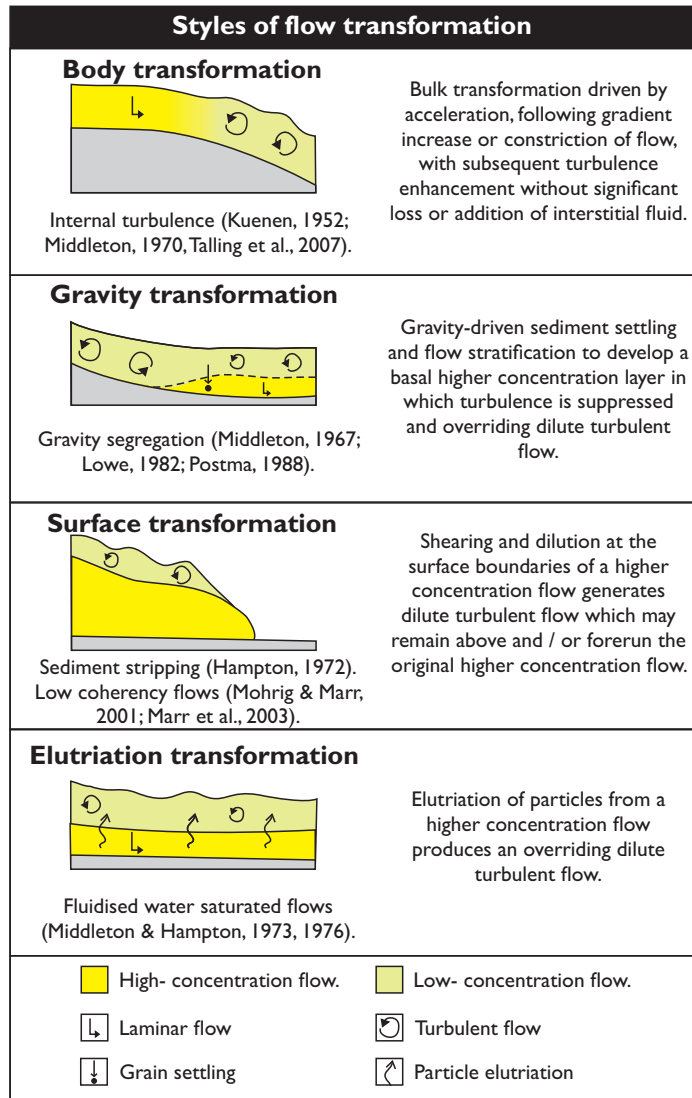


Figure 2.11. Examples of potential flow transformations during downstream flow run-out. Modified from Fisher (1983).

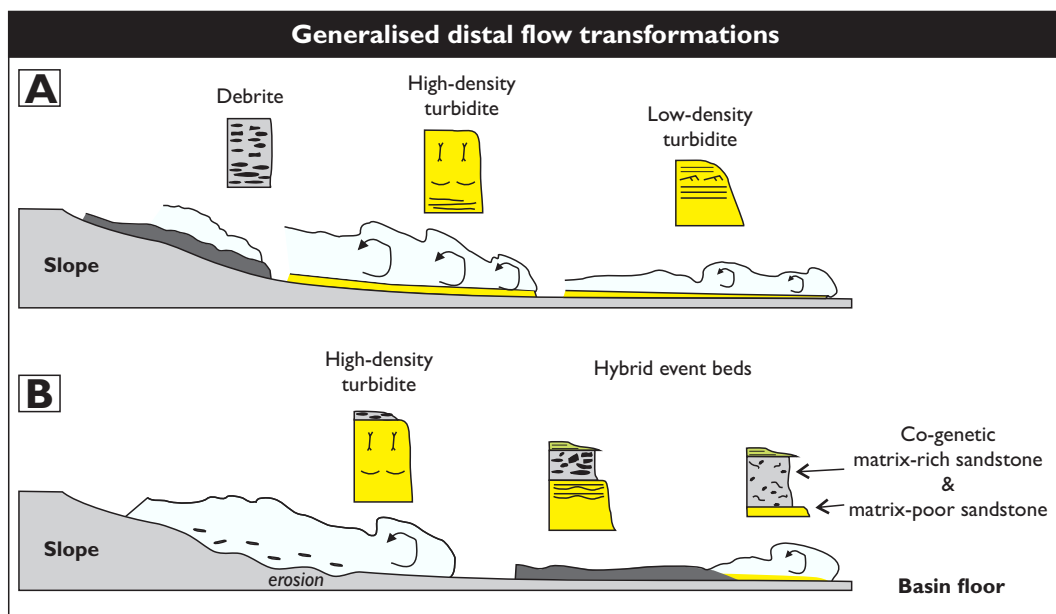


Figure 2.12. General trends of flow transformation during run-out downstream. **A)** Traditional facies tract for which the flow underwent increasing dilution and became increasingly turbulent distally. **B)** Emerging flow transformation trends whereby flow may become turbulence suppressed and cohesive distally. Modified from Haughton et al. (2003).

transformation (partially or wholly) from relatively non-cohesive turbulent flow into more cohesive, laminar-like, turbulence suppressed flow (Fig. 2.12b; Wood & Smith 1958; Haughton et al., 2003, 2009; Talling et al., 2004, 2007a; Baas et al., 2009, 2011; Sumner et al., 2009, 2012; Talling, 2013). This awareness has largely been driven by the recognition of individual beds containing co-genetic facies recording deposition from relative turbulent and more cohesive flow behavior occurring during a single SGF event (Wood & Smith 1958; Haughton et al., 2003, 2009; Amy & Talling, 2006; Barker et al., 2008; Kane & Pontén, 2012); such deposits form the focus of this research and are discussed further in section 2.4.

2.3.5 Interactions with sea-floor topography

SGFs may run out for long distances where the sea-floor topography is relatively simple or where they are channel confined (tens - hundreds km, Wynn et al., 2002b; Fig. 2.13). Where SGFs occur in more topographically complex settings, their potential run-out distance can be reduced, or increased, and their character, including that of the depositional system they emplace, can be modified by interaction with sea-floor topography (Miller & Smith, 1977; Fisher, 1990; Smith, 2004 and references therein). Such systems can contain commercial hydrocarbon reserves (e.g. Gulf of Mexico, Kendrick., 2000; West Africa, Gee & Gawthorpe, 2007; North Sea, Barker et al., 2008, Davis et al., 2009) as sea-floor topography can focus sand deposition and provide suitable traps through structural and or stratigraphic trapping (McCaffrey & Kneller, 2001; Prather, 2003). Sea-floor topography can take a variety of forms (e.g. salt or mud diapirs, Beaubouef et al., 2003; fault generated topography, Clark & Cartwright, 2009) and its expression on the sea floor may be static or dynamic depending upon sedimentation rates versus that of the processes generating topography (Prather et al., 1998; Grando & McClay, 2004; Mayall et al., 2010).

Interaction with sea-floor topography can modify SGFs in terms of their transport direction, velocity, turbulence and sediment concentration, suspension fall-out rate and rheology (Long, 1955; Pickering & Hiscott, 1985; Kneller et al., 1991; Edwards et al., 1994; Haughton, 1994; Kneller & McCaffrey, 1999; Lamb et al., 2004; Barker et al., 2008; Davis et al., 2009; Patacci et al., 2014; Figs 2.14 - 2.16). The nature of the modification depends upon a number of factors such as flow velocity, density, height, and degree of flow stratification, as well the height of the topographic obstacle (Fig. 2.14; Kneller & Buckee, 2000; Kneller & McCaffrey, 1999). Such topographically-driven modification of the SGF is referred to herein as flow confinement or confined flow, and may occur following flow interaction with a range of topographic features on the sea floor (Fig. 2.13, 2.15, Example B). Confined flows may also be contained (flow containment) where the height (Kneller & McCaffrey, 1999) and geometry of the topography is such that the majority of the flow is restricted within a depositional container; provided the flow is of sufficient magnitude such that it reaches the limits, and feels

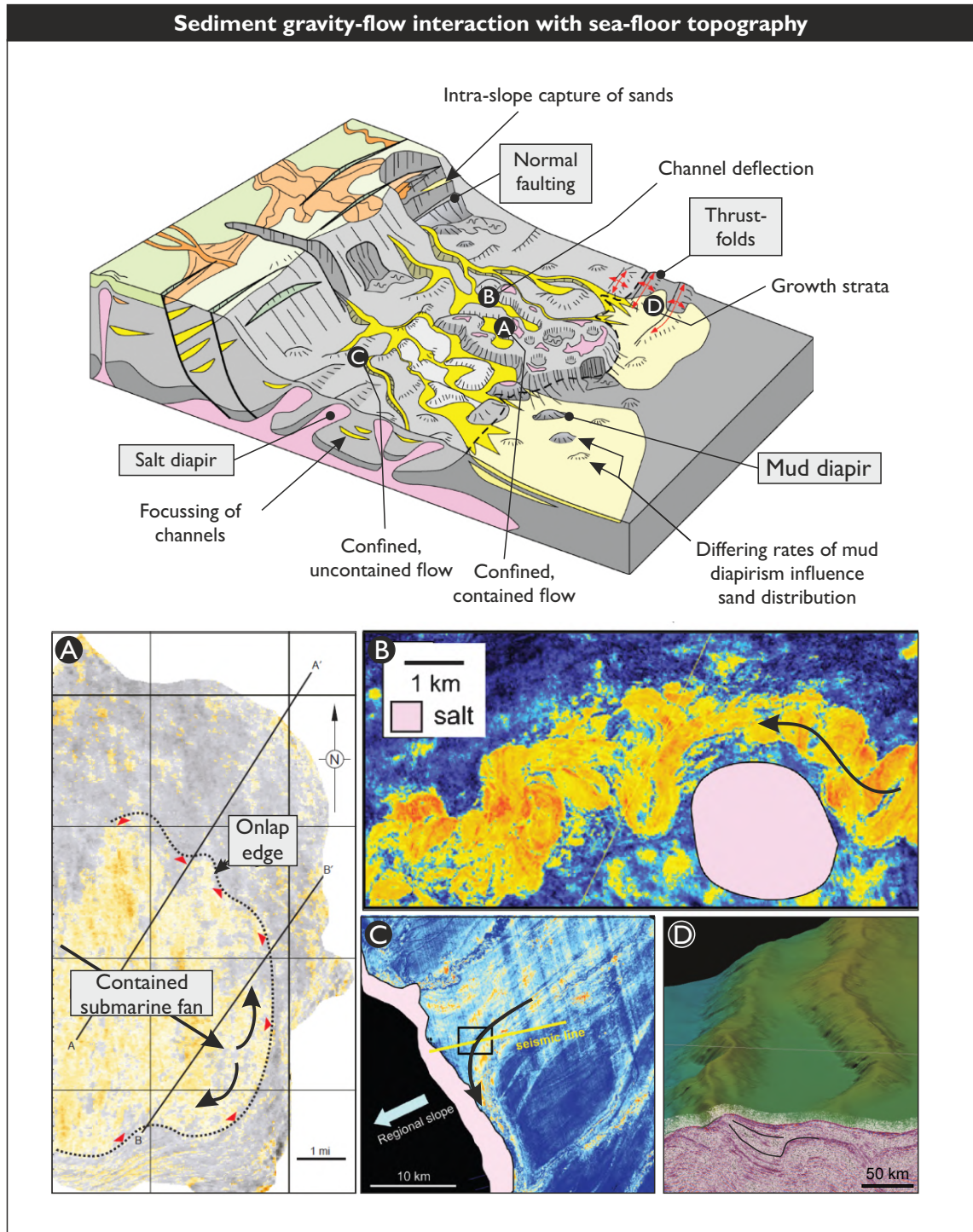


Figure 2.13. Schematic block model illustrating the influence of sea-floor topography upon shelf, slope and basin floor depositional systems. Terrestrial fluvial-delta systems (orange), sand-rich facies (yellow), deep-water fans (pale yellow), slope muds (grey) and salt (pink). Note the deflection and focussing of channels where flows are confined and that flows may or may not be contained entirely where flow confinement occurs. Modified from Mayall et al. (2010). Numbered examples correspond to scenarios on the upper block model. (A) from Prather et al. (1998); (B & C) from Mayall et al. (2010).

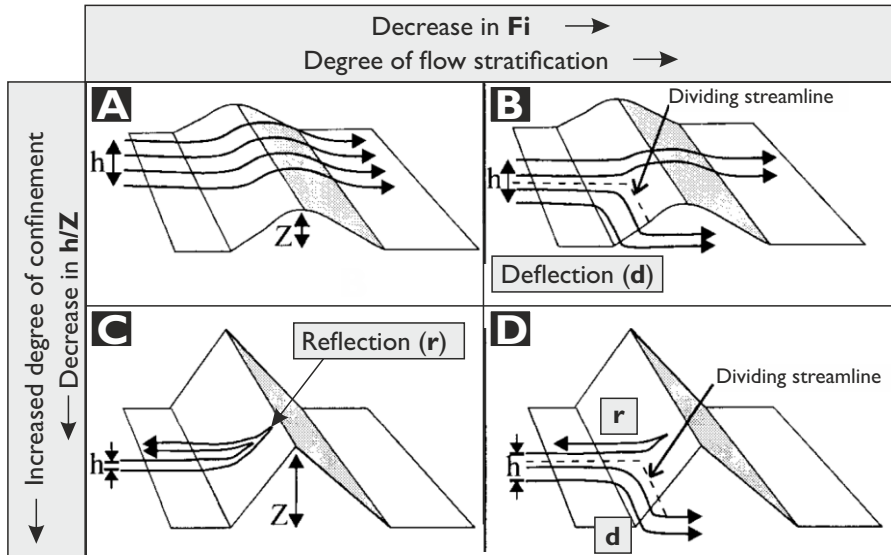


Figure 2.14. Schematic matrix illustrating scenarios of sediment gravity flow interaction with sea-floor topography with varying degrees of flow stratification and obstacle height. Where the F_i (ratio of inertial to gravitational forces) is high and the topography small, the flow has the ability to surmount the obstacle (A). With reduction in the F_i an increasing proportion of the upper flow (that above the dividing streamline) has sufficient energy to move up the counter-slope of the confining obstacle, with the actual height of the obstacle determining whether such flow passes over the obstacle (2) or collapses back down as a reflection (D). Denser flow below the dividing streamline is deflected laterally along the confining slope (B & D). Regardless of the F_i number, obstacles of sufficient height will not be surmounted by the flow (C), however the F_i number will determine the proportion of flow reflection and deflection. Modified from Kneller & McCaffrey, (1999).

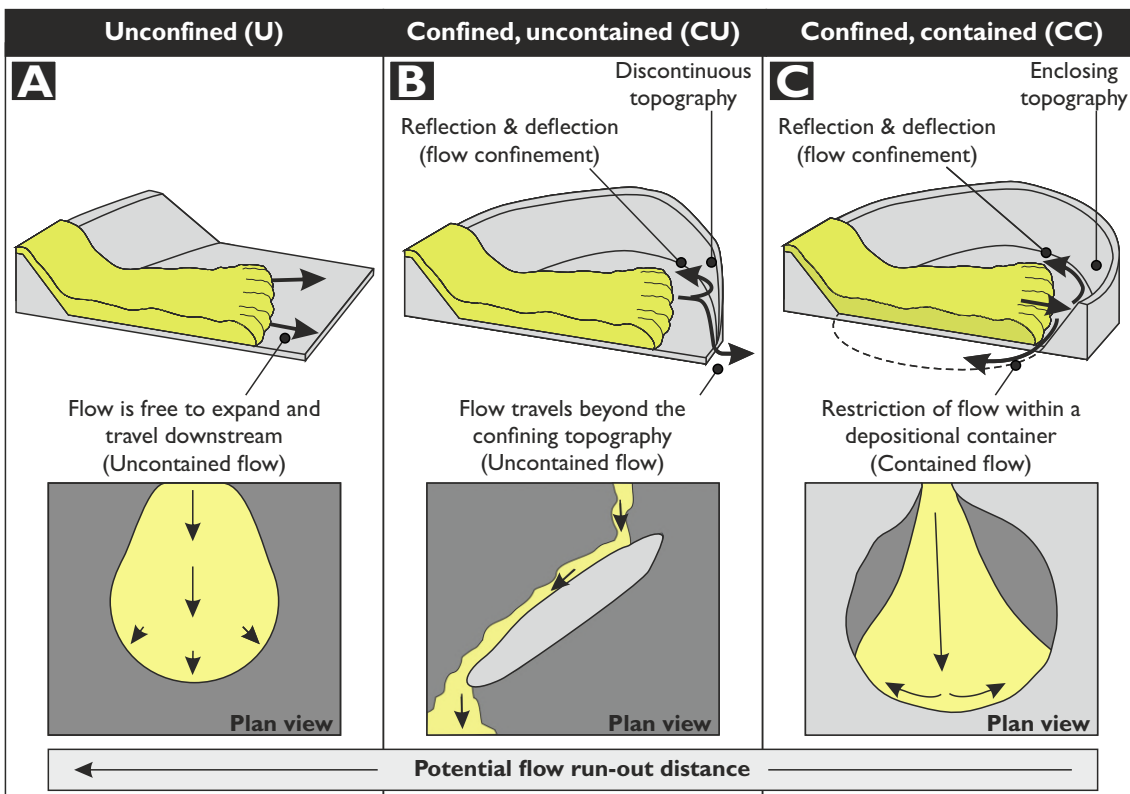
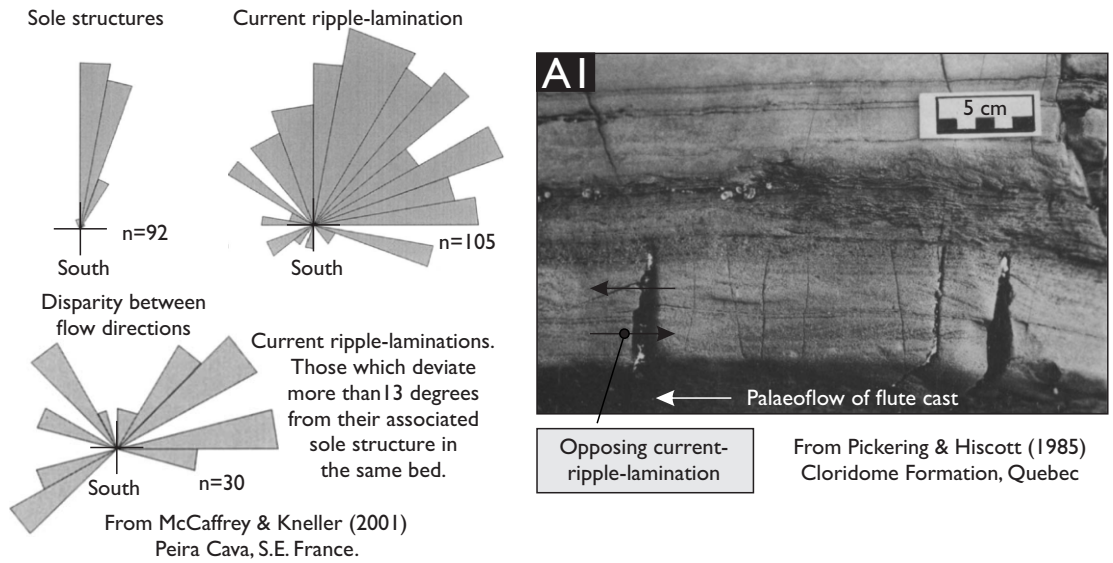
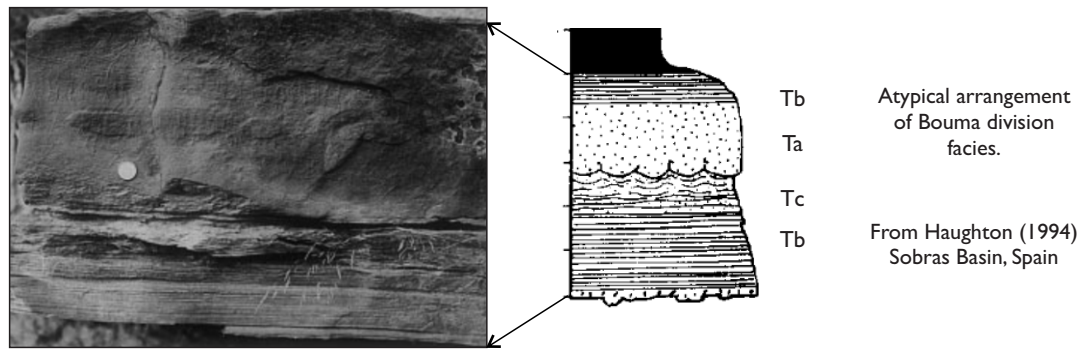


Figure 2.15. Classification of flows depending upon their interaction with sea-floor topography. Where there is no pronounced sea-floor topography, flows are free to radially spread and run out downstream (A). In the presence of sea-floor topography, modification of flow transport direction and other characteristics (flow confinement) occurs (B & C). Where the geometry of the topography is sufficient to retain the flows within a depositional container and the flow is of sufficient magnitude to reach the limits and feel the effects of this containment the flow is considered to be confined and contained (C).

A Disparity of palaeoflow direction within individual SGF beds



B Atypical grain size & facies arrangement



C Bed dominated by “combined flow” structures

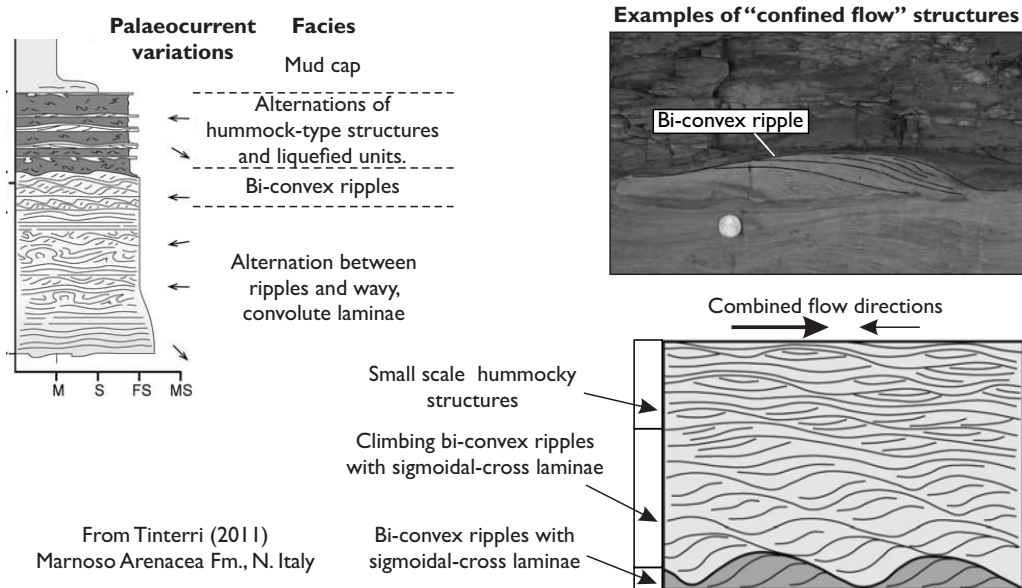


Figure 2.16. Examples of deposits emplaced by gravity flows which interacted with confining sea-floor topography **A)** Examples of discrete palaeoflow directions, often observed in a single bed (**AI**). **B)** Examples of atypical facies and grain size profiles. **C)** Examples of distinct sedimentary structures believed to reflect combined flow (i.e. competing incoming and confined flow directions).

the effects, of this containment (Fig. 2.15, Example C; Kneller & Buckee, 2000; Al Ja'Aidi et al., 2004). Such confined and contained flow may occur in salt withdrawal mini-basins (Prather et al., 1998) and in small intra-continental rift or fore-arc basins (Pickering & Corregidor, 2000). Thus SGFs, and the depositional systems that they emplace, can be classified depending upon whether they were: 1) unconfined (U); 2) confined and uncontained (CU); or 3) confined and contained (CC, Fig. 2.15, Examples A, B, C, respectively).

The effects of flow confinement can be manifested in the rock record (Fig. 2.16). Specifically, this may be indicated by the following relationships: 1) disparate palaeoflow directions (e.g. sole structures versus tractional sedimentary structures higher within the bed; Kneller et al., 1991; Haughton, 1994; Pickering & Hiscott, 1985; Kneller, 1995; Kneller & McCaffrey, 1999, McCaffrey & Kneller, 2001; Felletti, 2002; Fig. 2.16a); 2) complex grain-size grading and arrangements of sedimentary structures (e.g. Haughton, 1994; Pickering & Hiscott, 1985; Fig. 2.16b); 3) distinct “combined” sedimentary structures considered to record oscillatory “seiches” or multidirectional flow (Marjanac, 1990; Tinterri, 2011; Fig. 2.16c). Additionally, where confined flows also experience containment their deposits are typically characterised by greater thicknesses of both sandstone and overlying mud-caps compared with unconfined systems (e.g. ponded mud-caps Ricci Lucchi & Valmori 1980; Pickering & Hiscott, 1985; Haughton 1994).

2.4 Hybrid event beds: Introduction and adopted terminology

Deposits containing co-genetic matrix-poor and matrix-rich sandstone facies, indicative of deposition beneath non-cohesive and relatively more cohesive flow states respectively, have been documented in a suite of deep-water depositional systems (Wood & Smith 1958; McCave & Jones, 1988; Van Vliet, 1978; Ricci Lucchi & Valmori, 1980; Lowe & Guy, 2000; McCaffrey & Kneller, 2001; Haughton et al., 2003, 2009; Talling et al., 2004; Sylvester & Lowe, 2004; Puigdefàbregas et al 2004; Amy & Talling, 2006; Barker et al., 2008; Davis et al., 2009; Hodgson, 2009; Kane & Pontén, 2012; Lee et al., 2013; Talling, 2013; Fonnesu et al., 2015; Patacci et al., 2014; Terlaky & Arnott, 2014). Collectively referred to as hybrid event beds (HEBs) herein, they contain matrix-rich sandstone which: 1) overlies relatively matrix-poor sandstone, as observed in the vertical profile of a single bed; 2) becomes a greater proportion of the bed thickness, compared with matrix-poor sandstone, further along a downstream transect; or 3) both. HEBs are of economic significance as the matrix-rich sandstone, associated with poor-reservoir quality, introduces heterogeneity at an intra-bed scale (Sylvester & Lowe, 2004; Porten et al., submitted), influences the vertical and lateral flow of hydrocarbons within reservoir sandstone (e.g. Amy et al., 2009; Fonnesu et al., 2015) and can indicate the presence of better reservoir quality sandstone (matrix-poor) further upstream (e.g., Haughton et al. 2003, Hodgson, 2009; Kane & Pontén, 2012; Sumner et al., 2012).

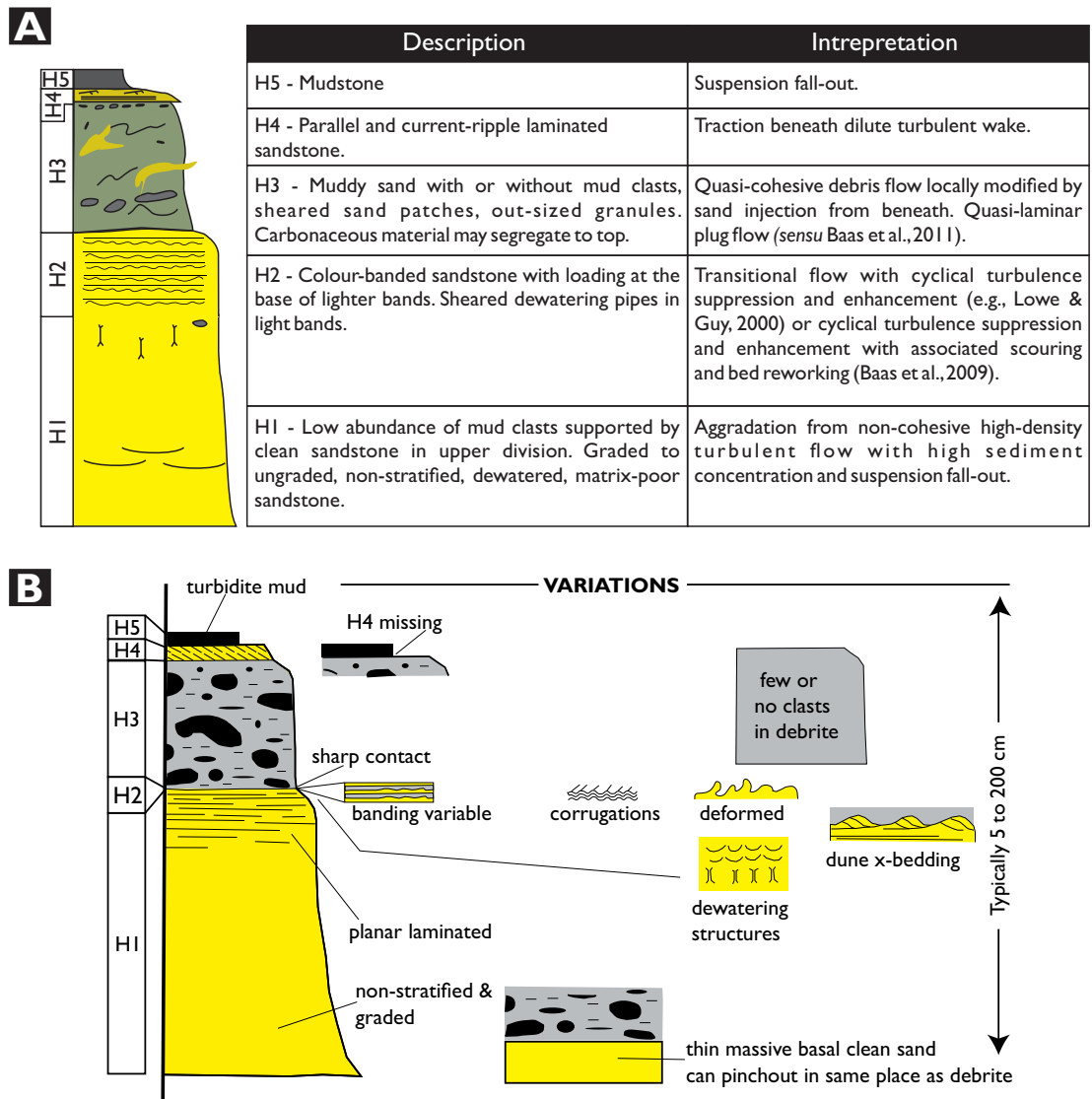


Figure 2.17. **A**) Idealised hybrid event bed (modified from Haughton et al., 2009) with interpretation of hybrid flow (compiled from Haughton et al. (2009) and Baas et al. (2011)). **B**) Examples of variations in HEB depositional character (from Talling, 2013).

HEBs are largely thought to record the downstream transformation of flows which became increasingly more cohesive (clay-rich) and turbulence-suppressed due to clay-enrichment either following the entrainment of muddy substrate and / or flow deceleration and reduction of flow shear stresses (Wood & Smith 1958; McCave & Jones, 1988; Haughton et al., 2003, 2009; Talling et al., 2004; Barker et al., 2008; Baas et al., 2009, 2011; Hodgson, 2009; Sumner et al., 2009; Kane & Pontén, 2012; Talling et al., 2013; Terlaky & Arnott, 2014). Using examples from ancient deep-water systems in the North Sea, Haughton et al. (2003, 2009) demonstrated the co-genetic relationship of matrix-poor and matrix-rich sandstone HEBs and proposed an “idealised” HEB sequence (Fig. 2.17). The authors interpreted the spatio-temporal evolution of flows to become increasingly cohesive and turbulence-suppressed downstream (hybrid flow *sensu lato*, herein), however, particular emphasis was placed on the development of rheological heterogeneity along the length of near-bed flow with a forerunning non-cohesive (clay-poor) flow passing rearwards into a region of increasingly cohesive, turbulence-suppressed flow (hybrid flow *sensu stricto*, herein).

Flow transformation, and the emplacement of HEBs, has also been suggested to result from the vertical redistribution of non-cohesive material within the flow and development of vertical rheological stratification within the flow (e.g., Talling et al., 2007a, Kane & Pontén, 2012) without significant longitudinal heterogeneity in near-bed flow structure. These conceptual models are supported by, or were based upon, observations from experimental, variably clay-rich, turbulence-suppressed “transitional” flow types (Figs 2.18, 2.19; Marr et al., 2001; Mohrig & Marr, 2003; Baas et al., 2009, 2011; Sumner et al., 2009). Experimental studies have demonstrated how co-genetic matrix-poor and matrix-rich sandstone can be deposited in the absence of a region of sandy non-cohesive flow (Sumner et al., 2009; Baas et al., 2011). Experimental studies of clay-rich flows have been valuable in demonstrating the influence of cohesive clay upon flow rheology style and vertical structure, as well as subsequent depositional character (Marr et al., 2001; Mohrig & Marr, 2003; Baas & Best, 2002; Baas et al., 2009, 2011; Sumner et al., 2009). However, the relatively short tanks or recirculating flume tanks used in these experiments means these are limited in terms of their ability to effectively simulate the longitudinal structure, and its behaviour, within clay-rich flows. Further, experimental flows were well mixed before being decelerated, and thus possessed no inherent flow structure, vertical or longitudinal, which might be expected in naturally occurring SGFs (Kuenen & Menard, 1952; Middleton & Southard, 1984; McCaffrey et al., 2003; Choux et al., 2004; Baas et al., 2005). Thus it is unclear how observations from these experiments relate to conceptual models concerning the longitudinal structure of clay-rich flow types (i.e., hybrid flows *sensu stricto*, Haughton et al., 2003, 2009).

In summary, HEBs record the association of fluidal, non-cohesive flow, through various styles of transitional flow, to cohesive, turbulence-suppressed flow during a single SGF event which may be expressed: 1) spatially across the flow (i.e. an instantaneous flow structure, Haughton et al., 2003, 2009); 2) temporally during larger-scale bulk transformation of the flow (Wood & Smith, 1958, McCave & Jones, 1988); or 3) both due to changing proportions of cohesive clay within the flow. The term hybrid event bed is used *sensu lato* herein as it makes no specific reference to a given flow rheology or flow structure and encompasses a wide range of potential flow character (i.e. cohesive or non-cohesive, turbulent or laminar).

2.5 Hybrid event bed depositional character

2.5.1 Vertical bed character

In their simplest form HEBs comprise underlying matrix-poor (i.e. clay-poor) sandstone facies and overlying matrix-richer (clay-rich) sandstone facies within a single event bed; the statistical significance of this arrangement, grain size profile and the absence of intervening hemipelagic mudstone are just a few of the features used to demonstrate that matrix-rich and matrix-poor sandstones were co-genetically deposited during a single SGF event (Haughton et al., 2003,

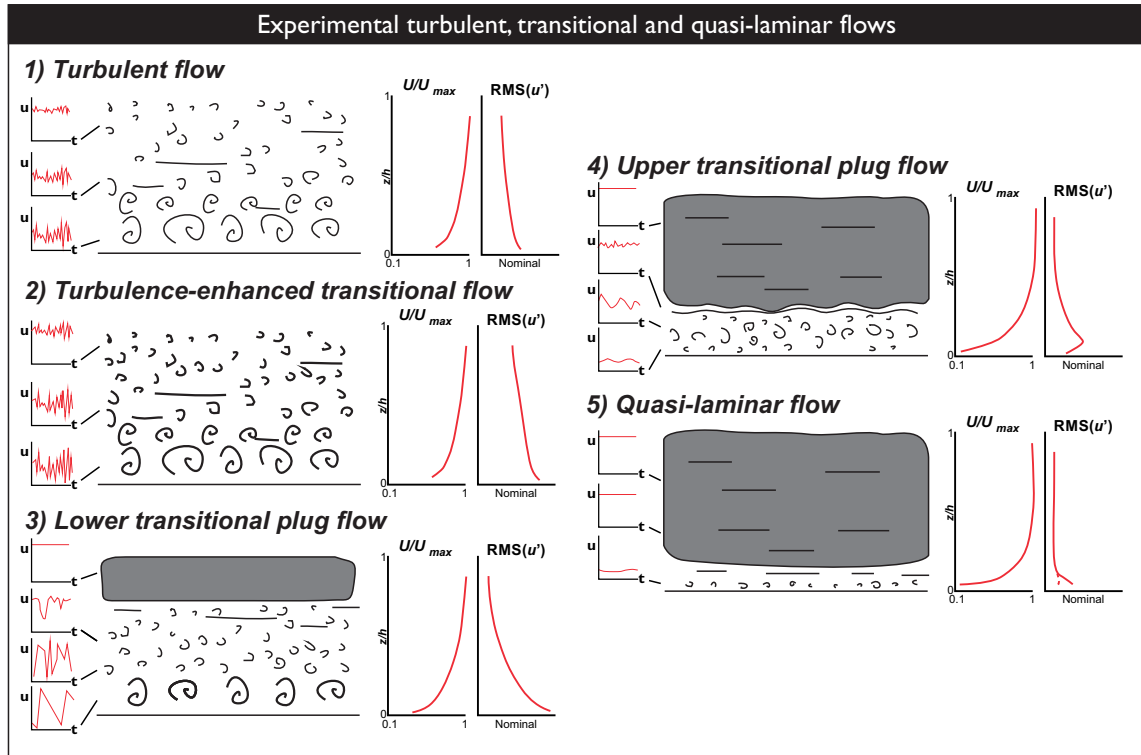


Figure 2.18. Schematic models illustrating documented change in the vertical rheological structure of experimental turbulent, transitional and quasi-laminar flow as clay concentration is increased (1 to 5, respectively). Graphs on the left denote characteristic velocity time series at various heights within the flow. Graphs to the right depict characteristic vertical profiles of dimensionless downstream velocity (U/U_{max}) and root-mean-square of downstream velocity ($RMS(u')$). Modified from Baas et al. (2009).

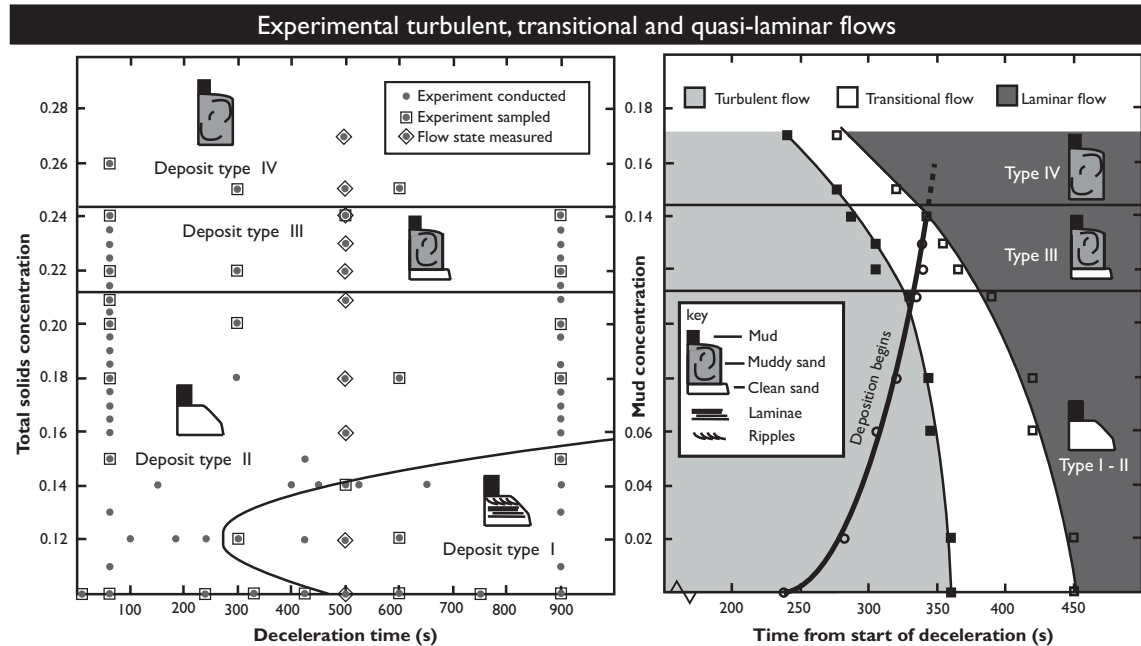


Figure 2.19. A) Graphs showing deposits from flows in which mud content and deceleration rate were varied. Deposit types I and II comprise normally graded sand overlain by a mud cap. Type I has planar lamination and may contain ripples, whereas Type II is non-stratified (structureless). Type III comprises clean sand overlain by ungraded muddy sand and a mud cap. Type IV comprises ungraded muddy sand with a mud cap. **B)** Graph to show how the state of the flow (turbulent, transitional or laminar) varies both with mud content and the time from the start of deceleration. Bold line indicates the onset of sand deposition from flows with different mud contents. Type I to II form when the flow is turbulent (non-cohesive) when sand deposition commenced. Type III deposits form when the flow is transitional at the onset of deposition with matrix-poor (clean) sandstone deposited from sand settling out of clay-rich cohesive flow due to insufficient yield strength in the flow. Type IV deposits form if the flow becomes laminar before deposition. From Sumner et al. (2009).

2009; Talling et al., 2004; Davis et al., 2009).

Whilst acknowledging that variants in HEB character occur, Haughton et al. (2009) proposed an idealised HEB sequence which summarises the key depositional characteristics of HEBs (Fig. 2.17a); variations on this HEB sequence were later summarised by Talling, 2013 (Fig. 2.17b). The matrix-poor, typically unstratified, H1 division of Haughton et al. (2009) has been interpreted to record either deposition from: 1) non-cohesive fluidal flow (Haughton et al., 2003, 2009); or 2) late-stage sand settling from relatively more cohesive flow in which the yield-strength was insufficient to support the entire sand fraction (Talling et al., 2004; Sumner et al., 2009). The banded sandstone H2 division, which can often be absent from HEBs, has been interpreted to record: 1) deposition from near-bed flow which transiently fluctuated between relatively cohesive and non-cohesive states due to changes in the concentration or degree of bonding of cohesive material (Lowe & Guy, 2000; Lowe et al., 2003; Baas et al., 2005; Barker et al., 2008); 2) reworking of the bed by a zone of near-bed turbulence-enhanced flow beneath transitional flow (*sensu* Baas et al., 2009, 2011). The overlying, non-stratified, matrix-rich H3 division, which is variably mud-clast-rich, is interpreted as the depositional product of a relatively more cohesive (clay-rich), turbulence-suppressed flow state (Haughton et al., 2003, 2009, Talling et al., 2004, 2007a, 2012a; Amy & Talling, 2006; Hodgson, 2009). The cohesive flow responsible for the H3 division can be considered in terms of a coherency continuum along which variation in the flow yield strength determined its ability to support coarser sand fractions or mud-clasts, and thus the depositional character of the H3 division (Marr et al., 2001, Mohrig & Marr, 2003, Talling et al., 2007a, 2012a; Baas et al., 2009, 2011; Sumner et al., 2009; Talling et al., 2013). HEBs are variably capped by a thin, stratified (current-ripple or planar laminated) sandstone, which may load into the underlying H3 division, and is interpreted as the product of a relatively dilute, turbulent wake in the rear of the flow event (Haughton et al., 2009; Baas et al., 2011).

2.5.2 Long length-scale facies tracts

Long length-scale (c.1000 – 1000s m) transects of individual HEBs (Amy & Talling, 2006; Fonnesu et al., 2015) and packages of HEB-bearing strata (Haughton et al., 2003, 2009; Barker et al., 2008; Davis et al., 2009; Hodgson, 2009) have documented a number of downstream facies tracts. Typically there is an overall increase in the proportion of matrix-rich sandstone (H3) at the expense of underlying matrix-poor (H1) sandstone distally (Haughton et al., 2003, 2009; Amy & Talling, 2006; Barker et al., 2008; Hodgson, 2009) (Fig. 2.20a). Exceptionally extensive exposure in the Miocene Marnoso Arenacea Formation, NW. Italy, display the downstream terminations of H3 divisions within HEBs (Amy & Talling, 2006; Talling et al., 2012a). Where the H3 division was mud-clast rich the H3 division pinched out rapidly with a dramatic reduction in bed thickness compared to more gradual pinch out and reduction of bed

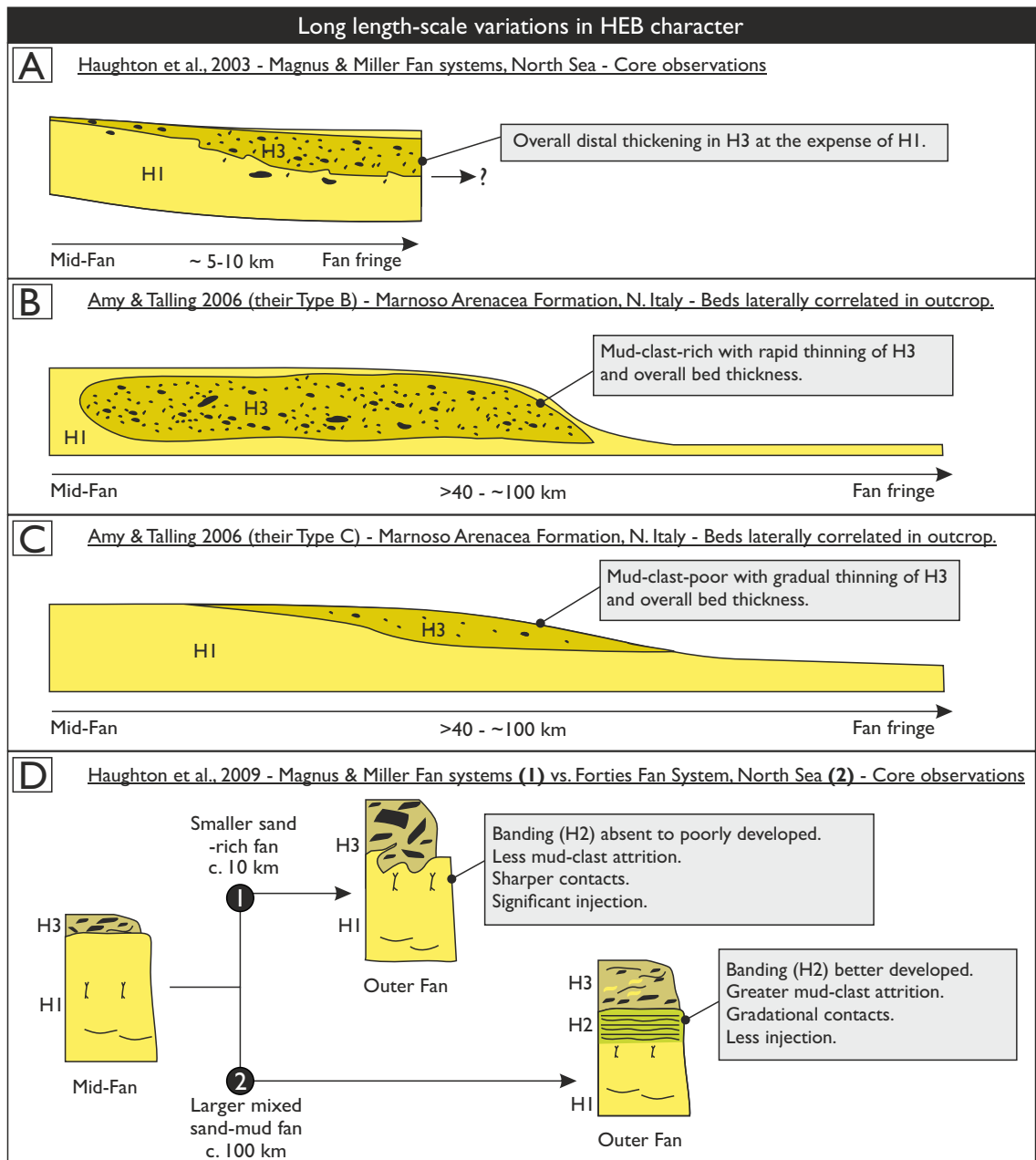


Figure 2.20. Summary of long length-scale variations documented in HEBs. **A)** Modified from Haughton et al., (2003); **B & C)** modified from Amy & Talling, (2006); **D)** modified from Haughton et al. (2009).

thickness where the H3 division was mud-clast poor (e.g. Type 2 and 3, respectively of both Amy & Talling, 2006; Talling et al., 2012a; Fig. 2.20b,c). A higher flow coherency has been suggested as a mechanism capable of generating H3 divisions that abruptly pinch-out and support a greater abundance of mud clasts (Talling et al., 2010, 2013). Both trends in H3 character were observed in a single bed and suggest that spatial variation can also occur in the coherency of flow associated with emplacement of the H3 division (Amy & Talling, 2006; Talling et al., 2012a).

Haughton et al. (2009) documented differences in HEB character between small sandy Jurassic systems and larger mixed sand-mud Palaeocene systems from the North Sea (Fig.

2.20d). In the larger mixed sand-mud systems, HEBs are characterised by a better-developed H2 division, mud clasts that are less abundant, smaller and corroded, a non-founded contact at the H3 basal boundary and gradational facies contacts. Focusing on the scale difference between these systems, Haughton et al. (2009) suggested that these differences arise due to the differing flow run-out distances and thus the degree of lateral flow partitioning and textural fractionation (i.e. rate of change in flow behaviour along the flow length); longer run-out distances result in greater partitioning, more gradational facies contacts and greater disaggregation of mud clasts. However, Haughton et al. (2009) overlooked the potential importance of variation in the sediment composition of flows between these systems. Lee et al. (2013) suggested that variations in initial sediment composition result relatively sandier and muddier HEBs in the same system.

2.5.3 Short length-scale facies tracts

Transects of individual HEBs over relatively short length-scales (10s -100s m), in strike and downstream orientation, reveal significant variation in the H3 division in terms of the proportion of H3 to the underlying H1 division, whereas bed thickness remains near constant (Hodgson, 2009; Fonesu et al., 2015; Southern et al. 2015) as well as the abundance and maximum size of mud clasts within the H3 division (Talling et al., 2012a, 2013). Such variations in H3 character are non-systematic and can be expressed in both downstream and across flow directions (Talling et al., 2012a; Fonesu et al., 2015; Southern et al. 2015).

2.6 Hybrid event bed distribution

Geographically HEBs typically occur in the following settings: 1) the distal and lateral fringes of distributive lobe systems (Haughton et al., 2003, 2009; Talling et al., 2004; Davis et al., 2009; Hodgson, 2009; Kane & Pontén, 2012; 2) adjacent and localised to confining sea-floor topography in confined, uncontained (CU) settings (Barker et al., 2008; Patacci et al., 2014); 3) in the lower parts of channel margin splays (Terlaky & Arnott, 2014); 4) in the upper parts of channel infill / backfill successions (Sylvester & Lowe, 2004; Haughton et al., 2009; Fig. 2.21). Stratigraphically (vertically) HEBs have been documented in the following arrangements: 1) restricted to the base of prograding lobe packages, when observed at a point (i.e., one dimensional core - Kane & Pontén, 2012); 2) restricted to basinward stepping lobe package(s) during fan initiation (progradation) and growth (aggradation) and absent during lobe bodies recording fan retreat (Hodgson, 2009); 3) restricted to turbidite systems during clastic switch-on and early basin infill after which there is no reoccurrence of HEBs (Haughton et al., 2009); 4) persistent throughout the succession and interleaved with traditional turbidite deposits

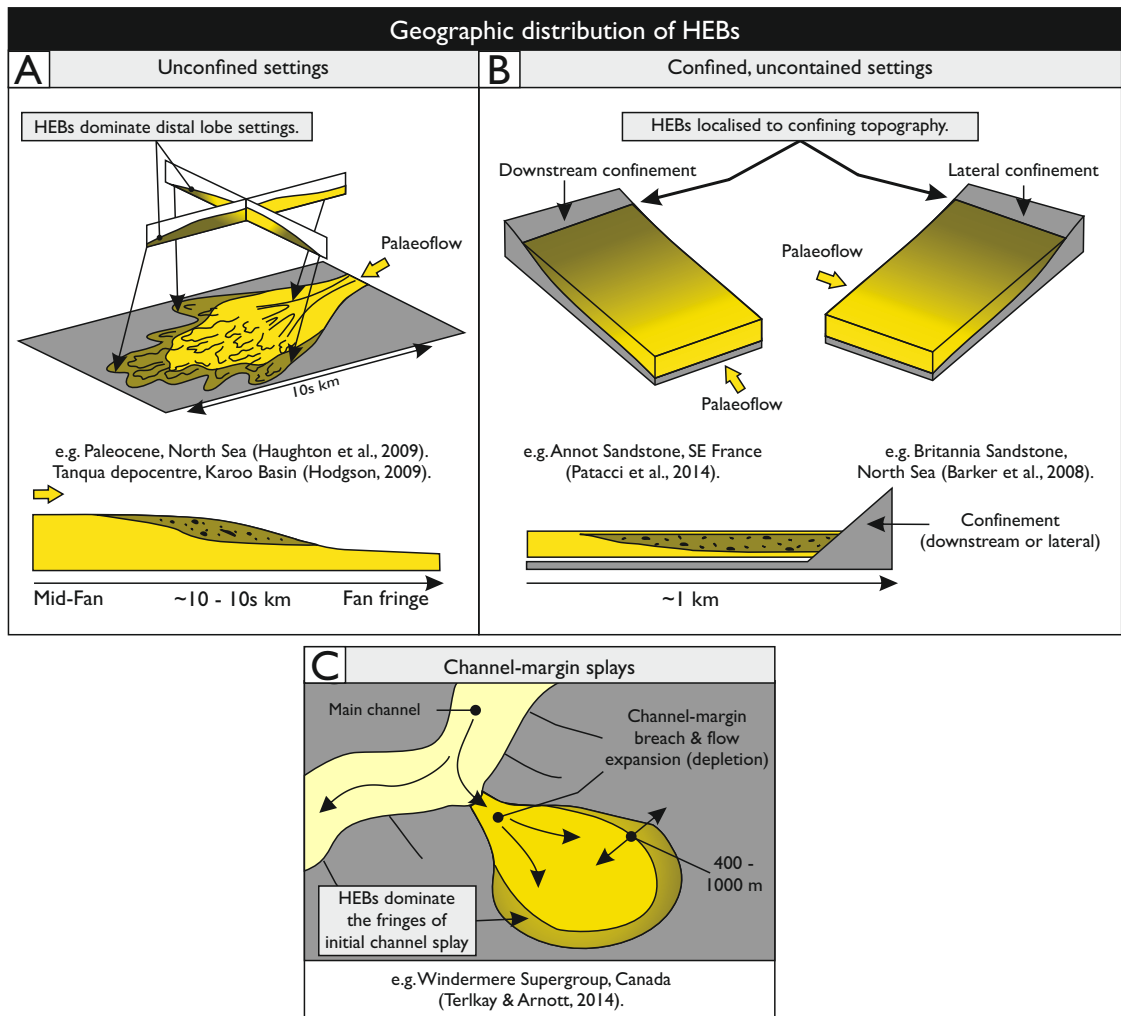


Figure 2.21. Documented geographical distribution of HEBs in deep-water systems.

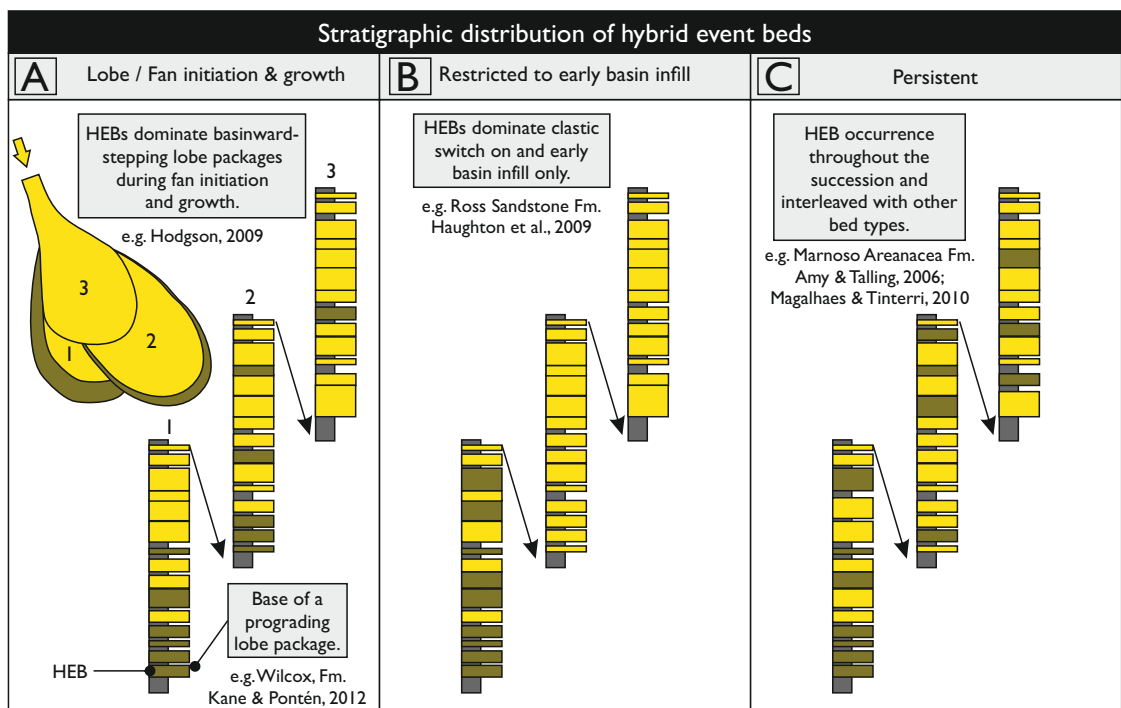


Figure 2.22. Documented stratigraphic distribution of HEBs in deep-water systems.

which are dominant (Amy & Talling, 2006; Magalhaes & Tinterri, 2010) or relatively subordinate (Haughton et al., 2009, their Fig. 13, Type 3; Fig. 2.22).

2.7 Hybrid flow development

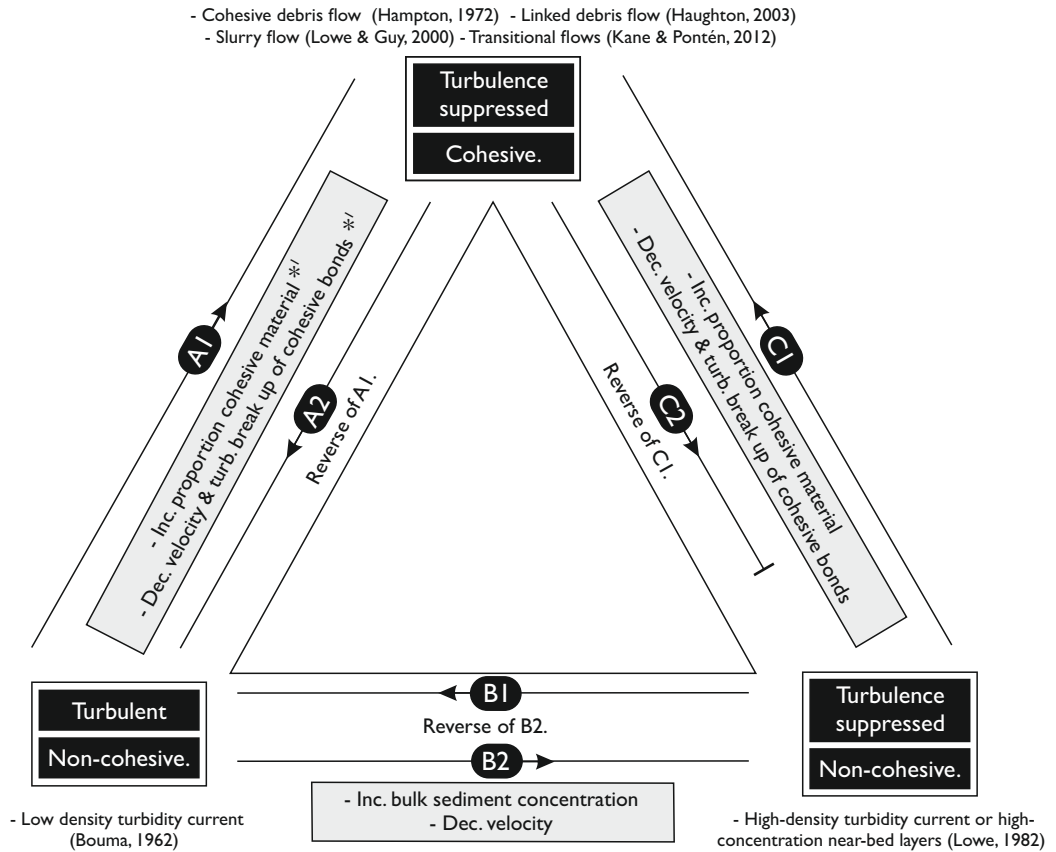
Models for the origin of co-genetic matrix-rich sandstones within HEBs have generally cited the transformation of initial cohesive, non-turbulent flow (partially or wholly) into more turbulent, non-cohesive flow downstream (Talling et al., 2004, 2007a) or transformation (partially or wholly) from non-cohesive to more cohesive flow (Haughton et al., 2003, 2009; Pritchard & Gladstone, 2009; Barker et al., 2008; Davis et al., 2009; Kane & Pontén, 2012). Thus, mechanisms driving modification of turbulent and cohesive flow characteristics are important in the development of hybrid flows (Fig. 2.23).

2.7.1 Turbulence enhancement

Turbulence intensity may be enhanced where flows accelerate (e.g. upon meeting steeper gradients or entering constrictions) (Figs 2.11, 2.23, Example A2), undergo a reduction in sediment concentration (Fig. 2.23, Example B1) or in the early stages of transitional flow development *sensu* Baas et al. (2009; Fig. 2.18). Dilution upon the surface of a cohesive high-concentration flow, due to shearing with the ambient fluid, can locally enhance fluid turbulence (Figs 2.11, 2.23, Example A2; Fisher, 1983; Marr et al., 2001; Mohrig & Marr, 2003). Gravity settling of particles into near-bed flow can reduce sediment concentration in overlying regions of flow to enhance turbulence at the expense of other grain-support mechanisms (e.g. Lowe, 1982; Fisher, 1983; Figs 2.11, 2.23, Example, B1), provided that the residual flow does not become significantly enriched in cohesive material to develop a cohesive strength capable of suppressing fluid turbulence.

2.7.2 Turbulence suppression

Turbulence suppression may occur with an increase in sediment concentration or an increase in the proportion of cohesive material (Fig. 2.18), or a reduction of flow velocity (Fig. 2.19). Suppression of turbulence with little change in cohesive strength can occur where clay-poor gravity currents undergo a deceleration (Kneller, 1995; Kneller & Branney, 1995) and in regions of the flow where settling of particles raises the concentration of near-bed flow (Fisher, 1983, Lowe, 1982, 1988; Fig. 2.23, Example B2). Gelation (bonding) of cohesive material within the flow, and thus the development of a flow yield strength, can suppress turbulence (Fig. 2.23, Example A1-2, C1-2). Development of a cohesive strength and turbulence-suppression within a flow can result from relatively small increases in the proportion of cohesive material within the flow (Marr et al., 2001; Baas & Best, 2002, Baas et al., 2009, 2011; Sumner et al., 2009). Variations in the proportion of cohesive material present



Modification:	Triggers of turbulence or cohesive strength modification:
<p>A1</p> <p>Turb. non-cohesive ↓ Turb. suppressed, cohesive</p>	<ul style="list-style-type: none"> Flow depletion driving deposition and / or reduction in turbulence (e.g. Talling et al., 2007; Barker et al., 2008; Sumner et al., 2009; Baas et al., 2011; Kane & Pontén, 2012). Hydraulic fractionation enriches mud in hindward regions of the flow (e.g. longitudinal segregation of Haughton et al., 2003, 2009). Entrainment of mud-clasts and their disaggregation to release mud (e.g. Haughton et al., 2003, 2009). <p>*1 The initial onset of cohesive bonding can be characterised by enhanced turbulence as cohesive bonds repeatedly form and then break due to fluid turbulence (cf. Baas et al., 2009, 2011).</p>
<p>A2</p> <p>Turb. suppressed cohesive ↓ Turb. non-cohesive</p>	<ul style="list-style-type: none"> Flow dilution driven by mixing with the ambient fluid on the flow's surface boundary (e.g. surface transformations of Fisher, 1983; Marr et al. 2001). Acceleration and increase in internal flow turbulence (e.g. body transformation of Fisher, 1983).
<p>B1</p> <p>Turb. suppressed non-cohesive ↓ Turb. non-cohesive</p>	<ul style="list-style-type: none"> Acceleration and increase in internal flow turbulence (e.g. reverse body transformation of Fisher, 1983). Dilution of the bulk flow via mixing with ambient fluid or sediment deposition (e.g. Lowe, 1988).
<p>B2</p> <p>Turb. non-cohesive ↓ Turb. suppressed non-cohesive</p>	<ul style="list-style-type: none"> Development of a high concentration near-bed flow layer (e.g. gravity transformation of Fisher, 1983).
<p>C1</p> <p>Turb. suppressed non-cohesive ↓ Turb. suppressed cohesive</p>	<ul style="list-style-type: none"> Entrainment of mud or mud-clasts into a high-concentration sandy flow with weak or no turbulence.
<p>C2</p> <p>Turb. suppressed cohesive ↓ Turb. suppressed less cohesive</p>	<ul style="list-style-type: none"> Dilution (driven by mixing with the ambient fluid) to become a lower coherency (less cohesive / lower yield strength) debris flow but not to the point where fluid turbulence exceeds cohesive strength (Marr et al., 2001).

Figure 2.23. Schematic diagram illustrating the range of processes which can trigger modification of turbulence and cohesive strength within a sediment gravity flow. Modifications in flow character are expected to occur in discrete regions of the flow (i.e., lower vs. upper flow, head vs. tail) as sediment gravity flows are characterised by inherently complex structure in terms of velocity, grain size and sediment concentrations.

within a flow can occur due to; 1) variations present in the original flow (Lee et al., 2013); 2) entrainment of cohesive substrate into the flow (Haughton et al., 2003, 2009); 3) redistribution and concentration of cohesive material in certain regions of the flow (Haughton et al., 2003, 2009); or 4) relative enrichment of cohesive material following deposition of non-cohesive particles (McCave & Jones, 1988; Talling et al., 2004; Barker et al., 2008; Sumner et al., 2009). Thus, flow transformation via cohesive-driven turbulence-suppression, and development of hybrid flow, is most likely to occur where proportions of cohesive material are higher and where shear rates are lower (Fig. 2.23), specifically in:

- 1) near-bed flow regions where mud enrichment occurs following entrainment and disaggregation of muddy substrate (e.g. Haughton et al., 2003);
- 2) upper, hind-ward or marginal regions of flow where lower velocity and shear promotes both preferential support (enrichment) of mud fractions due to their lower-settling velocities and a lower turbulence intensity (e.g. Baas et al., 2011);
- 3) flow events with an initial higher proportion of cohesive material compared to other flow events with lower proportions of cohesive material (Baas et al., 2008; Fig. 2.18);
- 4) Where flow depletion triggers a reduction in shear and the proportion of cohesive material present in the flow is sufficient for turbulence suppression to occur (Sumner et al., 2009; Fig. 2.19).

2.8 Styles of flow transformation associated with hybrid event bed development

This section outlines a number of flow-transformation mechanisms proposed to account for the range of HEB deposits based on studies of ancient and modern systems, as well as insights gained from experimental work. Such mechanisms involve transformation from an initial flow, which was either relatively cohesive and non-turbulent or non-cohesive and turbulent.

2.8.1 Transformation of an initial relatively cohesive non-turbulent flow

2.8.1.1 Flow dilution

Partial transformation of an original cohesive debris flow into an increasingly less cohesive turbulent flow has been suggested as a potential mechanism for HEB development (Haughton et al., 2003, Talling et al., 2004, 2007a; Fig. 2.24). Transformation is suggested to initiate on the upper and frontal surface of the flow due to dilution following shearing and mixing with the ambient fluid (Fig. 2.11c). The dilution generates a relatively dilute turbulent suspension which could out-run the parental debris flow and deposit sand from a turbulent flow prior to arrival of the debris flow and deposition of matrix-rich sandstone under a relatively cohesive turbulence suppressed flow. Marr et al., (2001) demonstrate how such a process is more signi-

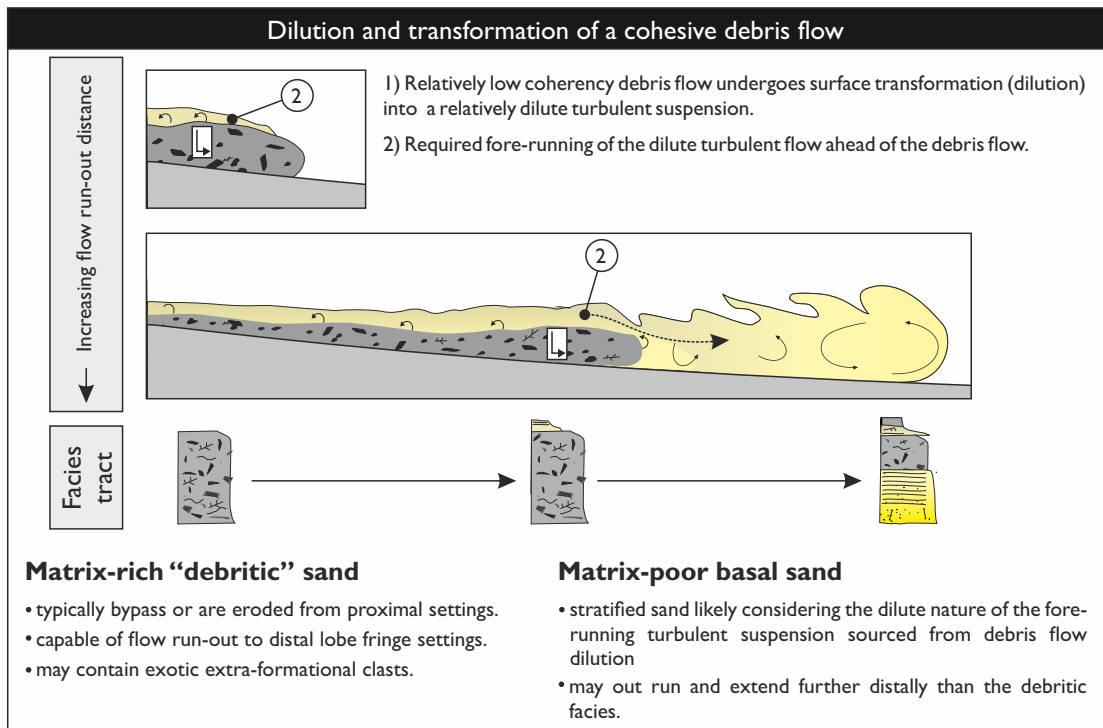


Figure 2.24. Emplacement of co-genetic matrix-rich and matrix-poor sandstone due to partial dilution of an initial cohesive debris flow into relatively dilute turbulent flow. Modified from Talling et al. (2004).

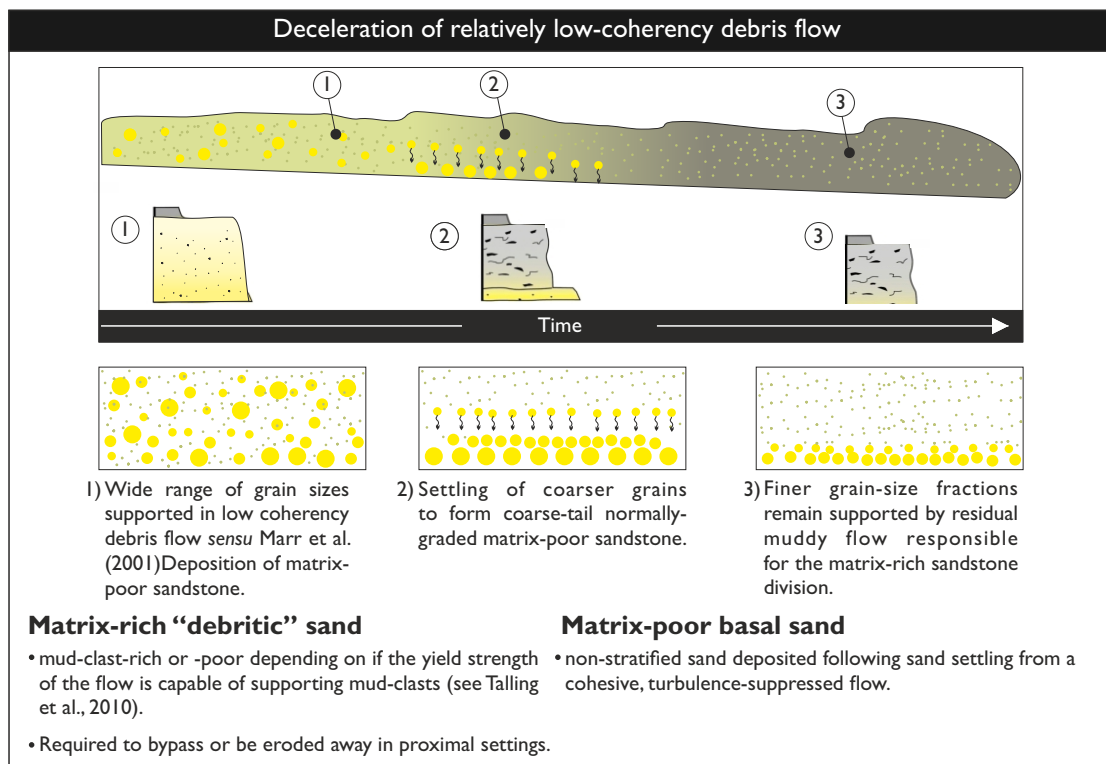


Figure 2.25. Emplacement of co-genetic matrix-rich and matrix-poor sandstone due to deceleration and sand settling from clay-rich flow. Modified from Talling et al. (2004).

ficant where the coherency (yield strength) of the debris flow is relatively low and thus its resistance to surface shearing and dilution is reduced (Fig. 2.5). Field examples of a debrite directly underlain by turbidite sandstone have been interpreted to record such surface dilution of debris flows sourced from local upstream slumps (Stanley, 1982; Strachan, 2008).

2.8.1.2 Deceleration of a lower coherency debris flow

Deceleration of a relatively lower coherency debris flow has been suggested as mechanism to promote HEB deposition (Talling et al., 2004; Sumner et al., 2009) (Fig. 2.25). Upon deceleration, a coarser portion of the sand fraction is no longer supported, resulting in emplacement of the matrix-poor sandstone, whilst the residual flow becomes relatively enriched in cohesive material capable of supporting finer sand fractions and deposits the overlying matrix-rich sandstone facies in a HEB. Such late-stage sand settling would be incapable of producing stratification in the basal matrix-poor sandstone (Marr et al., 2001; Sumner et al., 2009) and thus offers constraint to the applicability of this mechanism in HEB development. Both this and the previous mechanism require that debris flow typically bypass proximal settings unrecorded and travel over relatively shallow gradients. Talling (2013) suggested a relatively lower yield strength could promote such run-out; however it is unclear why relatively more plastic flow would repeatedly achieve comparable or greater run-out distances than that of turbulent flow.

2.8.2 Transformation of an initial relatively non-cohesive turbulent flow

An enrichment of cohesive material (detrital clay) in turbidity currents is thought to c

Non-cohesive flows can become increasingly cohesive and turbulence suppressed during their run-out downstream where there is a sufficient enrichment of cohesive material (i.e. detrital clay) within the flow (Fig. 2.23, Example A1, C1). The following sections outline various mechanisms that can trigger the transformation from non-cohesive to more cohesive flow and the eventual deposition of matrix-rich sandstone facies associated with HEBs.

2.8.2.1 Entrainment of muddy substrate

Haughton et al. (2003, 2009) suggested the entrainment of muddy substrate plays a role in turbulence suppression and establishment of cohesive strength within turbulent flows (Fig. 2.26). Initially, the mud clasts entrained into the flow may locally suppress turbulence in near-bed flow. The progressive disaggregation of mud clasts releases disseminated clay particles into the flow and increases the surface area, thus potential electrostatic bonding of cohesive material. Such material may be hydraulically fractionated into the rear of the flow and eventually lead to the development of relatively cohesive, laminar flow here (Haughton et al., 2003, 2009). The resultant longitudinal flow structure with turbulent frontal flow and increase-

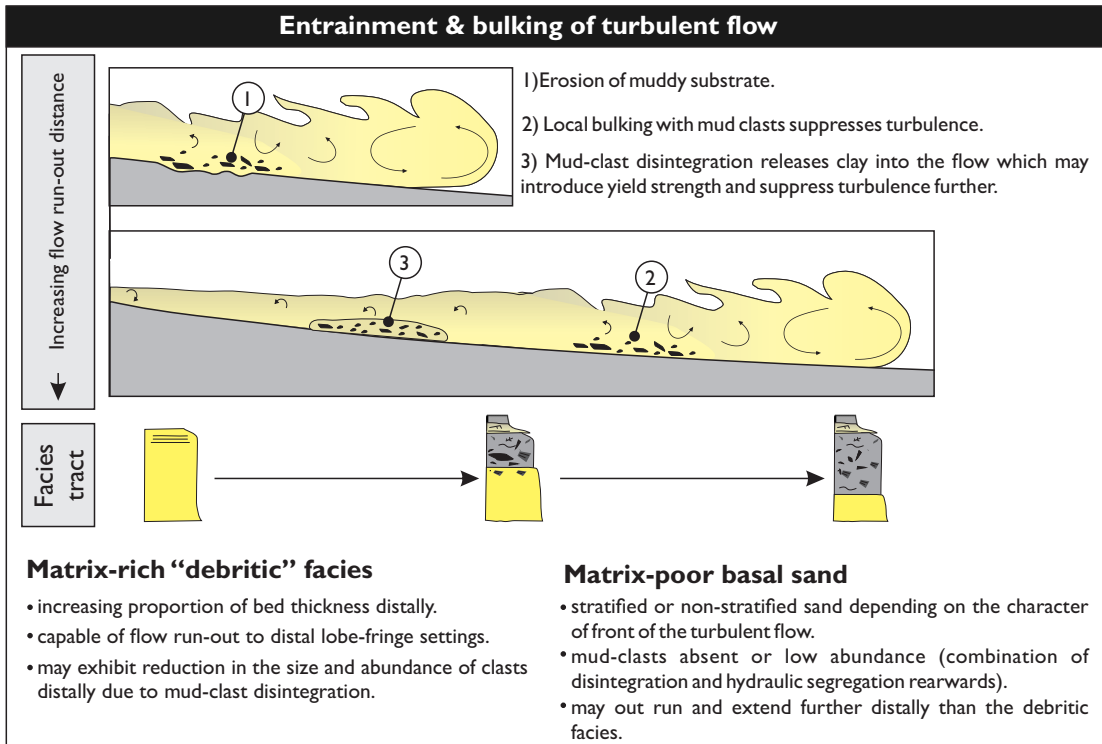


Figure 2.26. Emplacement of co-genetic matrix-rich and matrix-poor sandstone due to entrainment of muddy substrate. Mud clasts locally bulk the flow and modify the flow by suppressing turbulence. Disintegration of mud clasts during transport can release disseminated clay into the flow for further suppression of turbulence. Modified from Haughton et al., (2003).

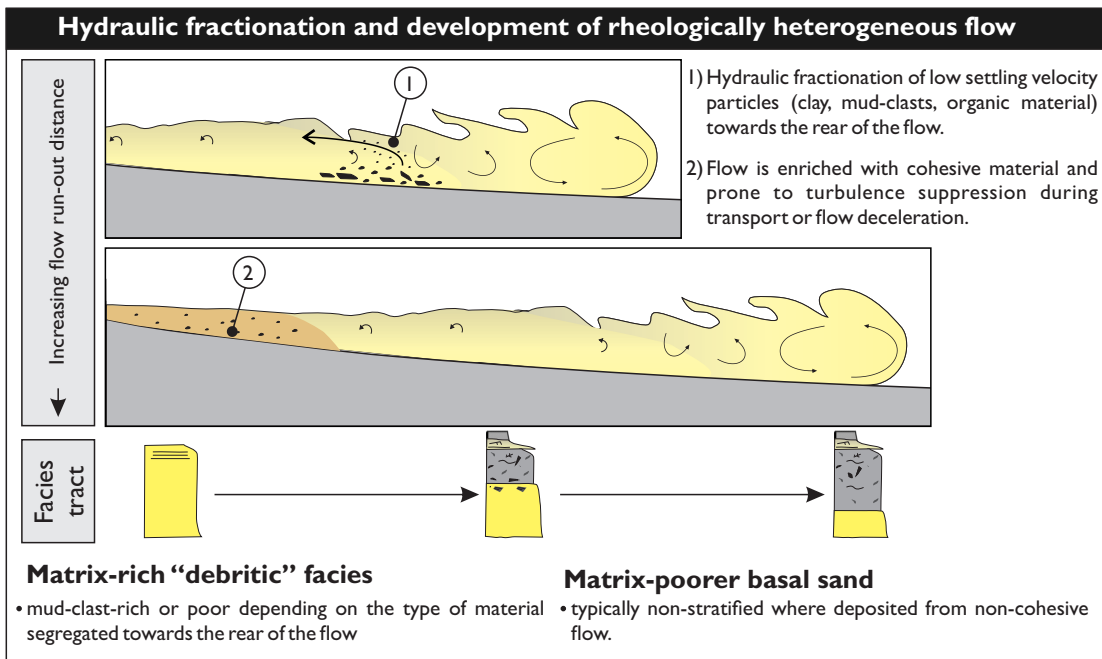


Figure 2.27. Emplacement of co-genetic matrix-rich and matrix-poor sandstone due to hydraulic fractionation (redistribution) of low-settling velocity particles (e.g. mud & silt, mud clasts and carbonaceous fragments) towards the rear of the flow. This process may result in pronounced longitudinal rheological heterogeneity across the flow with the rear of the flow becoming clay-enriched and cohesive whilst the front of the flow remains relatively clay-poor and non-cohesive (i.e. hybrid flow *sensu* Haughton et al., 2009). Clay-enrichment in the rear of the flow may be enhanced and prolonged by the release of mud during the disintegration of entrained mud-clasts (Haughton et al., 2009).

ngly mud- and mud-clast-rich laminar-like flow towards the rear can explain the emplacement of matrix-poor and overlying relatively more matrix- and mud-clast-rich sandstone in the HEB.

Significant volumes of muddy substrate may be entrained along above-grade flow paths (*sensu* Kneller, 2003) which are prone to incision (e.g. tectonically active or recently active feeder slopes and above intra-basinal bathymetry, Haughton et al., 2003, 2009; due to fan topography, Amy & Talling, 2006; Fonnesu et al., 2015) or following periods of high stand and reduced clastic supply to deep-water settings (Hodgson, 2009). Entrainment of muddy substrate on the basin floor is often apparently less voluminous compared to that present within HEBs. However, shallow entrainment can be relatively extensive and cryptic beneath SGFs (Eggenhuisen et al., 2011; Fonnesu et al., 2015). This interpreted mechanism is commonly favoured where HEBs dominate at particular levels within the stratigraphic succession which are considered to record periods of lobe or fan initiation and growth (Haughton et al., 2003, 2009; Davis et al., 2009; Hodgson, 2009), or during switch-on of clastic infill in basins with above-grade feeder slopes of intra-basinal bathymetry (Haughton et al., 2003, 2009). Thus, HEBs may also be prevalent during upstream channel entrainment and knick-point migration (Haughton et al., 2003, Sylvester & Lowe, 2004). The basal matrix-poor sandstone should exhibit evidence of deposition from a non-cohesive fluidal flow. Matrix-rich sandstone deposited in this manner should contain mud clasts from the slope or basin floor, however rare exotic clasts may still be present.

2.8.2.2 Hydraulic (longitudinal) segregation

Haughton et al. (2003, 2009) suggested that the action of vertical gradients in horizontal (downstream) velocity upon the vertical grain size distribution within the flow may be crucial (Fig. 2.27). Flow velocity declines with increasing height above the downstream velocity maximum and thus preferentially supports, and is enriched in, lower-settling velocity particles (e.g. finer particles, such as cohesive muds, less dense particles, such as organic fragments and platy particles – mica grains or platy mud clasts). This slower travelling region of flow may redistribute and enrich clay in the rear of flow, and be replenished by elutriation from underlying higher concentration flow which is non-cohesive (mud-poor) and variably turbulent (e.g. high or low density turbulent flow). Such processes would establish flows with discrete, longitudinally rheological zones which become increasingly cohesive and turbulence-suppressed towards the rear of the flow.

2.8.2.3 Flow deceleration

Experiments have demonstrated how the deceleration of variably clay-rich flows results in reduced shear stress and promotes bonding of cohesive material which may suppress fluid turbulence further (Baas et al., 2009, 2011; Sumner et al., 2009) (Fig. 2.28). These experiments

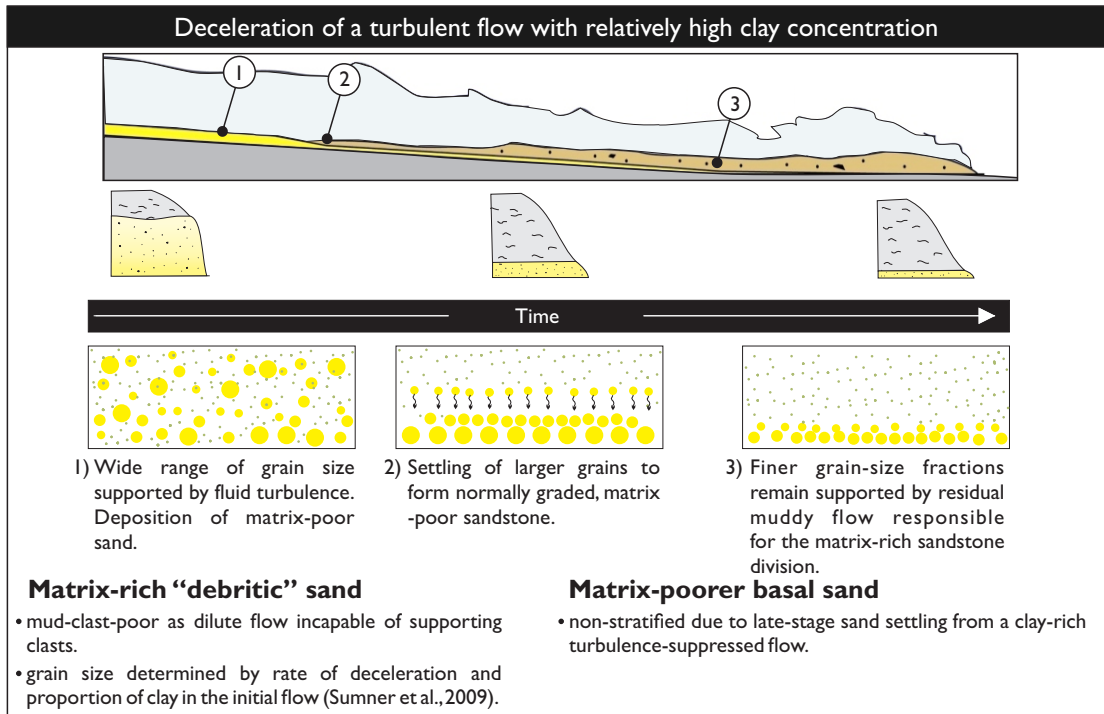


Figure 2.28. Deposition of co-genetic matrix-rich and matrix-poor sandstone due to deceleration of turbulent flow. Rapid deceleration (i.e. flow depletion *sensu* Kneller 1995) results in loss of coarse sand fractions to the bed with residual flow becoming clay-enriched and turbulence suppressed. Such flow can be capable of supporting the remaining sand fraction and eventually deposit matrix-rich sandstone (Baas et al., 2009; Sumner et al., 2009). Modified from Talling et al. (2004).

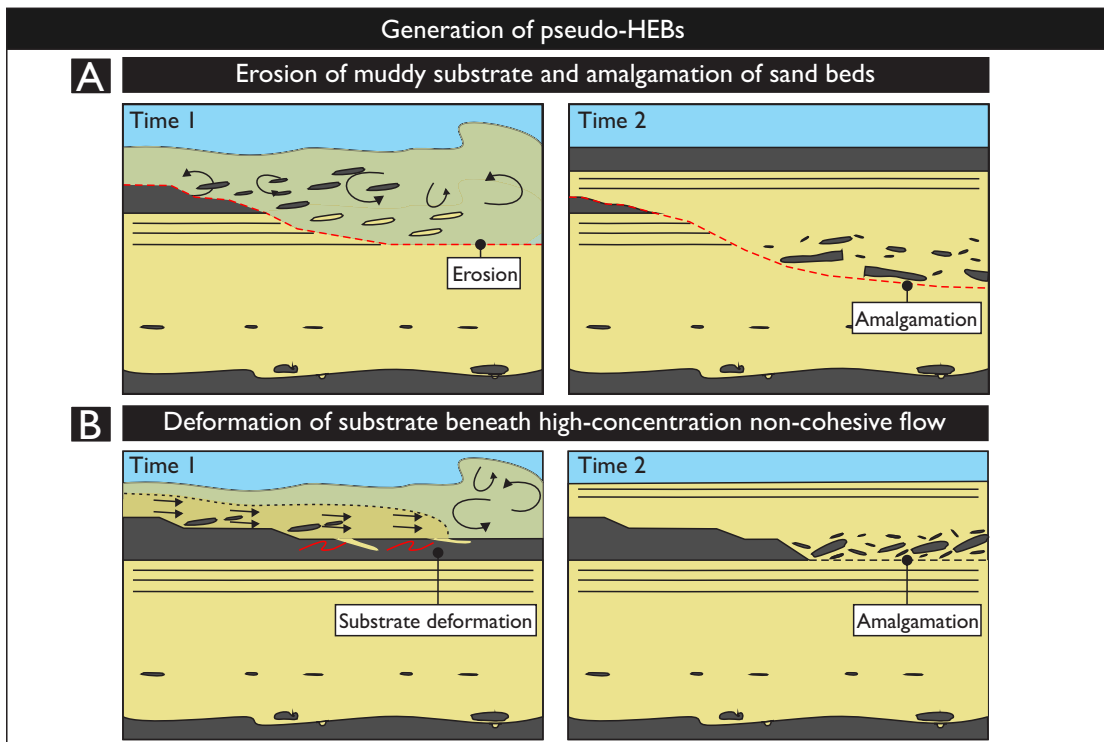


Figure 2.29. Processes that can result in deposits with a pseudo-HEB depositional character (i.e. sand encasing a mud-clast-rich layer) in which constituent facies were not deposited together from a single flow event as occurring in HEBs. Based on the ideas of Walker (1966) and Butler and Tavarnelli (2004), (A & B, respectively).

demonstrated that where the initial proportion of cohesive material was higher or the flow was subject to a faster rate of deceleration, much of the sand fraction was retained within the flow at the time of cohesive bonding and thus emplaced a deposit with a matrix-rich sandstone comparable to that in HEBs (Fig. 2.19). Gradually decelerated flows or flows with lower proportions of cohesive material deposit the majority of their sand fraction prior to gelation and emplace matrix-poor stratified sandstone more comparable to classical turbidites (Sumner et al., 2009). Flow transformations following spatial flow deceleration (flow depletion *sensu* Kneller and Branney 1995) have been invoked to account for the distribution of HEBs in topographically complex settings (Barker et al., 2008; Davis et al., 2009; Patacci et al., 2014, see below), at reductions in sea-floor gradient (Talling et al., 2007a) and where flows exit the channel mouth (Kane & Pontén, 2012) or breach lateral channel confinement in the form of splays (Terlaky & Arnott, 2014).

When driven by deceleration, flow transformation will initiate where shear stresses are lower and proportions of cohesive material are higher such as in the upper, rearward or margin parts of flows (Baas et al., 2011). Thus this trigger of flow transformation will be more likely in flows which are enriched with cohesive material compared to those depositing turbidites. Further, cohesive-driven turbulence suppression may be promoted where flows are rapidly decelerated (e.g. base of slope, expansion at the channel mouth, forced deceleration at a confining slope) such that a greater proportion of the sand fraction remains in the flow in order to deposit matrix-rich sandstone facies (i.e. Sumner et al., 2009).

2.9 Mechanisms emplacing pseudo-HEB deposits

2.9.1 Liquefaction

Post-depositional liquefaction of a sandstone bed may promote foundering of overlying mudstone into the bed (e.g. Higgs, 2010). However, in many HEBs the mud clasts within the H3 division are distinct compared to the overlying mudstone (Haughton et al., 2003, 2009; Amy & Talling, 2006; Hodgson, 2009) and do not show reduction in their contortion upwards or partial attachment to overlying strata (Haughton et al., 2003, 2010; Talling et al., 2004). Total HEB thickness is commonly near-constant over long distances (Amy & Talling, 2006), which would not be the case if these were the result of post-depositional liquefaction and mudstone foundering from above. Although commonly loaded at their bases, capping stratified sandstone beds (H4) are typically laterally persistent above many large mud clasts within the H3 division (Talling et al., 2012a; Fongnesu et al., 2015) suggesting they were not pierced by foundering mud clasts. Furthermore, this mechanism does not account for matrix-rich sandstone recording turbulence-suppressed flow (e.g. banded sandstone, H2) nor where the contact between relatively matrix-poor and matrix-rich sandstone is sharp.

2.9.2 Modification by succeeding flow events

Sandstone deposits with a sandwiched mud-clast-rich division can be produced following the interaction of a gravity current with underlying strata, either following erosion of muddy substrate and sandstone bed amalgamation (Walker, 1966a) or via shear deformation of underlying muddy substrate with partial sandstone bed amalgamation (Butler & Tavarnelli, 2006; Fig. 2.29). Neither of these mechanisms are considered plausible ways to produce HEBs where lateral tracing demonstrates that the bed does not part into separate sandstone beds separated by an intact mudstone (Amy & Talling, 2006). Mud-clast-rich sandstone intervals are commonly overlain by thin, stratified and relatively fine-grained sandstone recording deposition beneath relatively dilute turbulent flow which is unlikely to have been capable of such extensive erosion or modification of mudstone substrate.

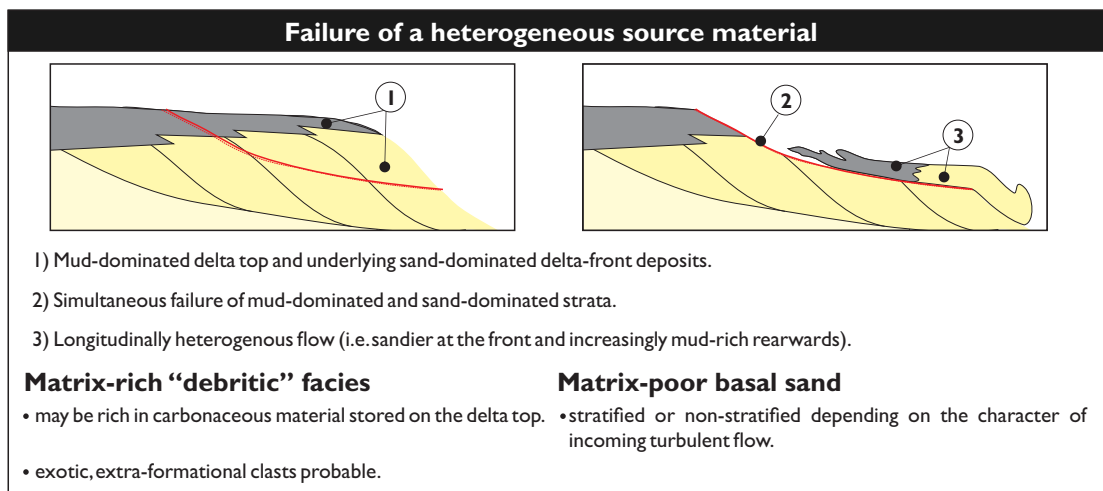


Figure 2.30. Deposition of co-genetic matrix-rich and matrix-poor sandstone due to failure of a heterogeneous source in which the sand-rich (non-cohesive) component consistently out-runs the mud-rich (cohesive) component of flow. Modified from Haughton et al. (2003).

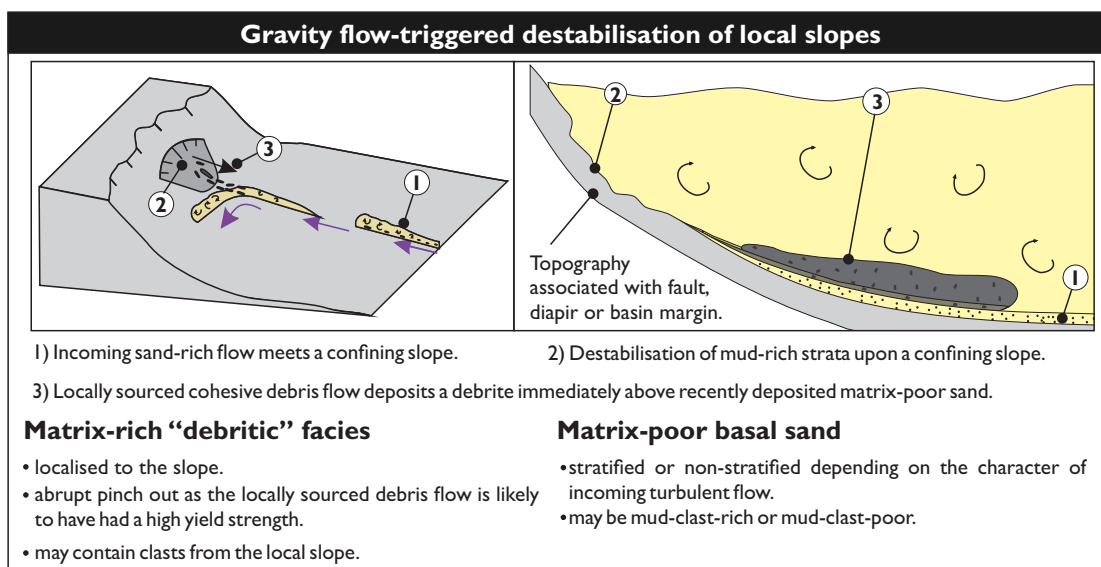


Figure 2.31. Deposition of co-genetic matrix-rich and matrix-poor sandstone due to gravity flow-triggered destabilisation of local confining slopes. Modified from McCaffrey & Kneller (2001).

2.9.3 Failure of a heterogeneous source area

Haughton et al. (2003) suggested that failure of a heterogeneous source (e.g. simultaneous failure of muddy delta top and sandy delta front strata) could potentially establish heterogeneity in the resultant SGF (Fig. 2.30). However they noted the fortuitous requirement for the sand-rich flow to repeatedly out run the mud-rich flow each time.

2.9.4 Intra-bed flow processes

Experimental studies have demonstrated how non-cohesive gravity flows can enter, and remain intact, within soft muddy substrates where bed shear stresses and flow density exceed the cohesive strength and density of the entered muddy substrate (Verhagen et al., 2013; Baas et al., 2014). The experimental deposits comprised sandstone encasing a mud-rich layer, such as that observed in HEBs, with significant loading along the base of the lower sand (Baas et al., 2014). This process is distinct from that associated with hybrid flows (*sensu lato*) as the mud-rich layer did not result from a cohesive flow state present within the sandier current entering the substrate. Instead the mud-rich layer passed across the front of the flow (Baas et al., 2014). It is currently uncertain how laterally extensive intra-bed flow deposits would be in the natural world and identification of the point of flow entry into the substrate would aid determination between intra-bed flow deposits and HEBs from flows with spatially or temporally heterogeneous rheology.

2.9.5 Gravity flow triggered destabilisation of local slopes

Gravity current-triggered destabilisation of muddy slopes on local sea-floor topography has been suggested to trigger synchronous linked debris flows which might result in the emplacement of matrix-poor sandstone overlain by matrix- mud-clast-rich sandstone within the same bed (Fig. 2.31; McCaffrey & Kneller, 2001). Such matrix- or mud-clast-rich sandstone would be expected to be localised to the slope with the bed becoming dominated by matrix-poor sandstone further away from the confining slope (McCaffrey & Kneller, 2001). Considering the local origin, the material in the triggered failure is expected to have been a relatively high yield strength (cohesive) flow and deposit a matrix- mud-clast-rich interval exhibiting limited disaggregation (e.g. large blocks or rafts with folding or shearing fabrics) near the confining slope. Such deposits, associated with a high yield-strength flow, may be expected to pinch out abruptly away from the slope or exhibit abrupt pinch out laterally as slumps and debrites often exhibit an irregular frond like geometry (Nelson et al., 1992; Twichell et al., 1995; Schwab et al., 1996). The presence of failure scars on the local confining slope, as well as isolated debrites, slumps or slides would indicate the instability of the slope (e.g. Puigdefàbregas et al., 2004).

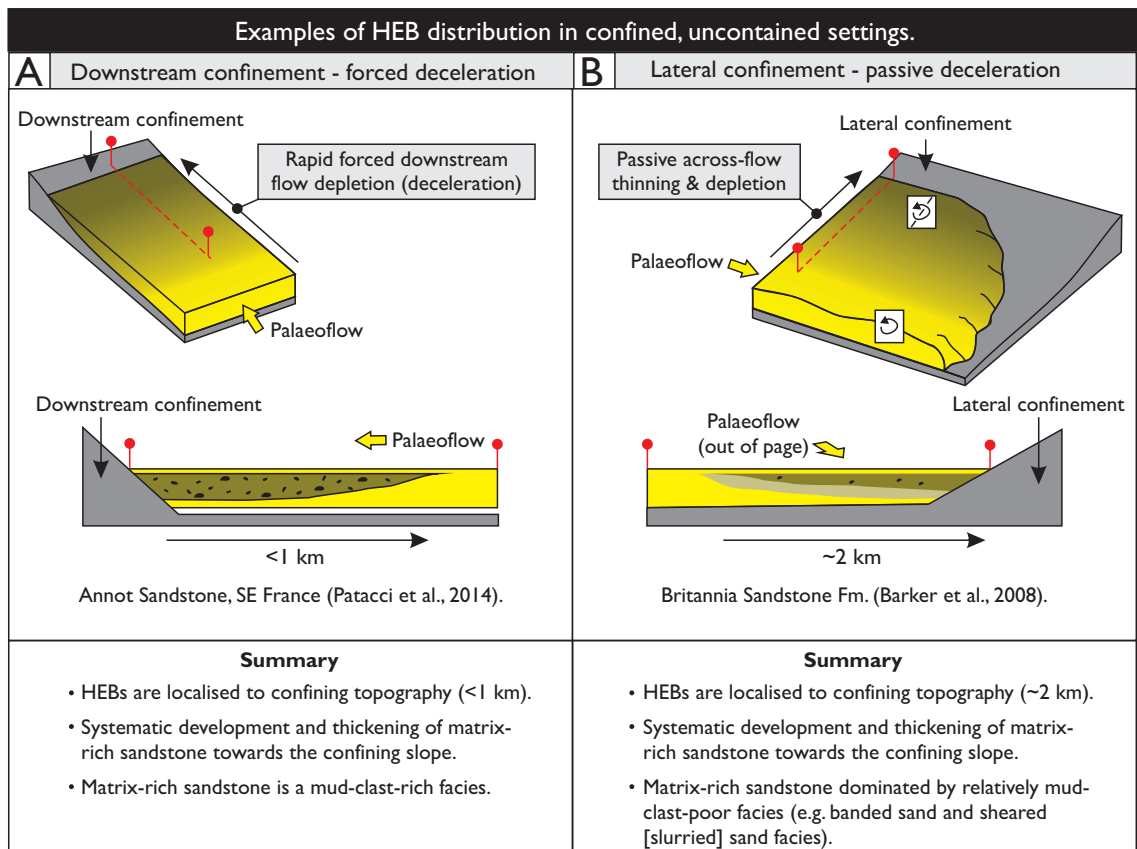


Figure 2.32. Summary of HEB depositional character and distribution in relation to downstream (A) and laterally (B) confining slopes as described by Patacci et al. (2014) and Barker et al. (2008), respectively.

This mechanism cannot account for HEBs developed in settings which lack confining sea-floor topography (Amy & Talling, 2006; Hodgson, 2009; Lee et al., 2013; Fonnesu et al., 2015). In the Eocene-aged Annot Sandstone, Braux, SE France, Patacci et al. (2014) noted significant lateral variability in the mud-clast-rich division (from mud-clast-breccia to well-mixed matrix-rich sand), which is not easily explained by local, short travelled failures which should exhibit similar degrees of disaggregation and mixing. Patacci et al. (2014) also proposed gravity current-triggered failures can be discounted where mud clasts are compositionally distinct to the confining slope and or mud-clast-rich divisions contain carbonaceous material which indicates sourcing along the flow pathway rather than failure of a confining slope distant from the shelf edge. These criteria may break down where the confining slope contains or is overlapped by similar deep-water strata which are subject to failure.

2.10 Hybrid event beds and sea-floor topography

Research characterising the lateral and stratigraphic distribution of depositional facies in topographically complex settings (e.g. Pickering & Hiscott, 1985; Haughton, 1994; Alexander & Morris 1994; Winker, 1996; Prather et al., 1998; Hurst et al., 2000; Satur et al., 2000; Sinclair, 2000; Sinclair & Tomasso, 2002; Felletti, 2002, 2004a; Amy et al., 2004; Brunt et al., 2004; Vinnels et al., 2010) has significantly advanced our understanding of systems in such settings by building upon early depositional models developed in relatively topographically simple settings

where SGF confinement and containment did not occur (e.g. Walker, 1978; Mutti & Normark, 1987; Richard & Bowman, 1998). However these studies focused upon traditional deposit types (e.g. high- and low-density turbidites) with no focus given to HEB character and distribution in topographically complex settings where multiple factors (e.g. topographic complexity promoting flow depletion or entrainment) seem to be favourable to their development.

Studies have begun to focus on the character and distribution of HEB in topographically complex settings (Barker et al., 2008; Davis et al., 2009; Tinterri & Magalhaes, 2011; Patacci et al., 2014). Davis et al. (2009) described the distribution of HEBs in the Paleocene Forties Fan (North Sea) and documented a downstream change from successions dominated by matrix-poor beds (e.g. high-density and low-density turbidites) to those dominated by matrix-rich beds (e.g. HEBs) when passing from areas between diapiric related sea-floor topography to regions of relatively simpler sea-floor topography. They suggested this can arise due to flow non-uniformity effects associated with a change from constriction (accumulative flow), with turbulence enhancement, to expansion (depletive flow) and turbulence suppression.

Two studies have documented the occurrence of HEBs as localised to confining topography, with systematic variation in their depositional character with increasing proximity to their onlap onto the confining slope of the topography (Fig. 2.32; Barker et al., 2008; Patacci et al., 2014); such trends might be used to infer proximity to confining topography in topographically complex settings. Barker et al. (2008) described a subsurface study of the Britannia Sandstone Member from the North Sea and documented a systematic thickening of matrix-rich sandstone at the expense of underlying, matrix-poor sandstone within event beds over: 1) short length-scales (<2 km), in an across-flow direction towards a lateral confining basin margin (axially to marginally), and 2) over longer length-scales (>4 km) in a downstream orientation where flow ran out unconfined by topography. This axial to marginal facies tract was suggested to record a flow that thinned towards the lateral confining basin margin resulting in relatively lower turbulence, earlier sand deposition and a greater susceptibility to turbulence suppression in such marginal locations compared to flows in more axial settings that were thicker in positions away from the lateral confining slope. The longer length-scale facies tract was thought to record downstream “textural fractionation” (longitudinal segregation) in the depositing flow with adjacent rheological zones passing from turbulent flow in the front, through transitional flow, to laminar flow in hindward flow.

Patacci et al. (2014) described outcrops at the Braux onlap section of the Annot Sandstone, where laterally extensive event beds can be confidently traced laterally over distances of 1.5 km towards their onlap onto an obliquely orientated downstream confining

slope at the basin margin. They documented a common trend in which a mud-clast- and matrix-rich sandstone, interpreted as a H3 division, is developed locally (<1 km) adjacent to the confining slope and exhibits an overall thickening at the expense of underlying matrix-poor sandstone (H1) with increasing proximity to their pinch out and onlap onto the confining slope. This localised facies tract was considered to record turbulent flows that were primed to transformation and turbulence suppression, following up-dip entrainment of muddy substrate and radial expansion, and their subsequent rapid transformation due to forced deceleration within 1 km of the slope.

2.11 Focus of the current work

The following chapters (3-6) detail the bed-scale expression of various HEBs as well as spatial variations in their character and distribution in three deep-water systems which were affected by discrete styles of basin physiography - the unconfined Cretaceous Vøring Basin (Chapter 3), the confined, uncontained Carboniferous Pennine Basin (Chapter 4 & 5) and the confined and contained Miocene Castagnola Basin (Chapter 6). Each system was studied in isolation with no intention to propose an all-inclusive bed classification due to the inherent difference in boundary conditions between these systems (i.e. source material, system size, basin physiography) and the range and complexity of processes which can drive flow transformation and the emplacement of HEBs. However, the findings of these separate case studies are integrated in Chapter 7 in order to provide generic insights and further understanding of HEBs and the flows that emplace them.

Chapter 3. Hybrid event beds dominated by transitional facies types: character, distribution and significance in the Maastrichtian Springar Fm. NW Vøring Basin, Norwegian Sea.

3.1 Introduction

Chapter 3 presents a subsurface study of Maastrichtian-aged deep-water sandstones (the intra-Springar Sandstone) from the NW Vøring, Norwegian Sea (Fig. 3.1). The Maastrichtian system represents a large (c. 140 km long), mixed sand-mud system that developed where sea-floor topography was relatively simple (i.e. unconfined, *sensu* Fig. 2.15a). Data and core (224.84 m cumulative thickness) from 5 wells (Fig. 3.2) were used to assess spatial (geographic and stratigraphic) trends in facies frequency and proportion, and thus bed character, to infer the spatio-temporal evolution of flows emplacing HEBs in an unconfined deep-water system.

Gravity currents are typically ascribed to two end-member flow types: 1) largely turbulent high- and low-density turbidity currents which deposit relatively matrix (clay)-poor turbidites (Bouma, 1962; Lowe, 1982); and 2) cohesive (clay-rich), laminar debris flows that deposit debrites (Hampton, 1972). Recent studies are increasingly demonstrating that deposits in which both matrix-poor and matrix-rich sandstone facies occur do not exclusively result from either of these two flow types *sensu stricto*, and may instead record deposition from flows with complex rheological heterogeneity or those which underwent rheological transformation (Lowe & Guy, 2000; Haughton et al., 2003, 2009; Talling et al., 2004, 2007a, 2013; Sylvester & Lowe, 2004; Barker et al., 2008; Sumner et al., 2009; Kane & Pontén, 2012; Terlaky, 2014). These deposits deviate from classical models predicting gravity current evolution during run-out (Bouma, 1962; Lowe, 1982; Mutti, 1992; Mulder & Alexander, 2001), in that individual beds record deposition from both non-cohesive and more cohesive flow states during a single flow event. In the sub-aerial realm, the development of multiple flow states, as well as evolution between them, within a single flow event has been documented in sub-aerial density flows such as pyroclastic flows, debris flows and lahars (McClung & Schaerer, 1993; Druitt, 1998; Iverson & Vallance, 2001). Commonly, examples of such deep-water “non-classical” deposits exhibit evidence of progressive aggradation beneath a passing flow, which evolved from non-cohesive (clay-poor), turbulent flow to relatively more cohesive (clay-rich), laminar flow in the rear (i.e. hybrid event beds Haughton et al., 2003, 2009).

Clay concentration is considered to be a significant modifier of flow rheology due to its capacity to provide cohesive (yield) strength grain-support and to suppress fluid turbulence, even at small concentrations (Baas & Best, 2002; Sumner et al., 2009). Clay enrichment of

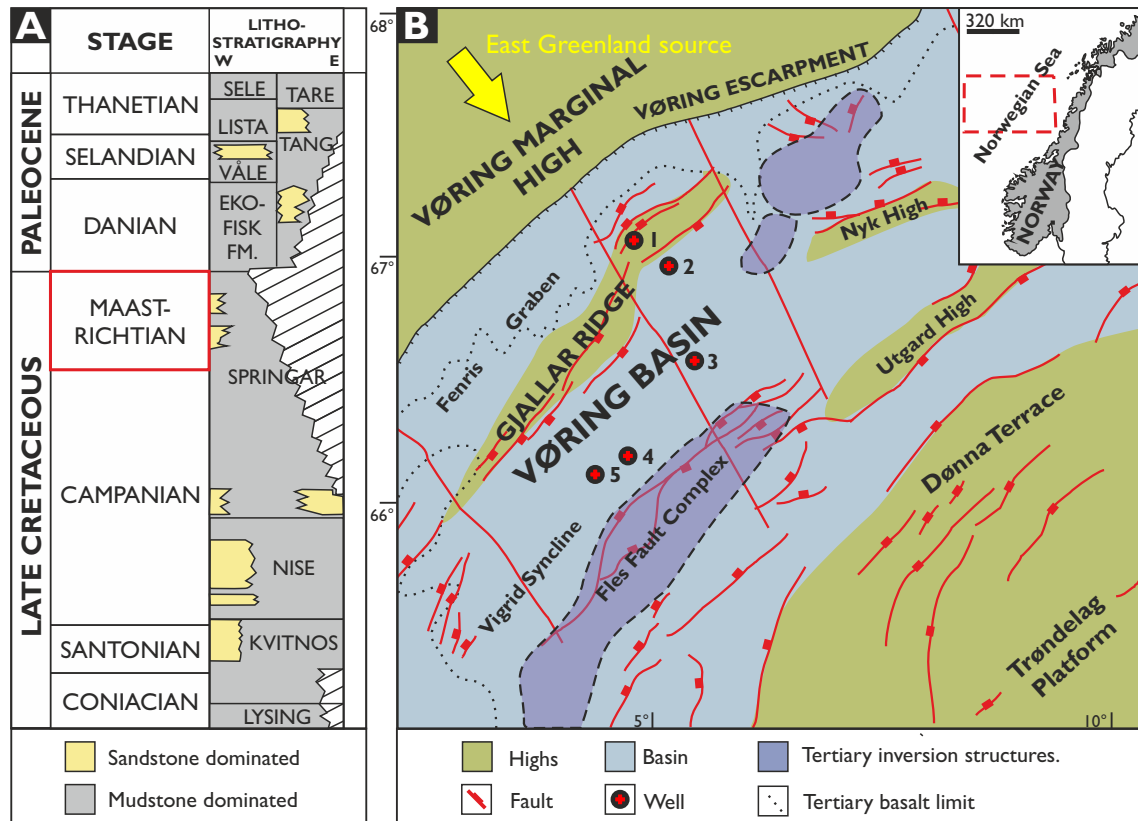


Figure 3.1. A) Stratigraphic column and B) Late Cretaceous to Paleocene palaeogeographic map for the NWVøring Basin, Norwegian Sea, with the position of studied wells indicated. Modified from Faerseth & Lien (2002). A supply from Greenland to the east has been demonstrated by Fonneland et al. (2004) and Morton et al. (2005).

Well	Formation	Cored interval (m)	Data
1) 6704/12-1	Springar	28.90	Core, wireline & plug
2) 6705/10-1	Springar	101.3	Core, wireline & plug
3) 6705/1-1	Springar	27.10	Core, wireline & plug
4) 6704/10-1	Springar	53.87	Core, wireline & plug, mini-permeametry & thin-sections
5) 6704/10-1	Springar	18.47	Core, wireline & plug, mini-permeametry & thin-sections

Table 3.1. Table summary of the data set.

gravity currents may occur via: 1) entrainment of muddy substrate (Haughton et al., 2003); 2) re-distribution of clay following rearward hydraulic fractionation of low-settling velocity material within a turbulent flow (Haughton et al., 2003); or 3) loss of the coarser sediment fraction, resulting in progressive downstream fining and clay-enrichment (Talling et al., 2007a, Barker et al., 2008; Sumner et al. 2009). Entrainment, hydraulic fractionation and depositional fractionation by gravity currents are controlled by a number of factors, including changes in basin-floor gradient, temporally evolving sediment supply characteristics and changes in flow confinement. Such sensitivity is reflected in the spectrum of hybrid event beds documented within the literature (Lowe & Guy, 2000; Haughton et al., 2003, 2009; Talling et al., 2004, 2007a, 2013; Sylvester & Lowe, 2004; Barker et al., 2008; Sumner et al., 2009; Kane & Pontén, 2012; Terlaky, 2014). However, our understanding of hybrid flow is in its relative infancy, and a

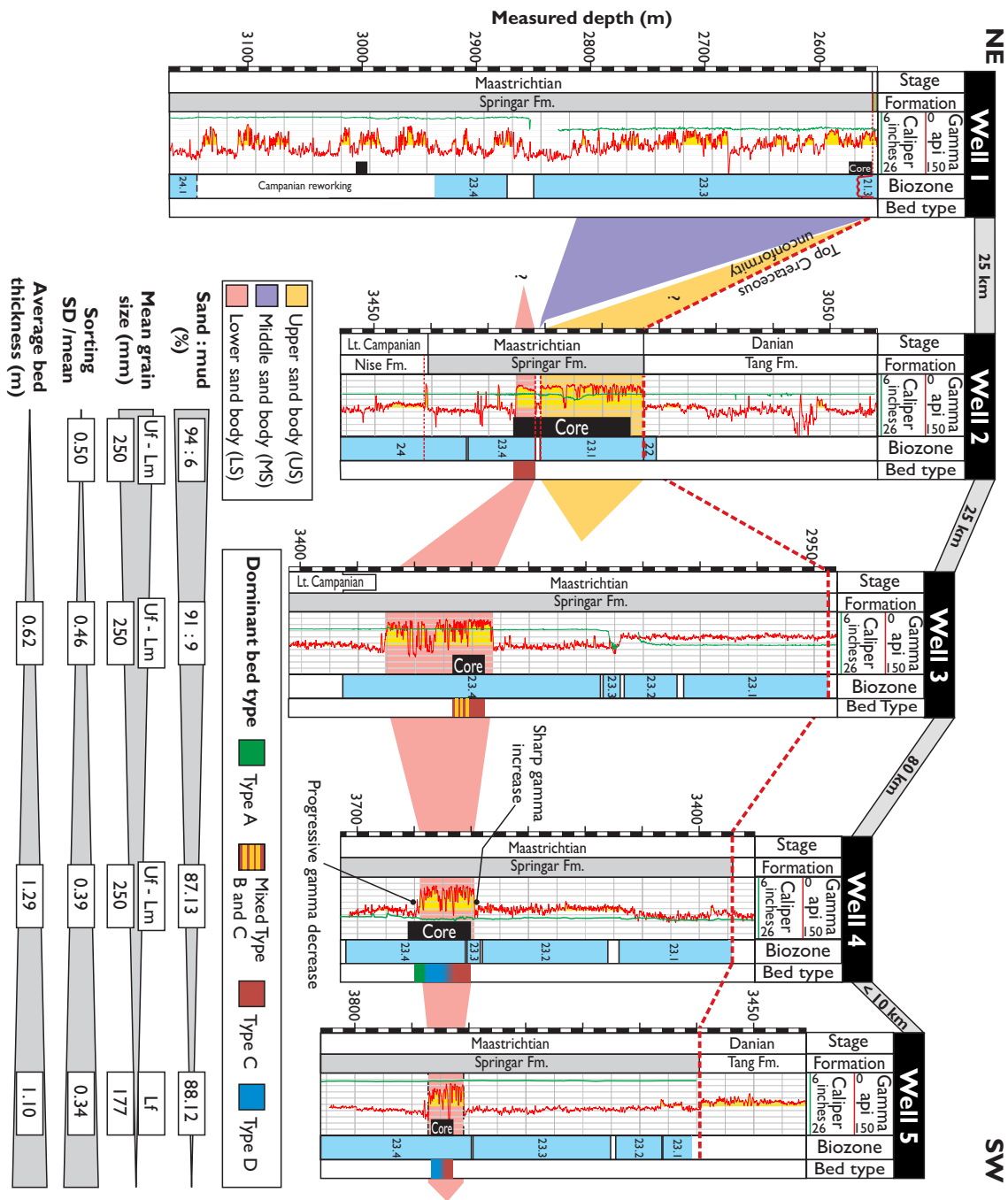


Figure 3.2. This study concerns deep-water sandstone of the Campanian to Maastrichtian aged Springar Formation which accumulated during rifting and an overall rise in sea-level (Surlyk, 1990; Riis, 1996). Well locations are shown on Fig. 3.1. Biostratigraphy highlights the presence of an Upper, Middle and Lower sand body (US, MS & LS, respectively). The LS is the most extensive and forms the basis of this study. The LS shows a downstream decrease in total thickness, sand-to-mud ratio and mean grain size with a concomitant increase in grain sorting and average event bed thickness from Well 2 to Well 5. Near complete penetration of the LS at Well 4 demonstrates a vertical change in the dominant bed type from Type A to Type D and finally Type C beds, a trend comparable to that in the partially cored LS at Well 5. Grain size abbreviations; **Lf**, lower fine sand; **Uf**, upper fine sand; **Lm**, Lower medium sand.

general consensus regarding the processes by which they evolve and deposit has not yet been reached.

This chapter presents a process model for the spatio-temporal evolution of hybrid flows (*sensu lato*, section 2.7.1) and emplacement of HEBs dominated by transitional facies (i.e. banded sandstone, matrix-rich non-stratified sandstone) using subsurface data from Maastrichtian-aged sandstones of the unconfined NW Vøring Basin, Norwegian Sea. Specific objectives are:

- 1) to document the intra-bed-scale heterogeneity of HEBs in terms of their texture and composition, and thus reservoir quality (porosity and permeability);
- 2) to describe depositional facies, and associated depositional processes, within beds;
- 3) to characterise spatial (geographic and stratigraphic) variations in facies frequency and their average proportion of bed thickness for different bed types
- 4) to infer how discrete zones of near-bed flow evolve during downstream flow run-out;
- 5) to discuss the above points in terms of the character and controls upon the spatio-temporal evolution of hybrid flows during their downstream run-out.

This study extends upon previous models concerning the spatio-temporal evolution of hybrid flows during their downstream run-out (Haughton et al., 2003, 2009; Kane & Pontén, 2012; Talling, 2013) and highlights how discrete styles of evolution of rheological zones within the flow contribute to the documented spectrum of hybrid event beds in deep-water systems. This improved understanding enhances predictive capacity with regards to the character and distribution of hybrid event beds in deep-water systems. Such deposits possess marked internal lithological heterogeneity, that are present in hydrocarbon reservoirs (Barker et al., 2008, Davis et al., 2009) and can act as potential seals or baffles within reservoirs (Amy et al., 2009).

3.2 Geological setting

The Vøring Basin lies 300 km west of Mid-Norway in the Norwegian Sea and formed during two regionally extensive rifting episodes during the Late Jurassic - Early Cretaceous, and Late Cretaceous – Paleocene (Skogseid & Eldholm 1989; Roberts et al. 1997) (Fig. 3.1a). Late Cretaceous rifting resulted in the deposition of mudstone-dominated marine successions; locally these contain deep-water fan sandstone accumulations that infilled basin-floor topography (Kvitnos, Nise & Springar Formations; Kittilsen et al., 1999; Færseth & Lien 2002; Lien et al., 2006).

This study concerns deep-water sandstones within the Campanian – Maastrichtian-aged Springar Formation, which accumulated during rifting and an overall rise in eustatic sea-

level (Surlyk, 1990; Riis, 1996; Fig. 3.1b). Siliciclastic sediment supply was derived from the uplifting East Greenland Margin (Fonneland et al., 2004, Morton et al., 2005) and transported eastwards via a narrow shelf, across both the proto-Fenris Graben and the developing and uplifting Gjallar Ridge (Lundin & Doré, 1997) and thence into the Vøring Basin (Færseth & Lien 2002, Lien et al., 2006). Here, deposits accumulated as a southwesterly dispersing gravity current system dominated by fine-grained, matrix-rich sandstones. Data from five exploration wells, penetrating intra-Springar sandstones in the NW Vøring Basin, form the basis of this study, which cover a downstream extent of approximately 140 km (Figs 3.2, 3.3; Table 3.1). The intra-Springar sandstones comprise very fine- to lower medium-grained sandstones of sub-arkosic composition, with detrital mud content ranging from 2-16 %, though typically less than 7% (Porten et al., submitted).

Proprietary biostratigraphic data highlight the presence of several sandstone bodies within the intra-Springar sandstone, informally referred to as the Lower, Middle and Upper sand bodies (LS, MS, US, respectively in Fig. 3.2). The US, penetrated in Well 2, is absent in Wells 3 to 5, suggesting it was of limited extent or offset from the latter wells. Its absence from Well 1 is most likely a result of removal by pre-Danian uplift and erosion. The MS is found only at Well 1, and its absence in Well 2 may either reflect confinement behind the Gjallar Ridge, or deposition and subsequent erosion and reworking during the emplacement of the US at Well 2. If deposited at Well 2, its absence from Wells 3 to 5 suggests the system was either offset in respect to these wells, as is considered for the US.

The LS is most extensive (Wells 2 to 5), and thus forms the focus of this investigation into spatial bed type distributions and facies trends within HEBs. Correlation of the LS with similar aged sands in Well 1 is problematic due to indeterminate biostratigraphy; furthermore, Well 1 is located on the upstream side of the Gjallar Ridge and could have been confined and separated from deposits of the LS in Wells 2 to 5. Limited thickness of the LS in Well 2 is thought to result from removal of the upper section through erosion or failure, based on the absence of biozones at the top. The LS thins basinwards with an overall decrease in grain size and sand-to-mud ratio with an overall improvement in grain sorting (Fig. 3.2). Seismic amplitude extractions illustrate the tendency for the development of weakly channelised sheets in proximal regions (Wells 2 and 3), and more lobate features in distal areas (Wells 4 and 5). Data coverage does not permit direct correlation of individual event beds between wells; thus, the analysis focuses upon proximal to distal trends across the LS fan system, and their inferred stratigraphic expression.

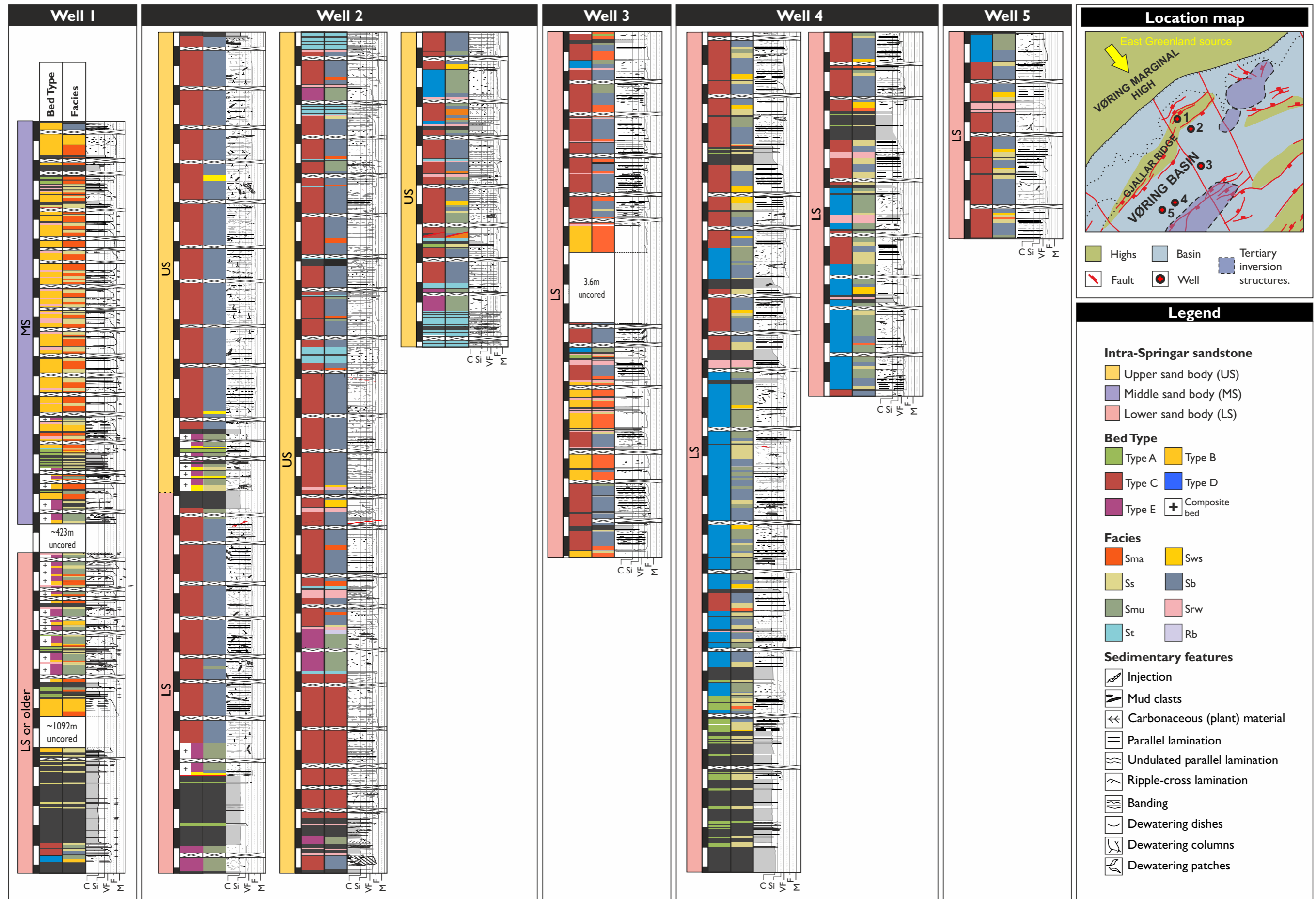


Figure 3.3. Graphic sedimentary logs summarising facies and bed types present within the studied wells 1 to 5. For well locations and the positioning of core taken from these wells refer to Fig.3.1 and 3.2, respectively.

3.3 Data and methods

Detailed sedimentary logs were described at 1:30 scale from 252.74 m of core taken from five exploration wells with intra-Springar sandstone penetration in the NW Vøring Basin (Figs 3.2, 3.3; Table 3.1). High-resolution (1 cm spacing) mini-permeametry data, plug data and point-counting of thin-sections taken from the most distal wells (4 and 5) allowed for detailed assessment of texture, composition and reservoir quality within selected HEBs. Using a petrographic microscope, 300 grain counts were used for volumetric determination of detrital and diagenetic minerals, matrix and porosity (*sensu* Walderhaug et al., 2012). Grain size was determined from measurements of the long axes of 300 grains using areal methods (*sensu* Johnson, 1994). Grain-size distribution and sorting values were then determined according to the method of Folk and Ward (1957). Underestimation of coarser grain sizes and slightly better apparent grain size sorting associated with thin section analysis (Johnson, 1994) were not corrected for, as the data still allow for assessment of relative textural changes vertically through the bed (Sylvester & Lowe, 2004; Kane et al., 2010a). Deposits within the studied wells were assessed in terms of geographic and stratigraphic variation in facies frequency and average facies proportions within bed, and thus for corresponding bed type distributions.

3.4 Results

3.4.1 Key bed types of the intra-Springar sandstone

Within the LS, eight sandstone facies and five bed types are recognised (Table 3.2; Figs 3.4, 3.5). Bed types are classified on the type, proportion and vertical arrangement of sandstone facies encountered, each of which are tentatively ascribed to a particular flow regime. Thus, an individual bed comprising more than one facies can record deposition beneath multiple flow regimes. This study focuses on the variability of facies characteristics (e.g. frequency and average proportion of total bed thickness) within key bed types, defined below, in order to understand gravity-flow evolution and resultant deposit character and distribution.

3.4.1.1 Bed Type A

Description: Type A beds comprise very thin- to medium-bedded (<0.3 m thick), plane-parallel and current-ripple laminated sandstone (facies Ss, Fig. 3.4b), that exhibit normal grading and are moderately- to well-sorted. Beds are mud-clast-poor with sharp, planar non-erosive bases and are most commonly encountered at the base of the LS in distal settings (Fig. 3.3, Well 4).

Facies	Colour	Grain size (µm) & sorting	Grading	Detrital clay %	Position	Structures	Interpretation
Sma Non-stratified sandstone	Medium – pale grey.	fL-mU (125 – 375); Moderate – poor.	Weak normal or ungraded.	4.0 – 7.0%, 5.5% average .	Lower bed; proximal.	Non-stratified relatively clean sand that sometimes contains mud-clasts aligned on horizons parallel to bedding.	1) Rapid suspension fallout from high density turbidity current (Lowe, 1982); 2) En-masse freezing of sand-rich flow (Allen, 1991); 3) Progressive aggradation beneath sustained turbidity current (Kneller & Branney, 1995), 4) syn- or early post-depositional transformation (Walker, 1965), e.g. sediment liquefaction.
Ss Stratified sandstone	Medium grey - beige	vfU-mU (94 – 375); Moderate.	Normal	4.3 – 9.0%, 6.2% average .	Lower – upper bed; distal.	Relatively clean sand with planar-parallel to wavy laminae (<5mm) and rarer ripple-cross-lamination. Laminae often lined with glauconite grains and rare mud-clasts.	Deposition beneath a tractional flow boundary zone below a dilute turbulent flow in lower to upper flow regimes (Allen, 1984a, Best & Bridge, 1992).
Sws Weakly stratified sandstone	Medium – pale grey	fL-mL (125 – 250); Moderate – poor.	Normal	4.6 – 9.3%, 7.0% average .	Lower bed; proximal-distal.	Faint colour banding with darker bands slightly clay-richer and finer-grained. Characteristics similar to both facies Ss and Sb.	Flow character that is transitional between flow states responsible for the emplacement of facies Ss and Sb.
Sb Banded sandstone	Medium grey - beige	fL-mU (125 – 375); Moderate.	Weak normal or ungraded.	5.3 – 9.3%, 7.3% average .	Lower – upper bed; proximal – distal.	Colour-banded sand with dark bands richer in detrital clay, mica and organics with relatively poorer sorting. Pale bands load into dark bands. Dewatering pipes and dishes are abundant and often pervasive.	Temporal fluctuation of near-bed flow clay concentration driven by cycles of poor and improved fluid turbulence thus sediment mixing (Lowe & Guy, 2000; Baas et al., 2005).
Smu Matrix-rich non-stratified sandstone	Medium – dark grey	fL-fU (125 – 250); Moderate – poor.	Ungraded - weak normal.	8.0 – 22.0%, 12.0% average .	Upper bed; distal.	Matrix-supported, non-stratified mud-rich sand that may contain mud-clasts typically 0.1 – 8 cm and sub-rounded. Clast alignment may be random or crudely bed-parallel.	En-masse deposition from a cohesive, turbulence suppressed flow with varying degrees of cohesive strength suggested by clast alignments (Talling, 2013).
Srw Reworked sandstone	Pale – medium grey	vfU-mL (94 – 250); Moderate – well.	Normal - inverse	No data	Isolated beds or bed-top; proximal - distal	Sharp tops, mud drapes; opposing current direction indicators; internal scouring; sharp grain size contrasts with underlying facies.	Depositional product of reworking and deposition by bottom currents (Sanders, 1962; Hubert, 1964; Lovell & Stow, 1981).
St Tractional lag sandstone	Pale grey.	fU-mU (177 – 375); Moderate.	Ungraded	No data	Isolated beds or bed-base; proximal.	Clay-poor sandstone can display crude tractional structures and elongate, sub-angular mud-clasts.	Winnowed tractional deposits remnant from multiple episodes of bypass above an erosion surface (e.g., base of channel, scour or bedform trough).
Rb Deformed strata	-	-	-	No data	Anywhere but most common proximally.	Sandstones or mudstones exhibit post-depositional soft (e.g., shear fold) to brittle (e.g., micro-faults) deformation structures. Often associated with variable scale ptigmatic sandstone dykes, lacking internal sedimentary structures. Present as <1-m thick units.	Secondary deformation of sandstones and / or mudstones attributed to slumping and or sand remobilisation and injection. Many are potential secondary slumps or debris flows triggered by incoming gravity currents (e.g., Stanley, 1982).
Mm Mudstone	-	Clay - fine silt.	-	No data	Inter bed; proximal – distal.	Laminated to massive mudstone which ranges from highly to unbioturbated.	Hemipelagic suspension fallout from the water column.

Table 3.2. Facies descriptions and interpretations.

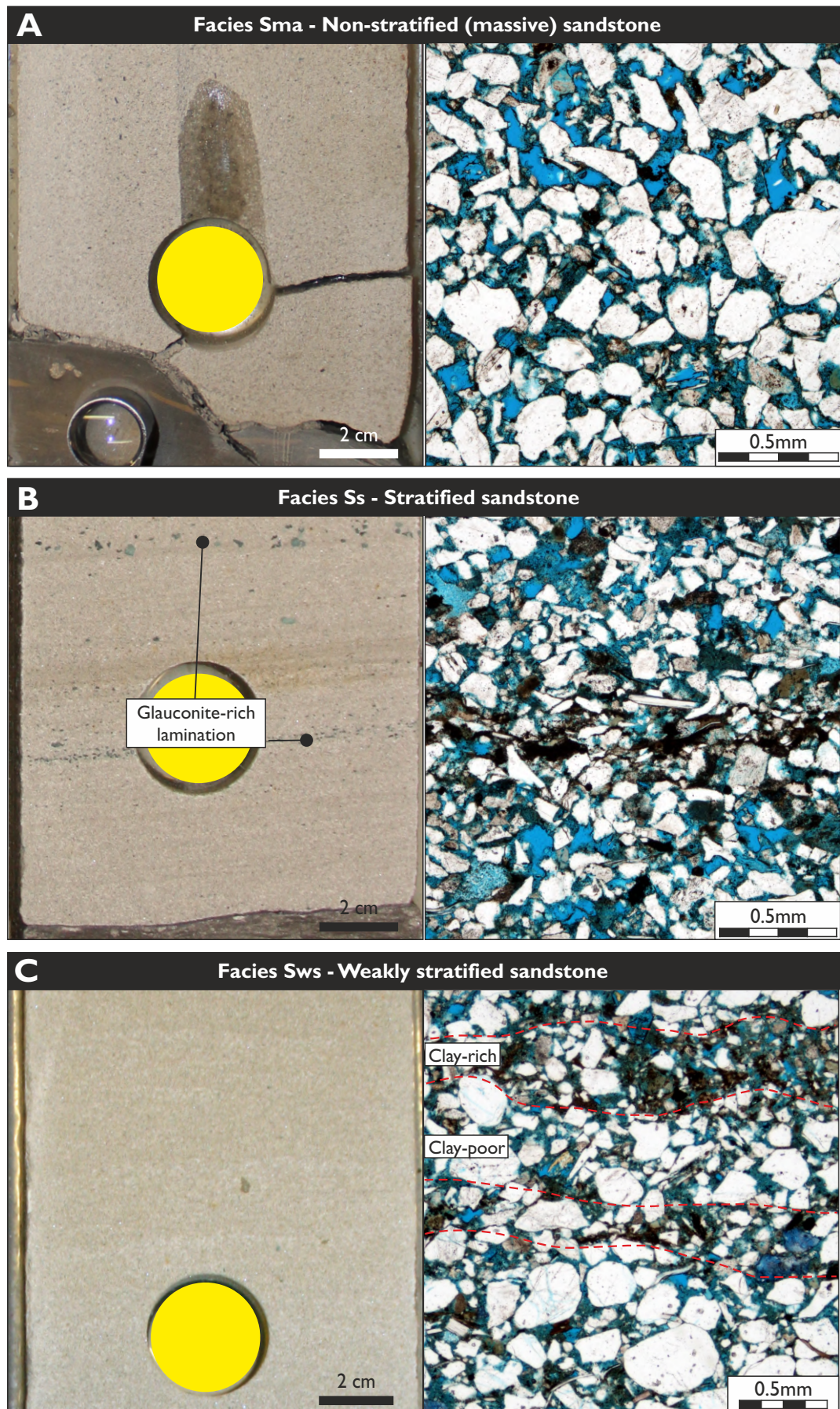


Figure 3.4. Core photographs and thin-section photographs demonstrating examples of facies present within the studied cores. See Table 3.1 for facies descriptions and interpretations.

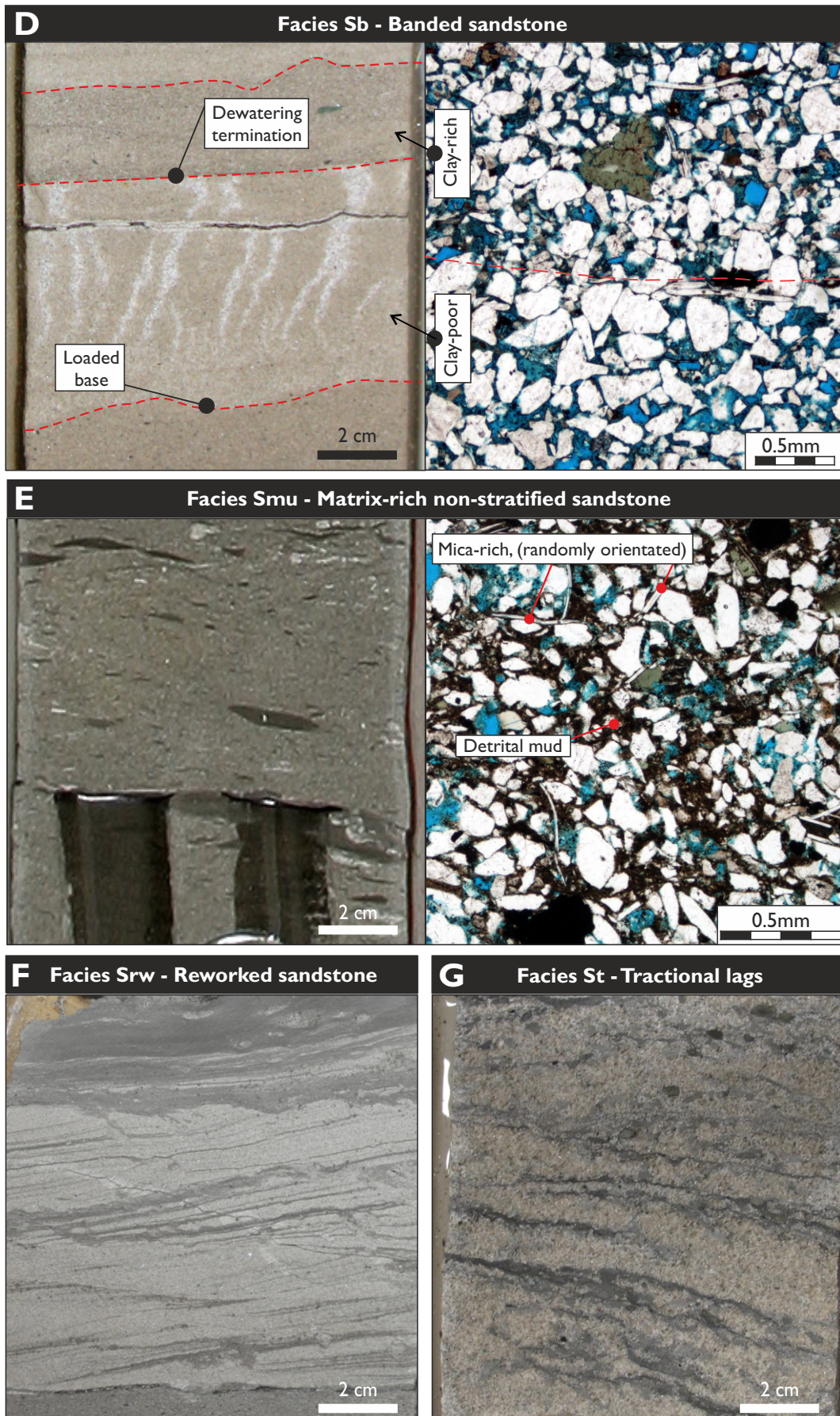


Figure 3.4 ctd. Core photographs and thin-section photographs demonstrating examples of facies present within the studied cores. See Table 3.1 for facies descriptions and interpretations. LB – Light band (detrital clay-poor); DB – Dark band (detrital clay-rich).

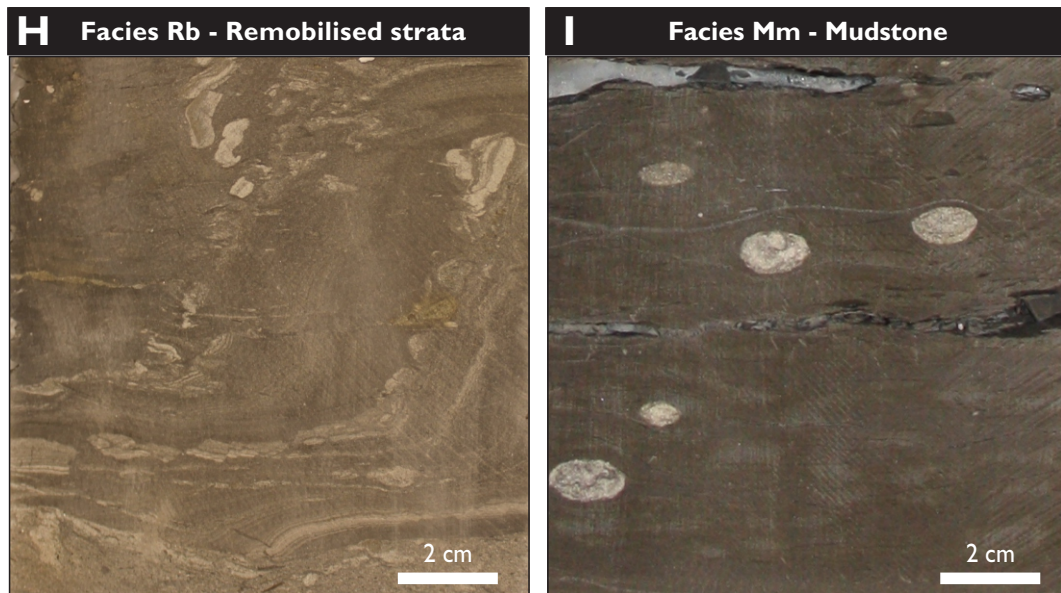



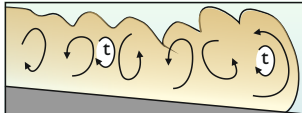
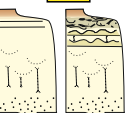
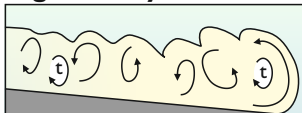


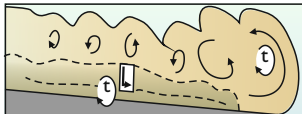
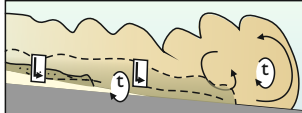




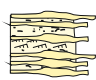
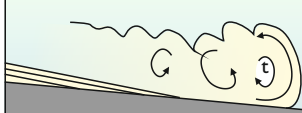

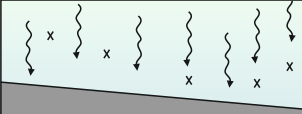
Figure 3.4 ctd. Core photographs and thin-section photographs demonstrating examples of facies present within the studied cores. See Table 3.1 for facies descriptions and interpretations.

Interpretation: Type A beds are interpreted as the deposits of dilute turbulent suspensions, in which fluid turbulence grain support, differential-grain settling and bed traction have emplaced graded stratified sandstones (e.g. low-density turbidity current, *sensu* Lowe, 1982; Bouma, 1962).

3.4.1.2 Bed Type B

Description: Type B beds typically comprise normally-graded, moderately- to poorly-sorted, medium- to very-thick-bedded (0.2-1.1 m) deposits of sandstone in which non-stratified matrix-poor sandstone (facies Sma, Fig. 3.4) are the dominant facies, both in terms of frequency and average facies proportion (Fig. 3.6). Facies Sma are typically overlain by thinner planar, parallel-laminated sandstone (facies Ss); rarer instances occur in which they are overlain by banded sandstone (facies Sb) which is in turn overlain by a thin, non-stratified matrix-rich sandstone (facies Smu). Small (<10 mm) bedding-aligned mud clasts and dewatering dish structures can be present. Bed bases are sharp with occasional sole structures suggesting that bed bases may often be erosive.

Interpretation: Type B beds are interpreted as the depositional products of largely high- to low-density turbidity currents (*sensu* Lowe, 1982). Bedding-aligned mud-clast horizons and normal grading suggests non-stratified sandstones were not emplaced *en-masse* following sudden loss of grain support and subsequent differential settling of grains according to density, a process capable of producing normally graded non-stratified sandstones (Lowe, 1982; Shanmugam, 1997). Instead, deposition is considered to have occurred progressively beneath high-density

Bed Type	Process interpretation
<p>A</p>  <p>Bed thickness: few cm to 30 cm. Grain size: silt to fine sand. Sedimentary structures: dominated by plane-parallel and ripple-cross lamination (facies Ss) normally graded.</p>	<p>Low-density non-cohesive turbulent flow</p>  <p>Competence-related deposition and tractional working by dilute low density turbidity current (Lowe, 1982; Hiscott, 1994a).</p>
<p>B</p>  <p>Bed thickness: 20 to 110 cm. Grain size: fine to medium sand. Sedimentary structures: dominated by non-stratified matrix-poor sandstone (facies Sma).</p>	<p>High-density non-cohesive flow</p>  <p>Deposition largely from a high density sediment gravity flow (<i>sensu</i> Lowe, 1982) with high suspension fall out rates.</p>
<p>C</p>  <p>Bed thickness: 40 to 200 cm, packages up to 18 m. Grain size: upper very fine to lower medium sand. Sedimentary structures: wide range of facies (facies Sma, Ss, Sb and Smu) with Sb thickness exceeding 30% of bed thickness and that of overlying facies Smu. Common dewatering structures. Mud-clast rich and mud-clast poor examples occur.</p> <p>D</p>  <p>Bed thickness: 5 to 200 cm. Grain size: upper very fine to lower medium sand. Sedimentary structures: wide range of facies (facies Sma, Ss, Sb and Smu) with Smu thickness exceeding 30% of the bed thickness and that of underlying facies Sb. Mud-clast-rich and mud-clast poor examples.</p>	<p>Mixed turbulent, cohesive and quasi-laminar flow characteristics</p> <p>Early stage</p>  <p>Late stage</p>  <p>Bed C: Significant deposition occurred from a flow regime that was dominated by near-bed flow which fluctuated between relatively turbulent and more cohesive states (e.g., Baas et al., 2005).</p> <p>Bed D: Flow in which there was a greater or more stable component of near-bed flow with a relatively cohesive, quasi-laminar state (e.g., deposition of facies Smu).</p> <p>t Turbulent L Laminar</p>
<p>E</p>  <p>Bed thickness: 20 to 65 cm. Grain size: clay to fine sand. Sedimentary structures: poorly sorted, ungraded, plastic deformation (fold and shear structures), weak to absent fabrics in mud-clasts. Facies Smu and Rb dominate.</p>	<p>Cohesive quasi-laminar flow</p>  <p>Deposition from muddy (cohesive) laminar debris flows (Lowe, 1982; Sohn et al., 1997).</p>
<p>F</p>  <p>Bed thickness: 1 to 35 cm. Grain size: very fine to fine sand. Sedimentary structures: mud drapes, plane-parallel and ripple-cross lamination in random sequences, variable grading, internal erosion surfaces and sharp tops (facies Srw)</p>	<p>Bottom current (contour current)</p>  <p>Tractional reworking of sand by bottom currents (e.g. Sanders, 1962; Hubert, 1964; Lovell & Stow 1981).</p>
<p>G</p>  <p>Bed thickness: from 1 cm, packages up to 300 cm. Grain size: medium to fine sand. Sedimentary structures: lenticular, sharp top & base, winnowed (clean) sand (facies St). Elongate rip-up mud clasts and irregular stratification.</p>	<p>Reworking & winnowing by gravity flows</p>  <p>Winnowed tractional deposit remnant from bypass above an erosion surface (e.g. base of a channel, scour or bedform trough).</p>
<p>Hemipelagite mudstone</p>  <p>Bed thickness: few mm to 450 cm. Grain size: clay to minor silt. Sedimentary structures: structureless or laminated (facies Mm).</p>	<p>Hemipelagic fallout</p>  <p>Hemipelagic suspension fallout from water column.</p>






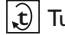



-  Planar lamination
  Current-ripple lamination
  Clasts
  Dewatering
  Banding
 Turbulent
  Laminar
 Non-cohesive  Cohesive 

Figure 3.5. Descriptions and process interpretations for event beds of the intra-Springar sands.

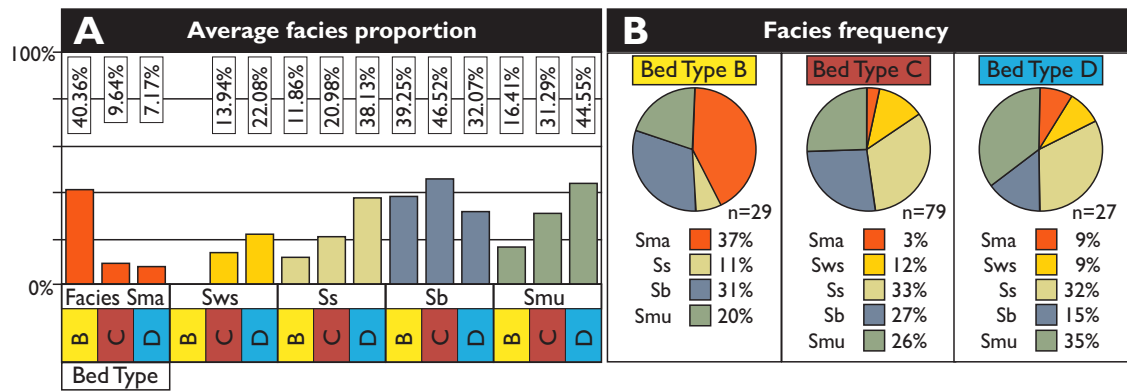


Figure 3.6. Average facies proportions of total event bed thickness (**A**) and facies frequency (**B**) within bed types B, C and D. Determination of facies characteristics did not include beds affected by amalgamation or reworking so as to avoid over-estimation of the thickness and probability of facies positioned lower in the bed.

turbidity currents with high sediment concentrations, in which grain collision support and a high rate of suspension fall-out inhibited tractional transport and development of associated sedimentary structures (e.g. direct suspension sedimentation, Middleton, 1967; Lowe, 1982, 1988; Arnott & Hand, 1989). High sediment concentration flows can easily exceed their flow capacity, e.g. the limit to the rate of suspended sediment transport per unit cross-sectional area (*sensu* Hiscott, 1994a), as the flow decelerates. Subsequently, above-capacity flows commence direct suspension sedimentation of a broad range of grain sizes, even grains whose settling velocities are less than the nominal suspension threshold of the flow, to emplace non-stratified poorly sorted sands. Grain size grading within progressively aggraded deposits suggest waning flow (Kneller, 1995) and the presence of a longitudinal grain size distribution within the flow (e.g. rearward fining). Succeeding, later-stage deposition of facies Ss records a change to deposition from relatively dilute, low-concentration flow comparable to that emplacing Type A beds. Instances where the thick facies Sma are instead overlain by facies Sb and Smu, such late-stage deposition is thought to mark the onset of turbulence-suppressed and relatively more cohesive conditions within the flow (see process interpretations in Section 3.4.1.3).

3.4.1.3 Bed Types C and D

Description: Type C and D beds comprise thick- to very thick-bedded (0.4-2.0 m) sandstone deposits with weak normal grading (Figs 3.7, 3.8). A range of sandstone facies occur within these beds which, when all present, are arranged into a common vertical succession: 1) a basal non-stratified, matrix-poor sandstone overlain by 2) plane-parallel laminated sandstone, weakly stratified sandstone (facies Sws, Fig. 3.4c), and 3) banded sandstone (facies Sb, Fig. 3.4d) with 4) matrix-rich non-stratified sandstone (facies Smu, Fig. 3.4e) at the bed top. Facies contacts are gradational over a few cm with no dramatic grain size changes. Overall, beds exhibit a vertical increase in the proportion of low-settling velocity particles (e.g. plant fragments, mica, detrital

clay; Figs 3.7, 3.8). Non-stratified, weakly stratified and stratified sandstone facies in lower bed positions typically have similar or better sorting and lower detrital clay concentrations compared to sandstone facies positioned higher in the bed. Banded sandstones comprise light-dark coloured bands, reflecting variability in depositional detrital clay content and grain sorting (Figs 3.7, 3.8). Thus, banded sandstones are often characterised by a distinct saw-tooth mini-permeability profile, reflecting variation in detrital clay-content concentration between sandstone bands, with the highest permeability correlating with matrix (clay)-poor light coloured sandstone bands (Fig. 3.7). Banded sandstones tend to be less well-sorted, and can be marginally coarser compared to matrix-poor stratified sandstone facies located lower in the bed (e.g. facies Ss and Sws). Matrix-rich non-stratified and banded sandstone facies (facies Smu and Sb) have reduced porosity and permeability values compared to cleaner (matrix-poor) sandstone (facies Ss, Sws, Sma; Figs 3.7, 3.8), except where quartz cementation has occurred in the latter. Quartz cementation can preferentially occur in matrix-poor sandstone due to the low proportion of detrital clay which prevents quartz cementation (Heald & Larese, 1974). In matrix-rich non-stratified sandstone, present in the upper bed, permeability exhibits the greatest decline whilst porosity values remain relatively high (Figs 3.7, 3.8) due to the high proportion of detrital clay in this facies which is characterised by micro-porosity (Fig. 3.4e; Hurst & Nadeau, 1995).

Dewatering structures (e.g. columns and dish structures) are common in banded sandstones, with vertical structures often terminating on the underside of dark (matrix-rich) less permeable bands (Fig. 3.7). Small-scale load and flame structures and shear fabrics are also common. Matrix-rich non-stratified sandstones can be mud-clast-rich, with clasts varying in size (<10 mm to greater than the core width) and arrangement (e.g. chaotic to crudely bed-parallel), or be relatively poorer in mud clasts. Although less common, bed tops can instead consist of plane-parallel laminated sandstones, but with higher detrital clay contents when compared to those present lower within the bed (e.g. 8% vs. 11% averages for lower and upper bed positions, respectively). Bed bases are sharp and can be either erosive, sometimes with sole structures, or non-erosive. Compared to Type B beds, Type C and D beds are less likely to contain non-stratified matrix-poor sandstone (Sma), which when present, is considerably thinner compared with those present in Type B beds (Fig. 3.6).

Type C and D beds contain similar facies in a comparable vertical arrangement, however, these bed types are distinguished on subtle differences in facies frequency and average proportion of total bed thickness (Figs 3.6, 3.7, 3.8). In Type C beds, the thickness of matrix-rich non-stratified sandstones neither exceeds that of banded sandstones, nor 30% of the total bed thickness, whereas within Type D beds the reverse is true of matrix-rich non-stratified sandstone thickness. Type D beds differ from Type C beds in terms of the following

Bed Type C characteristics

Bed: 3616.67-3618.22 m (RKB), Well 4

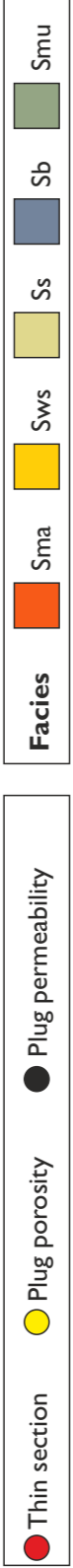
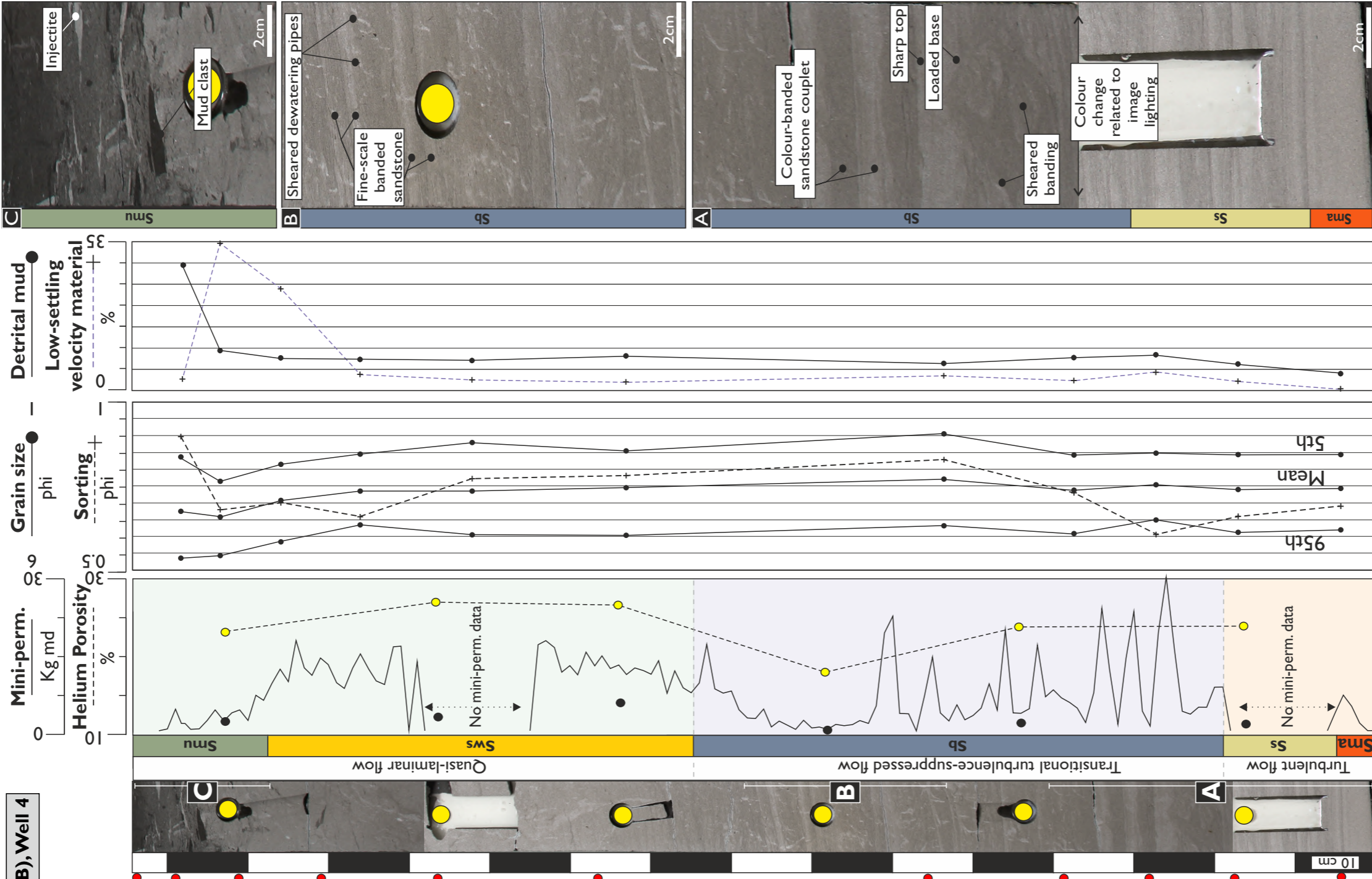
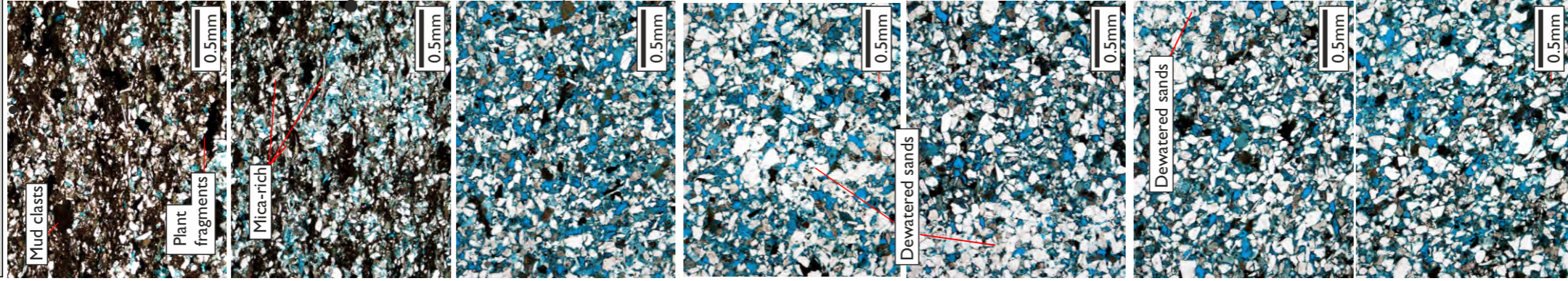


Figure 3.7. Type C event bed dominated by banded sandstone (Sb) with matrix-rich sandstone (Smu) comprising less than thirty per cent of total bed thickness. Banded sandstone (Sb) is associated with a saw-tooth mini-permeability curve with the highest permeabilities occurring in the relatively matrix-poor lighter coloured bands. An upward enrichment of particles with low-settling velocity (e.g., carbonaceous fragments, mica grains, mud clasts and detrital clay) occurs within event beds and is most pronounced within matrix-rich sandstone (Smu) commonly found at the top of beds. Permeability and porosity are governed by a complex interplay of grain size, sorting, packing and detrital clay content (Beard and Weyl, 1973; Heald and Laresse, 1974; Ehrenberg, 1997). Permeability determined from plug samples is comparable to that of the high-resolution (1 cm spacing) mini-permeability data. Permeability can be reduced in matrix-poor sandstones where quartz cementation occurs. High proportions of micro-porous clay in the upper bed result in porosity values remaining relatively high. Conversely, this increase in detrital clay drives a dramatic reduction in permeability. Grain size and sorting parameters were determined using methods outlined in Folk & Ward (1957).

Bed Type D characteristics

Bed: 3639.16-3640.82 m (RKB), Well 4

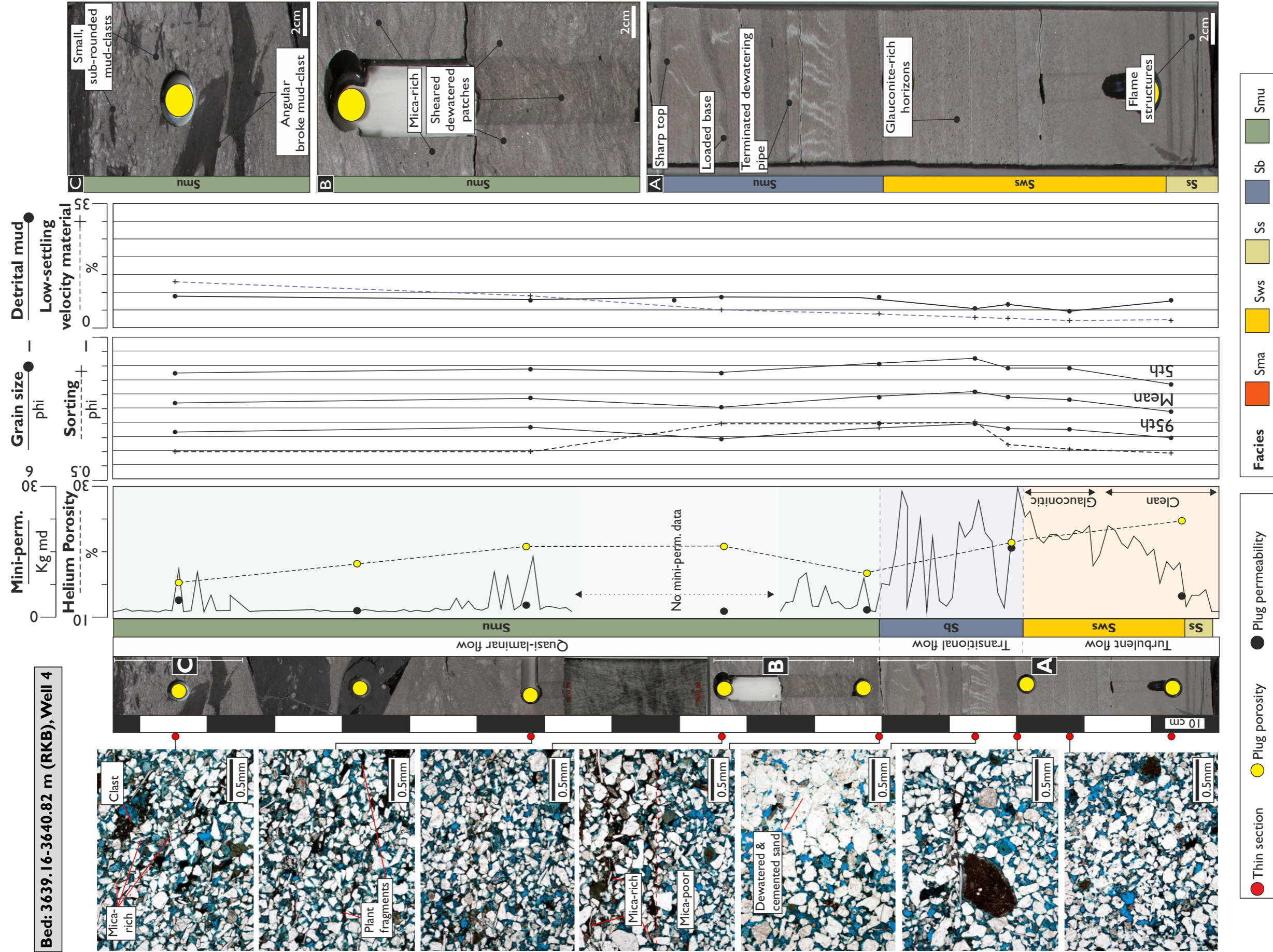


Figure 3.8. Type D event beds contain thick matrix-rich sandstone (Smu, greater than 30% of total bed thickness) and thinner banded sandstone (Sb) as well as thinner and less common matrix-rich sandstone (Facies Sma) compared to Type C event beds. Saw-tooth mini-permeability curves are associated with banded sandstone due to alternating matrix (clay)-rich and matrix-poor sandstone bands. Permeability and porosity are governed by a complex interplay of grain size, sorting, packing and detrital clay content (Beard and Weyl, 1973; Heald and Laesele, 1974; Ehrenberg, 1997). Permeability is at its lowest within the matrix-rich sandstone (Smu) at the bed top, whilst porosity remains relatively high due to the presence of micro-porosity in detrital clay. Grain size and sorting parameters were determined using methods outlined in Folk & Ward (1957).

characteristics: 1) matrix-rich non-stratified sandstones are more frequent in bed Type C (Fig. 3.6), are always found at the bed top and are typically richer in mud clasts, though mud-clast-poor examples are still common; 2) banded sandstones are less frequent and thinner in bed Type C (Fig. 3.6); and 3) non-stratified sandstones are more commonly absent from the base of bed Type C.

Interpretation: The exact process emplacing graded non-stratified sandstone (Sma) in Type C and D beds is ambiguous, as indicators of progressive aggradation are lacking (e.g. lamination, horizons of concentrated mud clasts). Plausible mechanisms for emplacement of graded non-stratified sandstone include: 1) progressive bed aggradation beneath a high-concentration flow with high suspension fall-out rates as considered for Type B beds (Section 3.4.1.2); 2) *en-masse* deposition following sudden loss of grain support; or 3) sand settling from a late-stage clay-rich flow which lacked sufficient yield strength for sand support (e.g. Type III deposits of Sumner et al., 2009; Baas et al., 2011). Mechanism 3 is unlikely, given that near-stationary late-stage flows would require a zone of complex vertically-stratified flow with repeated alternations of clay-rich and clay-poor sediment in order to deposit banded sandstone in the same bed. Such complex vertical flow stratification is not known experimentally or naturally; for example, banded sandstone was not encountered in the experiments of Sumner et al. (2009). If such flow existed, it is problematic to envisage how the complex vertical flow stratification and banded sandstone would not have been disrupted by late-stage sand settling. Light bands retain sharp contacts with underlying clay-rich dark bands even where their contacts are loaded (Figs 3.4, 3.7). Dark clay-rich bands form permeability barriers to dewatering, and thus may represent barriers to settling sand (Fig. 3.7). Furthermore, it might be expected that such cleaner, sometimes coarser, sands be found perched on top of mud clasts positioned lower in the bed; however, such instances did not occur. Both mechanisms 1 and 2 could emplace poorly sorted, normally graded non-stratified sandstone (Middleton, 1967; Lowe, 1982; Hiscott, 1994a; Kneller, 1995; Shanmugam, 1997). The vertical succession of facies within a deposit emplaced by flow freezing *en-masse* (Mechanism 2) would record the vertical structure of the flow, however the presence of banded sandstone would necessitate complex repeated vertical flow stratifications, which are considered unlikely. Non-stratified sandstones in Type C beds are interpreted to record progressive bed aggradation beneath flow with a high sediment concentration and high rate of suspension fall-out (Mechanism 1). The overlying plane-parallel laminated sandstone records a change to traction and deposition beneath a low-density turbulent flow, with a reduced sediment concentration and rate of suspension fall-out. Frictional freezing of bed-load layers (e.g. traction-carpets, Dżułyński & Sanders, 1962; Kuenen, 1966; Lowe, 1982; Hiscott, 1994b) are disfavoured as grain sizes are relatively fine (very fine- to lower medium-grained sand), grains are relatively well sorted, inverse grading is absent and laminae are thin (~1 mm).

The change to banded sandstones records a change in the character of near-bed depositional flow. Such near-bed flow may have undergone transient fluctuations between sand settling from relatively fluidal (turbulent) flow, emplacing light bands, to flow in which cohesive strength hindered suspension settling (e.g. 'slurry flows' of Lowe & Guy, 2000; Baas et al., 2005). Alternatively, Baas et al. (2011) suggest banded sandstone may develop during reworking of cohesive and non-cohesive sediment by a zone of near-bed turbulence-enhanced flow beneath an overall clay-rich transitional flow (i.e. turbulence-enhanced transitional flow and lower transitional plug flow *sensu* Baas et al., 2009). It is problematic to constrain which mechanism emplaced banded sandstone from the rock record alone, and future work should consider the expressions of banded sandstone potentially associated with these discrete mechanisms. Regardless of the mechanism, banded sandstones are considered to have developed quasi-progressively beneath a passing flow, rather than *en-masse* from a complex stratified flow, as repeated vertical changes in both texture and lithology are not known experimentally or in nature. Vertical dewatering features are often sheared in a common direction, reflecting the effect of over-passing flow shear (although such features have also been attributed to post-depositional creep; e.g. Del Pino Sanchez, 2006). The significant thickness of banded sandstone in the event beds suggests that a transiently turbulent-cohesive flow state dominated during deposition of the bed. Bed-top matrix-rich non-stratified sandstone (facies Smu) represents late-stage deposition beneath turbulence-suppressed, cohesive (clay-rich) quasi-laminar flow. Occurrences of crudely aligned mud clasts and a lack of mounding at the upper (bed top) or lower contacts of this facies suggests the yield strength of such cohesive flows was variable but relatively low (Talling et al., 2012a).

Within Type C and D beds, the recurrent vertical organisation of facies, whose contacts are relatively gradational and lack intervening mudstones, suggests such facies were emplaced during a single flow event that was characterised by discrete flow states and associated depositional processes. The repeated arrangement of relatively matrix (clay)-poor turbiditic sandstones (facies Sma, Ss and Sws) and overlying more matrix-rich sandstones (Sb and Smu) is comparable to the slurry beds of Lowe and Guy (2000), hybrid event beds of Haughton et al. (2003; 2009), co-genetic turbidite-debrites of Talling et al. (2004), and transitional flow deposits of Kane and Ponten (2012), as well as experimental deposits of transitional flows (Sumner et al., 2009; Baas et al., 2011). Such studies consider these deposits to record varying flow rheology during deposition, from relatively turbulent and clay-poor, to clay-richer, cohesive turbulence-suppressed flow (e.g. transitional or quasi-laminar flow). Subtle differences in the frequency and average proportion of facies between Type C and D beds are considered to reflect changes in the relative importance of a number of discrete flow rheological zones during deposition. Such evolution is further discussed in section 3.5.1.

3.4.1.4 Bed Type E

Description: Type E beds comprise thin- to thick-bedded (0.20 to 0.65 m), weak normal- to non-graded deposits of matrix-rich non-stratified sandstones or slumped heterolithic deposits (facies Rb, Fig. 3.4h). Matrix-rich sandstones often have poorer sorting compared to those present in Type C and D beds, due to the presence of coarser, outsized grains. Mud-clasts, and rarer sand-clasts, display a range of clast sizes and have variable orientations, from bed-parallel to chaotically arranged. Bed bases are non-erosive and occur with underlying mudstone or Type A beds. Bed Type E is most commonly associated with wells close to the Gjallar Ridge (Wells 1 and 2).

Interpretation: Type E beds are interpreted as the products of slumps and cohesive laminar debris flows (Lowe, 1982; Sohn et al, 1997).

3.4.2 Well Summaries

Fig. 3.9 summarises the palaeo-depositional environment of the intra-Springar sandstone, and the distribution of bed types within the LS and US of the studied wells.

3.4.2.1 Well 1

Several sandstones bodies are present within Well 1 which appear to have been either separate or confined (e.g. LS, 8.4 m, Figs 3.2, 3.3) or of a different age (e.g. MS 20.5 m, Figs 3.2, 3.3) to sandstones downstream of the Gjallar Ridge in Wells 2 to 5 (Figs 3.2, 3.3). Type A, B and E beds occur along with isolated deposits of bottom current reworked sandstone (Srw), and lesser occurrences of tractional lags (facies St, Fig. 3.4g; Fig. 3.3). In Well 1, inverse grading at the base of beds is more commonly observed than in other wells, suggesting that it is the most proximally situated within the study area (Kneller & McCaffrey, 2003).

In Well 1, deposits typically comprise a basal non-stratified sandstone (Sma) which is directly overlain either by matrix-rich non-stratified sandstone (Smu), or remobilised heterolithic deposits (Rb). Compared with Type C and D beds, these deposits lack intervening plane-parallel laminated (Ss) or banded (Sb) sandstone between these facies. Relatively matrix-poor non-stratified sandstone at the bed base often contain elongate sub-angular mud clasts, considered to represent relatively local upstream erosion. The absence of intervening planar-parallel or banded sandstone is distinct compared with HEBs elsewhere within the LS; these consistently have a banded sandstone between non-stratified and matrix-rich non-stratified sandstone facies types. Similar deposits are found at the base of the US in Well 2, also located close to the Gjallar Ridge (Fig. 3.10). Thus, these distinctive deposits are envisaged to

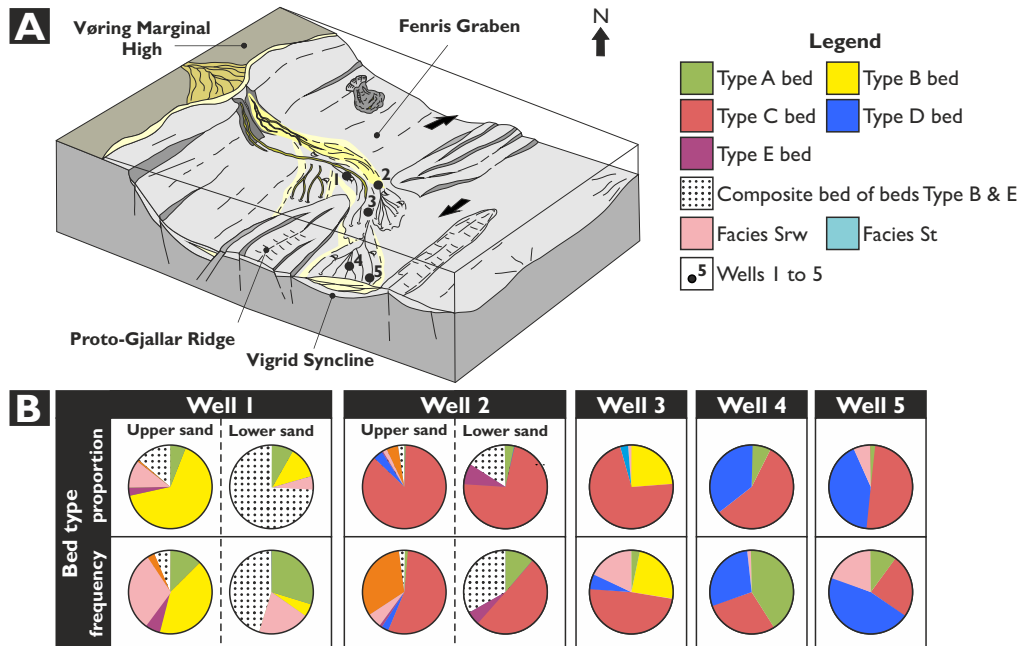


Figure 3.9. A) Palaeogeography and depositional model for the Maastrichtian intra-Springar sandstone. B) Summary of facies and bed type proportion and frequency within the studied wells I to 5.

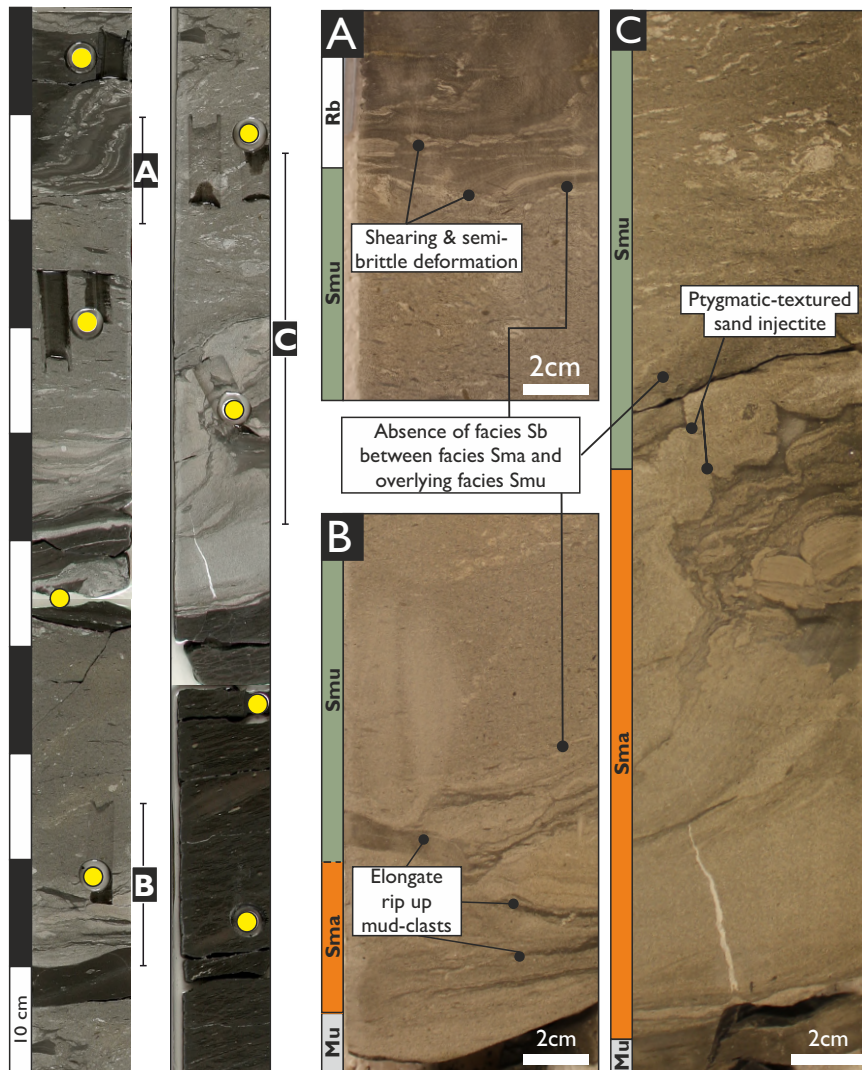


Figure 3.10. Composite deposits of Type B and E beds at Well 2. These deposits consist of relatively matrix-poor sandstone, often with abundant angular rip-up mud clasts, that are directly overlain by matrix-rich debritic sandstone or slumped heterolithics with no intervening planar laminated or banded sandstones as observed in Types C and D event beds.

represent composite deposits of Type B and E beds emplaced by gravity-current-triggered destabilisation of local bathymetry at the Gjallar Ridge (Stanley, 1982; Kneller & McCaffrey, 1999). Isolated debrites and slumps (Type E), lacking cleaner sandstone facies at their bases, are also most common within Wells 1 and 2 near the Gjallar Ridge, implying that local topography around the Gjallar Ridge influenced deposition, and promoted emplacement of these bed types which are absent from wells located further downstream (Fig. 3.3).

3.4.2.2 Well 2

The LS at Well 2 is 13.4 m-thick, with a sharp gamma decrease at its base. In core, this corresponds with the transition from mudstone into the LS sandstones (Fig. 3.2). Here, the LS is dominated by a thick (12.4 m) succession of banded sandstone, with abundant dewatering features; mudstone interbeds are absent. Rare subtle grain-size boundaries or changes in the degree of shearing of dewatering features are typically the only indication of cryptic amalgamated bedding surfaces. Based on the dominance of banded sandstone facies, and their occurrence at the bed base above amalgamation surfaces defined by grain-size breaks, these deposits are most comparable to Type C and D beds. The whole package is interpreted to be a succession of amalgamated Type C beds as the final bed at the top of the LS package is unaffected by amalgamation and possess only a thin facies Smu at the bed top. Type D beds, interpreted to be more distal deposits compared with Type C beds, are in Well 3 and suggests that Type D occurrence may be similarly limited in Well 2. The US is parted from the LS by a c.1 m-thick mudstone, and commences with distinct composite deposits of Type B and E beds, also recognised at Well 1 (Fig. 3.10). In Well 2, these composite deposits and the underlying m-thick mudstone coincide with a zone of indeterminate biozonation, suggesting that the underlying mudstone is condensed, or that these deposits reflect local slope destabilisation. These composite deposits are then overlain by thick successions of banded, dewatered and amalgamated beds similar to that in the LS.

3.4.2.3 Well 3

The LS is thickest at Well 3 (98.0 m), and is characterised by a progressive gamma decrease at the base and an abrupt gamma increase at the top (Fig. 3.2). Core taken from the upper part of the LS exhibits a mixed succession of bed Types B and C, in which Type C beds become more frequent upwards; Type D beds are rare throughout (Fig. 3.3).

3.4.2.4 Well 4

The LS is thinner (55.2 m) than at Well 3 and has complete core coverage in Well 4. The base of the LS has a serrate, upwards-decreasing gamma profile, reflecting a sandying-upwards trend

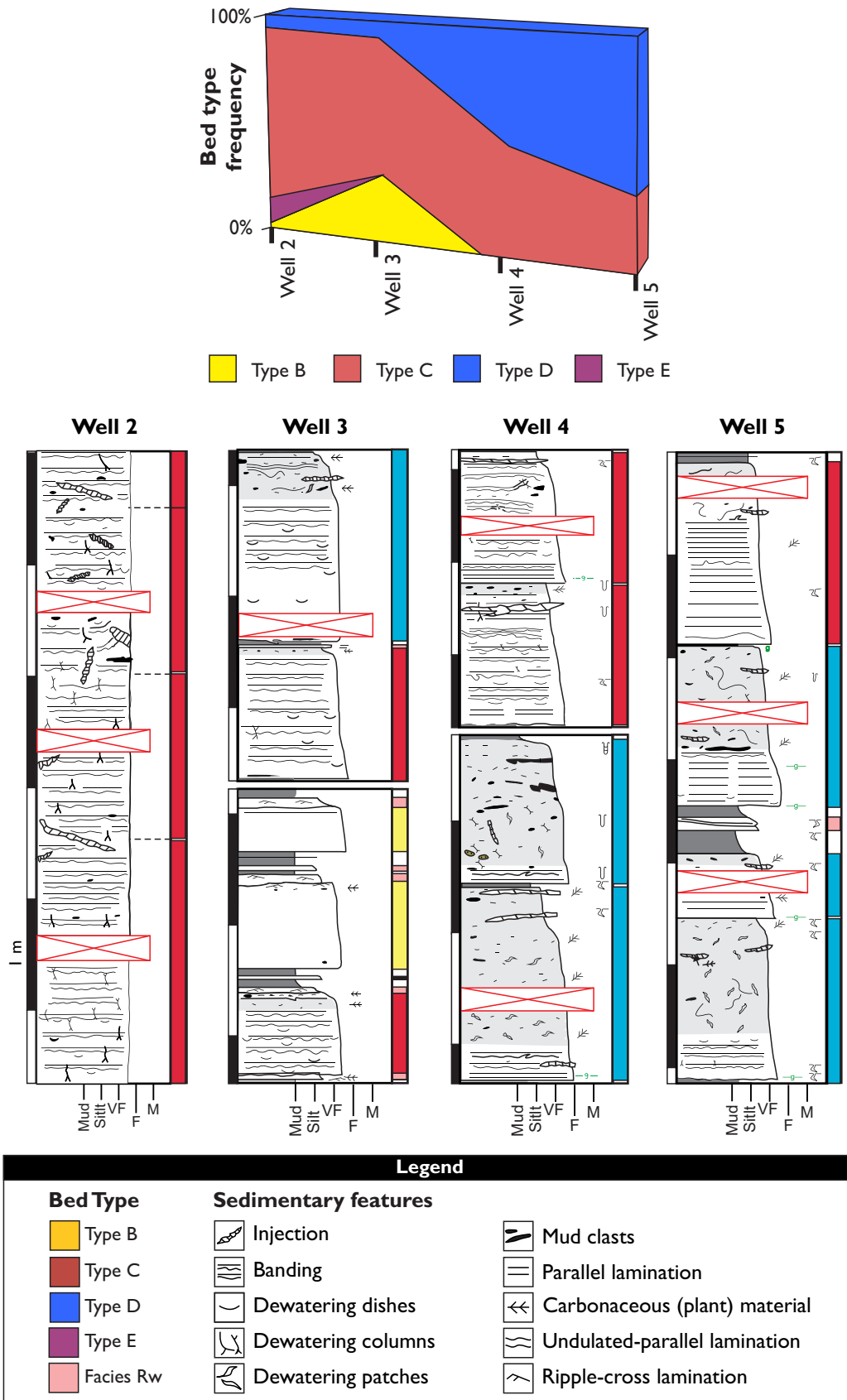


Figure 3.11. Distribution of key bed types across the lower sand (LS) body of the intra-Springar sandstone. There is an overall downstream change from Type C beds dominating relatively proximal Wells 2 and 3, where Type B beds are present, to Type D beds dominating distal Wells 4 and 5 where Type B beds are absent. This corresponds to a downstream decrease in the total thickness, sand-to-mud ratio and mean grain size of the lower sand body with a concomitant increase in grain sorting and average bed thickness as shown on Fig. 3.2.

in core, whereas the top is marked by an abrupt return to high gamma values. Type C and D beds dominate Well 4, whereas Type B beds are absent. Stratigraphically, the succession commences with a package dominated by Type A beds followed by Type D, then finally packages in which Type C beds are dominant.

3.4.2.5 Well 5

In Well 5, the LS is at its thinnest (35.0 m), comparable to Well 4 in that it exhibits the following features: 1) a serrate, upwards-decreasing gamma curve at its base, and a sharp increase at its top; 2) dominance of Type C and D beds and an absence of Type B beds; and 3) a stratigraphic change from a package dominated by bed Type D, to one dominated by bed Type C.

3.4.3 Bed-type distribution

3.4.3.1 Downstream bed-type distributions

The lack of distinctive marker beds within the large (>115 km axial extent) LS system prevents individual bed-to-bed correlation, and thus assessment of the downstream evolution of individual flows. However, assessment of the frequency of bed types downstream, as well as the facies frequency and average facies proportion within, has been conducted across the LS and used to infer downstream facies transitions related to flow evolution.

Within the LS interval, a downstream change in the dominant bed type is evident, with strata in proximal settings dominated by Type C beds, with subordinate Type B beds and an absence of Type D beds. Distal settings are dominated by Type D beds, whereas Type B beds are absent and Type C beds remain a significant bed type (Fig. 3.11). The average thickness of Type C and D beds shows an overall increase basinwards (Fig. 3.2, Well 3 to 5), and is considered to reflect flow events which became increasingly depositional in their character in the distal part of the system. Average bed thickness was determined using only complete, non-eroded and non-reworked beds. A reduction of average bed thickness in Well 5, less than 10 km away from Well 4, is thought to represent a relatively more distal or off-axis lobe setting, rather than distal fringe setting, as beds do not show dramatic thinning or grain size fining. Distal fringe settings are expected downstream of the most distal well (Well 5), and may be represented by Type A beds which dominate the distal 'switch-on' of the LS at the base of Well 4.

3.4.3.2 Stratigraphic bed-type distributions

Wireline data cannot be used to infer vertical trends within un-cored sections of the LS (e.g. lower Well 3), as packages dominated by Type C or B beds show no discernible difference in log character; reflecting the subtly differing proportions of comparable facies types in these beds, resulting in facies contrasts which are indistinguishable for the utilised well tool.

Therefore, high-resolution correlation within the LS is not possible. However, the sudden gamma increase at the top of the LS, representing a rapid shut down, has been used to infer an approximate time correlative horizon at the top of the LS. The preceding late-stage deposition of the LS was dominated by bed Type C in both proximal (Well 3) and distal (Wells 4 and 5) settings.

Within the LS there is a stratigraphic (vertical) change in the dominant bed type (Figs 3.2, 3.3). Proximally (Well 3), the dominant bed type in the lower un-cored portion of the LS is unknown, with no insight gained from gamma or ditch cuttings. Stratigraphically higher in Well 3, the LS comprises a mixed Type B and C package, passing upwards into a Type C dominated package. Distally (Wells 4 and 5), the dominant bed type changes vertically through the LS within an upwards succession of Type A, Type D and then Type C-dominated packages (e.g. Wells 4 and 5). Additionally, within the middle Type B dominated package, there is an upwards-reduction in the abundance of mud clasts within beds.

3.4.4 Spatial facies trends within HEBs

An assessment of facies frequency and their average proportion of total bed thickness was determined for Types B, C and D beds at Wells 3, 4 and 5 (Figs 3.12, 3.13). Facies frequency refers to the number of occurrences of a given facies with beds of a given bed type. Facies thicknesses, expressed as a percentage of the total thickness of their host bed, were used to determine the average proportion of a facies type within a given bed type at each well. Well 1 strata were excluded due to the uncertainty concerning their relationship with those in Wells 2 to 5 (see discussion in section 3.4.1.1). Well 2 was also excluded from this analysis due to the absence of non-amalgamated beds; inclusion of these beds would result in an over estimation of the frequency and average proportion of facies positioned lower within the bed where they are not affected by amalgamation.

3.4.4.1 Downstream facies trends

Bed Type C

Bed Type C is common in Wells 3, 4 and 5 and is more likely to contain non-stratified and banded sandstone facies types in proximal settings (Well 3) where these facies are at their thickest. Conversely, in distal settings (Well 4 and 5), stratified, weakly stratified and matrix-rich non-stratified sandstone facies types become more frequent and a greater proportion of bed thickness (Figs 3.12, 3.13).

Bed Type D

Type D beds are difficult to assess individually in terms of geographic facies trends as non-amalgamated examples are rare in Well 3. However, between the relatively closely spaced Well 4, and more distal or off-axis Well 5, Type D beds show subtle thinning of non-stratified

and banded sandstone facies types, whereas stratified and matrix-rich non-stratified sandstone types become thicker, a downstream trend also documented within Type C beds. Compared with overall trends observed in Type C beds, non-stratified and banded sandstone facies types within Type D beds are thinner and less frequent, whereas stratified and matrix-rich non-stratified sandstone facies are thicker and more frequent (Figs 3.12, 3.13). In summary, characteristics of Type D beds are most comparable to Type C beds located in distal settings (Well 4 and 5), and they show similar downstream or off-axis facies trends to those documented for Type C beds (e.g. thinning of facies Sma and Sb; thickening of facies Ss and Smu). Thus, Type D beds are interpreted to represent the downstream, more distal continuation of Type C beds.

3.4.4.2 Downstream variation in HEB bed base facies

An assessment of the spatial variation of facies frequency and thickness at the base of individual beds was conducted in order to gain insight into downstream changes in the character of deposition of the earliest flow.

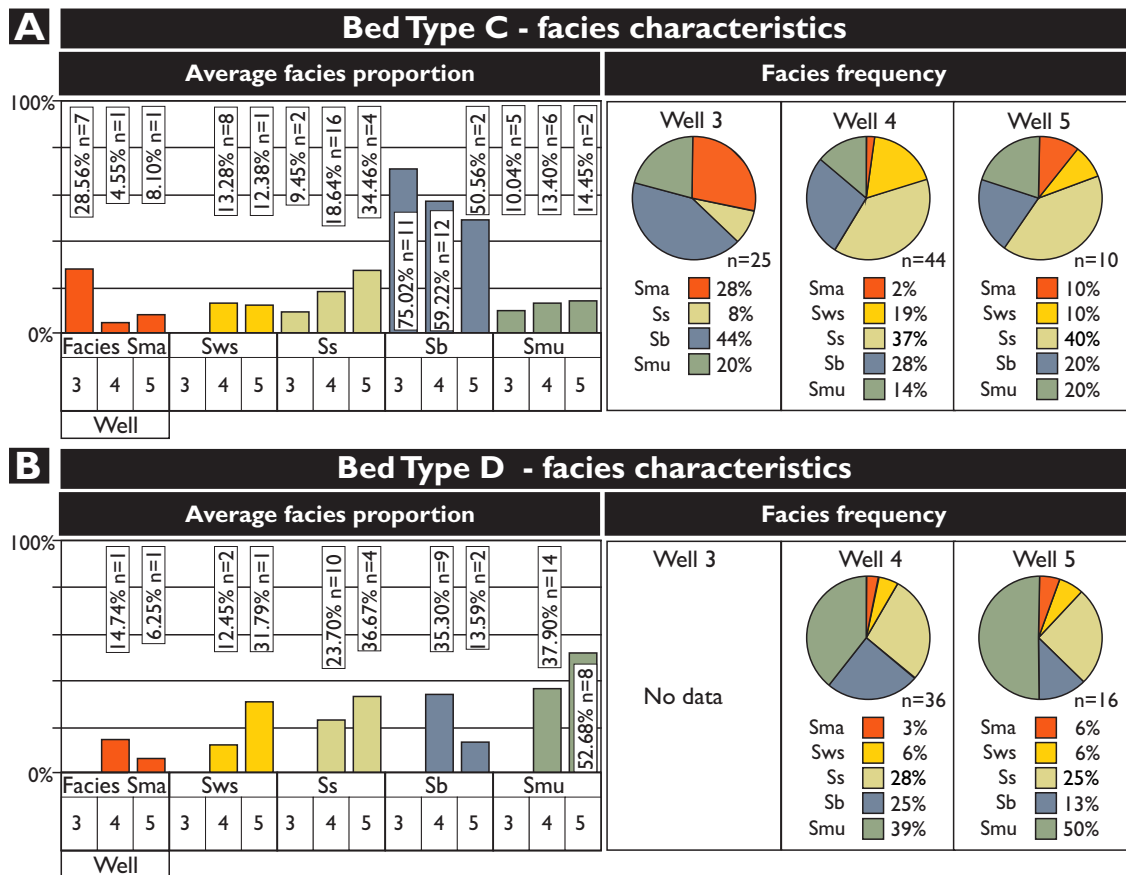


Figure 3.12. Graph illustrating spatial variation in the average facies proportion of bed thickness (left) and facies frequency (right) for facies types within Type C (A) and Type D (B) beds in Wells 3, 4 and 5. Type C beds exhibit a downstream decrease in the frequency and average proportion of facies Sma and Sb between Wells 3 through to 5, whereas facies Ss and Smu exhibit the reverse trend with a downstream increase in frequency and average proportion. Similarly for Type D beds in distal Wells 4 and 5, facies Ss and Smu are of a greater frequency and average proportion compared to facies Sma and Sb; this suggests similar downstream trends could have also occurred within Type D beds.

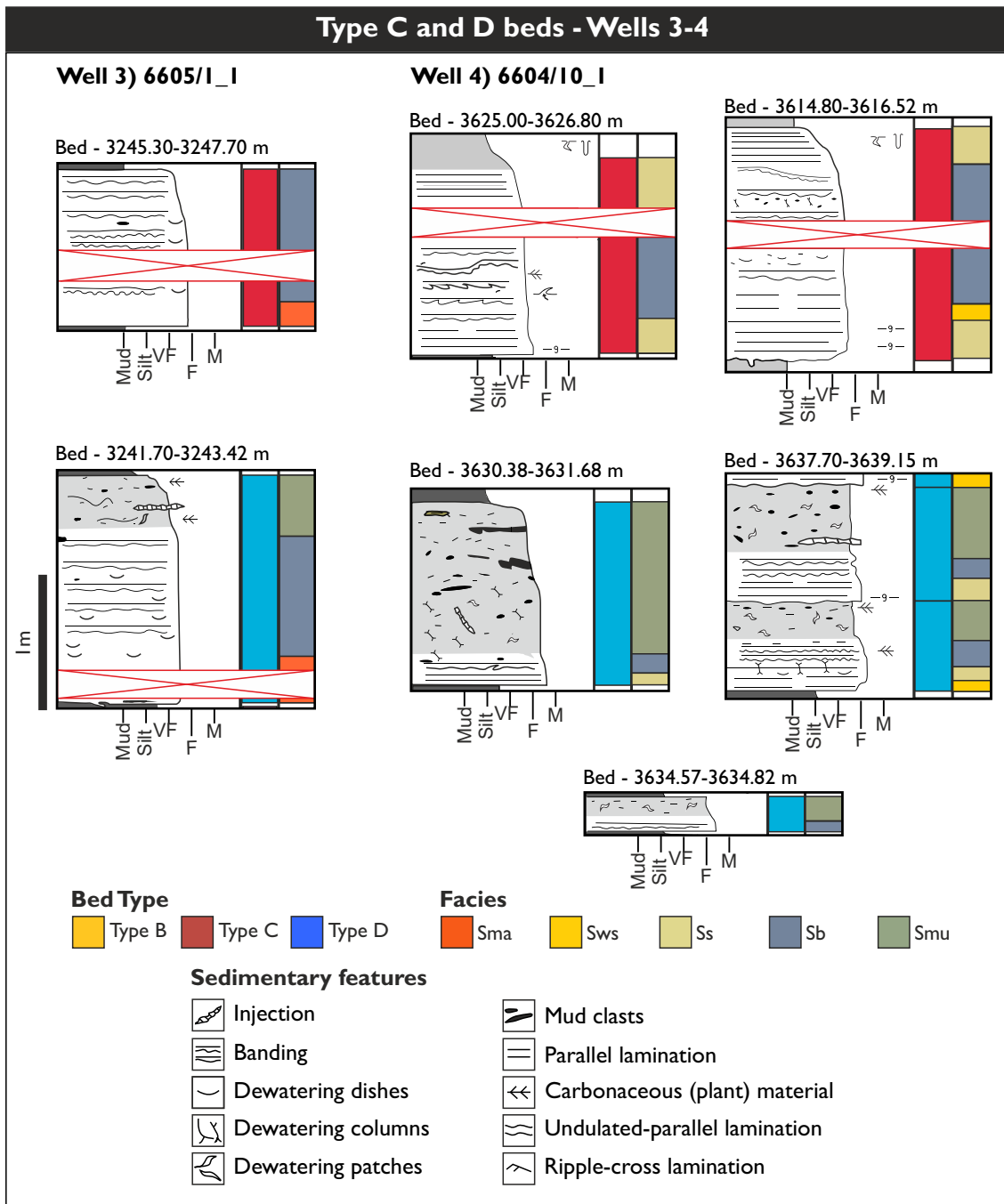


Figure 3.13. Graphic logs of Type C and D beds illustrating variation in facies proportions within beds and the facies type present at the bed base.

Bed Type C

Type C bed basal facies either comprise non-stratified or banded sandstone at Well 3, where these facies are at their greatest thickness; bed basal stratified sandstones were absent (Figs 3.13, 3.14). In distal settings, bed base occurrences of non-stratified or banded sandstone become far less frequent and thinner, whereas stratified sandstone bases are significantly more frequent (e.g. Well 4 and 5). Although the banded sandstone facies was absent, a similar downstream change from non-stratified to stratified (planar-laminated) sand at the base of beds containing a co-genetic matrix-rich, variably mud-clast-rich, sandstone, has been

documented in the Marnoso Arenacea Formation where correlation of individual beds downstream over c. 120 km is comparable to the downstream run-out in this study (Sumner et al., 2012).

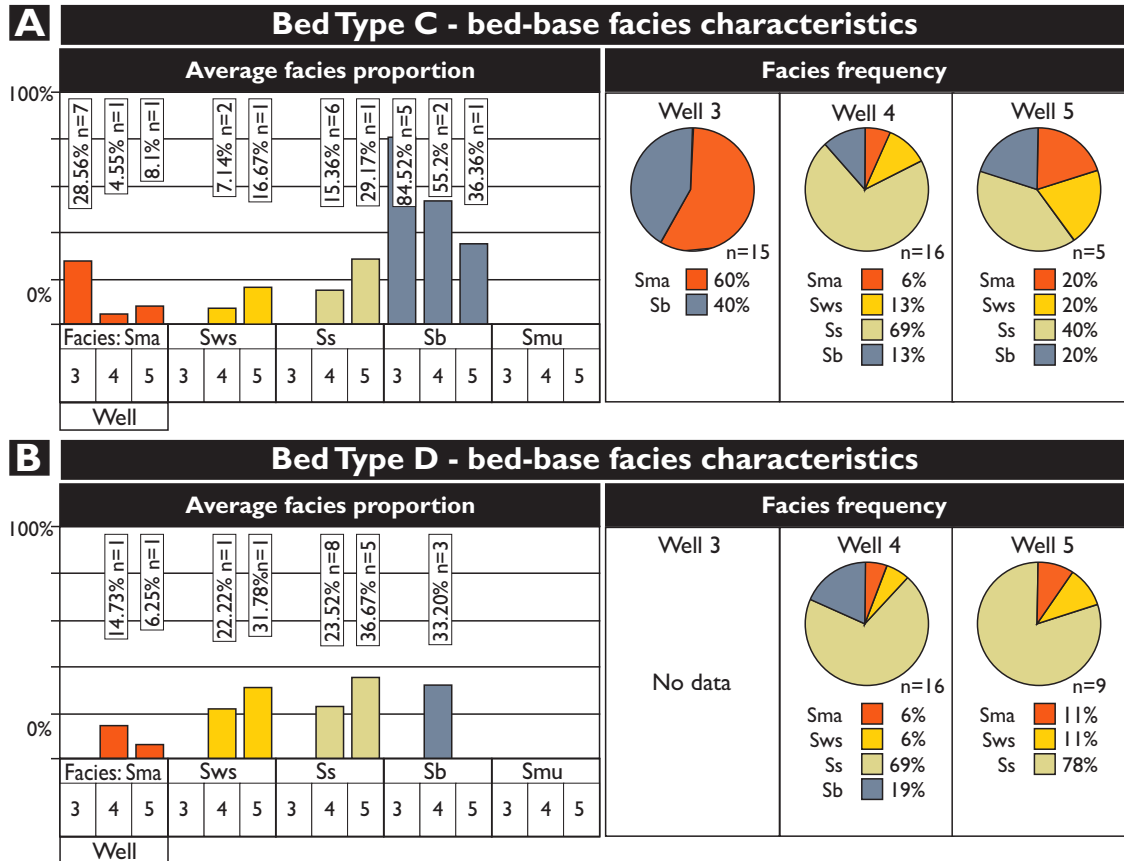


Figure 3.14. Graphs illustrating spatial variation in the average facies proportion of bed thickness (left) and facies frequency (right) of facies types present at the base of Type C (A) and Type D (B) beds in Wells 3, 4 and 5. Bed-basal facies are defined as those overlying mudstones or definitive amalgamation surfaces. Facies Smu does not occur as a bed-basal facies in Type C or D beds. In Type C beds, bed-basal occurrences of facies Sma and Sb exhibit a downstream decrease in frequency and average facies proportion from Well 3 through to Well 5 where as facies Ss exhibits the reverse with a downstream increase in frequency and average facies proportion. Similarly for Type D beds in distal Wells 4 and 5, bed-basal occurrences of facies Ss exhibit a higher frequency and average facies proportion compared to facies Sma and Sb.

Bed Type D

As previously discussed, assessment of downstream trends within Type D bed character, at a similar length-scale to Type C beds, is challenging as they are rare at Well 3. Similar to Type C beds, Type D beds can have a range of facies at the bed base (Figs 3.13, 3.14). In Type D beds, stratified sandstone is by far the most frequent basal facies type, whereas non-stratified and banded sandstone are less frequent and thinner if present at the bed base (Figs 3.13, 3.14). Such characteristics are most comparable to Type C beds in distal settings (e.g. Wells 4 and 5), thus Type D beds are considered to represent continued and relatively more distal deposition compared with Type C beds.

3.4.4.3 Stratigraphic facies trends

The aforementioned downstream variations in facies characteristics can also be expressed stratigraphically in stacked, successive event beds. Fig 3.15 shows example successions from Wells 3 and 4, which display an upwards-increase in gamma with concomitant decreases in sandstone bed amalgamation; the latter bed succession is capped by a mudstone with a sideritic cone-in-cone concretion related to a period of condensed deposition (cf. MacQuaker & Taylor, 1996). These packages are considered to represent increasingly distal deposition (e.g. a landward or axis to off-axis shift). Stratigraphically there is no significant change in grain size due to the narrow grain size range of the system. These successions, considered to represent increasingly distal deposition, display vertical facies trends in successive beds akin to those documented occurring downstream across the LS (e.g. decrease in thickness and frequency of non-stratified sandstone; increase and then decrease of banded sandstone thickness and frequency; increase of matrix-rich non-stratified sandstone thickness and frequency; Fig. 3.12, 3.14). Concomitant with the vertical replacement of Type B beds by Type C beds in Well 3, there is a successive upwards-thinning of non-stratified sandstone in favour of banded sandstone which in turn begins to thin in favour of matrix-rich non-stratified sandstones. At Well 4, within the succession of Type D beds, there is an upwards-loss of weakly stratified sandstones and thinning of banded sandstone at the expense of matrix-rich non-stratified sandstone.

3.5 Discussion

3.5.1 Hybrid flow development and sedimentary facies tracts

3.5.1.1 Insight from vertical facies arrangement within HEBs

Bed motifs (i.e. vertical facies arrangements within individual event beds), and their variation along the flow pathway, can provide insight into the character of depositing flows and their evolution during run out (Kneller & McCaffrey, 2003; McCaffrey et al., 2003; Kane et al., 2009; Stevenson et al., 2014). The vertical facies arrangement within beds emplaced by progressive aggradation beneath a moving flow provides a record of the temporal changes in character of near-bed flow, passing the deposition point. Such changes will largely reflect the longitudinal distribution of rheological zones within near-bed flow and instantaneous near-bed flow structure provided the rate of change in such flow structure is relatively low during run out (McCaffrey et al., 2003).

HEBs (e.g. Type C and D beds) are considered to have been largely emplaced by progressive aggradation (e.g. facies Ss, Sws, Sb; albeit with episodic flow freezing as an element of band formation, and potentially Sma). Late stage deposition of matrix-rich non-stratified

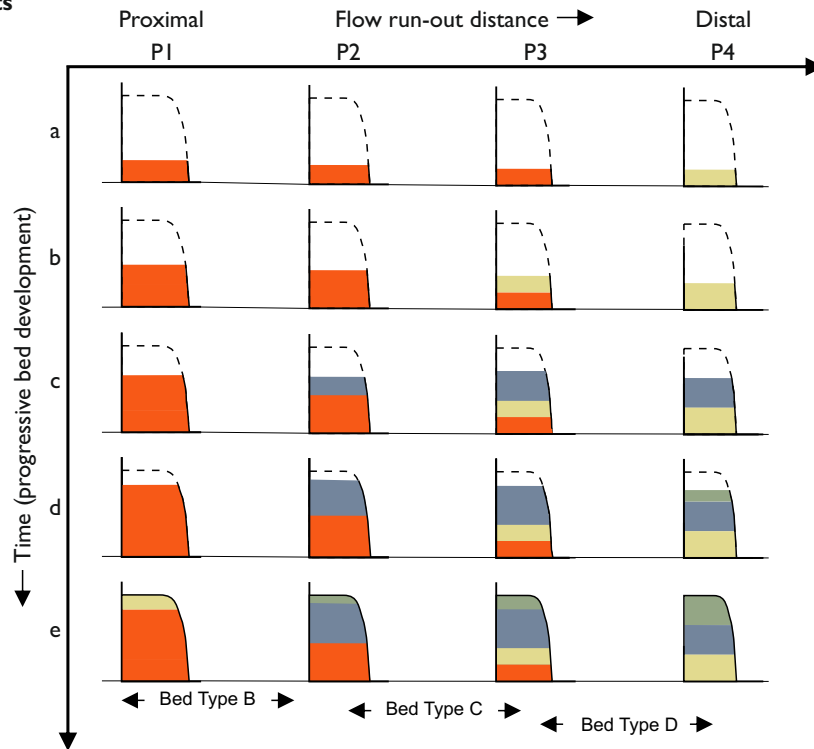
sandstone (Smu) from cohesive quasi-laminar flow occurred either incrementally, without differential-grain settling (Major, 1997), or via *en-masse* cohesive freezing. Flows emplacing Type C and D beds are considered to have been characterised by the presence of discrete rheological zones that were contemporaneous and distributed longitudinally within near-bed flow. These zones passed from clay-poor and relatively turbulent flow (facies Sma, Ss and Sws), to increasingly clay-rich transitional and quasi-laminar flow (Sb and Smu) zones from head to tail. Numerous studies focussing upon vertical and horizontal facies trends within beds in outcrop and experimental work have demonstrated the presence and evolution of multiple zones of flow state within individual gravity currents (Lowe, 1982; Fisher, 1983; McCave & Jones, 1988; Haughton et al., 2003, 2009; Talling et al., 2004; Amy & Talling et al., 2006; Barker et al., 2008; Sumner et al., 2009; Baas et al., 2009, 2011; Kane & Pontén, 2012).

Gravity currents are generally considered to be vertically stratified in terms of grain size, density, composition, and thus rheology (Garcia & Parker, 1993; Altinakar et al., 1996; Baas et al., 2009; Sumner et al., 2009). Flow stratification, whilst likely to be present, is not considered to have produced the observed bed motifs, which contain stratified sandstones indicative of incremental deposition beneath a moving flow (e.g. facies Ss, Sws and Sb), rather than *en-masse* freezing of the entire flow required to preserve vertical flow stratification structures in the deposit. The longevity of such vertical rheological heterogeneity within unconfined sub-aqueous flow is poorly understood, as experiments typically utilise open channel confined flow (cf. Baas et al., 2009, 2011; Sumner et al., 2009). Furthermore, it has been suggested that the relatively low yield strength of the “debris” flow emplacing matrix-rich non-stratified sandstone may have been insufficient to support mud clasts if located at an elevated position within the flow (Talling et al., 2012a; Sumner et al., 2009).

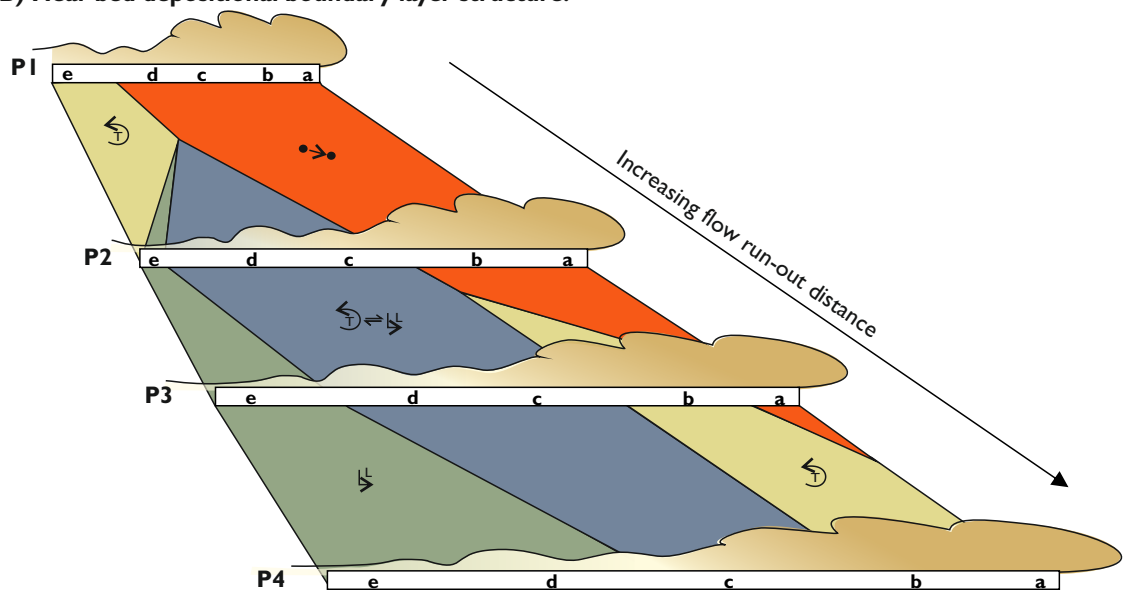
3.5.1.2 Insights from spatial bed type distributions and facies trends

Downstream and stratigraphic variations in facies presence and thickness, both between and within different beds (Types B, C and D), suggests subtle contrasts occurred in the type and significance of the rheological zones present within near-bed flow passing the depositional point (Figs 3.12-3.15). It is proposed that bed Types B to D form part of a longitudinal bed facies tract which represents longitudinal flow evolution from an initially non-cohesive relatively turbulent flow, to one characterised by an increasing proportion of transitional and quasi-laminar flow zones in the rear during basinwards run-out (Fig. 3.16). This interpretation is based upon observed downstream facies and bed type trends in addition to Type C and D



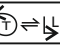

A) Deposits



B) Near-bed depositional boundary layer structure:



Character of the depositional boundary layer (near-bed flow):

-  Non-turbulent & non-cohesive flow (High-concentration flow, capacity-driven deposition)
-  Turbulent & non-cohesive flow (Low-concentration flow, competence-driven deposition)
-  Transiently turbulent-cohesive flow
-  Cohesive, non-turbulent flow

Facies:

-  Sma
-  Ss
-  Sb
-  Smu

Figure 3.16. Conceptual process model illustrating deposit accumulation **(A)** and inferred variation in the structure of near-bed flow character **(B)** at increasingly distal positions (P1-P4) along the flow pathway. The model was based on documented changes in the average proportion of facies in Type B, C and D beds (interpreted to represent increasingly distal deposit types, respectively, Fig. 3.6) and spatial changes in the average proportion of facies in individual bed types (Figs 3.12 & 3.12). During downstream run-out (P1-P4), near-bed flow character becomes increasingly heterogeneous along the length of the flow (a-e); the presence and relative importances of discrete rheological zones, and associated depositional facies, changes due to variations in either sediment concentration or the proportion of cohesive clay within the flow. Frontal regions of the flow become increasingly turbulent as sediment concentration declines where as more rearward regions of the flow become increasingly turbulence-suppressed and cohesive due to increase in the proportion of clay and flow deceleration.

bed characteristics in relation to one another, which include: 1) identical facies stacking patterns; 2) similar trends in facies characteristics in distal Wells 4 and 5 (e.g. both types show relatively thin and infrequent non-stratified and banded sandstone facies types in distal settings where matrix-rich non-stratified sandstones become more frequent and thicker); 3) increased dominance of bed Type D at the expense of bed Type C distally; and 4) Type D beds which are finer-grained and more matrix-rich compared with Type C beds (Porten et al., submitted). Thus, Type D beds are considered to represent deposition in a more distal location and a longer flow run-out distance compared to that associated with deposition of Type C beds. The increased significance of deposition from clay-rich turbulence-suppressed flow in distal settings (i.e. Facies Smu) is compliant with current models of hybrid event bed distributions within deep-water depositional systems (Haughton et al., 2003, 2009; Amy & Talling, 2006; Hodgson 2009; Kane & Pontén, 2012). Flow transformation is considered to be driven by an enrichment of cohesive clay via entrainment of muddy substrate, or relative enrichment by deposition of coarser sand fractions following deceleration (Baas & Best, 2002; Haughton et al., 2003, Talling et al., 2004, 2007a, b; Barker et al., 2008, Sumner et al., 2009); such processes may not be mutually exclusive. Type E beds, which also contain highly matrix-rich non-stratified sandstone, are not considered to be part of this facies tract as they are more frequent in proximal settings near topographic features (e.g. Wells 1 and 2, Gjallar Ridge).

A process model is presented in Fig. 3.16 for flow evolution and HEB emplacement based on facies and bed type observations made from the LS; the model represents a discrete style of evolution within the broader spectrum of flow evolutions envisaged with hybrid flow types. Flow is initially relatively clay-poor and of high concentration (e.g. high-density turbidity currents, *sensu* Lowe, 1982), being characterised by grain collisions, high sediment fall-out rates, and emplacement of Type B beds dominated by non-stratified sandstones. With clay-enrichment, a zone of transiently turbulence-suppressed flow is established, resulting in a reduction of non-stratified sandstone thickness and frequency in favour of banded sandstone (e.g. Type C beds). Concomitantly, during run-out and deposition of coarse sand fractions, the head of the flow transforms from high-concentration to low-concentration flow, characterised by fluid-turbulence grain support, lower sediment fall-out rates, and emplacement of structured sands (e.g. replacement of bed base facies Sma by facies Ss within Type C and D beds in distal settings). Rearward hydraulic fraction within this dilute turbulent suspension may have redistributed existing and entrained clay, and other low-settling velocity material (e.g. mud clasts and plant fragments), towards the rear of the flow. Such processes could be conducive to continued deposition of relatively clean sand, whilst enriching rearward regions of the flow in clay (e.g. preferentially developing more cohesive, transitional and quasi-laminar rheology in rearward flow zones). Further enhancement of clay concentration within the flow, either through entrainment or redistribution of clay, could promote the formation of a clay gel

or plug flow via clay flocculation (Blackbourn & Thomson, 2000; Baas & Best, 2002; Baas et al., 2009), to establish and progressively enhance a rearward zone of low yield strength quasi-laminar “debris” flow (e.g. leading to emplacement of matrix-rich non-stratified sandstone). Development and expansion of this quasi-laminar flow zone may drive the observed distal-most reduction of banded sandstone thickness and frequency within Type C and D beds (Figs 3.6, 3.12, 3.14), due to a reduction in the significance of the zone of transitional flow rheology responsible for banded sandstone facies (section 3.5.2.2).

3.5.2 Comparison to other studies concerning hybrid and transitional flow and associated deposits

3.5.2.1 Origin of relatively matrix-poor sandstone at bed bases

The complex flow evolution described in this study is, in part, comparable to other models concerning hybrid and transitional flows, in that deposition is interpreted to be increasingly characterised by cohesive, turbulence-suppressed flow (Haughton et al., 2003, 2009; Amy & Talling, 2006; Barker et al., 2008; Sumner et al., 2009; Kane & Pontén, 2012). In addition to these studies, the LS show a basinwards (c. 90 km) transition from non-stratified to stratified sandstone facies at the base of HEBs. Although non-stratified sandstone is most frequently documented at the base of HEBs (Haughton et al., 2003; Barker et al., 2008; Hodgson et al., 2009; Kane & Pontén, 2012), stratified bed bases have also been documented in previous studies (Amy & Talling, 2006; Talling et al., 2007b). However, downstream change between these two facies at the base of HEBs has not previously been discussed. This facies trend highlights that the earliest depositing portion of the flow (e.g. flow head) was, and remained, relatively clay-poor whilst evolving distally from a zone of high- to low-density turbulent flow (*sensu* Lowe, 1982). Such flow would remain capable of depositing relatively clean sand whilst the rear of the flow became clay-enriched, cohesive and turbulence-suppressed.

Hydraulic fractionation within the turbulent flow is thought to redistribute cohesive clay and other low-settling velocity material (e.g. mud clasts, mica, plant matter) towards the rear of the flow, suppressing turbulence once at critical concentrations (Haughton et al., 2003). HEBs of the LS are frequently enriched in such low settling-velocity material towards bed tops (Figs 3.7, 3.8). Hydraulic fractionation of clay toward the rear of the flow would limit clay concentration, and thus turbulence suppression, in the front of the flow, allowing for continued deposition of relatively matrix-poor sand and evolution from a high- to low-density turbidity current whilst the rear of the flow became clay-rich and turbulence-suppressed. Turbulent fluid scour and erosion, if occurring into a muddy substrate as observed beneath many HEBs of the LS, would introduce further clay to be fractionated rearwards within the flow, thus contributing further to potential flow transformation (Haughton et al., 2003, 2009). Studies in which HEB bases comprise non-stratified sandstone may reflect deposition in

relatively more proximal settings and that sand deposition continued further into the basin where stratified sandstone bases might be expected, provided the system was unconfined and relatively clean basal sand had been emplaced by a turbulent flow zone at the head of the flow.

Notably, Kane and Pontén (2012) documented a reverse longitudinal facies tract, inferred from repeated vertical stacking patterns interpreted as lobe progradation within the Paleogene Wilcox Formation, Gulf of Mexico. In this case, structured sandstone is replaced by non-stratified sandstone distally within bed bases. The authors also favour clay enrichment as the mechanism of flow transformation from clay-poor turbulent flow to clay-rich turbulence-suppressed flow. However, they proposed non-stratified sandstone facies represent late-stage sand settling processes (*sensu* Sumner et al., 2009). In their study, it may have been possible that the transformation from high- to low-concentration flow within the clay-poor front of the flow, as considered for the LS, was prevented by sudden or voluminous clay enrichment, which instead established cohesive (clay-rich), turbulence-suppressed flow. Dramatic clay enrichment may result from sudden flow expansion, deceleration, and deposition of coarser sand fractions (e.g. channel mouth, base of slope) or significant entrainment of muddy substrates associated with a hydraulic jump at the channel mouth (Wynn et al., 2002a). The latter process may be characterised by delayed flow transformation, as significant erosion likely requires an increase in turbulence intensity which may act against the cohesive effects of the higher concentration of clay, until eventual deceleration downstream.

3.5.2.2 Expanded thickness of banded sandstones

HEBs within the LS always contain banded sandstones (Sb), typically positioned at the junction between underlying relatively clean sandstone (Sma, Ss, Sws) and overlying matrix-rich sandstone (Smu); a position comparable to that documented in other studies (e.g. Lowe & Guy, 2000; Haughton et al., 2003, 2009; Barker et al., 2008; Davis et al., 2009; Sylvester & Lowe, 2004). In this study, banded sandstone is a greater proportion of HEB-bed thickness compared to these studies, with the notable exception of the Cretaceous, Britannia Sandstone of the North Sea (Lowe & Guy 2000; Barker et al., 2008). Haughton et al. (2009) noted that banded sandstone is more frequent within deposits of larger unconfined systems (e.g. Forties Fan ~300 km - Davis et al., 2009; Haughton et al., 2009) than in smaller systems with shorter flow run-out distances (e.g. ~20 km Upper Jurassic Miller-Kingfisher system, North Sea - Haughton et al., 2009). The authors suggested that the greater run-out distance in larger systems results in greater textural fractionation to establish more gradational contacts and zone of transitional rheology between relatively turbulent flow at the front and more cohesive flow at the rear. However in the LS, the proportion of banded sandstone in beds appears to decline in distal-most settings (Figs 3.6, 3.12, 3.13), which suggests that the significance of flow

that promoted banded sandstone can also decline with increasing run-out. Furthermore, banded sandstones within deposits of the LS are thicker than those occurring in the larger Forties Fan system, suggesting that factors other than flow run-out may have also contributed to banded sandstone emplacement (e.g. higher detrital clay concentrations present either in the initial flow, or due to greater entrainment). The decline in banded sandstone proportion in distal-most settings could correlate to the loss or weakening of a zone of near-bed turbulence-enhanced flow, as observed beneath late-stage transitional experimental flows (e.g. upper transitional plug flow and quasi-laminar plug flows with higher clay proportions or lower shear rates - Baas et al., 2009). If banded sandstone arises by such a mechanism, then their occurrence in a progressively aggraded deposit, interpreted to record longitudinally segregated flow, suggests overlap exists between conceptual models for hybrid flows (Haughton et al., 2003, 2009), and observations from clay-rich transitional flows in which flow rheology is observed to be vertically stratified (Baas et al., 2009, 2011).

3.5.2.3 *Bed-top stratified sandstones*

Numerous studies document the occurrence of bed-top planar- or current-ripple laminated sandstone overlying matrix-rich sandstone (Smu) in HEBs, interpreted as the deposits of late-stage trailing dilute turbulent flow at the rear of the flow event (Haughton et al., 2003, 2009; Amy & Talling, 2006; Davis et al., 2009). Bed-top planar or ripple-laminated sandstone overlying matrix-rich sandstone can occur in HEBs of the LS; however, their characteristics are indicative of later erosion and re-deposition by separate bottom-currents events (e.g. sharp tops, mud drapes, opposing current direction indicators, occasional internal scouring and sharp grain size contrasts to the underlying facies; Sanders, 1965). Absence of planar- or ripple-laminated sandstones associated with the same flow event emplacing facies lower within the bed suggests a late-stage trailing turbulent flow did not exist or was bypassed deeper into the basin. Distal-most deposition and switch on of the LS at the base of Well 4 consists of very fine grained and well laminated Type A beds of low-density turbiditic origin. Such beds could represent deposition of late-stage dilute turbulent flow which bypassed more proximal settings. Alternatively, it may represent distal-most deposition from the turbulent zone at the front of the flow which achieved a greater run-out distance than the sluggish, cohesive turbulence-suppressed flow (Kane & Pontén, 2012). Without high-resolution bed correlations, the origin of such sandstones cannot be explained.

3.5.3 Interaction with sea-floor topography

Well 2, positioned immediately downstream of the Gjallar Ridge, contains thick repetitive packages of dewatered, banded sandstone in both the LS and US (Fig. 3.3), which alludes to the potential overprinting effect of local topography upon flow character and deposition. Rapid flow deceleration may occur at the base of slope, or on flow expansion when exiting constrictions, such as channels, commonly incised on above-grade slopes (Clark & Pickering, 1996; Kneller, 2003). Subsequent rapid reductions in turbulence intensity would result in sudden reduction of the flow Reynolds number, and increase of flow concentration to establish a turbulence-suppressed flow (Talling et al., 2007a, b; Barker et al., 2008). Such turbulence-suppressed flow may emplace the thick, pervasively dewatered and relatively poorly sorted banded sandstone successions at Well 2 with poorly defined bedding (cf. Lowe, 1975; Vrolijk & Southard, 1997), and continue downstream as hybrid flows.

Erosion is common, both over above-grade slopes (Kneller, 2003) and at scour fields downstream of channel mouths (Wynn et al., 2002a), and if entrainment of muddy substrate occurs, this would enrich a flow's clay concentration, and hence potentially enhance further turbulence suppression and flow transformation during later deceleration downstream in distal parts of a fan. Thus, bathymetrically-driven flow non-uniformity associated with the Gjallar Ridge may provide the mechanism by which flows within the LS attained their hybrid character. Regardless of the type of mechanism, its influence appears to have been long lived in order to deposit stacked repetitive packages within the LS and US (e.g. implying a stable base of slope position or channel mouth position).

3.5.4 Influence of system evolution upon HEB distributions and proportions

A progressive decrease and sudden increase in gamma values at the base and top of the LS respectively, is considered to represent switch-on and progressive progradation, followed by sudden retreat or abandonment of the LS system (Fig. 3.2). The vertical succession of bed types representing the progressive increase in proximal forms is interpreted to represent a basinward shift of the documented longitudinal bed type facies tract, driven by system progradation which was subsequently translated into a stratigraphic distribution (i.e. Walther's Law, Middleton, 1973). System retreat would result in a return to distal bed types (Type A and D beds). However, if such retreat were rapid or absent (e.g. system abandonment), then successions of such beds in the late stages of the system would be limited in thickness, or absent, as in the case of the LS. The depositional consequence of such rapid abandonment is a relatively lower overall proportion of HEBs present within the earlier progradational phase, compared to other systems that might have experienced more prolonged periods of retreat prior to abandonment (Fig. 3.17). Thus, variations in the frequency, magnitude, and rate of system progradation and retrogradation events will contribute to both the distribution and

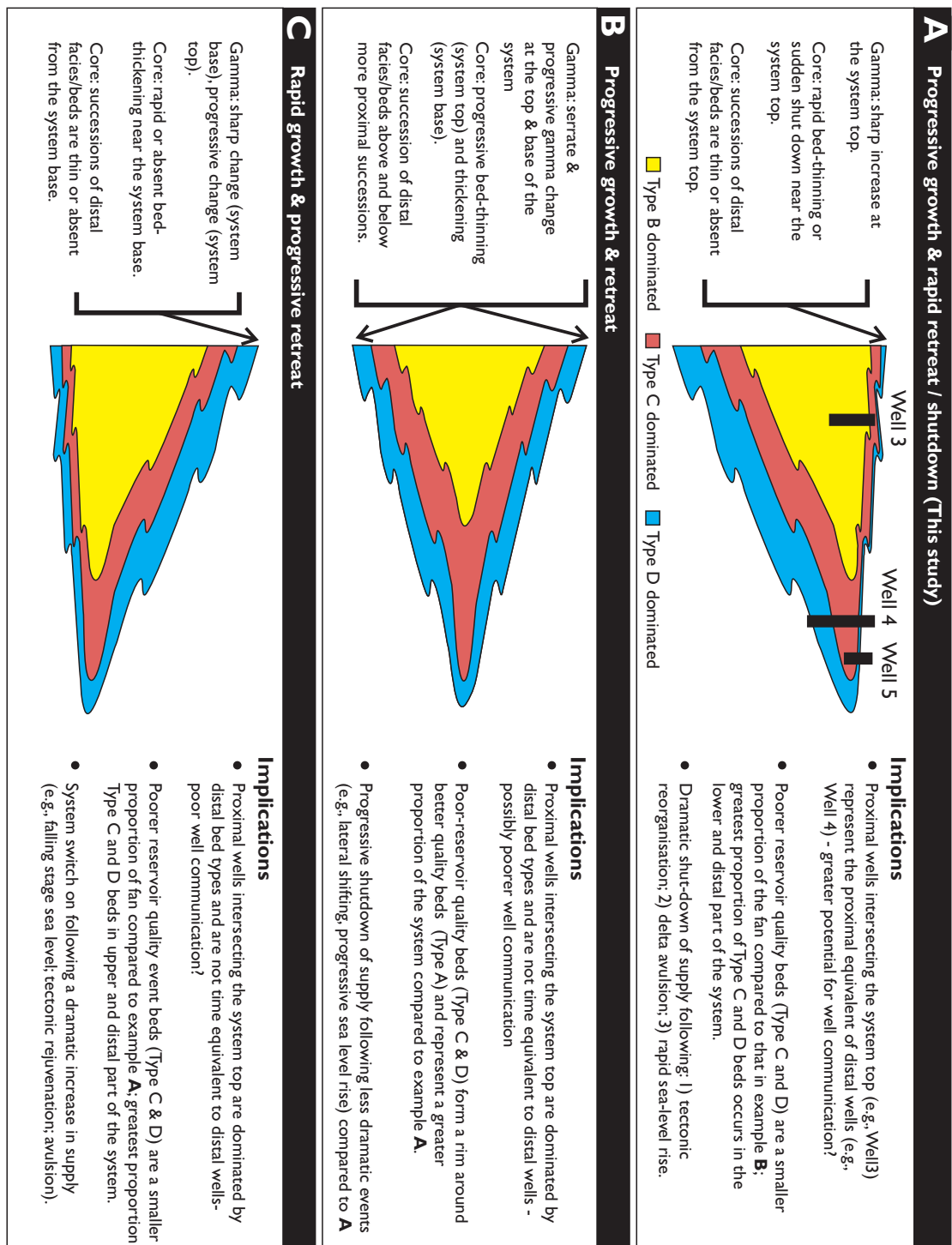


Figure 3.17. In HEB-prone systems, the relative rates of system progradation and retreat could influence the distribution and proportion of transitional deposits within the fan system. Systems with comparable phases of progradation and retrogradation have a more even distribution of transitional deposits (**B**) compared to systems in which one phase is more prolonged (**A,C**).

overall proportion of HEBs within a deep-water system (cf. Hodgson et al., 2009). Such patterns may also be expressed in small-scale cycles of progradation and retreat. Documentation of the stratigraphic distribution of HEBs in core can therefore provide insight into evolution of deep-water systems, and allow predictions of reservoir quality and distribution.

Although the documented bed type facies tracts and distributions have been discussed as a single downstream flow evolution, it is also possible that a temporal change to progressively relatively clay-poorer flow types could replicate the observed stratigraphic distribution of bed types rather than progradation of the system. It may be that progressive temporal reduction of clay within successive flows drives a reduction in the significance of the zone of cohesive flow in the rear of the flow which is translated as a reduction in the proportion of facies Smu in successive beds. Confident differentiation between stratigraphic facies changes driven by system progradation and those driven by temporal change in bulk flow character is not permitted by the data set available in this study; further, both processes have the potential to influence stratigraphic trends in combination with one another.

3.6 Conclusions

The range in HEB depositional character, and gravity currents as a whole (both within this study and in comparison to existing HEB studies), reflects the complexity of flow transformation (e.g. style, rate and magnitude) inherent in sedimentary systems controlled by a complex interplay of allogenic and autogenic controls. Distinct flow-event states (expressed in the variable character of discrete internal rheological zones) have potentially subtle differences in their run-out abilities, which will govern the size and shape of depositional elements as well as the distribution of depositional facies, and thus reservoir quality.

Analysis of spatial changes in bed character, both stratigraphically and geographically, within progressively aggraded deposits has highlighted the following:

- 1) the occurrence of discrete rheological zones within near-bed flow structure, whose relative importance evolved during flow run-out giving rise to a hybrid flow during a complex evolution of longitudinal flow structure;
- 2) the evolution of rearward regions of the flow from relatively clay-poor and turbulent to become increasingly transitional, clay-rich (cohesive), and turbulence-suppressed;
- 3) headward regions of the flow remained clay-poor with a decrease in sediment concentration driving an increase in downstream turbulence (e.g., a high- to low-density turbidity current evolution *sensu* Lowe, 1982);
- 4) flows may have been primed for transformation on meeting the base of slope or exiting the mouth of a channel near the Gjallar Ridge, due to the potential for extensive erosion of muddy substrates and rapid flow deceleration in such settings (Wynn et al., 2002a);

- 5) the frequency, rate, and magnitude of system progradational and retrogradational events contribute to both the distribution (geographically and stratigraphically), and proportion of HEBs within a system;
- 6) understanding transport and depositional processes of deep-water sandstones allows for the development of predictive facies and reservoir-quality models with utility in exploration and development phases;
- 7) the classification of gravity currents and their deposits in deep-water settings is proving ever more challenging as increasing data quality and density from the distal parts of deep-water fans illustrate the variability of HEB deposits.

Chapter 4. Influence of confining topography upon hybrid event bed character and distribution in a confined basin setting: insights from the Edale Basin, Carboniferous, U.K.

4.1 Introduction

Chapters 4 and 5 present an outcrop study of the Carboniferous (Pennsylvanian) deep-water infill of the confined, uncontained Edale Basin, N England (Fig. 4.1). Both chapters were written as manuscripts intended for publication. Chapter 4 provides an overview of the geological setting and relevant previous studies, as well as detailed facies and bed type descriptions and interpretations which are also relevant to Chapter 5. Chapter 4 focusses primarily on the character and distribution of HEBs in the Mam Tor Sandstones (MTS), with respect to a downstream confining basin margin (Fig. 4.2) whereas Chapter 5 details stratigraphic variations in occurrence of HEBs in both the MTS and the overlying Shale Grit Formation.

HEBs are common in the distal regions of deep-water systems, with a downstream transition from turbidite to HEB deposits occurring over relatively long distances (typically across 10 to 10s of km - Haughton et al., 2003, 2009; Amy & Talling, 2006; Hodgson, 2009; Kane & Pontén, 2012; Chapter 3; Fig. 2.21a). Such variation in depositional character is typically observed in unconfined settings where sea-floor topography was lacking or subdued, or where the size of the sedimentary system was small compared to that of the receiving basin (Haughton et al., 2009; Amy & Talling, 2006; Hodgson, 2009; Kane & Pontén, 2012; Fonesu et al., 2015). This commonly recognised facies tract is useful for the prediction of facies variation, and thus of reservoir quality in the sub-surface. However, shorter length-scale variations between turbidite and HEB have also been recognised, where flows interact with relatively more complex, confining sea-floor topography (Barker et al., 2008; Davis et al., 2009; Patacci et al., 2014).

HEB development has been suggested to be delayed or promoted by subtle changes in the degree of flow constriction between sea-floor features (e.g. diapirs) exhibiting positive relief (e.g. Palaeocene, North Sea, Davis et al., 2009), as well as subtle changes in sea-floor gradient and associated flow deceleration, or renewed entrainment (e.g. modern sea-floor, NW Africa - Talling et al., 2007a; Marnoso Arenacea, Miocene, N Italy - Magalhaes & Tinterri, 2010). HEBs have also been documented in confined, uncontained basins (Fig. 2.15b) adjacent to confining basin margins (e.g. Britannia Sandstone Member, Aptian, North Sea - Barker, 2008; Braux Unit, Annot Sandstone, Eocene, SE France - Patacci et al., 2014). In these cases deposit depositional variations, expressed as a transition from turbidite to HEB (i.e. development and



Figure 4.2. Viewpoint from Castleton Valley demonstrating the location of the Mam Tor succession and onlap of the Mam Tor Sandstones and Edale Shales onto the downstream southern confining basin margin. The basin margin is cored by a Carboniferous carbonate system (Derbyshire Massif) which was fringed by steeply dipping fore-reef slopes. Prior to deep-water clastic infill of the Edale Basin this margin was draped by mudstones of the Edale Shale but retained its relief as a prominent confining basin margin based on palaeoflow (Fig. 4.1) data and the lack of contemporaneous strata in downdip basins.

thickening of a matrix-rich sandstone facies in the bed), occur over relatively short distances towards, and adjacent to, the confining topographic feature (~2 km, Barker et al., 2008; <1 km, Patacci et al., 2014; Fig. 3.32). In these studies, flow deceleration (“flow depletion” *sensu* Kneller 1995), forced by run-up or lateral thinning onto the confining slope, were proposed to result in suppression of turbulence, flow transformation, and the deposition of HEBs containing relatively matrix-poor and overlying matrix-rich, sometimes mud-clast-rich, sandstone (Barker et al., 2008; Patacci et al., 2014). The recognition of such localised and short length-scale facies tract variations, where deposits onlap confining topography, is of considerable significance as stratigraphic traps commonly form attractive targets in sub-surface hydrocarbon systems (McGee et al., 1994; Winker, 1996; Pettingill, 1998; Barker et al., 2008).

This chapter focusses primarily on the character and distribution of HEBs in the MTS Sandstones, with respect to a downstream confining basin margin where flows were locally deflected (Figs 4.1c, 4.2). Two outcrops expose strata of the MTS situated within 1 km of their onlap onto the downstream confining basin margin (Mam Tor and Hope Quarry, Figs 4.1c, 4.2). At Hope Quarry, numerous variously orientated quarried cuts at multiple stratigraphic levels allow for an assessment of HEB character and distribution locally (up to within 1 km of the confining margin). Furthermore, smaller exposures of MTS located c. 7 km upstream of the confining basin margin allows for an assessment of HEB character and distribution over a longer length-scale (Wicken and Ashop, Fig. 4.1c). Despite palaeoflow indicators near the basin margin recording the long-lived effects of flow confinement (Fig. 4.1c), it can be shown that HEBs are not localised within a narrow region near onlap onto this confining topographic feature as documented in previous studies (Barker et al., 2008, Patacci et al., 2014). Specific study objectives are as follows:

- 1) to assess the character and distribution of HEBs within the confined Edale Basin in order to determine their relationship with a downstream confining basin margin;
- 2) to evaluate potential mechanisms for the origin of matrix- and mud-clast-rich sandstone facies within HEBs, including processes potentially associated with local flow confinement by the basin margin;
- 3) to explore how variations in basin physiography and associated flow run-out distances influence the character and distribution of HEBs, and depositional reservoir quality within basin infill successions.

4.2 Geological setting

4.2.1 Regional geological framework

The Edale Basin is one of several linked sub-basins that together form the Pennine Basin – the central part of the larger Central Pennine Province of northern England, which formed a broad depositional area during the Carboniferous (Collinson, 1988; Hampson, 1997; Fig. 4.1a). The Central Province formed in response to Late Devonian – Mississippian back-arc rifting related to the Variscan Orogeny, which established a network of rapidly subsiding extensional fault-bounded basins in which deep-water mudstone accumulated, whilst shallow-water carbonates accumulated atop intervening structural highs (Leeder, 1982, 1988; Collinson 1988; Lee, 1988; Gutteridge, 1991; Fraser & Gawthorpe, 2003). By the Late Mississippian, a significant sediment supply was sourced from Laurentia-Baltica to the distant northeast (Gilligan, 1920; Hallsworth et al., 2000; Morton & Whitham, 2002), which initiated infilling of the northern region of the Pennine Basin (Pendleian, Craven Basin - Collinson 1988; Martinsen, 1990, 1993, 1995; Kane et al., 2010b); by contrast, central and southern regions, including the Edale Basin, remained starved of siliciclastic detritus at this time (Collinson, 1988; Walker, 1966a). Infill of the Pennine Basin occurred via a series of turbidite-fronted deltas when sediment supply was initiated; channels bypassed sediment over the delta slope to feed deeper-water fan systems (Walker, 1966a; Collinson, 1988; Hampson et al., 1999). Sediment delivery to the deep-water basin depocentres was strongly influenced by inherited rift bathymetry, with successive infilling of sub-basins occurring in a southerly step-wise manner (Allen, 1960; Walker, 1966a; Jones, 1980; Collinson, 1988; Martinsen et al., 1995; Kane et al., 2010b).

The Edale Basin was c. 25 km in length (Allen, 1960; Walker, 1966a), with water depths of up to several hundred metres (Collinson, 1988), and was fed by sediment from the north-northeast (Gilligan, 1920; Walker, 1966a). The northern feeder slope was likely to be steep, considering its relatively recent formation and configuration as an up-thrown footwall block, capped by a carbonate ramp which was then later draped by deep-water mudstones of the Edale Shales (Fig. 4.1b). The downstream, southerly limit of the Edale Basin was delineated by a

high relief basin margin comprising an up-thrown fault block and its capping carbonate system (the Derbyshire Massif - Leeder, 1982; Lee, 1988), fringed by steeply dipping (20 to 27° inclined) fore-reef talus slopes (Wolfenden, 1958; Fig. 4.1c). This carbonate system was then draped by deep-water mudstones of the Edale Shale prior to siliciclastic basin infill during the Kinderscoutian (Collinson, 1988; Lee, 1988; Gutteridge, 1991; Fig. 4.1b). Due to insufficient outcrop, the lateral limits of the basin and location of lateral confining basin margins to the east and west are poorly constrained. Although palaeocurrent data collected across the study area do not indicate the local presence of lateral basin margins (Fig. 4.1a), such margins are expected to have been present further afield, considering the block-basin topography which characterised the Pennine Basin (Leeder, 1982; Lee, 1988).

4.2.2 Stratigraphy

By the end of the Alportian (Serpukhovian; 318.1 Ma), active rifting had largely given way to extensive regional thermal subsistence (Lee, 1988; Leeder & McMahon, 1988; Fraser & Gawthorpe, 2003). By the beginning of the Kinderscoutian (~318.1 Ma), more northerly sub-basins had largely been infilled, and the Lower Kinderscoutian delta occupied a position just north of the Edale Basin (Reading, 1964; Collinson, 1969, 1988; Hampson et al., 1999). Clastic sedimentation in the under-filled post-rift setting of the Edale Basin commenced with the deposition of the MTS and overlying Shale Grit Formation (Fig. 4.1b). Together, these units represent the deposits of sediment gravity flows in a relatively deep-water basin floor and base-of-slope setting, sourced from the approaching Kinderscoutian delta to the north (Allen, 1960; Walker, 1966a, b).

The Edale Basin was largely infilled by the Lower Kinderscoutian turbidite-fronted delta during the Kinderscoutian (R1c; Fig. 4.1), which emplaced a shallowing-upwards succession up to 600 m thick (Walker, 1966a). This succession comprises four lithostratigraphic units (Fig. 4.1b) which record a change from distal and relatively more proximal sedimentary gravity flow sedimentation on the basin floor and base-of-slope (MTS and Shale Grit Formation, respectively - Allen, 1960; Walker, 1966a, b), to delta-slope and shallow-water delta deposition (Grindslow Shales - Walker, 1966a; Collinson, 1969; McCabe, 1977), culminating in delta-plain deposition (Lower Kinderscout Grit - Reading, 1964; Collinson, 1969; McCabe, 1977; Hampson et al., 1997). The absence of time-equivalent deep-water strata in the North Staffordshire Basin directly to the south of the Derbyshire Massif (Fig. 4.1a), highlights the long-lived confining effect of the southern basin margin; when the Edale Basin was eventually infilled, more extensive shallow water sheet-like delta systems were established (e.g. Rough Rock - Bristow, 1993). Although the UK Carboniferous succession contains numerous laterally extensive goniatite-bearing marine bands, permitting regional correlation of sand bodies across northern England (Aitkenhead et al., 2002), such marine

bands and other distinct markers are absent from the MTS and Shale Grit; as such, the internal division and correlation of these units across the Edale Basin is problematic.

4.3 Data and methods

HEBs of the MTS outcrop in the north of the basin (Wicken and Ashop river cuts) and further south near to the downstream confining basin margin (Mam Tor and Hope Quarry [HQ]; Fig. 4.1c). At these localities detailed sedimentological logs (cumulative total 379 m, ranging from 1:5 - 1:10 scale) were collected, with a view to characterise the constituent facies within beds in terms of their lithology (composition and texture), sedimentary structures, vertical arrangement, relative proportion of total bed thickness, and the geometry of contacts between facies. Palaeocurrent readings (n=1119) were measured from sole structures (flute casts, groove and prod marks) and current ripple laminations from the MTS and lower Shale Grit at various localities across the Edale Basin (Fig. 4.1c).

In addition, laterally offset logs at HQ (Ordnance Survey SK 17650, 82750) were used to construct transects of individual beds, in order to: (1) characterise the lateral variability of depositional character; and (2) ascertain the presence of shorter length-scale trends with respect to increasing proximity towards the confining basin margin (Fig. 4.1c). Here, the lower MTS outcrop locally (c. 1 km) near the confining basin margin, and were traced laterally over distances up to c. 770 m where the exposure allowed, by walking out individual beds and correlating tabular successions cropping out on a series of variably-orientated quarried ledges. The orientation of mud-clast a-axes, or their vergence where folded, were measured from two beds to discern any preferential distribution that could elucidate on the origin of the mud-clast-rich division commonly found in HEBs.

4.4 Facies and deposit types of the Mam Tor Sandstones and Shale Grit Formation

Fig. 4.3 summarises detailed descriptions and provides processes interpretations for the ten facies types recognised in both the MTS and Shale Grit Formation. The association and organisation of these facies with respect to seven commonly occurring bed type groups is displayed in Fig 4.4.

4.4.1 Type A and B beds

Description. Type A and B beds are distinct from other bed types in that they contain a distinct, thick mud-clast-rich division in addition to a range of matrix (clay)-rich sandstone facies (Figs 4.5, 4.6a,g,i). Type A and B beds are thick- to very thick-bedded (0.4-2.8 m) and comprise: 1) a basal, variably matrix-rich, relatively mud-clast-poor sandstone (facies CS-U, Fig. 4.3a; facies AS-Cla, Fig. 4.3d); 2) a distinct mud-clast-rich division (facies HAS-Cla, Fig. 4.3f), ranging from

22 - 67% of the bed thickness; and sometimes 3) a relatively thin cap of very fine-grained laminated sandstone (facies AS-L or CS-L, Fig. 4.3b, e; <<10% bed thickness) that can load into the underlying mud-clast-rich division. The lower sandstone division is typically fine- to

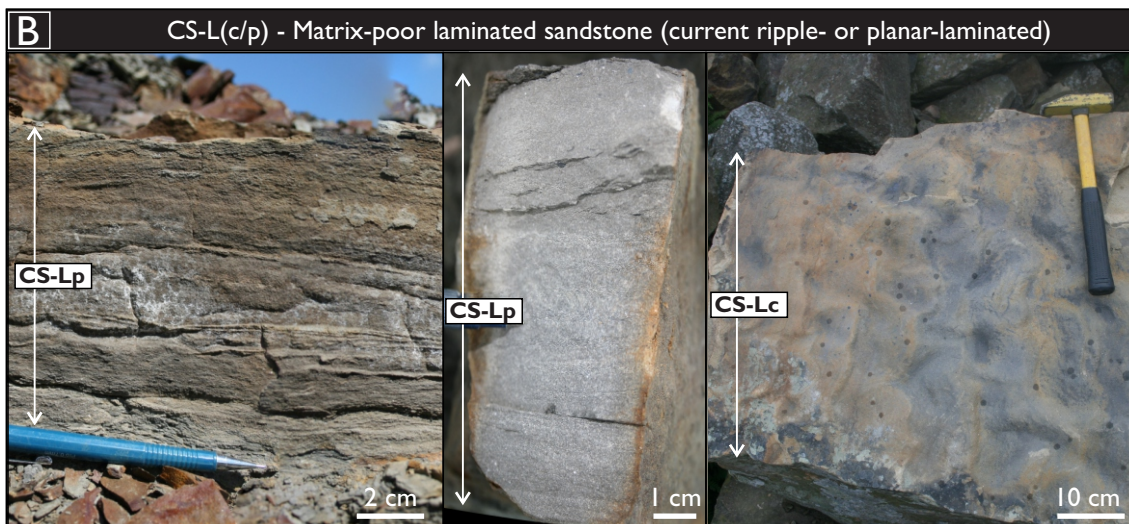


CS-U - Matrix-poor non-stratified sandstone

F grained (VFu - C); Non-stratified, moderate-well sorted, framework supported sandstone with crude normal grading and a relatively low proportion of clay, mud-clasts and carbonaceous material. Centimetre to decimetre scale mud-clasts (<10% vol) are sub-rounded and typically sub-parallel to bedding. Flute casts, groove and prod marks are common. Sub-vertical dewatering pipes (CS-Ud) can occur. Common in a range of bed types but dominant facies in Type G and many Type A beds.

Process

1) Rapid deposition or en-masse freezing of high concentration SGF dominated by grain interactions and hindered settling (e.g. concentrated flow sensu Mulder & Alexander; [2001]). 2) Basal flow with hindered settling. 3) Suspension fall-out from steady, dilute, turbulent sediment gravity flow (e.g. Bourma Ta, Bourma [1962]).



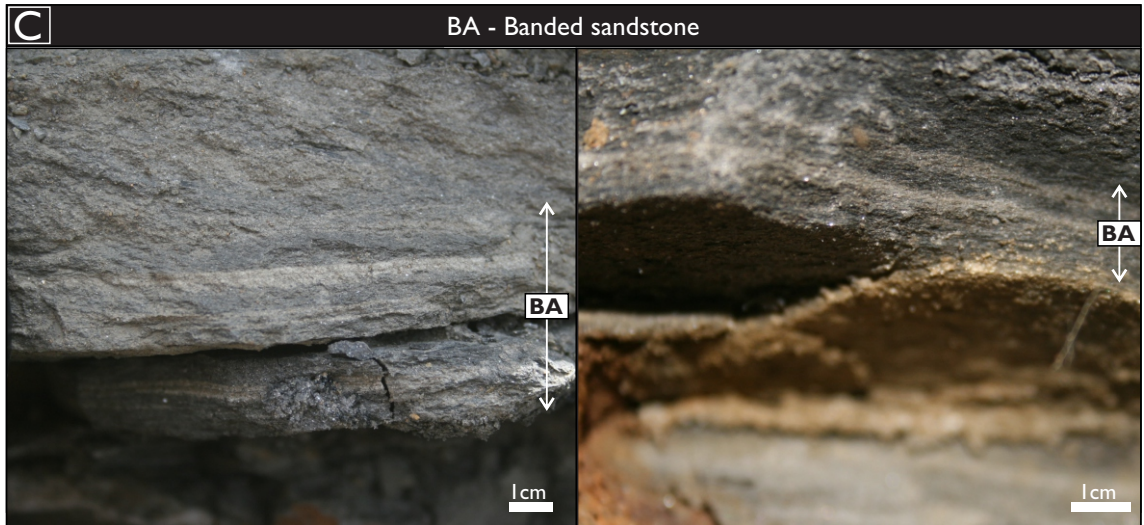
CS-L(cp) - Matrix-poor current ripple- or planar-laminated sst.

F grained (VFu - C); Laminated moderate- to well-sorted, framework supported normally graded sandstone with current-ripple lamination (<1 cm height, <6 cm wavelength; CS-Lr) or planar- to undulated lamination (<0.5 cm thick; CS-Lp). Mud-clast and carbonaceous material (<10% vol) are aligned sub-parallel with lamination. Typical occurrence in Type F beds, thin caps in Type G beds. CS-Lp can be present in the base of some Type A beds.

Process

1) Relatively dilute, non-cohesive turbulent flow capable of tractional bed form generation during waning of flow (e.g. Bourma Tb & Tc [Bourma, 1962]).

Figure 4.3 (continued overleaf). Photo examples, detailed descriptions and inferred process interpretations of lithofacies found in deposits of the Mam Tor Sandstone and Shale Grit Formation.

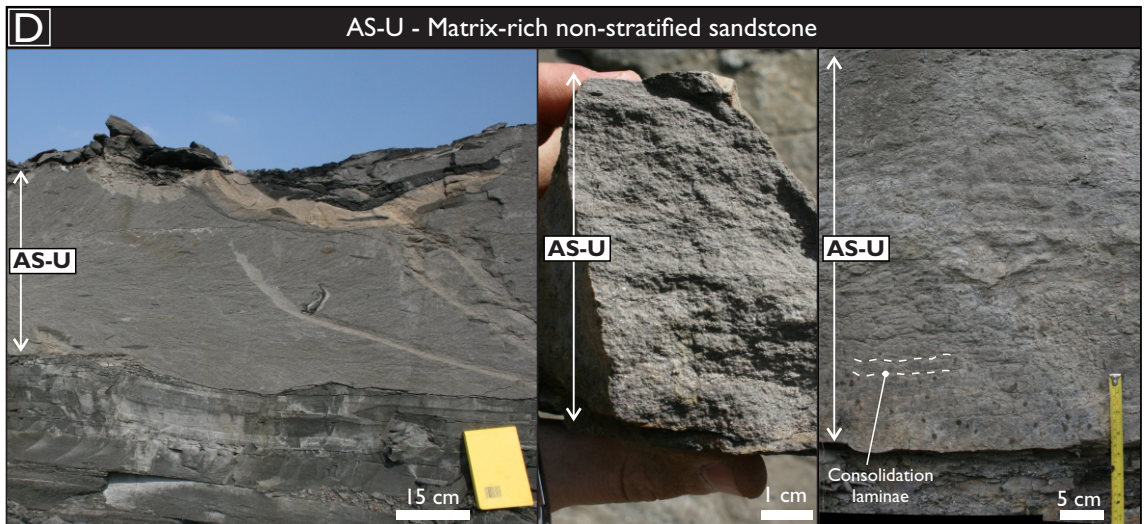


BA -Banded sandstone

F₁ grained (VF-M); Sandstone with alternating dark and light coloured bands on a millimetre scale. Dark bands are enriched in clay and carbonaceous material and exhibit internal shearing whilst light bands exhibit loaded bases into the underlying dark band. Typical occurrence as thin (<5cm) bed basal facies in Type B beds.

Process

Fluctuation between turbulent suppressed quasi-cohesive and more turbulent flow conditions following cycles of poor and improved sediment mixing affecting near-bed clay concentrations (Lowe & Guy, 2000; Baas et al, 2005) or turbulence enhancement beneath turbulence suppressed flows (Baas et al, 2011).



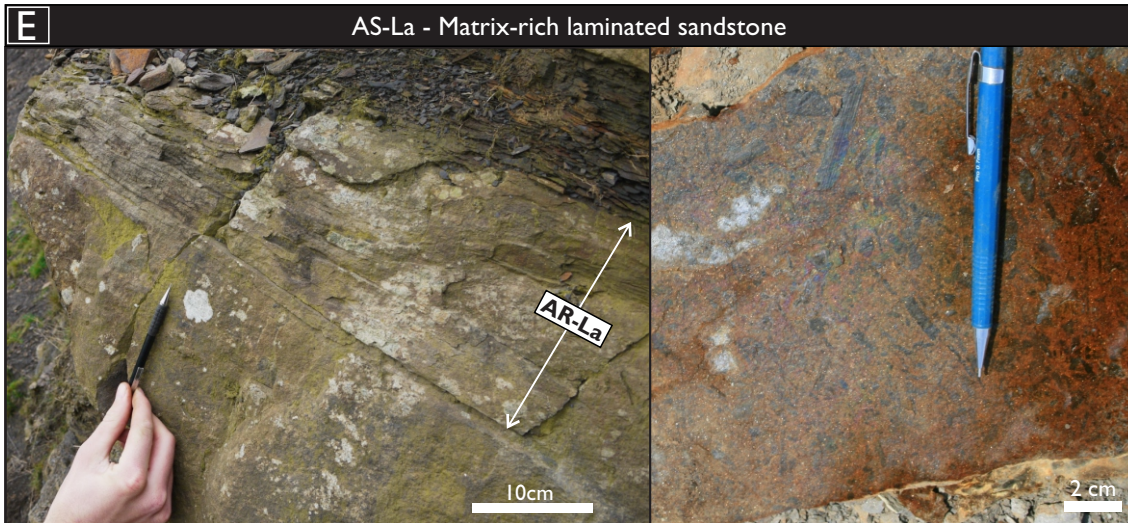
AS-U(d) - Matrix-rich non-stratified (dewatered) sandstone

F₁ grained (VFu – C); Non-stratified, poor- to moderately-sorted framework supported sandstone with crude normal grain size grading and a high proportion of clay and millimetre scales mud-clasts and carbonaceous fragments. Centimetre to decimetre scaled mud-clasts (<20% vol.) are sub-rounded to sub-angular and are variably orientated with respect to bedding. Larger out-sized mud-clasts (>3 cm) can exhibit a vertical increase in frequency. Groove and prod marks are more common than flutes casts. AS-Ud exhibit randomly distributed sheared ‘streaks’ (<8 cm across) of paler, clay-poorer dewatered sandstone of similar grain size to the host. Coarsest sand fractions can be concentrated near the bed base. Dominant facies in Type B beds.

Process

Deposition from turbulence-suppressed relatively cohesive (clay-rich) flow in which tractional bed-form generation was not possible (Baas et al, 2009; Sumner et al, 2009). The yield strength of the flow was sometimes incapable of supporting the coarsest sand fractions where concentrated at the base of the bed (see Marr et al, 2001; Sumner et al, 2009). Dewatered examples may record higher water contents or faster deposition trapping greater interstitial fluid and susceptibility to syn- or post-depositional dewatering.

Figure 4.3. ctd.

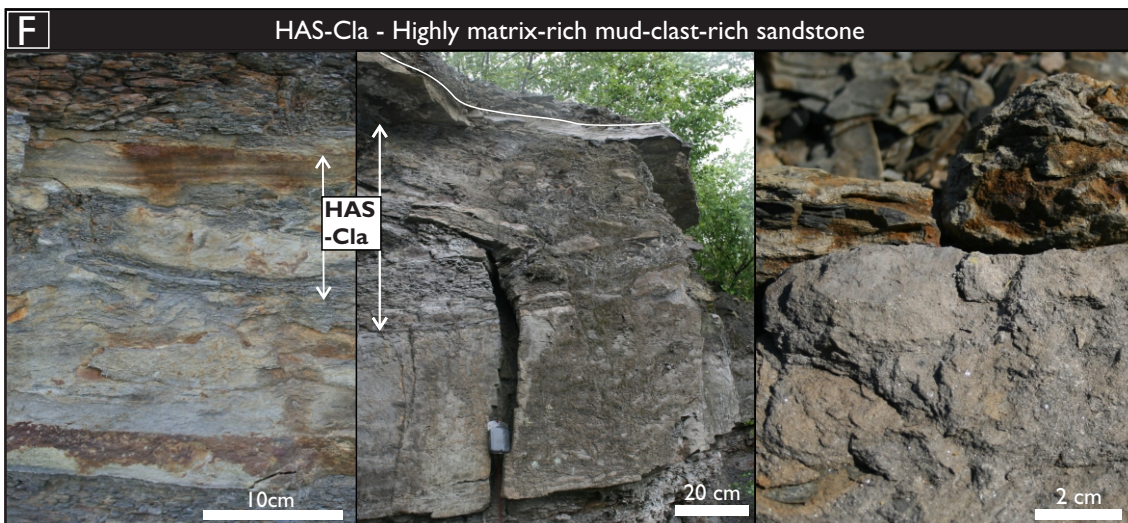


AS-L - Matrix-rich stratified sandstone

Vfu grained (VF-M); Moderately-sorted, framework supported sandstone with weak normal grading. Bedding parallel laminations form splitting planes enriched with disseminated carbonaceous material, mica platelets and millimetre scaled mud-clasts. Typical occurrence as upper bed facies.

Process

Quasi-laminar-cohesive flow of lower yield strength compared to AS-U such that crude stratification and alignment of clasts and plant fragments sub-parallel to bedding was possible. Perhaps with lesser degrees of turbulence suppression.



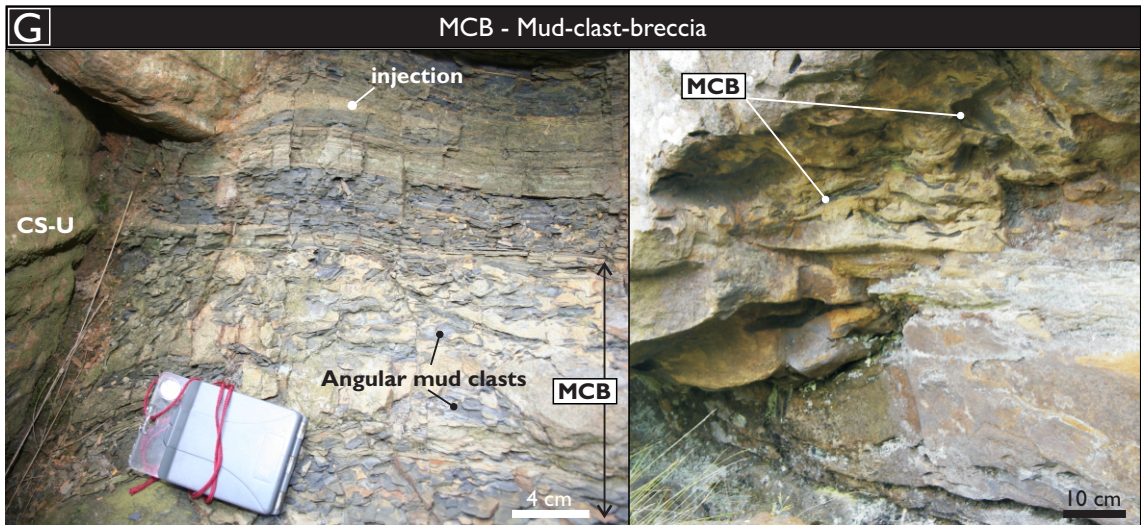
HAS-Cla - Highly matrix-rich mud-clast-rich sandstone

F grained (VFu - C); Chaotic arrangement of mud-clasts (cm to m-scaled) and carbonaceous fragments supported in highly argillaceous, mica-rich sandstone. Mud-clasts range from millimetre to metre scaled in length, are chaotically arranged and can be steeply inclined with respect to bedding (<math><70^\circ</math>). Longer decimetre to metre scaled clasts can be bulked or folded over: HAS-Cla is never present as a bed base facies, does not transition laterally into intact mudstone and is often injected from underlying facies (AS-U or CS-U) and loaded by overlying facies (AS-L).

Process

Most cohesive and turbulence-suppressed flow state due to the high proportion of clay and mud-clasts. Subsequently free movement of grains and bed traction are hindered whilst large mud-clasts are supported and sheared during transport. Repeated occurrence above AS-U or CS-U suggests strong temporal linkage between these facies and suggests mud-clasts were supported in the rearward portion of a progressively depositing flow or upper part of a flow depositing en-masse. Fully laminar and cohesive flow (high-yield strength debris flow sensu Talling 2013) is not thought to occur as mud-clasts do not protrude from bed tops and HAS-Cla is laterally continuous over 100s m within individual beds.

Figure 4.3.ctd.



MCB - Mud-Clast breccia

M graded (Fu – C); Discontinuous lenses of well-sorted, mud-clast-rich, framework supported sandstone winnowed of clay and finer sand grade material. Mud-clasts are elongate, sub-angular and may be partially attached to the local substrate. Typical occurrence above incision surfaces.

Process

Basal-lags following local and upstream erosion and winnowing beneath high capacity (sensu Kneller, 1995), largely bypassing sedimentary gravity flows.



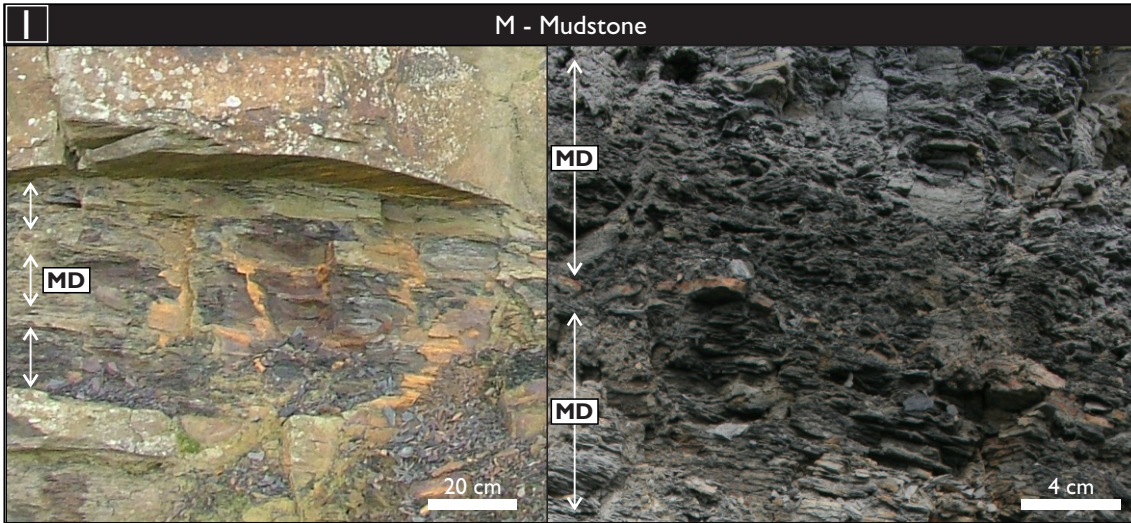
MD – Mud-dominated packages with thin fine grained sand laminae and beds

Mud dominated packages containing thin, very fine grained sandstone as starved ripples or planar laminated silts. Association with incision surfaces of facies MCB.

Process

Packages recording significant sediment bypass downstream with deposition from dilute flow tails (Mutti & Normark, 1987; Hubbard et al, 2014).

Figure 4.3. ctd.



M - Mudstone

Process

Clay-silt; Massive fissile mudstones punctuated by occasional silty or very fine Background hemi-pelagic sedimentation and late stage SGF sand laminae or thin beds. Relatively thick homogeneous mudstone dominates suspension fall-out punctuated by SGFs. the Edale Shales and contains a goniatite bearing marine band (Reticuloceras.reticulatum) locally at the junction with the overlying Mam Tor Sandstones.

Figure 4.3.ctd.

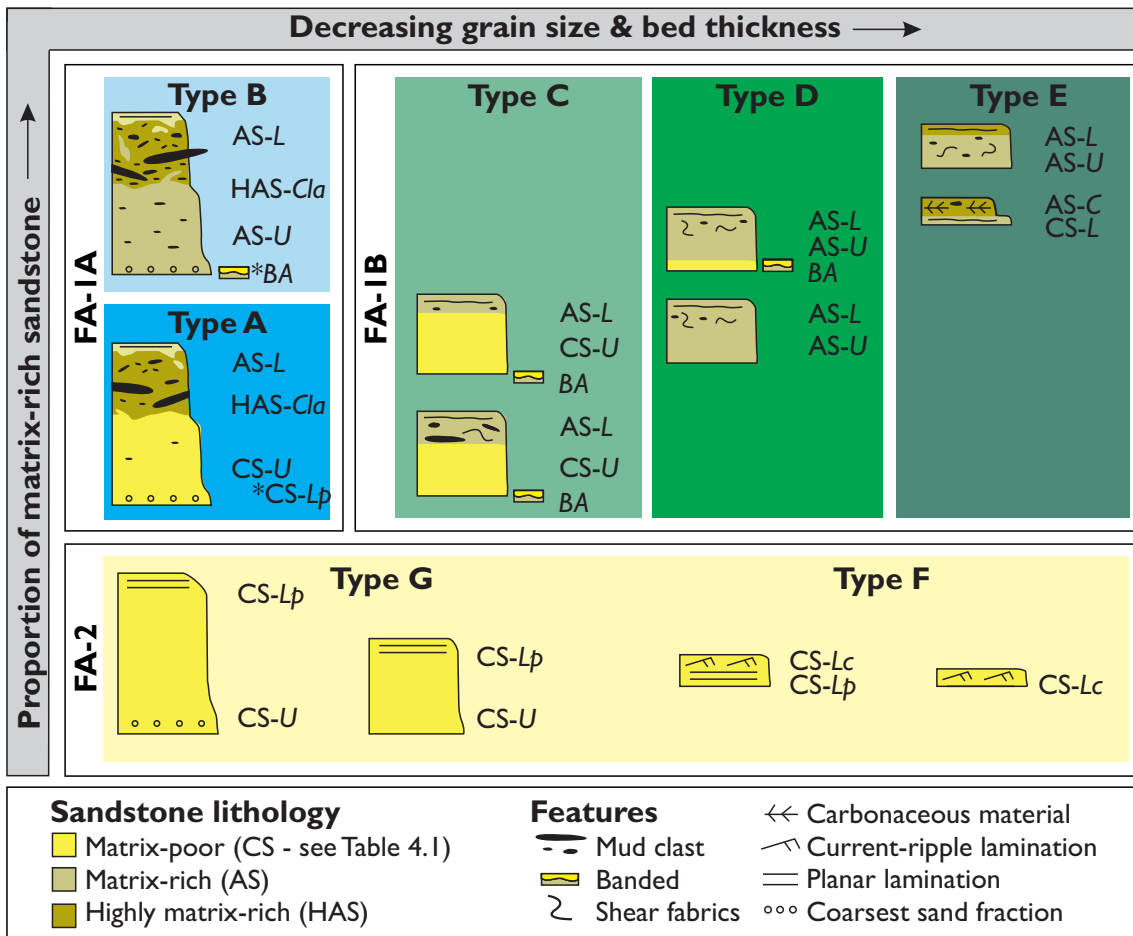


Figure 4.4. Bed types and their facies associations (FA-1A, FA-1B & FA-2) arranged according to grain size, bed thickness and the proportion of matrix-rich sandstone within the bed.

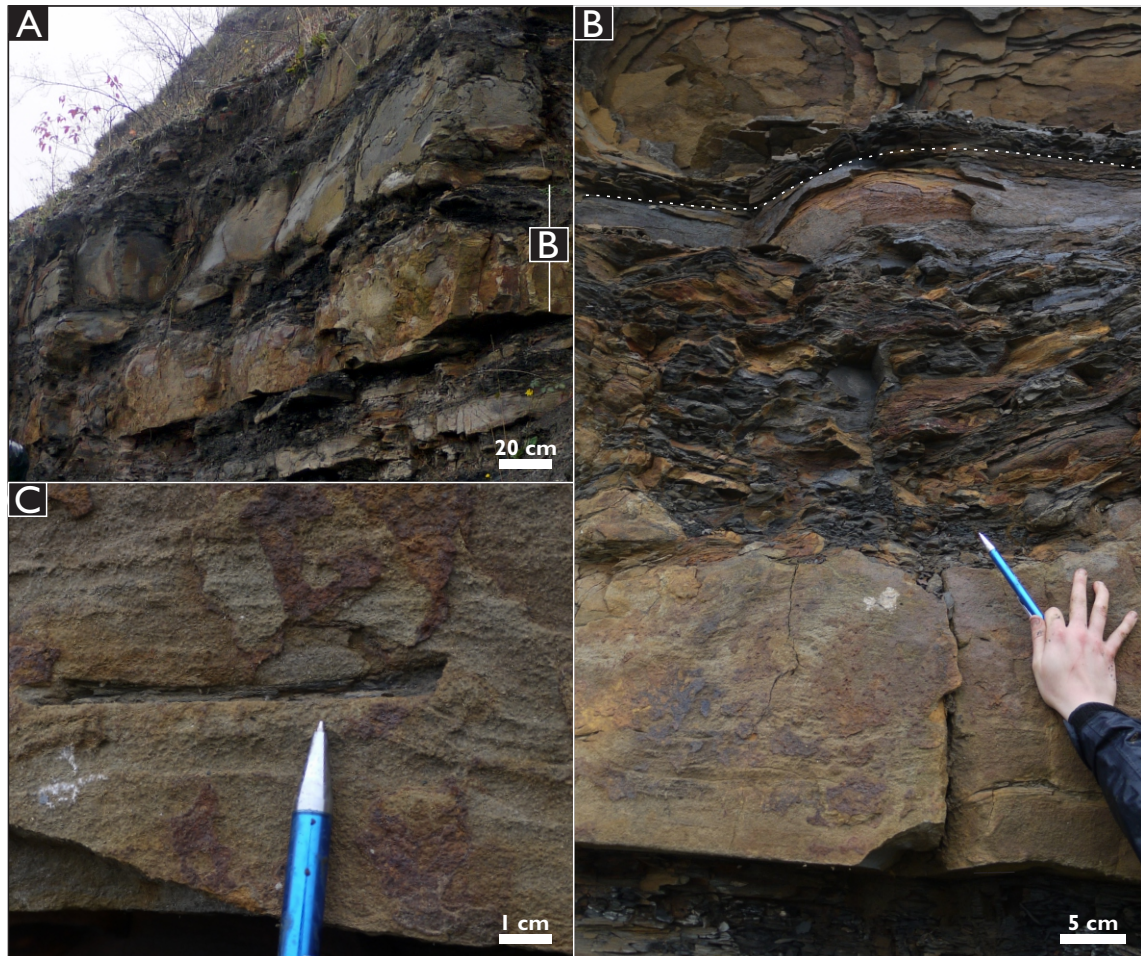


Fig. 4.5. Characteristics of matrix-rich mud-clast-rich deposits (FA-1A, Type A beds). **A)** Type A bed in which the lower sandstone facies is relatively clean (matrix-poor) compared to matrix-rich sandstone in base of the overlying Type B bed, weathering often highlights this contrast. **B)** Typical tripartite character of Type A beds in which relatively mud-clast-poor basal sandstone (facies CS-L) is overlain by a mud-clast and matrix-rich sandstone division (facies HAS-Cla) with a thin, fine grained, laminated sandstone (facies AS-L) at the bed top. **C)** Stratification within sandstone lower in the bed and underlying the mud-clast-rich division indicates deposition occurred progressively beneath a passing flow.

medium-grained, and typically non-stratified, though crude-spaced stratification can occur. This is either matrix-poor (facies CS-U, Fig. 4.3a; Bed Type A, Fig. 4.5b), or matrix-rich (facies AS-U, Fig. 4.3d; Bed Type B, Fig. 4.5b). Mud clasts are less abundant and typically smaller than those in the overlying mud-clast-rich division; mud clasts up to c. 35 mm were locally encountered at the bed base where recently entrained from the underlying mudstone (Fig. 4.6k). When matrix-rich, the lower sandstone division is typically more poorly sorted (moderate-poor sorting), and the lowermost part can exhibit banded sandstone (Fig. 4.3c), or a concentration of the coarser sand fraction (Fig. 4.6c, d, f). Further, when matrix-rich, a higher abundance of smaller mud clasts is observed compared with matrix-poor lower sandstone divisions. This abundance increases upwards prior to the development of the mud-clast-rich division (Fig. 4.6g, h). Though dominantly non-stratified, matrix-poor lower sandstone divisions are more prone to stratification than matrix-rich sandstone bases, which often exhibit pervasive consolidation lamination (Fig. 4.6e).

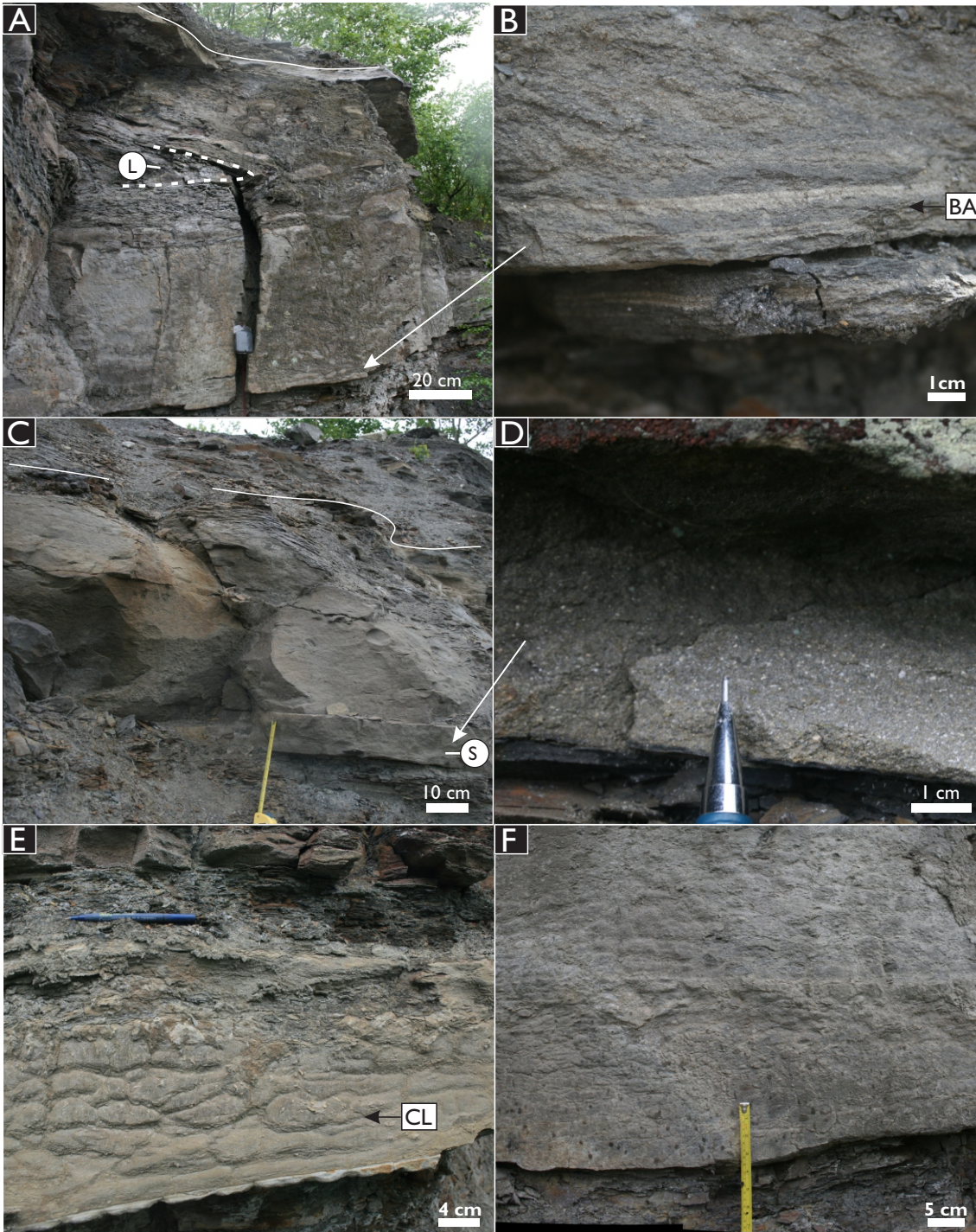


Fig. 4.6. Characteristics of matrix-rich mud-clast-rich deposits (FA-1A, Type B beds). **A)** Tripartite bed character consisting of unstratified argillaceous sandstone (facies AS-U) overlain by mud-clast-rich, matrix-rich sandstone (facies HAS-Cl_a), often with deformed mud-clasts (L), capped by argillaceous laminated sandstone (facies AS-L). **B)** Often bed bases can exhibit thin banded sandstone (facies BA). **C)** Tripartite bed character in which coarser sand fractions are concentrated in the bed base (S) resulting in a “starry night” appearance **(D).** **E)** Type B bed with consolidation laminae (CL), recording syn- or post-depositional disruption of stratification, and banded sandstone (facies BA) at the bed base **(F).**

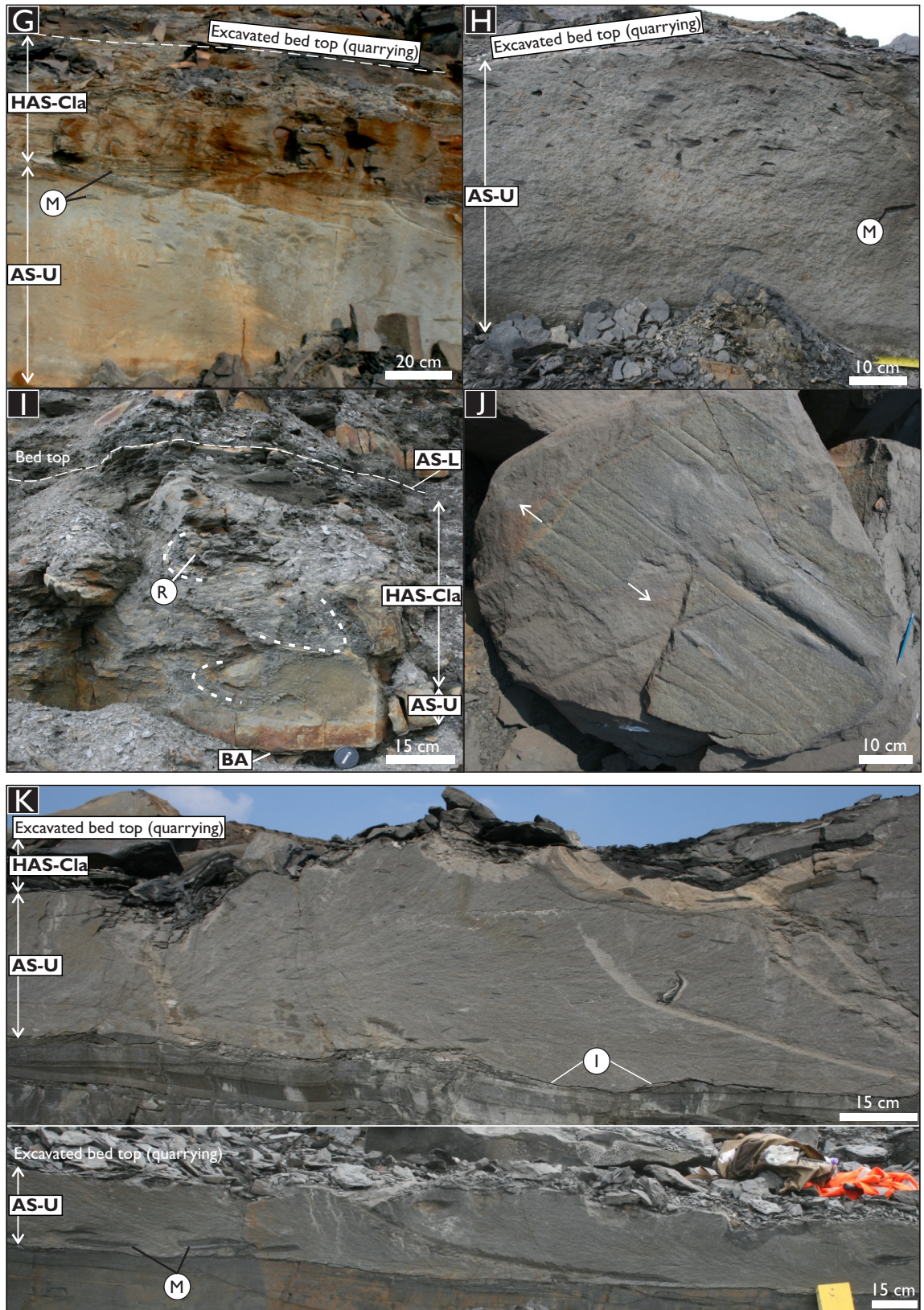


Fig. 4.6 ctd. Characteristics of matrix-rich mud-clast-rich deposits (FA-1A, Type B beds). **G & H)** The abundance and size of mud clasts (M) increases though the lower AR-U division prior to larger (c. 30 cm) mud clasts in the HAS-Cla division (G only). **I)** Examples of large, contorted mud-clasts (R) in the HAS-Cla division in a Type B bed with thin (<1 cm) banded sandstone (BA) at the bed base. **J)** Tool mark sole structures on the underside of Type B beds. Flute casts are uncommon and crude in form (not shown). **K)** Examples of shallow substrate incision (I) and entrapment of mud clasts (M) along the base of a single Type B bed.

In the mud-clast-rich division, mud clasts are predominant (i.e. clast-clast contacts are frequent and supporting sandstone matrix is sparse), and range widely in size from several cm to several m in length (Figs 4.5a, 4.6a,g,i,k). The mud-clast-rich division was never present at the bed base, and is often capped by a relatively thin, very-fine grained stratified sandstone (<<10% bed thickness). Clasts within the mud-clast-rich division are supported by highly matrix-rich sandstone or sandy siltstone (Fig. 4.3f), and large mud clasts can be folded (Fig. 4.6a). The contact with underlying relatively mud-clast-poor sandstone is often rugose (Figs 4.6b, k), despite the total-bed thickness remaining near-constant, with injections or inclusions of the relatively less matrix-rich sandstone beneath. Bed bases are sharp and can exhibit entrainment of underlying substrate (Fig. 4.6k). Bed bases display groove and gutter casts, occasionally with mud clasts at their terminations, and prod-marks (Fig. 4.6j); all of these features exhibit a wide range in width (~5 mm to 0.12 m). Flute casts are rare and, when present, are crude. In rare cases where the mud-clast-rich division is lacking in Type B beds, non-stratified matrix-rich sandstone in the lower bed passes directly up into the finer-grained, carbonaceous-rich and crudely laminated sandstone commonly found at the top of the bed; Type B beds are still distinct from Type C to E beds due to their greater thickness (0.40-2.80 m).

Interpretation. Many characteristics of Type A and B beds (e.g. vertical transition from relatively matrix-poor to matrix-rich sandstone, banded sandstone facies, matrix- and mud-clast-rich sandstone divisions, rarity of sedimentary structures associated with fluid turbulence) are comparable to those described from HEBs (Haughton et al., 2003, 2009; Barker et al., 2008; Talling et al., 2012a; Patacci et al., 2014; Fonnesu et al., 2015), and are similarly considered to be the depositional products of rheologically variable flow (spatially, temporally or both), in which flow became increasingly cohesive (clay-rich), turbulence-suppressed and mud-clast-rich. The repeated association of matrix- mud-clast-rich divisions (facies HAS-C1a) with underlying relatively mud-clast- and matrix-poorer sandstone facies demonstrates their co-genetic relationship with deposition during a single flow event; co-genetic relationships have been documented in previous studies of similar deposits (Haughton et al., 2003, 2009; Barker et al., 2008; Talling et al., 2012a; Fonnesu et al., 2015). Flows emplacing such deposits are considered to have been relatively clay-rich, compared with those depositing Type G and F beds, following entrainment of muddy substrate (Haughton et al., 2003, 2009; Fonnesu et al., 2015), or flow deceleration (Talling et al. 2004; Sumner et al., 2009; Kane & Pontén, 2012). The origin and significance of Type A and B beds with respect to the downstream confining margin of the Edale Basin is discussed later in this chapter. Chapter 5 further discusses Type A and B beds with respect to wider controls upon their occurrence and currently established models for clay-rich turbulence-suppressed flow types.

4.4.2 Type C, D and E beds

Description. Comparable to Type A and B beds, bed Types C, D and E also exhibit a vertical change from matrix-poor to matrix-rich sandstone facies and greater mud-clast abundance higher in the bed (Fig. 4.7). However, Type C - E beds differ from Type A and B beds in that mud-clast abundance and maximum size is lower, and a distinct, thick mud-clast-rich division (facies HAS-C1a) is lacking (Fig. 4.7a, c, d, e). Type C - E beds comprise thin- to thick-bedded (0.01- $<$ 0.65 m), very fine- to fine-grained sandstone deposits in which there is a crude vertical grain size grading and increase in the abundance of mud clasts and carbonaceous plant material (Fig. 4.7c, e, f). Matrix-poor sandstone at the base of the bed is typically thin ($<$ 20% of the bed thickness), and exhibits banding, crude planar lamination or a non-stratified character (Fig. 4.7c, e, a, respectively). The overlying matrix-rich sandstone may be non-stratified with internal shearing fabrics. It often contains a mud-clast-rich horizon, in which mud clasts are relatively small (0.01 – 0.20 m, max 0.46 m), sub-parallel to bedding, and low in abundance such that clast-clast contacts are rare and clasts “float” in the supporting sandstone matrix (Fig. 4.7c, d). Often, the top of the bed comprises crudely stratified matrix-rich sandstone due to an enrichment of small mud clasts ($<$ 20 mm), and carbonaceous (plant) fragments whose bed-parallel orientation forms splitting planes at the top of the bed (Fig. 4.7e, f). Type E beds are the thinnest and most fine-grained beds, and are notable in that they are dominated by this carbonaceous-, matrix-rich sandstone. The contacts between constituent facies within the bed remain relatively planar laterally within the bed. Locally, bed bases are sharp and planar with an abundance of prod and groove marks, implying flows transported mud clasts and carbonaceous debris, and that substrate erosion may have been cryptic (i.e. shallow, Eggenhuisen et al., 2010).

Interpretation. As for Type A and B beds, many characteristics of Type C - E beds are comparable to characteristics documented in deposits inferred to record deposition, in full or in part, from relatively cohesive, turbulence-suppressed flow (Haughton et al., 2003, 2009; Barker et al., 2008; Kane & Pontén, 2012; Talling et al., 2012a; Terlaky & Arnott, 2014). Similarly, flows emplacing Type C to E beds are considered to have been clay-rich, with enrichment achieved following entrainment of muddy substrate (Haughton et al., 2003, 2009; Fonesu et al., 2015), or flow deceleration and loss of coarser sand fractions (Talling et al. 2004; Sumner et al., 2009; Kane & Pontén, 2012). The thinner-bedded and finer-grained nature of Type C - E beds, which lack an abundance of mud clasts, evokes either more distal or smaller flow events compared to those emplacing Type A and B beds. The origin and significance of Type C - E beds with respect to the downstream confining margin of the Edale Basin is discussed later in this chapter.

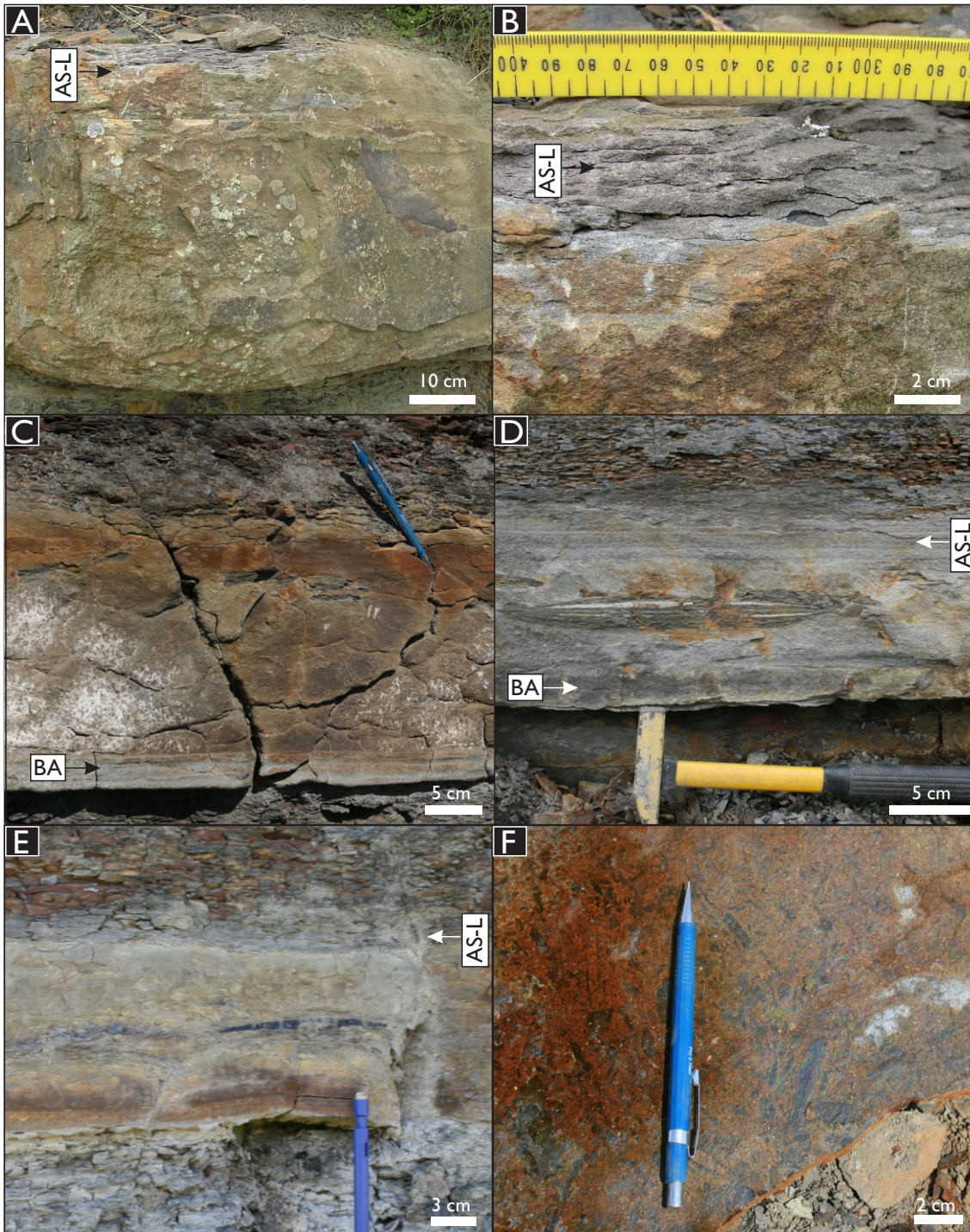


Fig. 4.7. Characteristics of matrix-rich, relatively mud-clast-poor deposits (FA-1B, Type C-E beds) interpreted to be the depositional products of cohesive (clay-rich) relatively turbulence-suppressed flow. **A)** Type C bed comprising relatively clean unstratified sandstone (facies CS-U) capped by a thin matrix-rich laminated sandstone (facies AS-L) with splitting planes defined by horizons enriched in carbonaceous material and small mud-chips **(B).** **C)** Type D bed commencing with banded sandstone (facies BA) overlain by unstratified matrix-rich sandstone (facies AS-U) which becomes mud-clast-rich upwards. **D)** Type D bed in which the overall bed exhibits normal grading with facies AS-L present at the bed top. **E)** Thin Type E bed dominated by facies AS-U with a cap of facies AS-L at the top of the bed which is enriched in carbonaceous (plant) fragments **(F)** which define splitting planes sub-parallel to bedding.

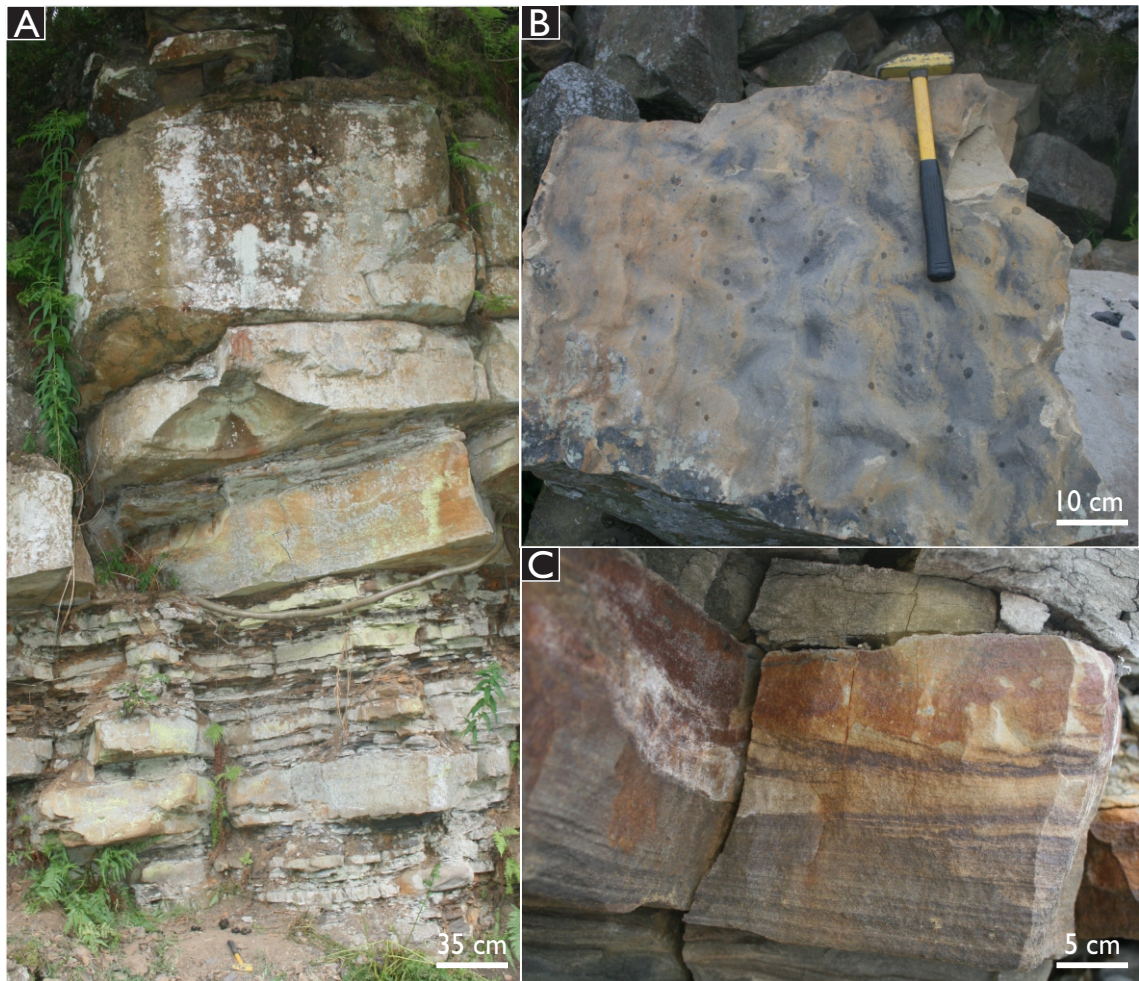


Fig. 4.8. Characteristics of matrix-poor deposits (FA-2, Type F & G beds) interpreted to be the deposits of non-cohesive (clay-poor) relatively turbulent flow. **A)** Interbedded thick Type G and thinner Type F beds. **B)** Current-ripple lamination cap at the top of a Type G bed. **C)** Planar lamination succeeded by current-ripple lamination in a Type F bed.

4.4.3 Type F and G beds

Description. Bed types F and G lack distinctly matrix-rich sandstone facies, and are dominated by matrix-poor sandstone which can contain carbonaceous material, albeit in a lower abundance compared to that found in Type A-E beds (Fig. 4.8). Type F beds are very thin- to thick-bedded (typically 0.01-0.38 m), normally-graded, and are dominated (>50% of bed thickness) by moderately well-sorted, laminated matrix-poor sandstone (facies CS-Lp or CS-Lr; Fig. 4.8c). Bed bases are typically non-erosive and, when present, tool marks are small (<5 mm width). Type G deposits are typically more thickly bedded (typically 0.25-1.40 m) and are dominated by a greater proportion of moderately sorted, non-stratified matrix-poor sandstone (facies CS-; >50% bed thickness), which may or may not be succeeded by a thin cap of planar or current-ripple laminated sandstone (facies CS-Lp or CS-Lr) at the bed top where normal grain size grading is most pronounced (Fig. 4.8a,b). Bed bases are commonly erosive, and

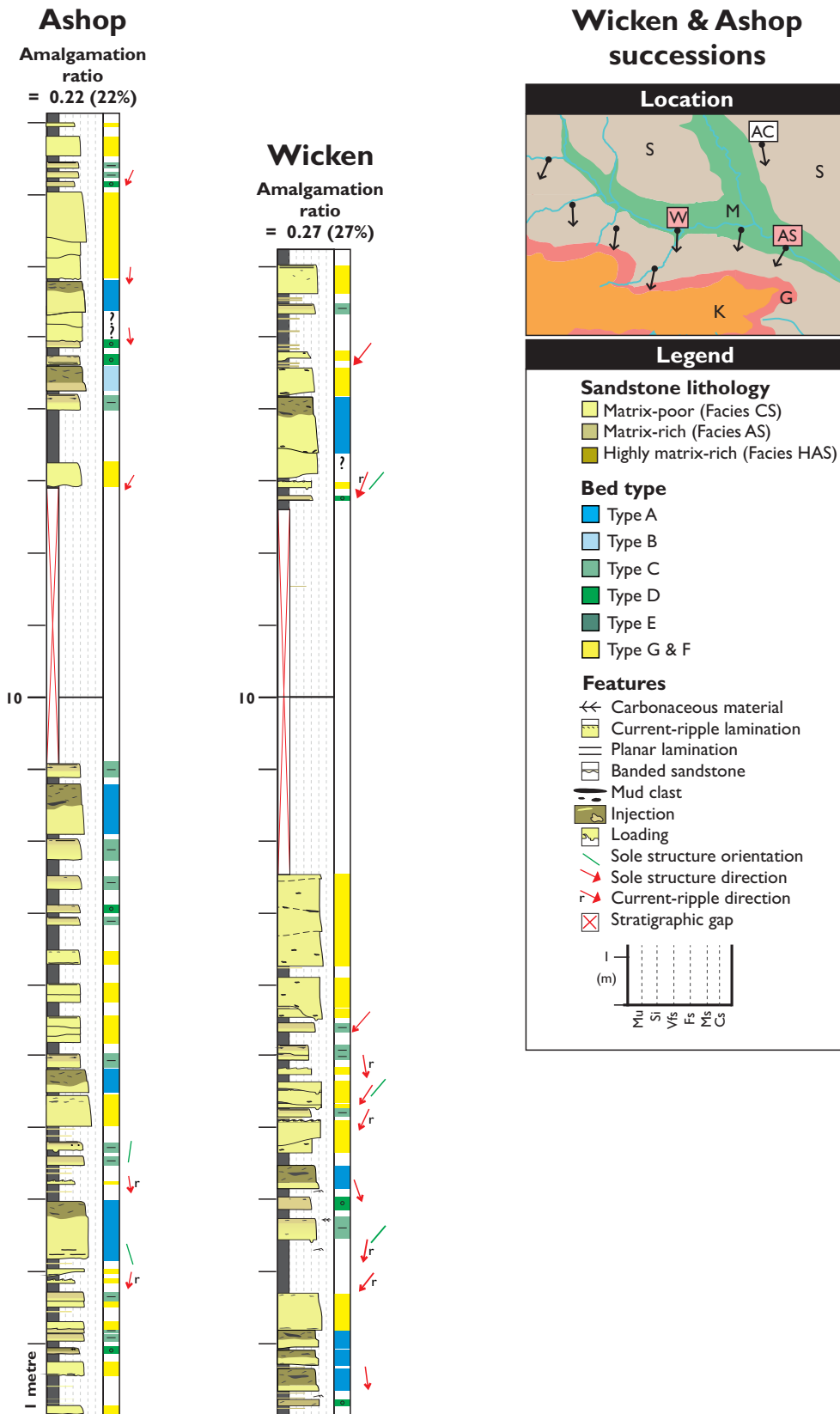


Figure 4.9. Sedimentary logs of exposures of the Mam Tor Sandstones, Ashop and Wicken river-cut sections. Depositional packages exhibit an upwards replacement of HEBs by matrix-poor Type G beds (FA-2), often with an increase in grain size and the degree of amalgamation.

exhibit sole structures (flute casts, groove marks, prod marks). Mud-clast rip-ups occur locally in association with amalgamation of Type G beds into thick successions.

Interpretation. Bed types F and G record deposition from non-cohesive (clay-poor) sandy flows with varying sediment concentration. Type F beds record progressive deposition beneath relatively dilute (low-concentration), non-cohesive turbulent flow (i.e. lamination, grading, flute casts; low-density turbidite *sensu* Bouma, 1962 & Lowe, 1982). Conversely, Type G beds record deposition and high sediment fall-out beneath high-concentration, non-cohesive flow (i.e. dominance of non-stratified sandstone, flute casts, normal grading; high-density turbidite *sensu* Lowe, 1982). Type F and G beds are inferred to have been deposited from relatively clay-poor flow, compared with flows emplacing Type A - E beds. Clay-poor flows may reflect: 1) a relatively proximal depositional region, where cohesive, turbulence-suppressed flow had not yet developed, or was not yet depositional; or 2) flow events in which factors promoting clay-enrichment did not occur (i.e. insufficient entrainment of muddy substrate - Haughton et al., 2009; insufficiently timed or rapid flow deceleration - Sumner et al., 2009).

Throughout the remainder of Chapter 4, bed types of the MTS and Shale Grit Formation are discussed in terms of the following facies associations.

- Facies association 1A (FA-1A) – Bed Types A and B.
IB (FA-1B) – Bed Types C - E.
- Facies association 2(FA-2) – Bed Types F - G.

4.5 Depositional character and distribution with respect to the confining basin margin

4.5.1 Strata upstream and distant from the confining basin margin

4.5.1.1 Wicken and Ashop river sections

Small exposures (< 20 m thick) of the MTS are located approximately 6 - 7 km upstream of the southern confining basin margin (Wicken and Ashop River localities, respectively; Fig. 4.1c).

Palaeoflow

Sole structures (flute casts and groove marks) and current-ripple lamination record palaeoflow towards the south-southwest (Fig. 4.1c), and are thus comparable to the majority of palaeoflow trends recorded across the basin. This indicates that flows were travelling downslope across the basin, unaffected by the downstream confining basin margin.

Sedimentology

Strata comprise a mixture of FA-1 and FA-2 deposits arranged into thickening-upwards cycles where FA-2 is dominant (Fig. 4.9). Shallow scouring and bed amalgamation is more frequent (22-27%, amalgamation ratio, *sensu* Romans et al., 2009) compared to that in downstream

exposures. FA-2 deposits are common, and typically exhibit erosive bases and bed tops which can be enriched in sparse mud clasts or carbonaceous material. FA-1 deposits include those of FA-1B and FA-1A which typically exhibit matrix-poor non-stratified sandstone as the basal sandstone facies, rather than matrix-rich sandstone facies.

4.5.2 Localities adjacent to the downstream confining basin margin

4.5.2.1 Mam Tor

A south-facing landslide scar on Mam Tor exposes a c. 124 m-thick succession of interbedded deep-water sandstones and mudstones of the MTS (Fig. 4.10), first described in detail by Allen (1960) and more recently by Davis (2012). The succession commences close to the contact of the MTS with the underlying Edale Shales, which locally coincides with the *Reticuloceras reticulatum* marine band (Stevenson & Gaunt, 1971; Waters et al., 2009).

Palaeoflow

Description. The succession at Mam Tor can be stratigraphically subdivided into three intervals (0-25 m, 25-71 m, 71-124 m), based on the dominant palaeoflow direction inferred from sole structures (n=50), parted by thick mudstone-dominated packages (Fig. 4.10, c. 25, c. 71 m); the lower two palaeoflow zones were first documented by Allen (1960). Palaeoflow zones record flow either towards the southwest or south-southeast and southwest (Fig. 4.11). Rare examples of current-ripple lamination record more disperse palaeoflow typically towards the north, away from the confining basin margin (Fig. 4.11). Both sole structures and current ripple-lamination record palaeoflow which deviates compared to those observed further upstream away from the confining basin margin (Fig. 4.1c).

Interpretation. The sand rich packages are interpreted as confined lobe complexes adjacent to the basin margin, with intervening muddy intervals recording shut down of lobe sedimentation, at least locally. Palaeoflow deviations, concerning incoming flow trends approaching confining topography, are commonly described from confined deep-water depositional systems (Haughton, 1994; McCaffrey & Kneller, 1995; Kneller & McCaffrey, 1999; McCaffrey & Kneller, 2001; Felletti, 2002), and have been demonstrated experimentally (Kneller et al., 1991). Many studies have also documented deviation between sole structure and current ripple lamination palaeoflow indicators near confining topography (Pickering & Hiscott 1985; Kneller et al., 1991, McCaffrey & Kneller, 2001; Southern et al., 2015 – Chapter 6). The discrete trends in palaeoflow direction inferred from these types of sedimentary structures near the basin margin of the Edale Basin are interpreted to record the effects of flow confinement (cf. Kneller et al., 1991; Kneller & McCaffrey, 1999), with dilute regions of the flow collapsing back down the counter slope as reflections towards the north (depositing current-ripple lamination), whilst

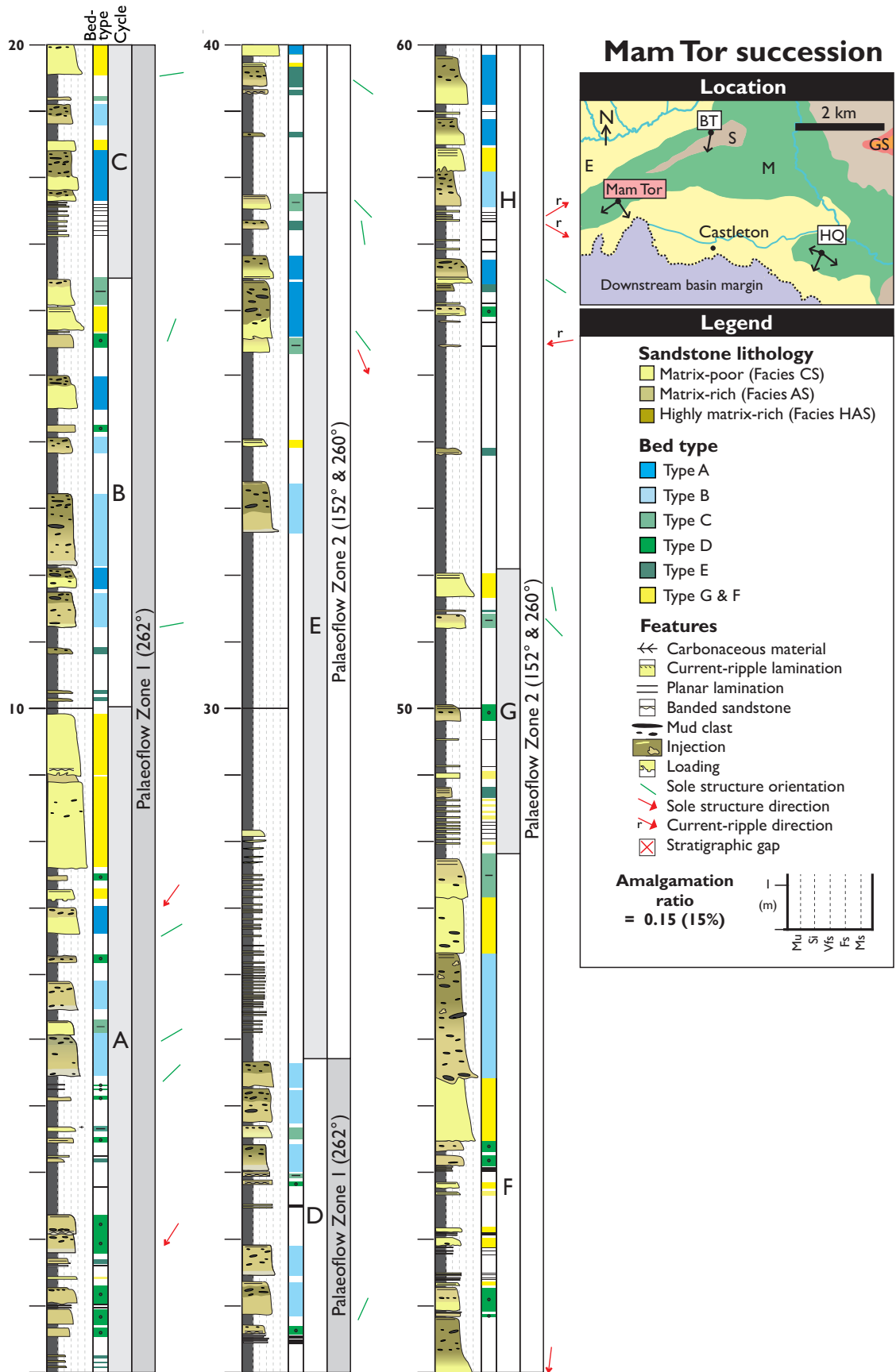


Figure 4.10 (continued overleaf). Sedimentary log of the Mam Tor Sandstones at Mam Tor with bed types, depositional packages and palaeoflow zones A to P indicated. Vertically through the succession there is an overall reduction in the proportion of matrix-rich bed types (Type A-E, FA-1) at the expense of matrix-poor bed types (Type F-G, FA-2). Matrix-rich bed types also exhibit variations in their proportion within smaller scale depositional packages.

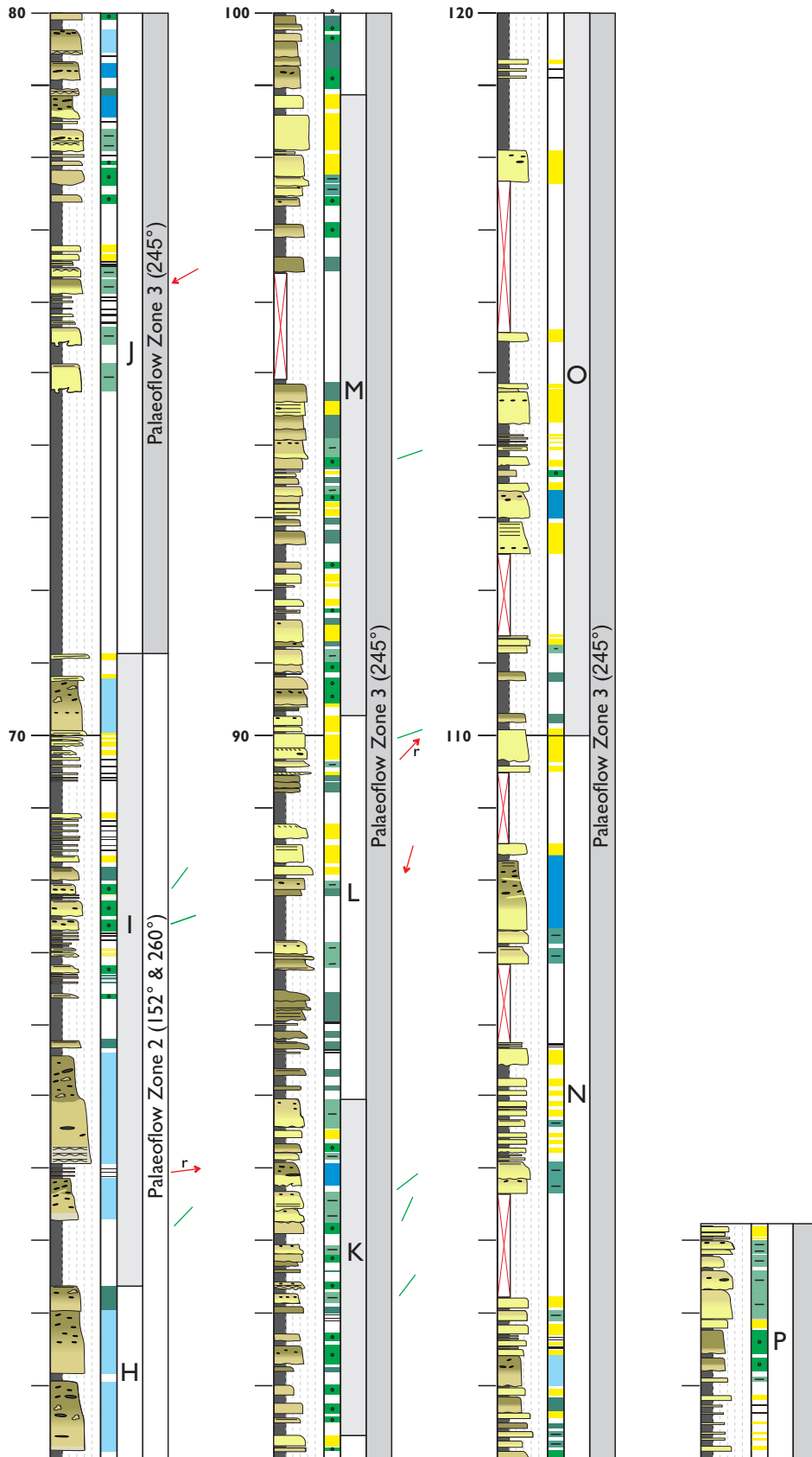


Figure 4.10.ctd.

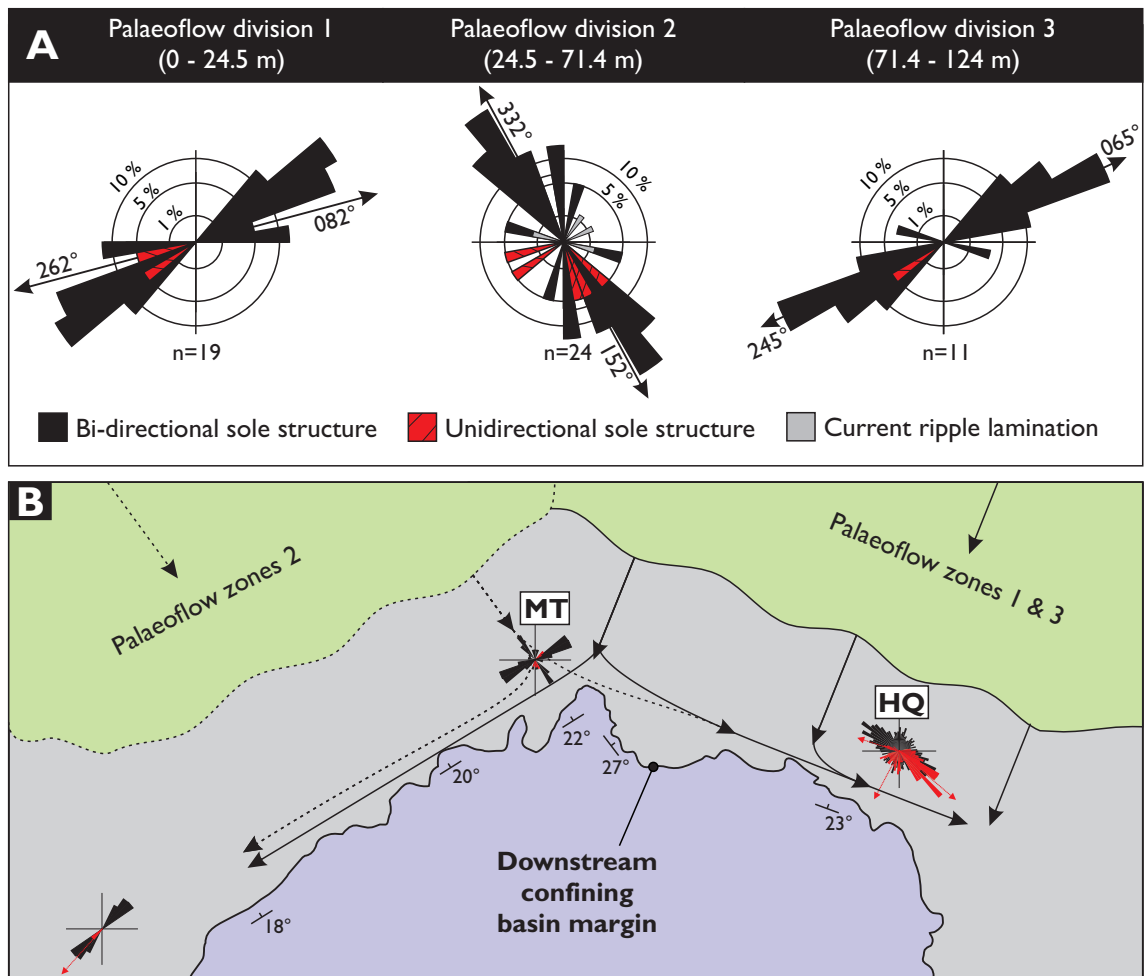


Figure 4.11. A) Stratigraphic subdivision of the Mam Tor succession into 3 palaeoflow divisions separated from each other by mudstone-dominated successions. **B)** Schematic illustration of palaeoflow zonation resulting from changes in the lobe position and subsequent changes in the approach direction of incoming flows prior to incidence with the confining basin margin.

denser regions of the flow (generating sole structures) were deflected laterally along the confining basin margin towards the southwest.

Stratigraphic changes in the dominant palaeoflow direction following re-establishment of lobe sedimentation may record lobe switching, driven by lobe compensation processes, or changes in the position of the feeder channel along the shelf edge (Walker, 1978). Outcrop constraints prevent differentiation of whether shut-down was a local phenomenon related to lobe compensation processes or occurred basin-wide; the Mam Tor outcrop is c. 240 m across, and other exposures with distinct correlative features are lacking. However, multiple feeder channels and changes in their position along the shelf and slope edge are expected, considering the broad geographical extent and high rate of sediment supplied to the Kinderscoutian delta system (Collinson, 1968, 1969; Hampson, 1997; Hampson et al., 1999). Numerous channels with turbiditic infill are described from proximal basin-floor and slope strata (Shale Grit and Grindslow Shales, respectively - Walker 1966b; Collinson, 1969, 1970),

whereas a number of channels and incised valleys with fluvial infill are cut into the top of the slope succession (Collinson, 1970; McCabe, 1977; Hampson, 1997; Hampson et al., 1999). Thus, changes in the active feeder position occurred during infill of the Edale Basin, and are expected to result in the development of discrete zones of deposition on the basin floor, and subsequent changes in palaeoflow direction. Palaeoflow Zone 2 records incoming flows from the northwest, which appear to have deflected near to the Mam Tor locality (i.e. developing subordinate trends to the southwest; Fig. 4.11a). Conversely, Palaeoflow Zones 1 and 3 record flow already travelling sub-parallel to the strike of the confining basin margin (073-253°, Stevenson & Gaunt, 1971), indicating flows approached from a more north-easterly direction, or that flow incidence with the confining basin margin occurred relatively further east of Mam Tor (Fig. 4.11b). Upon meeting the confining basin margin, flows were partitioned and deflected both southeast, (towards HQ) and southwest along the confining basin margin (Fig. 4.11b). Such flow partitioning around obstacles has been demonstrated experimentally (Al Ja'Aidi et al., 2004), and is considered likely given the high angle of incidence with the confining margin of the Edale Basin, and the complexity of palaeoflow observed at HQ (Figs 4.1c, 4.11b). The stratigraphic persistence of deflected palaeoflow trends demonstrates the long-lived confining effect of the basin margin during deposition of the Mam Tor succession (Fig. 4.10)

Sedimentology

The succession at Mam Tor contains a mixture of FA-1 and subordinate FA-2 deposits (Type F and G beds), often arranged into discrete cleaning-upwards packages, exhibiting a reduced amalgamation ratio (11%, *sensu* Romans et al., 2009) compared with that further upstream (Fig. 4.9). FA-1A deposits are common, and their mud-clast-rich division (facies HAS-C1a) is typically laterally extensive, always underlain by relatively mud-clast-poor sandstone facies (facies CS-U or AS-U), and can comprise decimetre-scaled mud clasts, which are often floating and supporting in a matrix-rich sandstone matrix.

The position, extent (c. 240 m), and sub-parallel orientation of the Mam Tor outcrop (055-235°) with respect to the basin margin (073-253°), places strata c. 250 - 300 m away from their point of onlap onto the basin margin. Such limited lateral change, in terms of distance from the confining basin margin (c. 50 m), is considered insufficient to express any variations in local depositional character, and inferred flow rheology, that might have arisen from proximity to, and confinement by, the confining basin margin; as such, lateral tracing of individual beds, as carried out at HQ, was not undertaken at MT.

4.5.2.2 Hope Quarry

A c. 74 m-thick succession of deep-water sandstones and mudstones outcrops in a series of variously orientated and previously undocumented exposures at HQ (Figs 4.1c, 4.12, 4.13). At the base of the succession, a c. 5m-thick mudstone, containing the goniatite bearing *Reticuloce-*

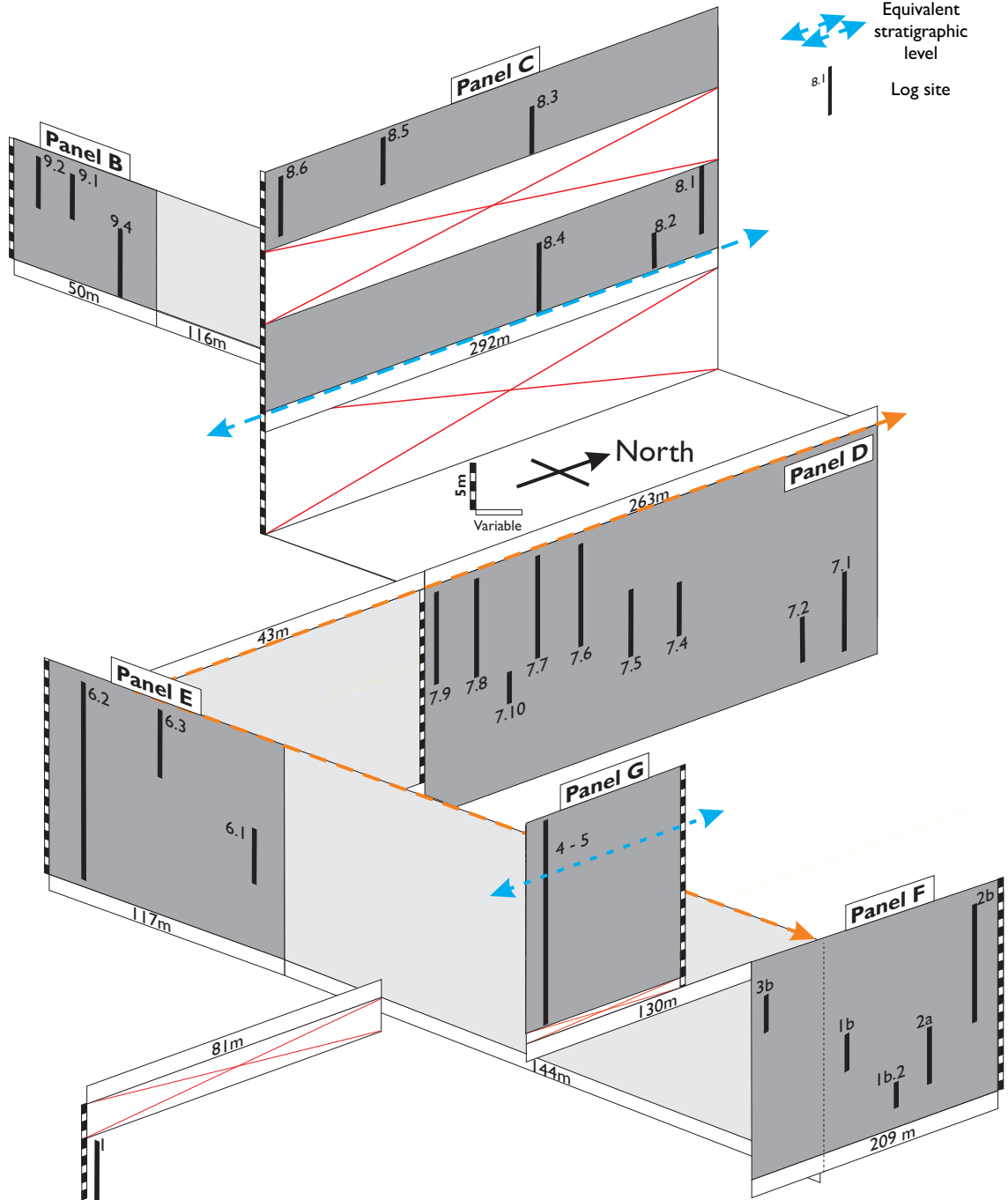
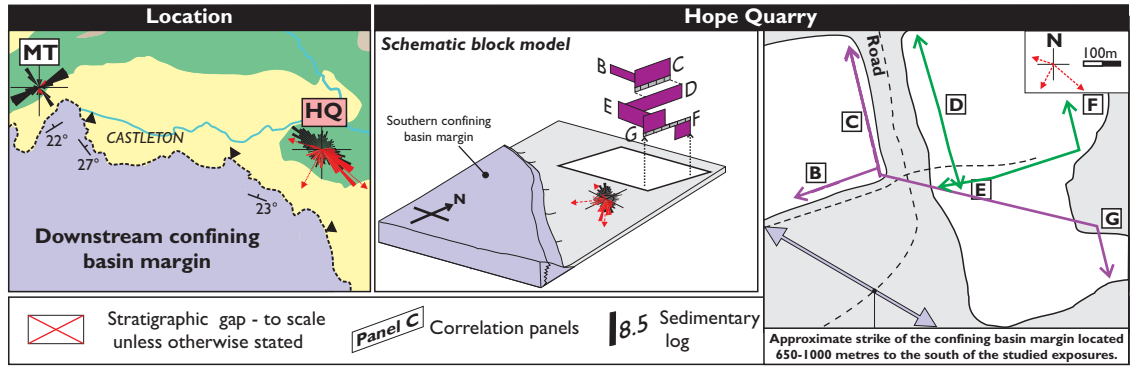


Figure 4.12. Location map and fence diagram indicating the location and orientation of exposures of the Mam Tor Sandstone in quarried faces at Hope Quarry.

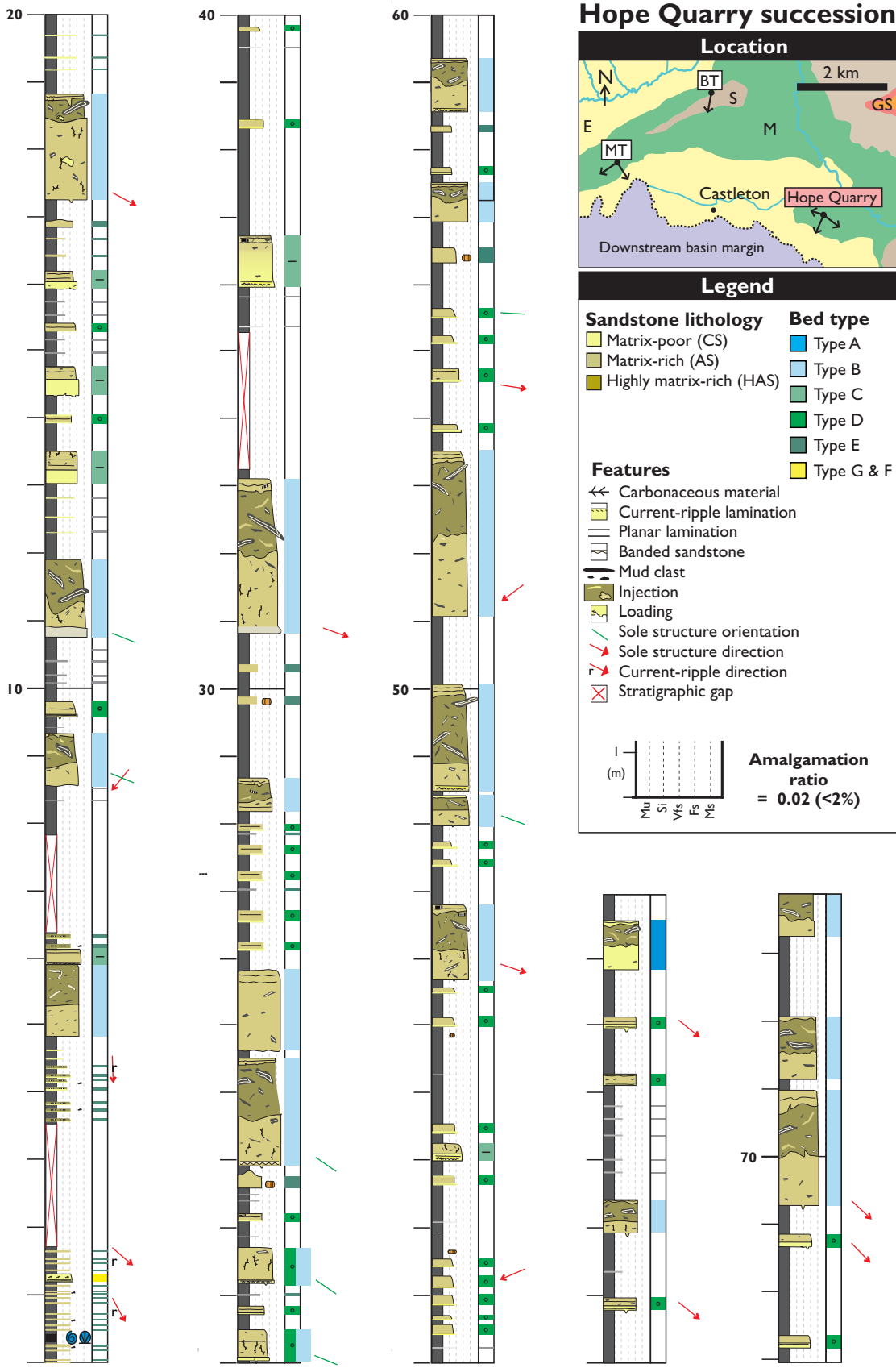


Figure 4.13. Stratigraphic succession collated from correlated exposures of the lower Mam Tor Sandstones, Hope Quarry. The Mam Tor Sandstones succession commences after a mudstone dominated succession (0-5 m) containing the *Reticuloceras reticulatum* marine band which marks proximity to the boundary with the underlying Edale Shales. The succession is dominated by Type A to E beds (FA-1), has a very low amalgamation ratio and, in contrast to the succession at Mam Tor, exhibits no stratigraphic subdivision according to palaeoflow direction or depositional trends.

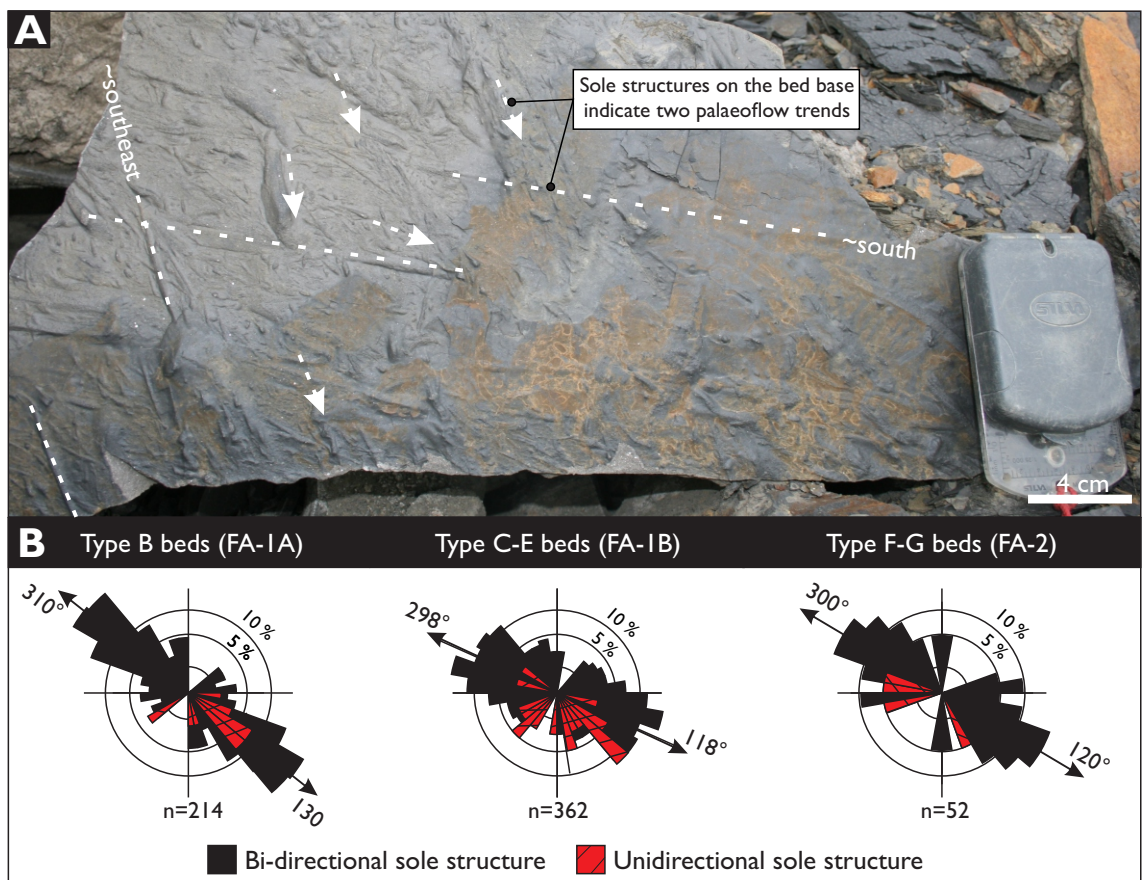
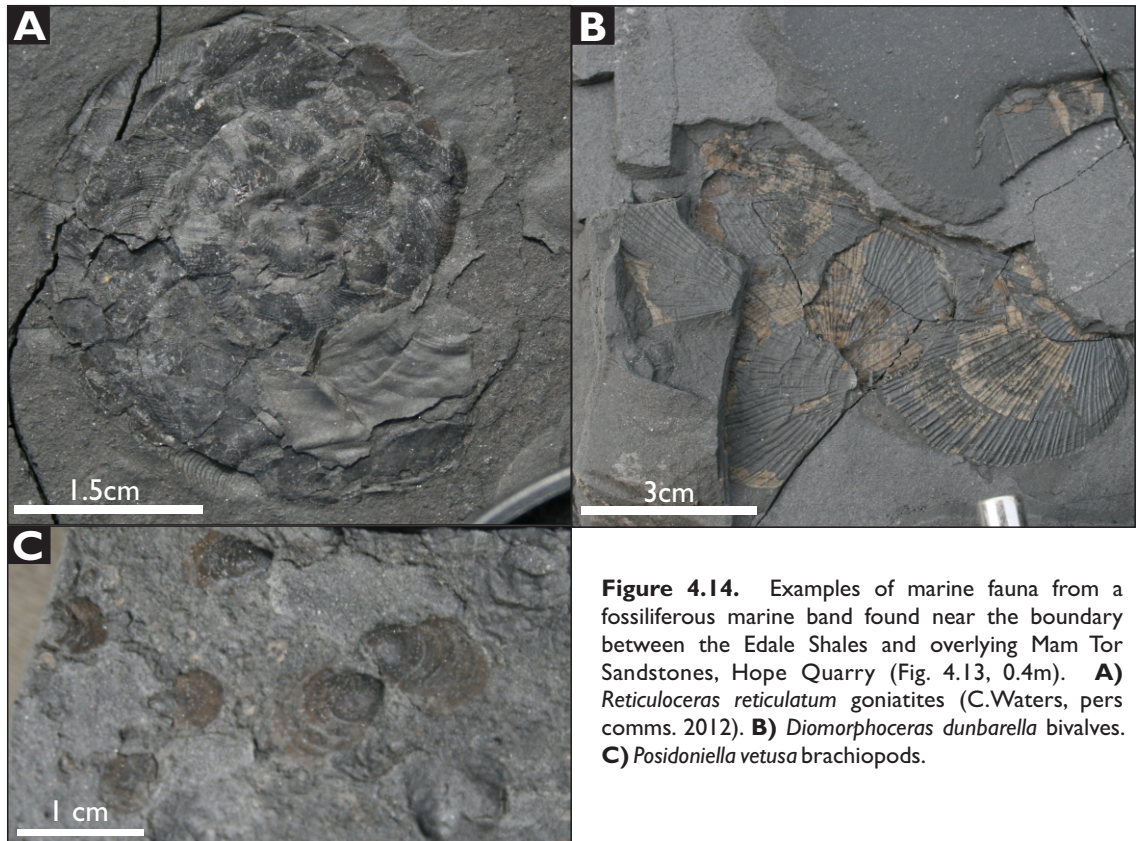


Figure 4.15. A) Example of bimodal palaeoflow on the underside of a Type B bed from Hope Quarry in which neither trend shows a tendency to crosscut the other suggesting both trends were created during the same event. **B)** Palaeoflow directions from discrete facies associations at Hope Quarry.

ceras reticulatum marine band (C. Waters pers. comm), indicates that the overlying siliciclastics are those of the lower MTS (Figs 4.13, 4.14; Stevenson & Gaunt, 1971) and are largely time-equivalent to the lower part of the succession at Mam Tor. Structure contour mapping of the basin margin into the sub-crop places strata at HQ between 650 and 1100 m from their point of onlap onto the confining basin margin slope, depending upon stratigraphic height within the succession.

Palaeoflow

Description. Sole structures (n=628) record dominant palaeoflow towards the south or southeast, with a subordinate trend to the northwest; the latter two trends deviate from that of incoming flows approaching the confining basin margin (Fig. 4.1c). Commonly, a single bed base can exhibit palaeoflow indicators recording flow both to the southeast and south (Fig. 4.15a). Of all the facies associations, FA-1A exhibits the least spread and is dominated by palaeoflow towards the southeast (Fig. 4.15b). Vertically, palaeoflow directions record sustained confinement by the confining basin margin during deposition of the HQ succession. However, palaeoflow directions do not group into zones similar to those documented at Mam Tor; instead palaeoflow can frequently change from bed to bed (Fig. 4.13).

Interpretation. The range in palaeoflow trends observed at HQ are interpreted to record the combined signature of incoming flows (travelling south), and flows deflected (southeast or northwest) along the strike of the confining basin margin (*sensu* Kneller and McCaffrey, 1999). Bimodal and cross cutting palaeoflow indicators on beds indicate flows passing HQ could comprise both incoming flow, and flow which had previously been deflected southeast along the confining basin margin following confinement further upstream along the confining basin margin (Figs 4.1, 4.15). Frequent changes in the dominant palaeoflow direction between successive event beds are in contrast with the stratigraphically discrete palaeoflow zones observed at Mam Tor, and are thought to record changes in the relative proportions of incoming flow and flow deflected in either direction along the confining basin margin. Such changes are likely driven by shifts in the position of the depositional lobe and position of incidence along the confining basin margin as discussed previous. The persistence of deflected palaeoflow trends throughout the HQ succession demonstrates the pertinacity of the confining basin margin during the deposition of this succession.

Sedimentology

Strata are tabular and rarely exhibit amalgamation (2% amalgamation ratio; Fig. 4.13). FA-1A deposits are common and are almost exclusively of the matrix-rich-based kind (i.e. Type B beds). Similar to Mam Tor, the succession exhibits the full spectrum of FA-1 deposit types with subordinate occurrences of FA-2 as Type F beds. However, matrix-rich based Type B beds are

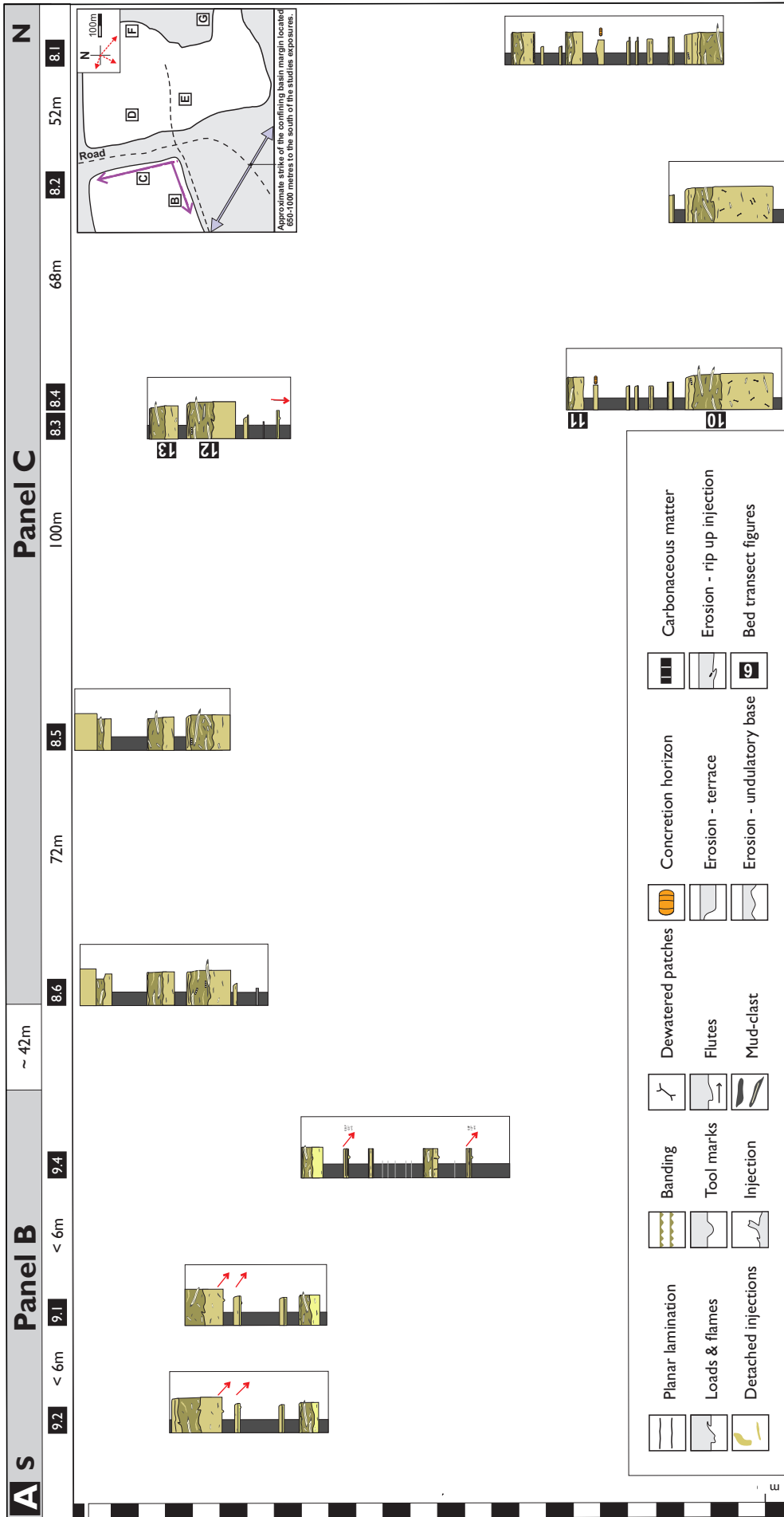
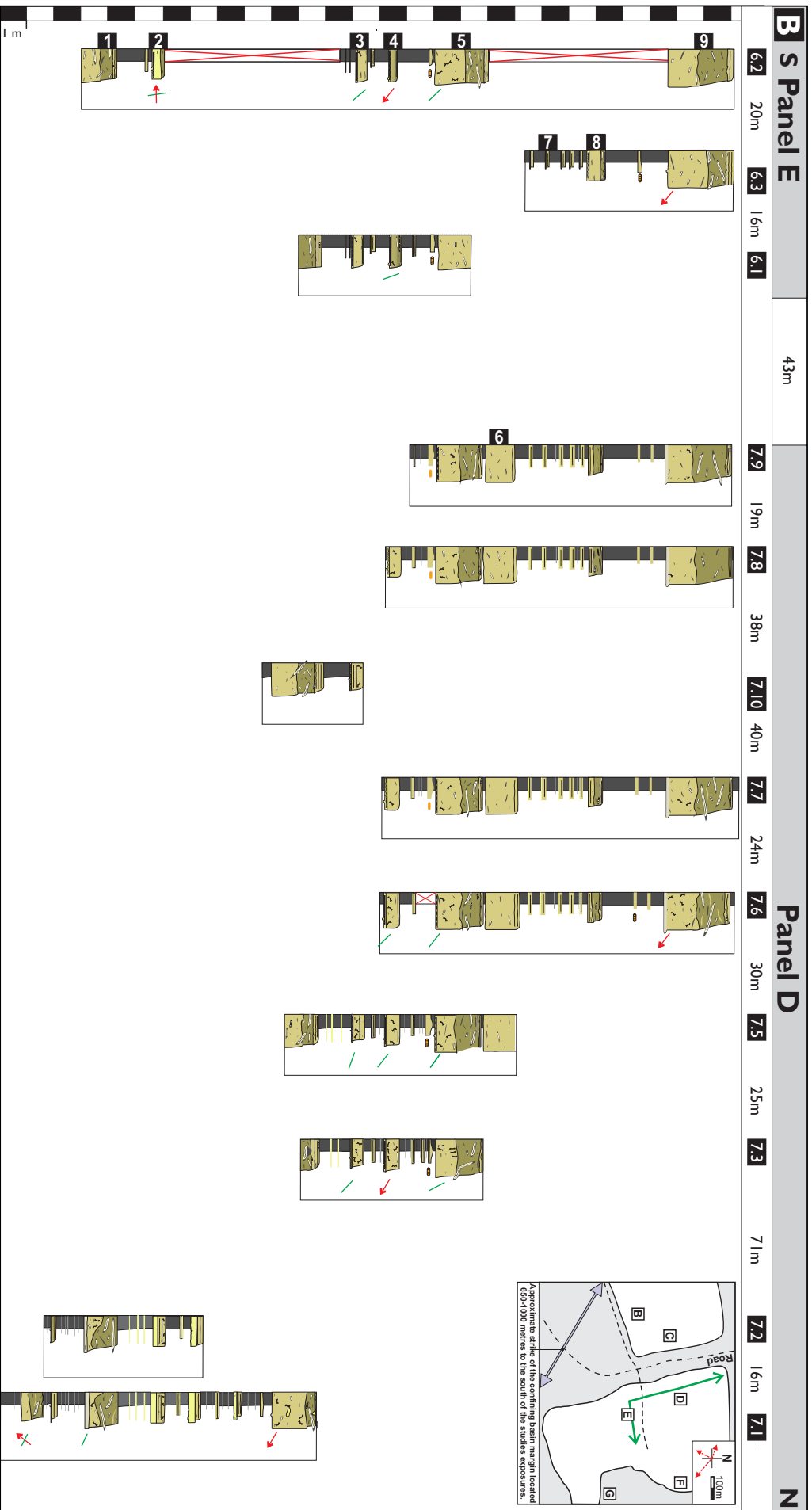


Figure 4.16 (continued overleaf). A-D) Lateral correlation of a series of sedimentary logs collected from variously orientated quarried facies at Hope Quarry. Strata can be traced laterally with respect to palaeoflow direction and increasing proximity towards the nearby downstream confining basin margin of the Edale Basin. Inset map shows the location of panels which comprise these correlations whilst stratigraphic relation to one another are shown in Fig.4.12.



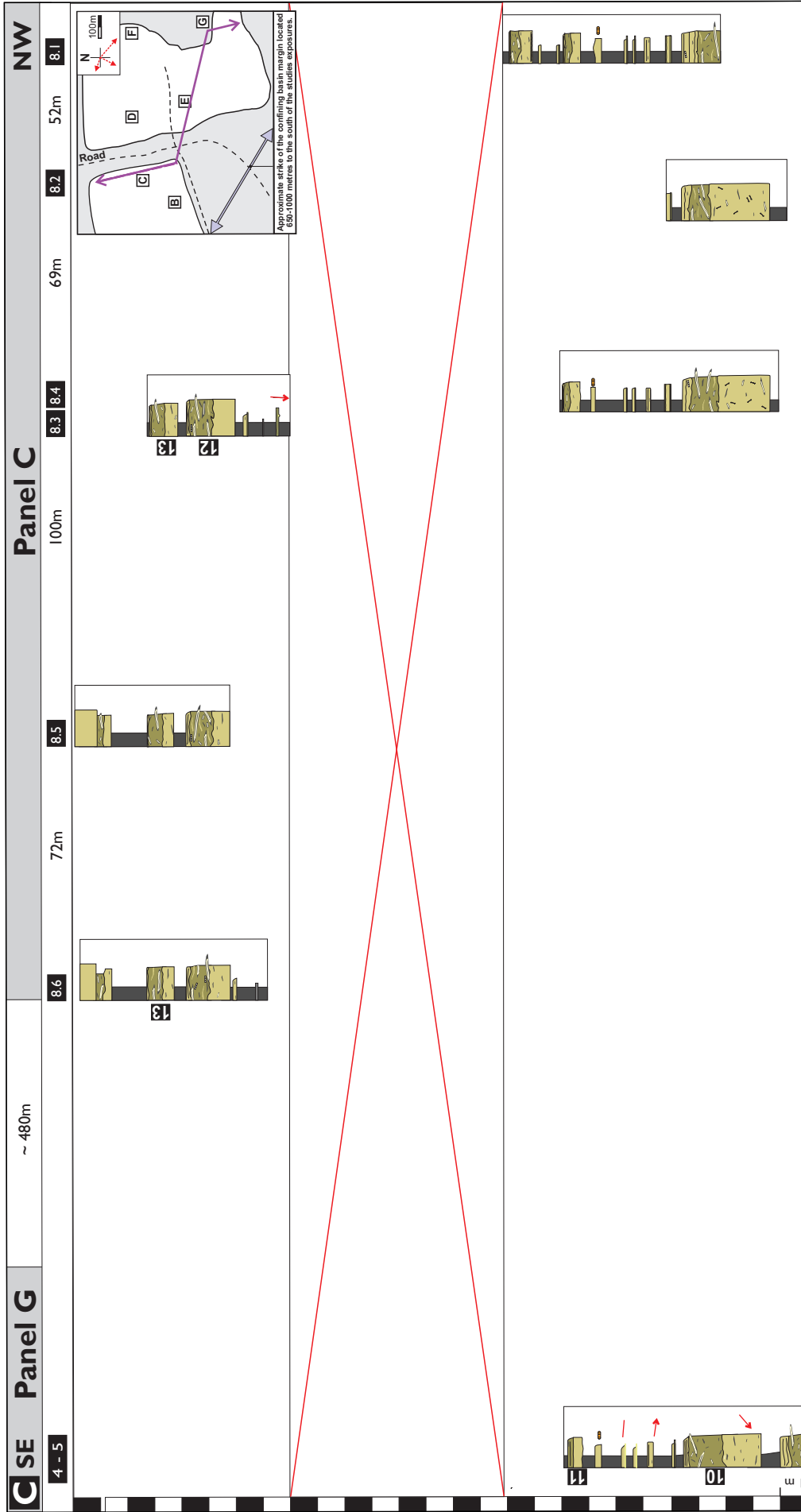


Figure 4.16. ctd C) Correlation of logged sections from Panel G to C. (See A) for the legend for sedimentary features. See Fig. 4.12. for the spatial context of logged sections and correlated panels.



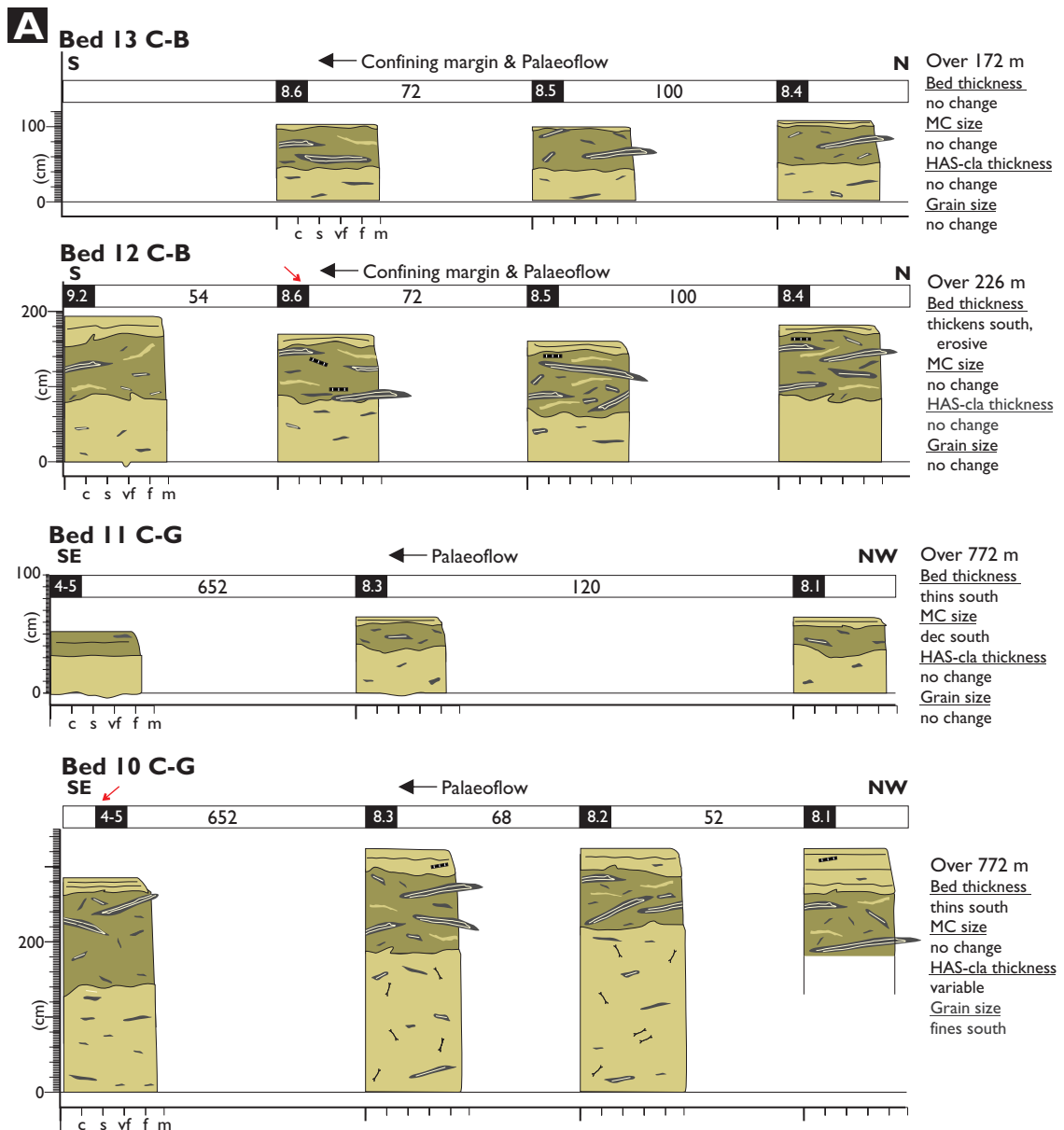


Figure 4.17 (continued overleaf). A-D) Individual beds can be traced laterally with respect to palaeoflow direction and proximity to the nearby, downstream confining basin margin. Lateral tracing of beds reveals variation in their depositional character (i.e., facies present at the bed base, proportion of facies - particularly that of the mud-clast-rich division, subtle variation in grain size) however these are non-systematic with respect to palaeoflow or proximity towards the basin margin. Beds containing matrix-rich sandstone facies, including thick mud-clast-rich divisions are found up to 1.1 km upstream of the confining basin margin locally at Hope Quarry. See Figs 4.12 and 4.16 for the distribution of log sites and panels and see Fig. 4.16a for the legend to sedimentary features. MC, mud clast.

a greater proportion of the FA-I deposits when compared with a similar thickness of strata in the lower Mam Tor succession where a mixture of Type A and B beds occurs (Figs 4.11, 4.13)

Lateral tracing of beds and variation in depositional character towards the confining basin margin

Individual beds can be traced laterally over distances up to c. 250 m at HQ (Figs 4.16a-d, 4.17a-d). Bed transects can be orientated at a high angle to the strike of the confining basin margin, such that any lateral variation in depositional character can be assessed with respect to increasing proximity towards the confining basin margin.

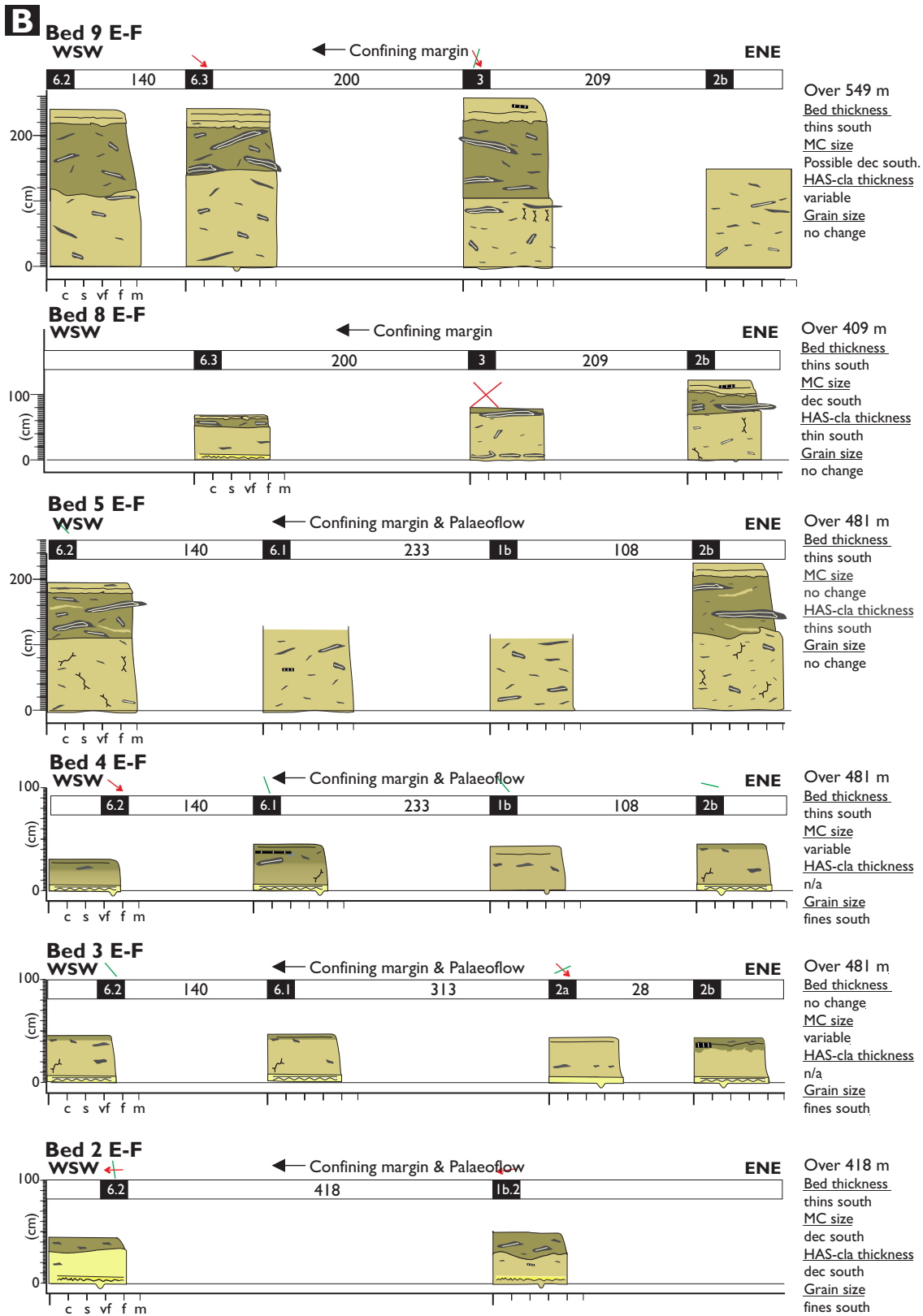


Figure 4.17 ctd.

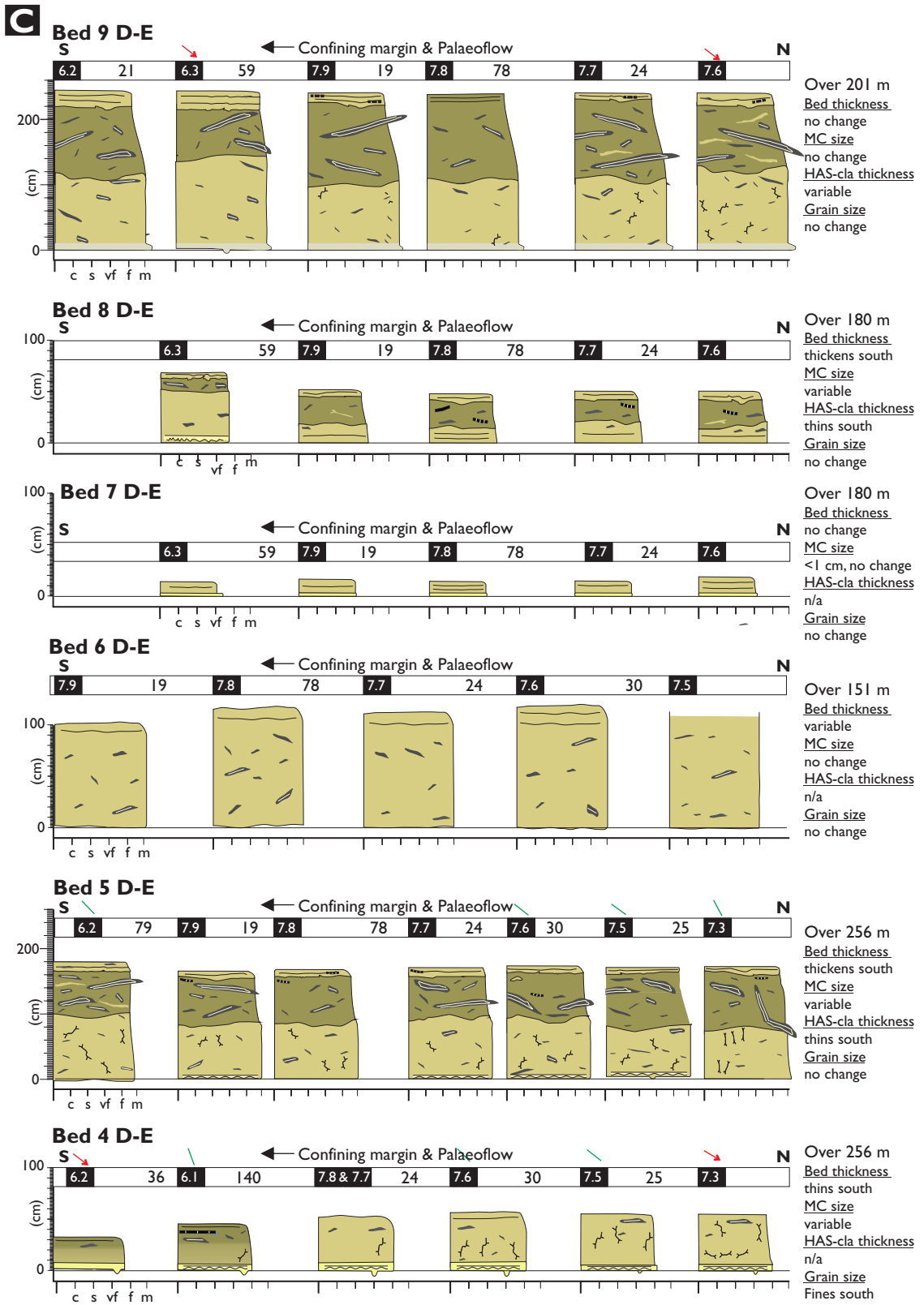


Figure 4.17 ctd.

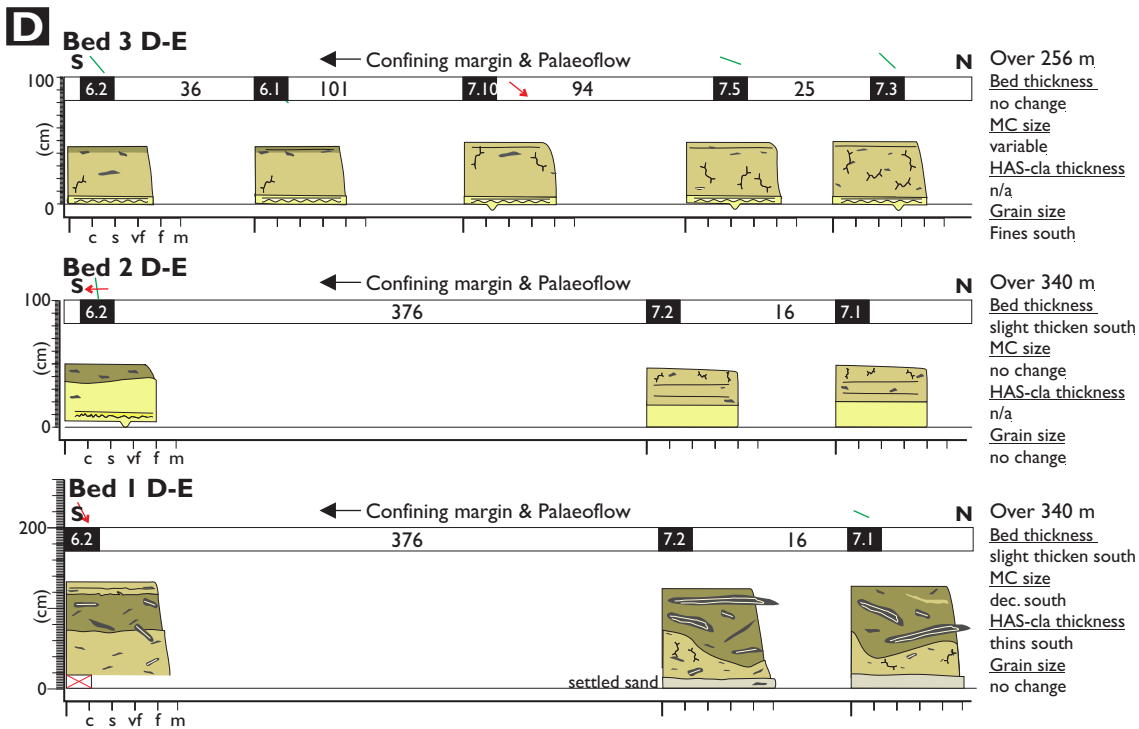
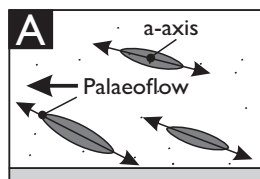
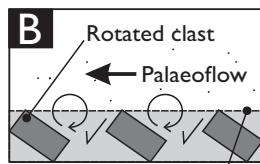


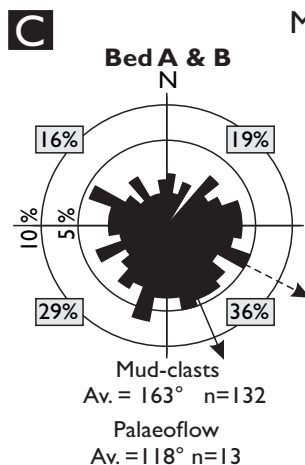
Figure 4.17 ctd.



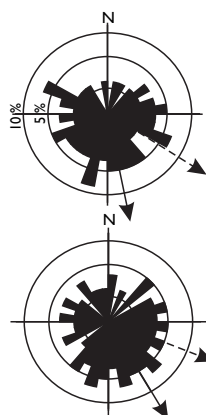
Clasts transported within gravity flows can develop inclination in their long axis (a-axis) with the elevated end of this axis orientated in the downstream sense of palaeoflow (Postma et al., 1988).



Passing flows may deform underlying substrate and generate clasts which are inclined in an upstream direction (Butler & Tavarnelli, 2006).



Mud-clast fabric



Bed A
 Mud-clasts: Mean = 174° n=65
 Non-uniform distribution (Von-Mises)
 at 5% confidence level

Palaeoflow: Mean = 123° n=7

Bed B
 Mud-clasts: Mean = 150° n=67
 Non-uniform distribution (Von-Mises)
 at 1% and 5% confidence levels

Palaeoflow: Mean = 112° n=6

Figure 4.18. A) The long axis of mud-clasts can become elevated in the direction of palaeoflow where transported within flows (Postma et al., 1988). **B)** Mud-clast rotation and alignment by an overriding gravity flow with mud-clast long axis elevated in the direction of sole structures found on the underside of beds (modified from Butler & Tavarnelli, 2006). **C)** Distributions of mud-clast fabrics collected from the mud-clast-charged division of two FA-1A (Type B) beds. Statistically, mud-clast fabrics exhibit a weak preferential distribution (Von-Mises) towards the south-east; this mud-clast-inferred palaeoflow direction is comparable to the palaeoflow indicated by sole structures on the base of the base of the bed.

Laterally, strata and beds remain at a near-constant thickness towards the confining basin margin (Figs 4.16a-d, 4.17a-d). In FA-1B and FA-1A deposits, matrix-rich sandstones are present, and comprise a significant proportion of bed thickness (~55%) as far away as 1 km upstream of the confining basin margin (Fig. 4.17a-d), as are the matrix and mud-clast-rich divisions of FA-1A beds (Fig. 4.17c). FA-1B and FA-1A do not transition laterally between one another, nor into other deposit types. FA-1B deposits exhibit minimal lateral variation in terms of facies type and their relative proportions, with any changes in their depositional character largely driven by subtle changes in mud-clast presence and abundance (Fig. 4.17a-d). In FA-1A deposits, the basal, thin, matrix-poor banded sandstone can pinch-out; however there is no consistency in the direction of pinch-out in respect to proximity to the basin margin or palaeoflow (Fig. 4.17c, Bed 5). The mud-clast-rich division in FA-1A beds is extensive, but varies in thickness significantly (22-67 % of bed thickness) and repeatedly over short length scales (tens of m) at the expense of underlying mud-clast-poor sandstone, despite minimal change in overall bed thickness (Fig. 4.17d, Bed 3). Similar variations in the thickness of mud-clast-rich divisions have been described from confined (Southern et al., 2015 – Chapter 6) and unconfined deep-water systems (Hodgson, 2009; Fonesu et al., 2015). Thus, whilst variations in depositional character (e.g. facies presence and proportion, mud-clast abundance) do occur, these are random and non-systematic with respect to increasing proximity towards the confining basin margin.

Mud-clast fabrics within FA-1A

Previous studies have demonstrated how mud-clasts orientation can record palaeoflow direction, where transported within flows, or where present as the deformed remnants of intact substrate deformed beneath overriding flow (Postma et al., 1988; Johansson & Stow, 1995; Butler & Tavarnelli, 2006). In these cases, the orientation of the elevated end of the a-axis is considered to record the direction of palaeoflow (Fig. 4.18a,b). Palaeoflow direction can also be inferred by the inclination direction of fold nose axes in sheath-folded clasts, transported within flows such as that observed in slumps (Miyata, 1990; Bradley & Hanson 1998; Debacker et al., 2009). The direction of the elevated end of the mud clast a-axis (n=106), and inclination direction fold noses axes (n=26), were measured from the mud-clast-rich division of two FA-1A beds with comparable palaeoflow directions (Fig. 4.18c). Structural restoration of the data was not required, as the structural dip on beds was negligible (<5°).

Cumulatively, the distribution of the measured mud-clast directions in these beds exhibits significant spread; however, there is a higher frequency of mud clasts directed towards the south (65%) compared to the north, with 36% directed towards the south-east (Fig. 4.18c). Using the EZ-ROSE computer program of Baas (2002), a statistical analysis of mud-clast orientations was conducted separately for Bed A and Bed B (Fig. 4.18c). In Bed A the

distribution of the mud-clast population is uniform when considered at a 1% confidence level however the distribution is considered non-uniform (Von-Mises) with a mean direction towards 174° for a 5% confidence level. The mud-clast population in Bed B exhibits a non-uniform distribution (Von-Mises) at both 1% and 5% confidence levels with a mean towards 150°; this mean is comparable to the mean for Bed A at a 5% confidence level (174°). The preferential distributions of mud clasts in Beds A and B (174° and 150°, respectively) are comparable to both directional sole structures recording palaeoflow in these beds (112° and 123°, respectively) and the dominant palaeoflow trend observed at HQ.

The weak preferential distribution of the mud-clast population may reflect a number of factors. As discussed prior, a flow event passing HQ is interpreted to comprise both incoming flow and flow already deflected by, and travelling parallel to the strike of, the confining basin margin; such complexity may cause the spread in the distribution of mud-clast directions. Furthermore, variations in mud-clast size, shape, or density may favour discrete styles of transport within the flow (rolling, dragging, clast buoyancy), resulting in discrete alignments; particle size is known to influence grain fabric orientations within sandstones (Baas et al., 2007). An element of measurement error may also be a factor as it is difficult to accurately record shallowly inclined mud clasts (<5°).

4.6 Discussion

Several studies have documented the localised development of deposits similar to FA-I in onlap settings adjacent to confining topography features and proposed a range of mechanisms for their development (McCaffrey & Kneller, 2001; Puigdefàbregas et al., 2004; Barker et al., 2008; Patacci et al., 2014). In this study, the origin of FA-I deposits within the Edale Basin is discussed with respect to the downstream confining slope on the southern basin margin. Building upon insights gained from this, and through comparison with other studies, the control flow run-out distance, as determined by basin physiography, is explored in terms of the influence it may exert upon the character and distribution of HEBs in basin infill successions.

4.6.1 Origin of FA-I deposits

4.6.1.1 Failure from the confining basin margin

Slope failures upon topographic features on the sea floor are common, and may be spontaneous (Giles & Lawton, 2002), or triggered by other gravity currents (Kneller & McCaffrey, 1999; McCaffrey & Kneller, 2001). In the latter case, it is suggested that turbidity current incidence with a confining slope can trigger failure or large-scale delamination of muddy strata, in the form of a synchronous debris flow travelling away from the confining slope, which results in the deposition of mud-clast-rich divisions encased within sandstone

beds locally near onlap settings (e.g. Annot Sandstone, Braux - Kneller & McCaffrey, 1999; Puigdefàbregas et al., 2004).

FA-IA beds containing mud-clast-rich divisions are not thought to originate following gravity current triggered destabilisation of confining slopes *sensu* Kneller and McCaffrey (1999) or Puigdefàbregas et al. (2004). The tabular nature of FA-IA beds, and the lateral extent of mud-clast-rich divisions (up to 772 m) in which material typically does not exceed 1 m in length, and exhibits no reduction in disaggregation towards the confining basin margin (Fig. 4.17), suggests material was not derived from local slope failure. Considering the thickness and extent of mud-clast-rich divisions (Fig. 4.16), it is expected that the failure and transport of such material should disrupt underlying strata however, mud-clast-rich divisions never truncate through multiple layers of stratigraphy, and are always underlain by a laterally-persistent sandstone facies (Fig. 4.17). The preferential distribution of mud-clast fabrics with respect to the direction of palaeoflow, inferred from sole structures on the bed base, suggests such material was transported within the flow depositing the basal sandstone, as opposed to discrete outbound failure travelling north away from the confining basin margin (Fig. 4.18c)

4.6.1.2 Substrate deformation and delamination

Butler and Tavarnelli (2006) described the deformation and entrainment of mudstone-dominated substrate beneath high concentration flows in the Gorgoglione flysch, Italy in which the substrate took on a chaotic character (minor thrusts, mud-clast rotation and folding, sandstone injection, flame structures). The fabric of deformation (fold noses and sheared flame structures) and rotated mud clasts verge in the direction of sole structures on the overlying sandstone, indicating substrate modification was syn-depositionally linked to the overlying bed (Butler & Tavarnelli 2006); in places, substrate modification penetrates down to an underlying sandstone bed (Butler & Tavarnelli 2006, their Fig. 7c) and resulted in a composite deposit with a pseudo-HEB character (i.e. mud-clast-rich interval encased between underlying and overlying matrix-poor sandstone).

The majority of mud-clast-rich divisions in FA-IA deposits are not thought to result from substrate deformation and generation of a composite bed. These divisions are typically overlain by thin (<10% of bed thickness), finer-grained laminated sandstone, interpreted to be the product of relatively dilute trailing flow not thought capable of laterally extensive and deep modification of substrate (Fig. 4.17). Examples of composite deposits are recognised which differ from typical FA-IA deposits, in that the capping sandstone is notably thicker (>25% bed thickness) and is of comparable grain size and facies to that normally found at the base of FA-I deposits (banded sandstone, non-stratified sandstone; Fig. 4.19). In some cases, the mud-clast-rich division was present in the earlier deposited event bed (Fig. 4.19a); in other examples it is clear that substrate deformation contributed, at least in part, to the chaotic character of the

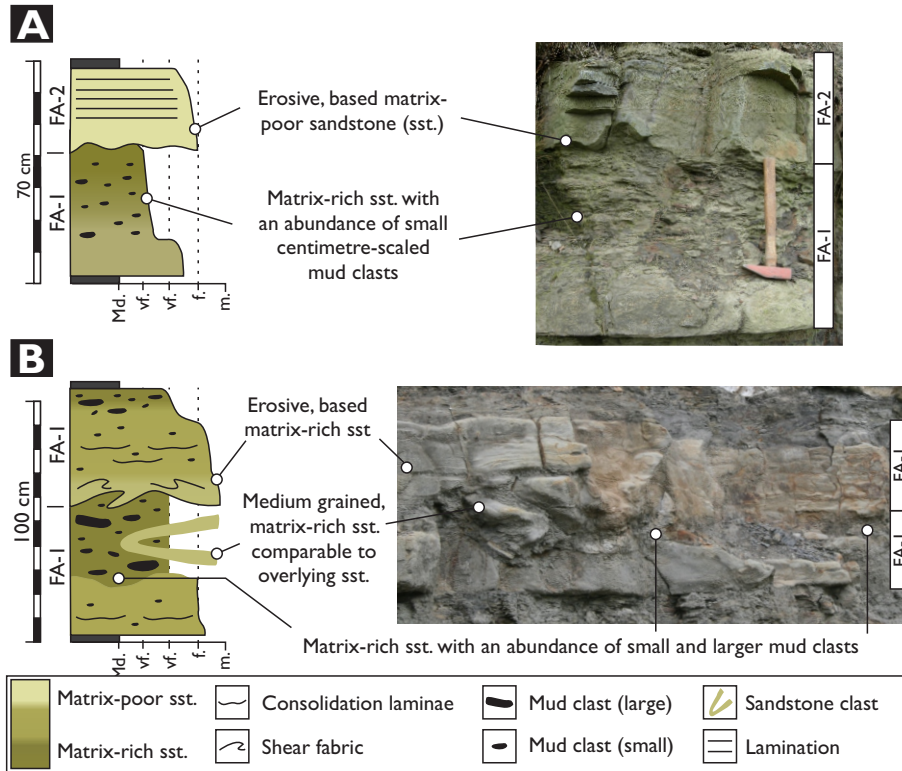


Figure 4.19. A & B Examples of composite deposits, produced by more than one depositing flow, contain a mud-clast-rich division encased within sand which is comparable to that seen in HEBs (FA-1A) deposited by one flow event. Composite deposits are distinct where the capping sandstone above the mud-clast-rich division is coarser grained than underlying sandstone and has a greater proportion of the bed thickness compared to that in FA-1A beds.

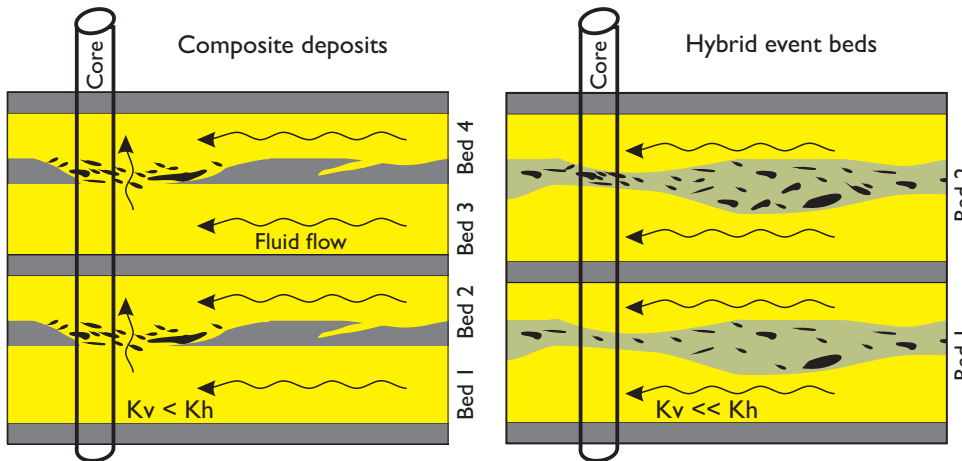


Figure 4.20. Implications of interpreting a one dimensional core as a succession of composite beds (A) or hybrid event beds (B). A) Composite beds are associated with higher bed amalgamation and thus a greater vertical permeability (K_v). B) Hybrid event beds typically exhibit infrequent bed amalgamation and thus K_v is dramatically reduced compared to that in A.

mud-clast-rich division (Fig. 4.19b), which may or may not have been associated with the earlier deposited bed. Although not observed in this study, lateral transition of the mud-clast-rich division into intact mudstone substrate would indicate instances where this division was solely a product of substrate modification. Thus, deposits with a pseudo-HEB character can be produced by substrate modification between separate event beds, rather than by flows transporting a region of mud-clast-rich turbulence-suppressed flow.

Misinterpretation of HEBs as pseudo-HEBs, or *vica versa*, has implications for inferring the spatial character and temporal behaviour of depositional systems (see Haughton et al., 2009 and Hodgson, 2009), and thus the distribution and volume of reservoir heterogeneity away from one-dimensional core-data (Fig. 4.20)

4.6.1.3 Confinement-driven flow transformation

Studies from confined systems have documented the local development and systematic thickening, of matrix-rich or mud-clast- matrix-rich sandstone within beds at the expense of underlying cleaner sand in the same bed with increasing proximity towards confining slopes (Britannia Sandstone, North Sea - Barker et al., 2008; Annot Sandstone, Braux, SE France - Patacci et al., 2014; Fig. 2.32). To account for these facies distributions, the effects of flow confinement (lateral flow thinning, Barker et al., 2008; downstream flow obstruction, Patacci et al., 2014) were suggested to result in confinement, turbulence-suppression, flow transformation, and the development of localised facies tracts near the confining slope (<1 km from onlap - Patacci et al., 2014). The occurrence of matrix-rich facies in Type A-E beds, located 7 km upstream of the confining basin margin (Fig. 4.9), is in marked contrast to these previously documented localised distributions, and indicates a hybrid flow character was developed during earlier flow run-out, prior to flow confinement at the basin margin. HEBs in the Edale Basin are interpreted to record flows which had become clay-enriched upstream, following entrainment of muddy substrate (i.e., Haughton et al., 2009) and / or flow depletion (Sumner et al., 2009; Kane & Ponten, 2012) and are discussed further in Chapter 5. The observations demonstrate that systems developed in topographically complex settings do not necessarily develop HEBs which are local to onlap settings. Thus, HEBs are not necessarily indicators of proximity to confining topography in such settings and matrix-rich, mud-clast-rich sandstone, with less desirable reservoir quality, can be distributed more extensively across the basin fill.

It is unclear as to whether established hybrid flows underwent further localised flow transformation upon their eventual confinement at the downstream basin margin. Lateral tracing of individual beds at HQ revealed no systematic variations in depositional character towards the confining basin margin (Fig. 4.17) and could suggest that incoming clay-rich flows, predisposed to deposit HEBs, were more resistant to confinement-driven transformation and

the development of slope-localised depositional trends compared with that documented in previous studies (Barker et al. 2008; Patacci et al., 2014); as such, depositional trends may be expressed elsewhere or over length scales greater than that of the available exposure at HQ. At HQ, the higher proportion of FA-IA deposits with a matrix-rich sandstone base (Type B beds), compared with those at Mam Tor, is not considered to indicate non-axial settings as grain sizes are comparable with FA-IA deposits at Mam Tor. Bed thicknesses cannot be used to further constrain this as beds are inherently thinner at Mam Tor due to its closer proximity to the confining basin margin. Nor does the dominance of Type B beds at HQ simply reflect depositional contrasts which have arisen due to variations in proximity of these locations to the confining basin margin (Fig. 4.1c). Sections 4.5.2.1 and 4.5.2.2 outlined how HQ is situated downstream of Mam Tor, as well as how flows passing HQ could comprise both incoming flow approaching the basin margin from the north and flow which had already been deflected (in the vicinity of Mam Tor) to travel south-west towards HQ (Figs 4.11, 4.15). As such, the higher proportion of matrix-rich based Type B beds at HQ, located downstream of Mam Tor, may indicate that flow confinement exerted a local modification of flow and deposit character.

Experimental studies using relatively turbulent, yet clay-rich, flows have shown how flow deceleration results in a reduction of shear stresses in the flow, with collapse of the flow towards the bed and the development of relatively cohesive, turbulence-suppressed flow as bonding of cohesive material present within the flow becomes more significant (Baas et al., 2009, 2011; Sumner et al., 2009). Where deceleration rates were faster, such as that likely to occur adjacent to the steep margin of the Edale Basin, a higher proportion of the sand fraction was retained and supported by the cohesive, turbulence-suppressed flow and was later deposited as a matrix-rich sandy deposit (Sumner et al., 2009). As such, the dominance of FA-IA beds with a matrix-rich sandstone base (Type B beds) at HQ, compared with Mam Tor, may indicate a confinement-driven transformation to cohesive, turbulence-suppressed flow in the earliest depositing (frontal) region of the flow, following confinement and deflection which had occurred further upstream along the confining basin margin. These observations suggest that relatively non-cohesive flow, located in the front of flows characterised by longitudinal rheological heterogeneity (i.e., hybrid flows *sensu stricto*, see Chapter 5, section 5.5.2), can be subject to flow transformation upon deceleration, such as that arising from confinement at the basin margin. Whether the front of the flow undergoes such transformation upon confinement, is expected to be influenced both by the proportion of cohesive material in the flow prior to confinement (as determined by the initial flow composition, entrainment processes or deceleration of the flow), as well as the rate of flow deceleration which was experienced upon flow confinement (see Sumner et al., 2009 and Baas et al., 2011).

4.6.2 Influence of the proximity of confining topography upon HEB character and distribution

Hybrid flows were developed by processes which promoted clay-enrichment and flow transformation prior to confinement at the basin margin. Such processes, initiated upstream, may require time, and therefore flow run-out distance, to operate and drive flow transformation. For example, there may be a lag time during which entrained mud clasts are redistributed towards the rear of the flow as well as a lag time in their progressive disintegration and release of cohesive clay into the flow (cf. Haughton et al., 2003, 2009). Variations in mud-clast disaggregation and redistribution have been suggested to account for variations in HEB character observed between relatively smaller and larger deep-water systems with contrasting run-out distances (Haughton et al., 2009)

The potential run-out distance of a flow is influenced by inherent flow characteristics (i.e. flow efficiency *sensu* Mutti, 1979, 1992; Normark, 1978; Mutti & Normark, 1987; Laval et al., 1988; Normark & Piper, 1991; Gladstone et al., 1988), and in topographically complex settings, is further influenced by basin physiography (i.e. basin size or the location of intra-basinal topographic features within). Contrasts in the character and distribution of FA-I deposits with respect to confining topography in the Edale Basin and Annot sub-basin (Patacci et al. 2014), may reflect variation in the available flow run-out distance in these systems (c. 25 vs. 10 km, respectively), and thus the timing and style of flow transformation driving emplacement of FA-I deposits (i.e. prior to, or as a consequence of interaction with the confining basin margin).

4.6.2.1 Proximally-confined flow

Where flow run-out distance is limited by basin physiography (i.e. reduced basin length, or relatively proximally-located intra-basinal topography), flow transformation processes initiated upstream may be overprinted by flow confinement effects. In such cases, HEB deposition may be localised in a narrow region in onlap settings with facies variation from turbidite to HEB occurring over relatively short length scales (i.e. ~1 km, Patacci et al., 2014; Fig. 4.21a).

4.6.2.2 Distally-confined flow

Where flow run-out distance is relatively longer (i.e. due to increased basin length, or a relatively more distal location of intra-basinal topography), there may be sufficient time for upstream-triggered flow transformation processes to operate prior to confinement by sea-floor topography. Consequently, HEBs may not be localised to confining topography, may be distributed over a greater lateral extent within the basin infill, and may exhibit facies variations expressed over longer length-scales (10s to 100s km), from upstream to more distal settings (Haughton et al., 2003; Edale Basin - this study; Fig. 4.21b). Thus, HEB distributions may be more comparable to those observed in unconfined systems, where HEBs dominate in distal and marginal fan settings (Haughton et al., 2003, 2009; Hodgson, 2009; Kane & Pontén, 2012).

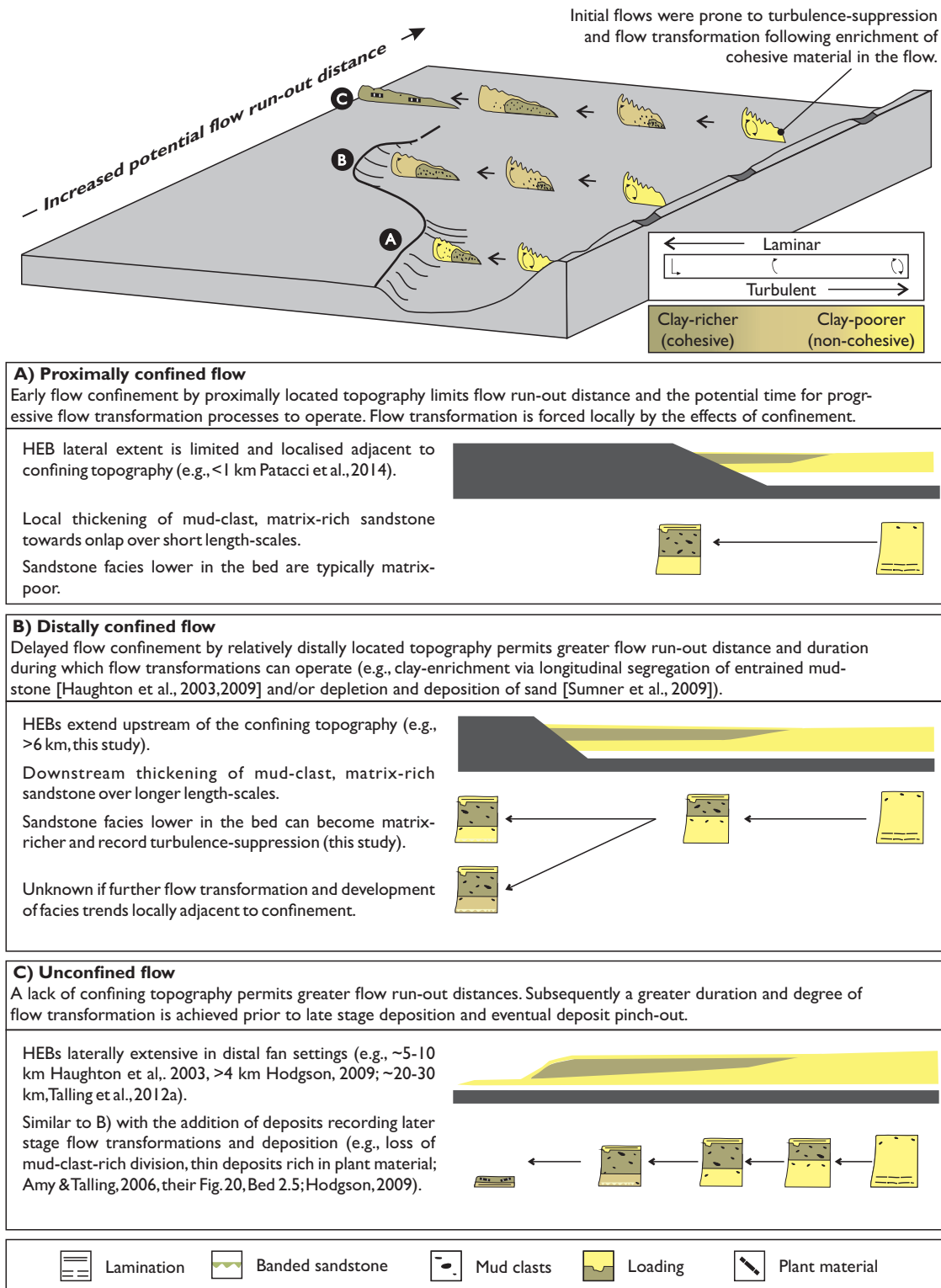


Figure 4.21. Schematic block model illustrating the effect of flow run-out distance, as determined by basin physiography, exerts upon flow transformation processes and the distribution of HEB in basin infill successions.

Observations here suggest HEB depositional character, and inferred flow character, may vary after flow confinement and deflection with replacement of matrix-poor sandstone bases by matrix-rich sandstone bases in FA-IA deposits following the collapse, re-concentration and turbulence-suppression in the flow head. The expression of topography on the sea floor during

basin infill can be dynamic, therefore scenarios may arise where the generation of intra-basinal topographic features may dissect a depositional system and reduce the flow run-out distance, resulting in a change from distally-confined to proximally-confined HEB distributions (Fig. 4.22b, c respectively).

4.6.2.3 *Unconfined flow*

Where flows are small in relation to the size of the basin, or where confining topography is lacking, flow efficiency is the limiting factor upon flow run-out distance, and deposits pinch out naturally without forced onlap onto confining topography (Fig. 4.21c). HEBs are expected to be distributed in distal and marginal fan settings as observed in other unconfined systems (Fig. 2.21a), with facies variations expressed over long-length scales, and occurrences of the distal-most expression of these deposits (Amy & Talling, 2006; Hodgson, 2009; Kane & Pontén, 2012). Amy and Talling (2006) describe such long length-scale (tens of km) facies tracts, and note the rapid distal downstream thinning of HEBs into deposits enriched with carbonaceous plant material (Facies tract 2A of Amy & Talling, 2006; Talling et al., 2012a) - similar to that observed in some FA-IB deposits in this study. Similar thin HEBs enriched in plant material are also found in the large unconfined Permian-aged Tanqua Depocentre (<100 km run-out) of the Karoo Basin (Hodgson, 2009). Where sedimentation is sufficient to bury and remove the expression of topography on the sea floor, previously confined settings, with relatively limited HEB distributions, may become unconfined, and come to exhibit more extensive, unconfined HEB distributions (Fig. 4.22).

Flow run-out distance, and thus the duration of the period in which flow transformation processes operate, may also be influenced by other factors in addition to the relative proximity of confining topography. The relative position at which flow transformation processes are initiated upstream with respect to that of downstream confining topography is also likely to be an important controlling factor. Flows can entrain substrate at various locations along the flow pathway, including the slope (Haughton et al., 2003, 2009) or basin floor (Amy & Talling, 2006; Fonnesu et al., 2015), or may be enriched in such cohesive material upon initiation (Lee et al., 2013). Furthermore, the time required for flow transformation to occur may also vary, depending upon the rate at which such processes are permitted to operate within the flow, likely influenced by a number of flow characteristics (i.e. Reynolds number, velocity and concentration structure). Examples of thin-bedded carbonaceous-rich deposits (FA-IB) in the Edale Basin (comparable to the distal expression of HEBs observed in unconfined systems, Amy & Talling, 2006; Hodgson, 2009), suggest that, despite the presence of confining topography, flow efficiency is also an important factor influencing the character and distribution of HEBs, and associated reservoir heterogeneity in confined settings. This study highlights the need for greater awareness and understanding of the factors influencing flow

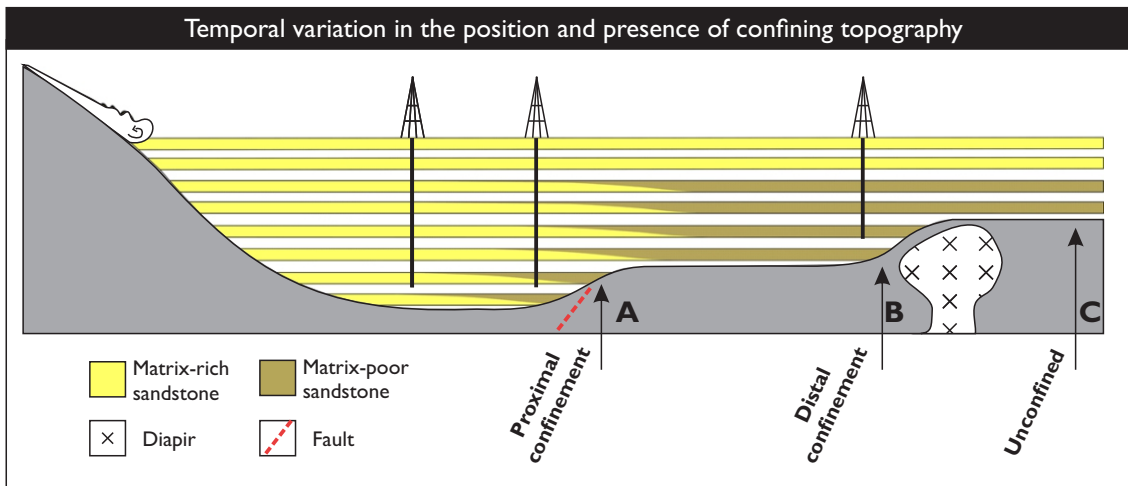


Figure 4.22. Schematic model illustrating how temporal variations in the position or presence of confining topography, and subsequent flow run-out distance may affect the stratigraphic distribution of HEBs within a basin infill succession.

transformation processes (i.e., rates and durations), as well as their interplay and variation over time, in order to improve confidence in sub-surface reservoir characterisation.

4.7 Conclusions

Gravity currents entering the Edale Basin from the north were confined and deflected along a steeply-inclined, downstream, confining basin margin. HEBs are widely distributed across the basin, and are encountered at least 7 km upstream of the confining basin margin; they do not exhibit systematic variation in depositional character towards the confining basin margin. Successions from the deep-water MTS exhibit downstream variation from turbidite (FA-2) to HEB (FA-1) dominated successions over several km. Such character and distribution of HEBs in the confined Edale Basin is in contrast to that observed in other, smaller, confined sub-basins, and indicates that HEBs did not result from confinement-driven flow transformation at the basin margin.

Contrast in the distribution of HEBs between these systems is interpreted to result from contrasts in the available flow run-out distance, controlled by basin physiography and the innate run-out potential of the flows, which determined whether flow transformation, turbulence suppression, and HEB deposition resulted following processes triggered upstream, or due to local confinement-driven flow transformations adjacent to confining topography. Observations from outcrops distributed along the confining basin margin suggest further local flow transformation may occur after confinement, with deflected flows being prone to collapse, reconcentration and turbulence suppression in frontal regions of the flow which were previously less cohesive prior to confinement. Thus, in addition to variation in depositional character towards the confining basin margin (cf. Barker et al., 2008; Patacci et al., 2014), HEBs may also exhibit variation along strike of the confining basin margin in regions downstream of where deflection occurred.

The flow run-out distance, and thus character and distribution of HEBs, can vary depending upon basin physiography (i.e. presence and position of confining topography). In settings where confining topography is located relatively early along the flow pathway, it is suggested that any upstream-triggered flow transformation processes that might eventually promote HEB deposition can be prematurely cut-short, or prevented by forced flow transformation at the confining basin margin. In such scenarios, HEBs may replace cleaner (matrix-poor) turbidite deposits over relatively short distances, and be localised in a narrow region adjacent to the confining slope (e.g. Patacci et al., 2014). Where confining topography occurs later along the transport pathway, upstream-triggered flow transformation processes may result in extensively distributed HEBs, which, despite the confined setting, may be distributed in an arrangement more comparable to that in entirely unconfined settings.

Given that the axial distance to confining topography must increase during basin infill, and that tectonic processes may rejuvenate intra-basinal topography, flow run-out distances may vary during the infill of a basin. Consequently, the overall character and distribution of HEBs within a basin-fill succession may evolve spatially and temporally. In addition to the relative position of downstream confining topography, the position at which upstream flow transformation processes were triggered and the flow magnitude can also modify the occurrence and distribution of HEBs. Awareness of these factors, and of their interplay and variation temporally, are important in developing improved models for subsurface prediction of facies and reservoir quality in both confined and unconfined settings, with implications for sub-surface reservoir characterisation.

Chapter 5. Character and occurrence of deposits from flows transitional between fully turbulent and cohesive flow behaviours: insights from the deep-water infill of the Edale Basin, Carboniferous, UK

5.1 Introduction

Chapter 5 focusses further on the deep-water infill of the Edale Basin with an emphasis on the stratigraphic occurrence of HEBs on a number of scales, in both the Mam Tor Sandstones (MTS) and the younger Shale Grit Formation (Fig. 4.1b,c). Chapter 5 considers the potential controlling factors upon HEBs in the wider context of the basin fill compared to that in Chapter 4 and discusses the character of HEBs in light of conceptual (Haughton et al., 2009, 2009) and experimental models (Baas et al., 2009, 2011; Sumner et al., 2009) for clay-rich, turbulence-suppressed flows believed to emplace HEBs. Chapter 4 provides an overview of the geological setting as well as facies and bed descriptions and interpretations which form the necessary background for Chapter 5; this material is not duplicated here.

HEBs have been described using a variety of nomenclature (e.g. slurry beds - Lowe & Guy, 2000; hybrid event beds - Haughton et al., 2003, Talling, 2013; co-genetic turbidite-debrite beds - Talling et al., 2004; transitional flow deposits - Sumner et al., 2009; Kane & Pontén, 2012). Such deposits are interpreted to record clay-enriched flows resulting from entrainment of muddy substrate (Haughton et al., 2003, 2009), or through flow depletion with subsequent redistribution or deposition of the non-cohesive sand fraction (Baas & Best, 2002; Talling et al., 2007a ; Sumner et al., 2009; Kane & Pontén, 2012; Baas et al., 2009, 2011; Terlaky & Arnott, 2014). Haughton et al. (2003, 2009) proposed the development of hybrid flows (*sensu stricto*), longitudinally variable in their rheology, either following entrainment of muddy substrate, or hydraulic fractionation and redistribution of cohesive material into the flow (Figs 2.26, 2.27). The subsequent flow structure is thought to exhibit a broad transition from non-cohesive, relatively turbulent flow at the front, through to cohesive, mud-clast-rich relatively turbulence-suppressed flow in the rear, thought to be expressed via progressive aggradation, in the vertical evolution of depositional character within HEBs (Haughton et al., 2003, 2009; Amy & Talling, 2006; Fonnesu et al., 2015). More recently, experimental work has also highlighted how the vertical redistribution of non-cohesive material, following flow depletion and settling of coarser sand fractions, may drive the development and downward thickening of a clay-rich, turbulence-suppressed, laminar-like plug in the upper flow (Figs 2.18, 2.19; Baas et al., 2009; 2011; Sumner et al., 2009). Where there is rapid flow depletion (*sensu* Kneller & Branney, 1995), the accompanying abrupt reduction in turbulent shear allows the yield strength

of the cohesive material in the flow to support a significant proportion of the sand fraction (Figs 2.18, 2.19; Hampton, 1975; Baas & Best, 2002; Sumner et al., 2009; Baas et al., 2011). As such, these experimental flows can emplace matrix-rich sandstone (Sumner et al., 2009, Baas et al., 2011) and exhibit settling of the coarsest sand fraction towards the base of the flow due to the relatively low yield strength of these cohesive, quasi-laminar flows (i.e., Marr et al., 2001; Sumner et al., 2009). Thus, flow transformation associated with clay-enrichment may affect discrete regions within the flow, or alter the flow on a larger scale.

The development and distribution of HEBs are widely proposed to be associated with the evolution of their hosting depositional system. Specifically, HEBs are suggested to record: 1) periods when the flow pathway was in disequilibrium, and prone to significant incision of muddy substrate (Haughton et al., 2003, 2009; Muzzi & Tinterri, 2010); 2) periods of fan initiation and growth (Fig. 2.22b; Haughton et al., 2009), perhaps linked to relative sea-level fall during incision of the preceding highstand mudstones (Fig. 2.22a; Hodgson, 2009); 3) periods of lobe progradation or lateral migration and back stepping where lobe successions exhibit a vertical increase or decrease in HEB abundance, respectively, due to the dominance of HEB in fan fringe settings (Fig. 2.22a; Kane & Pontén, 2012).

Using sedimentary logs collected across the deep-water infill of the Carboniferous Pennine Basin of N England, specific aims of this study are as follows:

- 1) to document the character and distribution (lateral and stratigraphic) of the range of HEBs present across the greater deep-water fill of the Edale Basin;
- 2) to consider the significance of HEBs in terms of system evolution, particularly in response to observed upstream cycles of incision and infill at the base of slope;
- 3) evaluate the role of discrete flow transformation processes upon deposit character and distribution in light of conceptual models of hybrid flow *sensu stricto* (e.g., Haughton et al., 2009) in which the flow becomes rheologically heterogeneous longitudinally and recent experimental work on clay-rich turbulence-suppressed flows, i.e., transitional flows *sensu stricto* (e.g., Baas et al., 2009, 2011; Sumner et al., 2009, Kane and Ponten 2012).

5.2 Data and methods

The MTS and younger Shale Grit Formation represent the deep-water component of the siliciclastic infill of the Edale Basin and were studied at several localities distributed across the basin (Figs 4.1c, 5.1). From these localities, detailed sedimentary logs (ranging from 1:5 - 1:25 in scale, and totaling 447 m in cumulative thickness), cover the majority of the stratigraphic thickness present in the MTS and Shale Grit Formation (Fig. 4.1b). Sedimentary logs were

taken to characterize spatial variations in HEB depositional character (i.e. texture, composition, sedimentary structures, proportions of facies within beds) and distribution in the Edale Basin, in order to gain insight into flow transformation processes within the basin.

5.3 Studied localities

Despite the occurrence of regionally extensive marine bands in underlying and overlying strata (Hampson, 1997, 1999), distinct correlative surfaces with chronostratigraphic significance are lacking within the deep-water infill of the Edale Basin. Subsequently individual exposures of the MTS and Shale Grit Formation located across the basin are compared and framed in terms of their position within the basin infill, based on lithostratigraphy and their relative spatial or stratigraphic position to one another (Fig. 5.1).

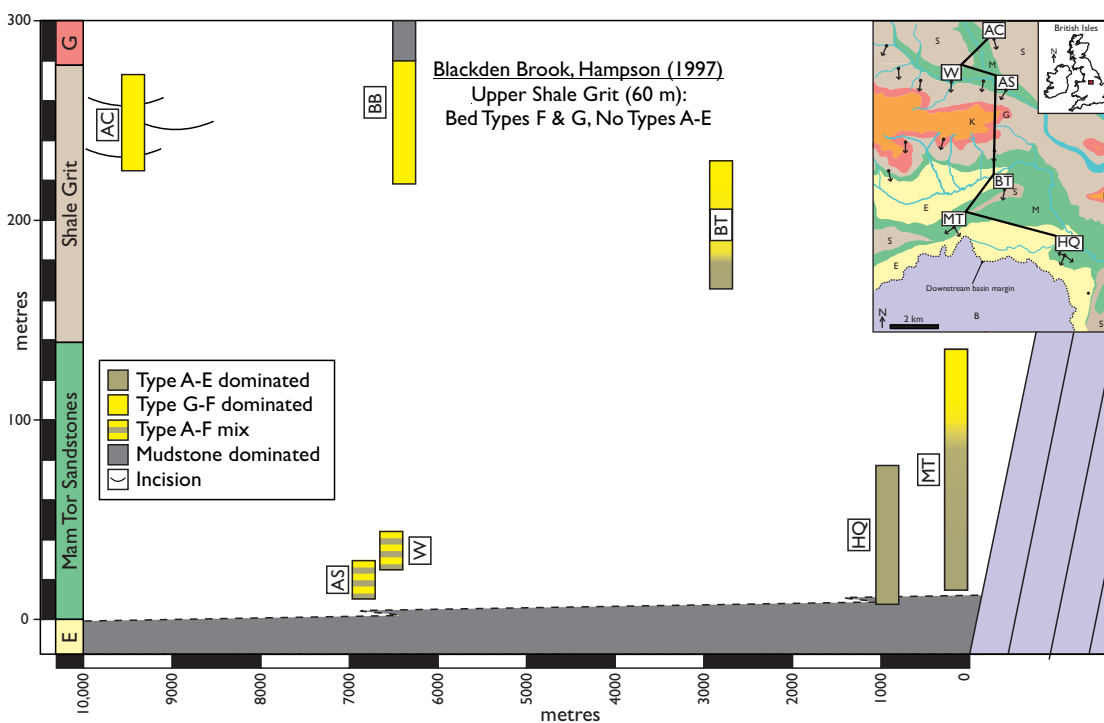


Figure 5.1. Distribution of studied localities with respect to the downstream confining basin margin (Derbyshire Massif). Correlation between outcrops is prevented by the lack of extensive or distinctive correlative surfaces as well as the lack of suitably sized or numerous outcrops across the basin. The abundance of HEBs (Type A-E) exhibits an overall decline upwards through the deep-water Mam Tor Sandstones and Shale Grit Formation at the expense of Type G & F beds with variations also occurring on a smaller scale in individual exposures (i.e., Mam Tor, Back Tor, Wicken and Ashop). The Ashop and Wicken exposures contain HEBs which are located 6-7 km upstream of the downstream confining basin margin. **AC**, Alport Castles; **W**, Wicken; **AS**, Ashop; **BT**, Back Tor; **MT**, Mam Tor; **HQ**, Hope Quarry.

5.3.1 Hope Quarry, Mam Tor & Back Tor

Three exposures of the MTS (Mam Tor and HQ) and Shale Grit Formations (Back Tor) occur in the distal part of the basin, upstream of the southern confining basin margin (Fig. 4.1c); these are described below.

5.3.1.1 Mam Tor

The succession at Mam Tor comprises nearly the entire thickness of the MTS (Walker, 1966a), with an amalgamation ratio of 15% (*sensu* Romans et al., 2009). Traditionally, the strata have been interpreted as a succession of deep-water turbidites (Allen, 1960; Walker 1966a), however the full range of gravity flow deposits illustrated in Fig. 4.4 are recognised here, and thus record the range of gravity flows that infilled the Edale Basin. Stratigraphically (vertically), the succession can be subdivided on a number of scales in terms of bed-type dominance and grain size (Fig. 4.10).

At the largest scale (c. 124 m), the succession exhibits a change in the dominant bed type, with replacement of mud-clast-rich matrix-rich deposits (Type A & B beds) by matrix-poorer deposits (Type F & G beds), with subordinate occurrences of mud-clast-poor matrix-rich deposits (Type C-E; Fig. 4.10). Such upwards-cleaning of bed types is paralleled by an overall reduction in mud clasts, regardless of bed type, maximum grain size, and bed thickness. This trend is driven by changes in the character of successive, decametre-scaled packages, defined by discrete changes in palaeoflow direction following periods of thick mudstone accumulation (Fig. 4.10, c. 32.7 & 74.8 m; Fig. 4.11a), and interpreted as discrete shifts in lobe position (Chapter 4 section 4.5.2.1; Fig. 4.11b). Each palaeoflow package exhibits a range of bed types, however, successive packages display a reduction in mud-clast- matrix-rich bed types (Type A & B) compared to matrix-poor bed type (Type G; Fig. 4.10).

Superimposed on these larger-scale trends are depositional packages exhibiting variations in depositional character on a smaller scale which can mimic or differ from those observed at the larger scale. A repeated trend in the lower palaeoflow zone is expressed as an overall upwards-coarsening and thickening of beds as matrix-rich bed types (Type A-B, D-E) are replaced and become subordinate to matrix-poor bed types (Type G; Fig. 4.10, Cycles A, B, C). Initially, deposits exhibit an increase in mud-clast abundance as Type D and E beds are replaced by Type A and B beds, prior to mud-clast abundance decrease as Type G beds become more dominant. Variation from this trend is recognised in Cycle D, where no reduction in mud-clast abundance is noted, despite an overall upwards-cleaning of beds prior to deposition of a thick mudstone-dominated package and the succeeding palaeoflow zone 2.

In other instances, an overall coarsening and increase in the proportion of matrix-rich sandstone is noted within beds, with minimal change in mud-clast abundance (Fig. 4.10, Cycles H, lower I). This is followed by a reverse of the trend, whereby beds become thinner, finer-grained, mud-clast-poor and relatively matrix-poor (Fig. 4.10, Cycle upper I), prior to the deposition of a thick mudstone-dominated package and the succeeding palaeoflow zone 3 succession. Stratigraphically higher in the succession, where matrix-poor beds dominate, trends comparable to those in lower cycles (Cycles A, B, C) occur, with beds thickening,

coarsening, cleaning, and losing mud clasts (Cycles L, M lower, M upper, N lower); these also nest to produce a similar trend on a larger scale (Cycles J, K, L, M; Cycles J-M). In the uppermost part of the succession trends, the definition of depositional cycles is problematic due to intervals of poor exposure.

5.3.1.2 Hope Quarry (HQ)

The exposure at HQ comprises a c. 74m-thick succession of gravity current deposits, which rapidly replaced accumulation of deep-water mudstones of the Edale Shales, and mark the abrupt onset of siliciclastic sedimentation in the Edale Basin. A fossiliferous marine band (*Reticuloceras reticulatum*) found in the uppermost Edale Shales here indicates that overlying gravity current deposits are those of the lower MTS (see Waters & Davies, 2006). Although direct correlation (and contemporaneity) with lower strata from the Mam Tor succession cannot be established, palaeoflow data at both localities indicate that flows in the vicinity of Mam Tor were often deflected south-eastwards towards HQ (Fig. 4.1c). The HQ succession contains a similar range of bed types, although depositional cycles are poorly defined, or lacking (Fig. 4.13). The absence of such trends at HQ is likely to result as a consequence of re-routing of gravity flows around the irregularly striking, southern confining basin margin (Chapter 4 section 4.5.2.1; Fig. 4.11b).

5.3.1.3 Back Tor

Direct correlation between Mam Tor and Back Tor (located c. 2 km to the north-east) is not feasible (Fig. 4.1c). Locally, the contacts between these shallowly dipping ($<5^\circ$) conformable strata are visibly inclined towards the east on valley sides, indicating that at a given height along strike, strata become younger towards the east, towards Back Tor. Structure contouring demonstrates that the base of the Back Tor succession is stratigraphically higher than the top of the succession at Mam Tor. However, the difference in stratigraphic height is difficult to constrain, due to lack of reliable dip magnitudes in a region affected by modern landslides, but is expected to range between c. 13 - 80 m, depending on the local dip ($2-4^\circ$). For overlap to occur between these successions, a local dip of $<1.5^\circ$ would be required.

When comparing with the Mam Tor succession, strata at Back Tor are coarser-grained with a higher amalgamation ratio (25%) and a lower proportion of matrix-rich bed types (Fig. 5.2). Sole structures (flute casts and groove marks) indicate palaeoflow towards the south-southwest (Fig. 4.1c). An upwards replacement of matrix-rich bed types by matrix-poor bed types is observed, similar to that observed at Mam Tor (Fig. 4.10). However, cleaning at Back Tor is associated with an overall coarsening and thickening of beds, a trend not recognised at Mam Tor. Bed cleaning is also observed in smaller-scale depositional packages in the lower

succession, and is accompanied by bed thickening, coarsening, and amalgamation or scouring towards the top of the depositional package (Fig. 5.2, Cycles A, B, C).

5.3.1.4 Wicken and Ashop

The Wicken and Ashop are two small river-cut exposures which occur c. 6-7 km north of the Mam Tor succession and the downstream confining basin margin (Fig. 4.1c). Strata here are considered to be the lower MTS, based on their proximity to the underlying Edale Shales as well as their grain size, which does not exceed upper medium-grained sand, and the amalgamation ratio (22% Ashop; 27% Wicken) compared to Back Tor. In this upstream succession, the full range of matrix-rich and matrix-poor bed types are present with the dominant bed type being those of the matrix-poor type (Fig. 4.9). Despite the limited stratigraphic thickness, vertical trends of bed-cleaning (replacement of matrix-rich beds), thickening, and coarsening accompanied by increased amalgamation (similar to those at Mam Tor and Back Tor) are observed succeeding thick mudstone deposits (Fig. 4.9).

5.3.1.5 Alport Castles

At Alport Castles, a c. 60 m-thick succession of the Shale Grit Formation crops out in a cliff face (c. 400 m in length) as a series of lenticular and sheet sandstone bodies, connected by erosional surfaces, or parted by more thinly bedded strata. This is overlain by an abrupt change to thin-bedded mudstone and siltstone strata at the top of the exposure (Figs 4.1c, 5.3). The geometry of these bodies has previously been interpreted as a series of stacked, multi-storey channel-fill sandstones cut into a finer grained slope succession (Clark & Pickering, 1996; Pringle et al., 2004). Within this existing framework, further investigation of facies (particularly those near the margins of incision surfaces) was aimed at providing insight into the temporal variation in flow processes, and transfer of sediment downstream during channel incision, bypass, and infill in the Edale Basin.

Channel bodies

Channel elements are sharp-based, and overlie incision surfaces which can exhibit a terraced geometry, commonly mantled by coarse-grained, clean (winnowed) sandstone supporting sub-angular mud clasts (facies MCB, Fig. 4.3g; Fig. 5.3, Element 3; Fig. 5.4). A step in the incision surface is seen to truncate deposits of facies MD (Fig. 4.3h) and facies MCB (Fig. 5.3, Element 3, Log C; Fig. 5.4); the latter is injected by sandstone from the sandy channel infill at this location (Fig. 5.4). Within facies MD, sandstones consist of laminae, or very thin beds, of starved ripples with notably finer-grain sizes (very fine-grained sand) than other sandstone facies locally.

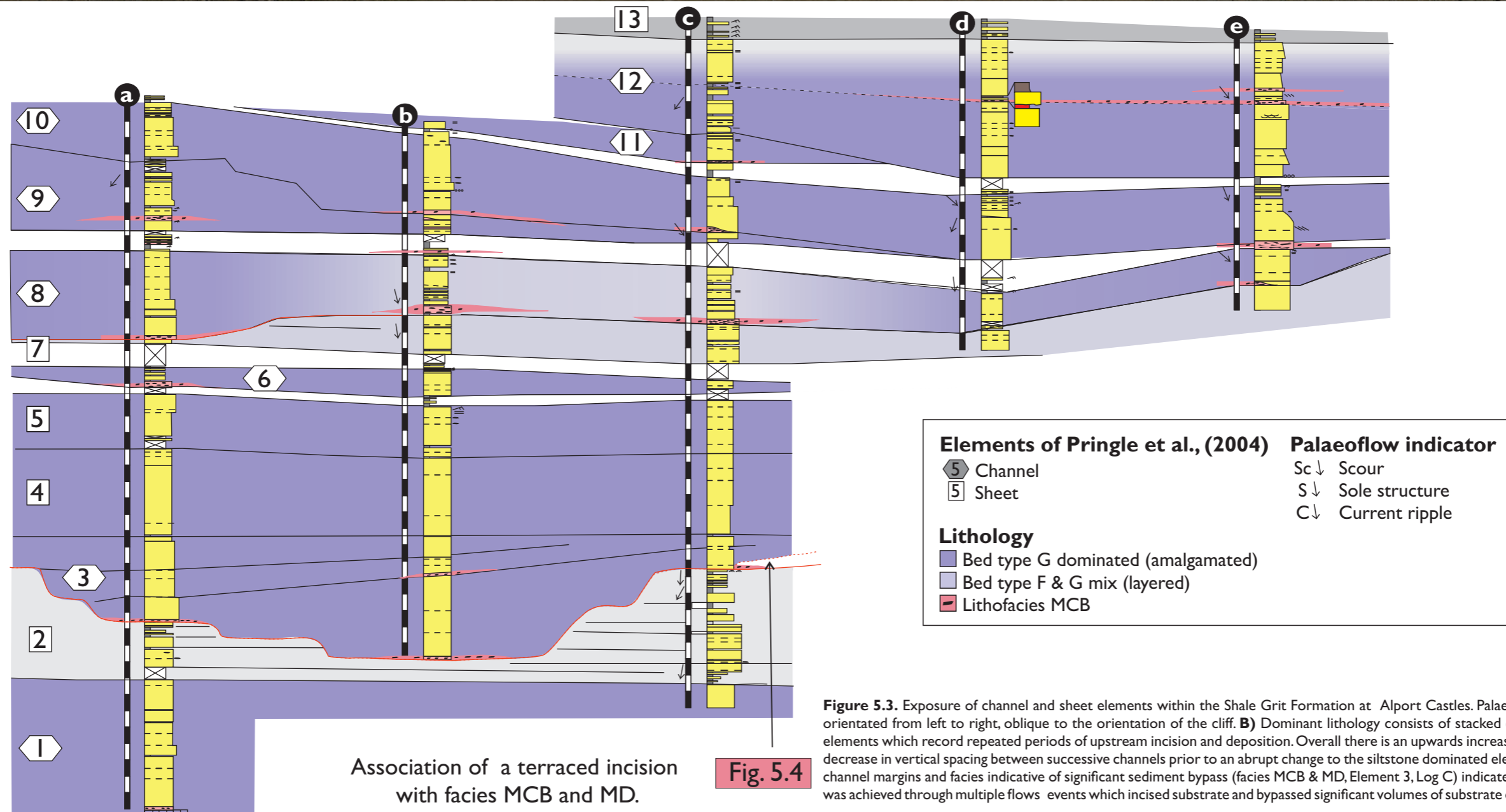
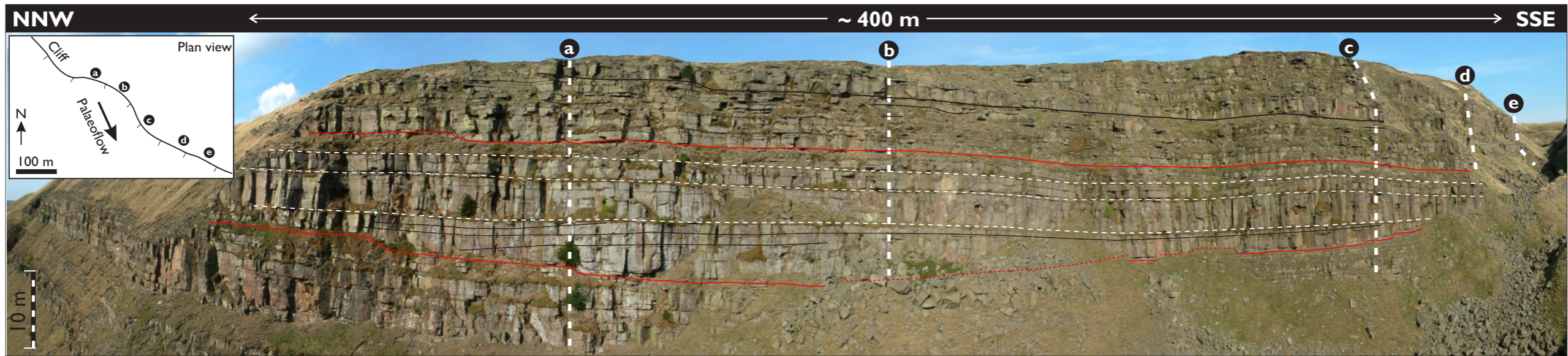


Figure 5.3. Exposure of channel and sheet elements within the Shale Grit Formation at Alport Castles. Palaeoflow direction is orientated from left to right, oblique to the orientation of the cliff. **B)** Dominant lithology consists of stacked channel and sheet elements which record repeated periods of upstream incision and deposition. Overall there is an upwards increase of grain size and decrease in vertical spacing between successive channels prior to an abrupt change to the siltstone dominated element 13. Terraced channel margins and facies indicative of significant sediment bypass (facies MCB & MD, Element 3, Log C) indicate channel sculpting was achieved through multiple flows events which incised substrate and bypassed significant volumes of substrate downstream.

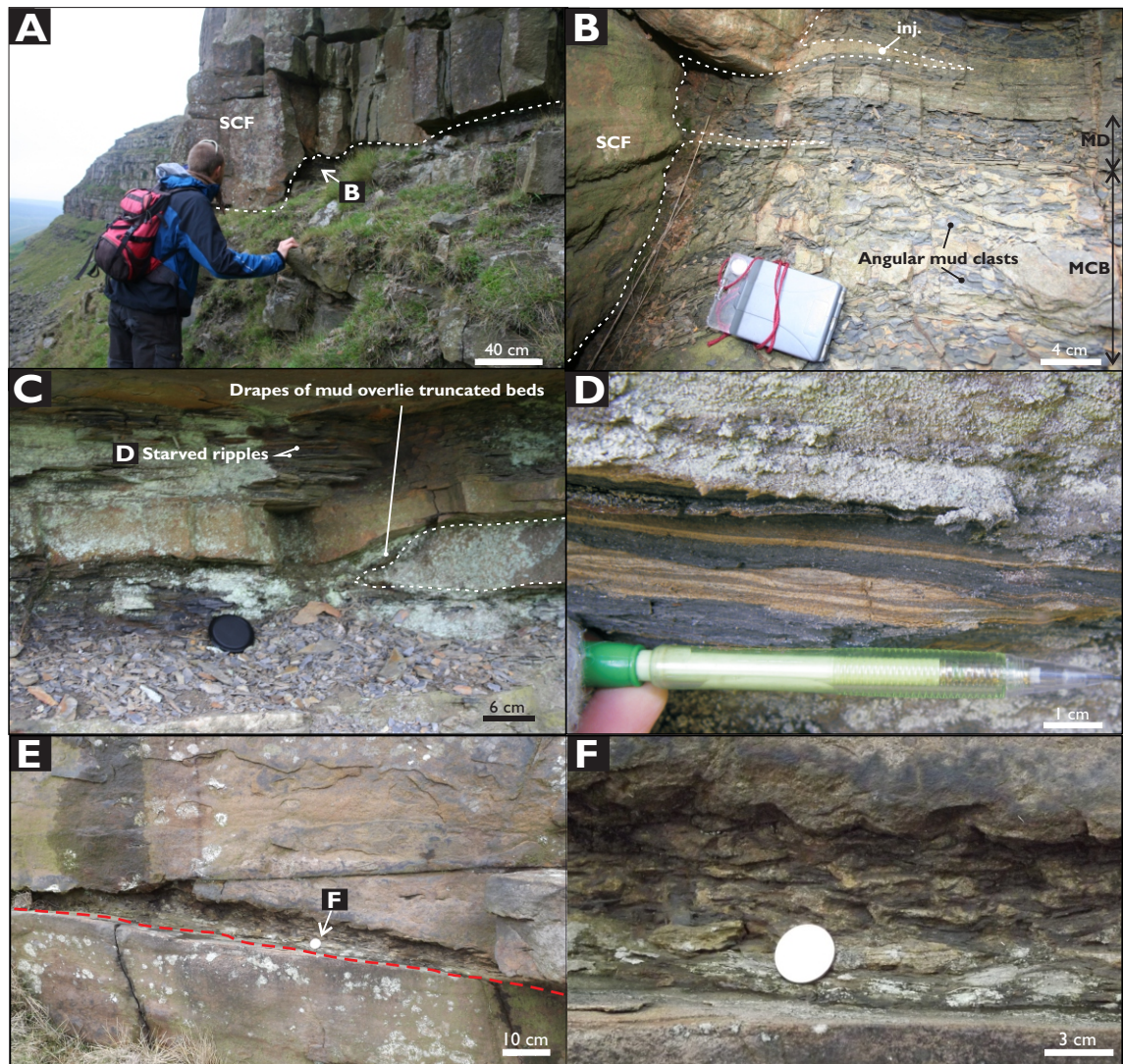


Figure 5.4. **A)** Terraced geometry of the incision surface underlying Element 3 (Fig. 5.3, Log, C). **B)** Close up showing how the incision surface beneath the sandy channel fill (SCF) truncates earlier facies recording previous local incision and bypass (facies MCB and MD). The association of these facies indicate that multiple flows of varying character sculpted channel incision surfaces during which incision magnitudes varied. **C & D)** Mud-draped scours and starved ripples in facies MD. **E)** Angular relationships around incision surfaces demonstrating how angular mud clasts (facies MFB, **F)** overlie incision surfaces and underlie channel fill.

The sandy channel infill appears to have been emplaced by a relatively small number of events, is dominated by amalgamated matrix-poor deposits (Type G), sometimes with low angle stratification or granule and pebble trains at their bases, and periodically displays inclined discontinuous lenses of facies MCB. Overall successive channel bodies exhibit a slight upwards-increase in grain size, and decrease in vertical channel body spacing (Fig. 5.3). Ground penetrating radar studies suggest that channel bodies stratigraphically higher in the succession are more deeply incised behind the cliff face (Pringle et al., 2004) prior to an abrupt transition into overlying thin-bedded mudstone and siltstone strata (Fig. 5.3, Element 13).

Sheet bodies

Sheet elements are not associated with facies MCB, inclined bedding, or significant incision surfaces that truncate bedding. Sheet elements typically comprise thick amalgamated matrix-poor deposits (Type G), where they overlie channel bodies (Fig. 5.3, Element 4 & 5), or

comprise more thinly bedded, less amalgamated interbedded Type G and F deposits (Fig. 5.3, Element 2).

5.3.1.6 Location interpretations

The succession at Mam Tor was constructed by at least 3 episodes of lobe deposition; successive lobes underwent subtle changes in their position and incidence with the confining basin margin (Fig. 4.11b), and likely record an overall temporal waning and/or retrogradation of the system as beds become thinner and finer grained. The return of coarser-grained and thicker-bedded deposits, with a dramatic increase in amalgamation ratio in younger strata at Back Tor, records a marked waxing and/or progradation of the system into the basin, and deposition in a more proximal fan setting. Strata at Wicken are considered to be relatively more proximal compared with downstream deposits of the MTS at Mam Tor.

At Alport Castles, channel incisions are interpreted as composite incision surfaces, sculpted by numerous flow events which incised substrate and bypassed the majority of sediment downstream. Repeated incision events are implicated by the occurrence of facies MCB and MD, recording discrete styles of incision and bypass (Table 1; Mutti & Normark, 1987; Hubbard et al., 2014), both of which are truncated by an incision surface beneath the sandy channel infill (Fig. 5.4). Facies MCB are clear indicators of local incision and sediment bypass, whereas incision associated with facies MD is ambiguous, as the majority of the flow bypassed and was not locally depositional. Although the bulk character of flows sculpting incision surfaces is unknown, such flows clearly had the capacity to incise and entrain local substrate and winnow deposits locally.

Transition from periods dominated by incision, to those dominated by incision infill at Alport Castles, marks a reduction in the volume of sediment transported downstream, potentially driven by waning flow energy and an overall backstepping of the system. During these latter periods of incision, infilling deposition occurred from non-cohesive (sandy) high density turbidity currents (Type G beds). Occurrences of facies MCB within channel fills is indicative of periods of overall infilling that were punctuated by events which incised and bypassed sediment downstream. Sheet bodies of thinner bedded, less amalgamated deposits record periods of relatively unconfined (non-channelised) deposition, perhaps recording greater waning of flow energy and retrogradation of the system. The presence of channel bodies which are more deeply incised higher in the succession (Pringle et al., 2004) may record the overall large-scale progradation of the fan system into the basin, as inferred from the Back Tor succession. Cycles of incision, bypass and infill, recording waxing-to-waning of flow energy, are repeated throughout the succession, and indicate the dynamic nature of flows, and the transfer of sediment downstream. The significance of changes in matrix-rich and matrix-poor bed type proportions, as observed on a number of scales throughout successions, is discussed

further below in light of these upstream incision and infill events, in addition to other potential controlling factors.

5.4 Discussion

5.4.1 Evolution of basin infill and implications for the character and distribution of matrix-rich bed types

Early interpretations of the evolution of the Edale Basin envisaged the southward advance of facies belts (i.e. fan slope and delta top), and proposed the Shale Grit and MTS were contemporaneous deep-water fan deposits, with the latter being the distal equivalents of the former (Walker, 1966a). Hampson (1997) later reassessed the basin infill in terms of sequence stratigraphic concepts. After recognising a number of features in the upper part of the basin infill succession (e.g. regional erosion surfaces, deep fluvial-infilled incisions, sharp depositional environment changes interpreted as a forced regression surface and condensed mudstones; Fig 4.1b), Hampson (1997) recognised the influence of sea-level upon the large scale evolution of the basin infill. The MTS and Shale Grit were interpreted as a lowstand system tract, developed during incision of upstream feeder channels, which were later infilled during early transgression and passive backfill as downstream sediment supply was removed.

Sea-level variability can account for many of the large-scale characteristics of the deep-water basin infill. The abrupt onset of deep-water siliciclastic sedimentation following deposition of condensed mudstones (Fig. 4.13) suggests that sediment supply was driven by an overall period of falling and low-stand sea level during which feeder channels were opened and incised upstream. Similarly, the abrupt end of deep-water fan deposition (as indicated by thick amalgamated turbidites of the Shale Grit Formation being abruptly overlain by condensed mudstones, Blackden Brook (Hampson, 1997), and mudstone-siltstone dominated strata (Fig. 5.3), records a period of significantly reduced sediment supply into the basin, associated with sea-level transgression. However, the occurrence of repeated cycles of incision, bypass, and deposition at Alport Castles indicates that similar processes of fluctuating flow character and sediment supply operated on a range of scales. These small-scale fluctuations could reflect allocyclic controls of smaller-scale fluctuations in sea-level superimposed on the larger sea-level curve (see Figueiredo et al., 2013), autocyclic controls or a combination of the two. Upper Carboniferous successions in the Central Pennine Basin and NW Europe often exhibit clear evidence for coherent cyclical fluctuations in relative sea-level driven by glacio-eustasy (Maynard & Leeder, 1992; Davies, 2008; Waters & Condon, 2012 and references within). Despite tectonic influences on the earlier infill of the Central Pennine Basin (Kane 2010b,c), evidence for tectonic activity during the Upper Carboniferous (Pennsylvanian) is lacking. The frequency of cut and fill events at Alport Castles, expressed on an element scale, suggests that

autogenic controls may have predominated, but does not necessarily discount the role of smaller-scale fluctuations in sea-level. Regardless of their origin, periods of incision and infilling record the dynamic nature of flow processes occurring during channel incision, bypass, and infill, with subsequent temporal variation in the character of flows which influenced deposition of the MTS and Shale Grit downstream.

5.4.1.1 System evolution and distribution of matrix-rich deposits

The succession at Mam Tor represents an overall waning and retrogradation of the system, with a loss of mud-clast-rich, matrix-rich deposits (Type A & B) and dominance of matrix-poor (Type G & F) and matrix-rich deposits (Type D & E) which are relatively mud-clast-poor and finer grained compared to Type A and B beds. The character of the upper portion of the succession may indicate an overall shift in the region of muddy-substrate incision further upstream of the depositional site. Mud-clast-rich matrix-rich bed types, interpreted as HEBs, are observed to undergo rapid pinchout of the mud-clast-rich division accompanied by significant bed thinning (Amy & Talling, 2006). Thus, mud-clast-poor matrix-rich Type D and E beds may represent the distal expression of Type A and B beds, and record incision in a more landwards location. Type D and E beds are notably enriched in carbonaceous matter, a common characteristic of matrix-rich deposits in the distal areas of long run out systems (Hodgson, 2009). Alternatively, Type D and E beds may indicate a reduction in the magnitude of muddy-substrate incision, with distal flow transformation and deposition driven by flow depletion of finer-grained, clay-rich flows (Sumner et al., 2009; Baas et al., 2011; Kane & Pontén, 2012). Alternations of matrix-poor and matrix-rich bed types in the upper Mam Tor succession are not thought to reflect temporal changes in the original composition of flows entering the basin, considering the frequency at which they occur. Instead, these alternations may record: 1) the downstream expressions of small-scale incision cycles occurring further upstream (Fig. 5.3); or 2) variation in periodicity of flow recurrence, and thus the availability of muddy substrate for entrainment.

An additional influential factor on the downstream expression of deposits may be evolution of the gradient at the base of slope. The Mam Tor succession marks the onset of siliciclastic basin-infill within a previously clastic-starved, post-rift setting. As such, the rate of change in gradient at the base of slope and rate of flow deceleration at the base of slope could have undergone an overall reduction as the basin infilled. Experimental work by Sumner et al. (2009) has highlighted the importance of the rate of flow deceleration upon gravity flow transformation and the character of their deposits. In these experiments, it was demonstrated that faster rates of flow deceleration were more favourable to the development of cohesive turbulence-suppressed flows capable of depositing matrix-rich sandstone facies. Thus, the reduced significance of beds with matrix-rich sandstone facies, both vertically through the Mam

Tor succession and overall reduced significance in the succeeding Back Tor succession may reflect change to more gradual gradient breaks at the base of slope.

The return of mud-clast- and matrix-rich bed types (albeit a limited proportion), and their rapid replacement vertically in the Back Tor succession compared to that in the preceding Mam Tor succession, could reflect a number of controlling factors. Haughton et al. (2009) suggest that temporal reduction in the degree of muddy substrate incision, and subsequent reduction of HEBs, may arise where the feeder slope is progressively eroded closer to an equilibrium profile. This is a feasible interpretation in the case of the Edale Basin, given the onset of siliciclastic sedimentation in an early post-rift, clastic-starved basin, characterised by inherited rift topography and thick mudstone accumulations (Collinson, 1988). Alternatively, a temporal reduction in the availability of muddy substrate may have occurred after progradation of the system deeper into the Edale Basin. Substrate induration (hardening) may have resulted due to the more frequent recurrence of flows with erosion of soft substrates down to a more consolidated mudstone, in addition to the shorter periods now available for soft muddy substrate accumulation. Further, the proportion of sandy (non-cohesive) deposits in substrates may have increased during later stages of basin infilling, resulting in a reduction in the availability of muddy substrate. Thus, changes in substrate composition or strength may have affected subsequent downstream flow evolutions (i.e. Sanford, 2008). The most likely factor driving the loss of matrix-rich bed types in the Back Tor succession (compared to that in the Mam Tor succession) could simply be the progradation of the system further into the basin with establishment of relatively proximal depositional settings where flow transformation was relatively incomplete; similar trends and interpretations have been made for small-scale depositional packages interpreted as prograding lobe packages (Kane & Pontén, 2012).

5.4.1.2 Small-scale evolution and distribution of matrix-rich deposits

Vertical changes in the dominant bed type can occur on a smaller-scale, as documented in a number of successions across the basin (Figs 4.9, 4.10, 5.2). A common vertical trend is an upwards-thickening, coarsening, and a reduction of mud clasts within beds, with the dominant bed type changing from matrix-rich to matrix-poor. (Figs 4.9, 4.10, Cycles A, B and C, Fig. 5.2). Such a trend is thought to record periods of upstream incision, and bypassing of sediment downstream during lobe growth with a reduction in the volume of muddy substrate, and/or progradation driving the upwards-loss of matrix-rich bed types. The occurrence of thin, relatively mud-clast-poor matrix-rich deposits (Type D-E) at the very base of these packages may represent the deposition of distal equivalents of mud-clast-rich matrix-rich deposits (Type A and B), with the site of incision migrating down the slope, and/or the magnitude of incision increasing, during opening of conduits on the slope. Similar trends of matrix-rich deposits being

replaced by matrix-poorer bed types vertically though individual lobe depositional packages has been documented in other systems, and interpreted as a record of progradation (Hodgson, 2009; Kane & Pontén, 2012), or a record of greater muddy substrate availability during lobe initiation (Hodgson, 2009).

Variations in depositional character in other packages are harder to relate to simple cycles of upstream incision and infill (Fig. 4.10, Cycles D, H, I) suggesting that such events were more complex, and / or depositional character was influenced by additional factors. Much of our understanding of channel evolution is focussed on later stages as inferred from the infill of these conduits. As such, temporal variation in the magnitude of substrate incision during channel development, and bypass of sediment downstream is poorly understood. Rather than a simple waning of the volumes of incised material during channel development, the magnitude may have been relatively constant, or may have increased. Multiple and varying incision events during the early stages of channelisation are indicated by the range of bypass facies and complex incision surfaces at Alport Castles (Fig. 5.4). Provided there were sufficient volumes of entrained muddy substrate, mud-clast-, matrix-rich bed types may persist throughout depositional packages (Fig. 4.10, Cycle D), or have increased upwards (Fig. 4.10, Cycles H, I lower) prior to an eventual waning of mean flow energy (Fig. 4.10, Cycle I upper). There may have been temporal variations in the availability of muddy substrate, as postulated for larger-scale depositional trends, occurring on a smaller scale during deposition of these packages.

It is also feasible that a single depositional package is not representative of a single cycle of upstream incision, and that a channel could remain as an open conduit bypassing sediment whilst multiple depositional packages are deposited downstream. If significant incision persisted during such bypassing, whilst shifting in depositional lobes occurred on the basin floor, matrix-rich bed types may have persisted through depositional packages (Fig. 4.10, Cycle D). The abrupt end of Cycle D, succeeded by sandstone laminae and very thin beds prior to deposition of a successive lobe with discrete palaeoflow suggests an abrupt shift in the lobe position was the primary cause of cessation of the deposition package in this location.

Despite the likely contemporaneity of the lower MT succession with the HQ succession, the latter does not exhibit well-defined depositional cycles. This is expected to result from complex gravity flow routing at the confining basin margin, with deposition at HQ influenced by both incoming flow approaching the confining basin margin, and flow which had already been deflected near Mam Tor towards HQ (Fig. 4.11b)

5.4.2 Implications for models describing types of hybrid and transitional flow

Type A to E beds exhibit a number of depositional characteristics (e.g. vertical transitions from clean to matrix-rich sandstone; development of banded sandstone facies; presence of co-genetic mud-clast-rich division in the upper bed; the rarity of sedimentary structures associated with fluid turbulence) which are comparable with those associated with HEBs (Haughton et al., 2003, 2009) and transitional flow deposits (Sumner et al., 2009; Baas et al., 2011; Kane & Pontén, 2012). These studies interpreted such deposits as the products of: (1) an initially relatively turbulent flows which underwent partial or total transformation to turbulence-suppressed, cohesive more laminar-like flow following deceleration, reduction of shear stresses and heightened bonding of cohesive material in the flow (Sumner et al., 2009; Baas et al., 2011; Kane & Pontén, 2012); or (2) following the entrainment, break-up and redistribution of entrained muddy substrate to develop rheological heterogeneity along the length of the flow, with rearward flow being more cohesive and turbulence-suppressed (Haughton et al., 2003, 2009). Experimental studies have highlighted how flow deceleration drives the vertical redistribution of non-cohesive material, via settling into near-bed flow or onto the bed, and results in the development of downward-thickening of a clay-rich, turbulence-suppressed plug in the upper flow (e.g. transitional flows of Baas et al., 2009; 2011; Sumner et al., 2009).

The co-genetic, thick, MCR division within Type A and B beds is comparable to that occurring within HEBs, as described from a suite of deep-water depositional systems (e.g. Haughton et al., 2003, 2009; Amy & Talling, 2006; Hodgson, 2009; Fonesu et al., 2015). Periodic planar lamination in matrix-poor, graded sandstone at the base of Type A beds indicate progressive aggradation, at least of the lower bed, and that material which comprises the co-genetic MCR was transported in a more rearward, later-depositing, region of the flow which was MCR, clay-rich and turbulence-suppressed; this inferred longitudinal segregation of the flow structure is comparable to that envisaged for hybrid flows *sensu stricto* Haughton et al., (2003, 2009). The lower matrix-rich sandstone (facies AS-U) in Type B beds is indicative of deposition from a more cohesive, turbulence-suppressed flow state (e.g., poor-sorting, matrix-rich sandstone, lack of structures associated with fluid turbulence; Sumner et al., 2009; Talling et al., 2010; Baas et al., 2011), than that interpreted for the frontal regions of flows depositing Type A beds. As such, it is more challenging to deduce whether Type B deposits reflect longitudinal or vertical segregation of the flow.

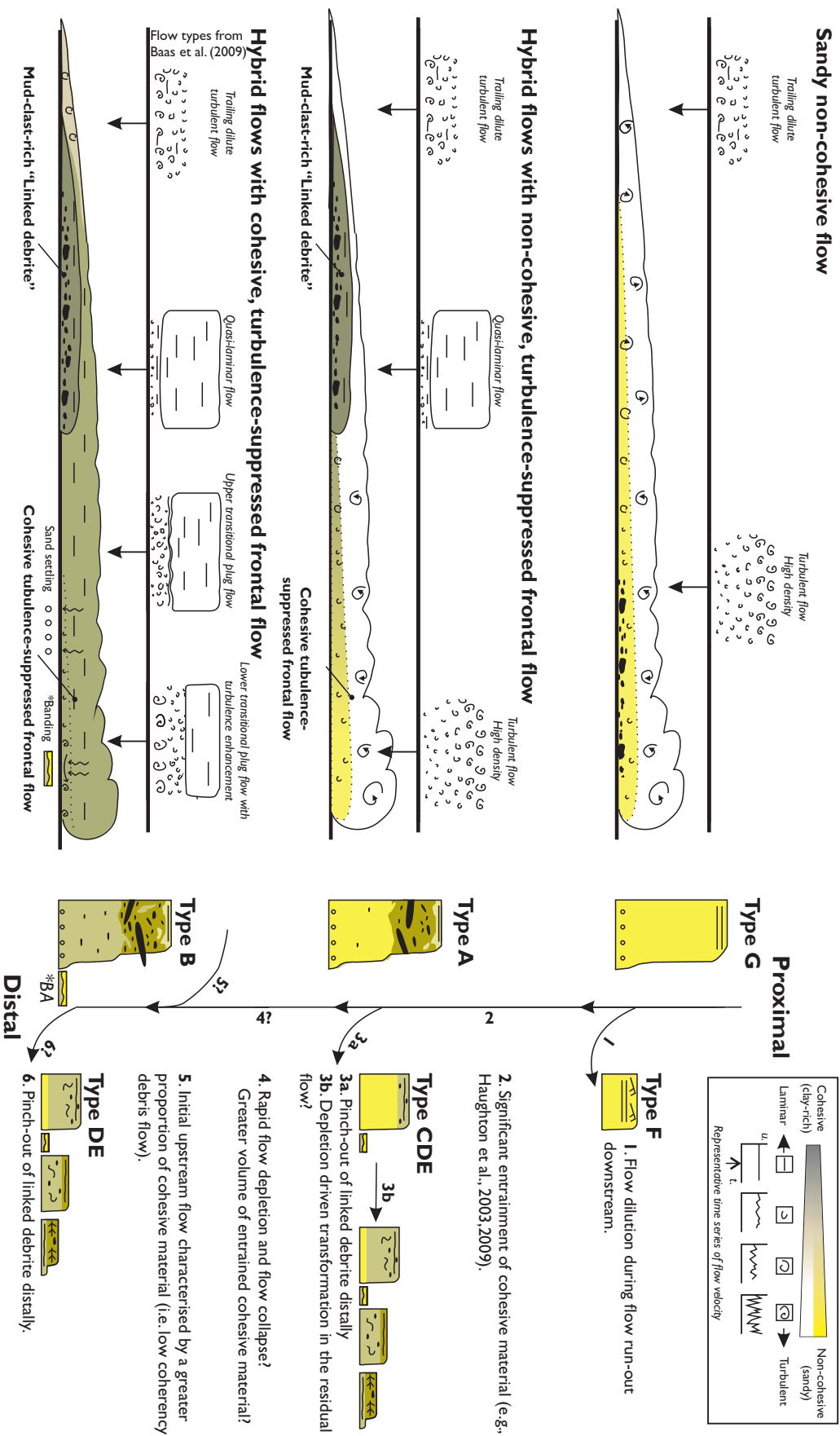


Figure 5.5. Left - Conceptual models illustrating flow processes which account for the deposition of matrix-poor or matrix-richer sandstone beneath co-genetic mud-clast-rich divisions (Type A and B beds, respectively). Right - Styles of flow transformation during downstream flow run-out, and suggested causative factors, which are thought to produce bed types recognised in the Mam Tor Sandstones.

Banded sandstone at the base of the bed (beneath the lower matrix-rich sandstone, Fig. 4.6a, b, e), are interpreted as stratification in that they represent progressive development beneath a passing flow. Models for the origin of banded sandstone have proposed either: 1) fluctuation between turbulent and more cohesive flow due to transient increases in the concentration and/or gelation (bonding) of cohesive material in near-bed flow (Lowe & Guy, 2000; Blackbourn & Thompson 2000; Baas et al., 2005); or 2) a zone of near-bed, turbulence-enhanced flow (observed beneath experimental clay-rich flow sensu Baas et al., 2009) which reworks matrix-poor sand deposited earlier during the same flow event (Baas et al., 2011). Based on model 1, as well as the typical occurrence of banded sandstone between matrix-poor and overlying matrix-rich sandstone in HEBs (Lowe & Guy, 2000; Haughton et al., 2003, 2009; Barker et al., 2008), Haughton et al., (2009) interpreted banded sandstone as a record of a region of transiently fluctuating flow positioned between fore-running, non-cohesive flow and more rearward, cohesive flow within a longitudinally segregated hybrid flow. Instances of bed-basal banded sandstone beneath matrix-rich sandstone in this study may be natural examples of model 2 and suggest that a range of flow characters may produce banded sandstone. Where occurring at the bed base, banded sandstone suggests a limited availability of sand either due to: 1) a limited proportion, or absence, of preceding less cohesive flow (sensu Haughton et al., 2009); and/or 2) intense reworking beneath more cohesive flow (sensu Baas et al., 2011). Where banded sandstone overlies a greater thickness of matrix-poor sandstone, as typically documented in previous studies, it implies: 1) a greater proportion of sand was deposited from preceding relatively turbulent, less cohesive flow, prior to the passage of more cohesive flow; and 2) reworking beneath the flow (sensu Baas et al., 2011) was not intense and preserved matrix-poor sandstone at the bed base. Regardless of the exact mechanism of emplacement, banded sandstone in Type B beds indicates progressive development beneath a passing flow in which material comprising the matrix-rich, MCR division was positioned in more rearward flow region such as that envisaged for hybrid flow (sensu stricto Haughton et al., 2009). Further, consolidation lamination in Type B beds alludes to the presence of primary stratification (Lowe & LoPiccolo, 1974; Lowe, 1975; Hurst & Cronin 2001) and thus an element of aggradation during deposition of Type B beds; aggradation could have occurred via the collapse of relatively laminar near-bed shear layers such as that observed in non-cohesive, but high-concentration turbulence-suppressed flows (Vrolijk & Southard, 1997; Sumner et al., 2008).

Type A and B beds are comparable in that they are interpreted as the depositional products of longitudinally segregated flow, which exhibited an overall increase in mud-clast abundance, clay-concentration and turbulence-suppression towards the rear of the flow. However, they differ in terms of how matrix-rich the lower sandstone division was beneath the MCR division. Such contrasts indicate that flows which can be classified as longitudinally

segregated hybrid flows (sensu Haughton et al., 2009), can exhibit discrete characters in terms of the dominant rheology of the frontal, earlier depositing regions of the flow which is either non-cohesive or more cohesive and turbulence-suppressed, emplacing Type A and B beds, respectively (Fig. 5.5). Occurrences of Type A or Type B beds are expected to reflect variations in the concentration of clay in the flow (i.e. that present on flow initiation or that entrained into the flow) and thus its response to deceleration upon meeting the basin-floor or the confining basin margin further downstream (section 4.6.1.3). These findings highlight the dynamic nature of the frontal regions of longitudinally segregated flows, and build further on the findings of Chapter 3 (section 3.5.1) which demonstrated how frontal regions of the flow can undergo separate, discrete downstream flow transformation compared to that occurring in the rear of the flow event. Further, these findings suggest that models for the development of hybrid flow (Haughton et al., 2003, 2009) and clay-rich transitional flow (sensu Baas et al., 2009, 2011; Sumner et al., 2009; Kane & Ponten, 2012), need not be considered in isolation, and both may drive and characterise flow transformations during a single gravity flow event (Fig. 5.5). The potential for the combined influence of these models upon flow transformation is unsurprising, considering the range and complexity of processes operating spatio-temporally within gravity flow events (Kneller & McCaffrey, 2003; Choux et al., 2005; Stevenson et al., 2014).

5.5 Conclusions

The sediment gravity flows infilling the Edale Basin are interpreted to have been controlled by relatively small-scale autogenic factors (arising from some combination of local sediment supply variability, lobe-switching and bed-scale compensation) superimposed on a larger cycle of sea-level fall and rise. Additional meso-scale fluctuations in sediment supply were likely a result of both smaller changes in sea-level (Figueiredo et al., 2013; Davies, 2008; Water & Condon, 2011), and autogenic processes.

Vertical trends of bed-thickening, coarsening, and reduction in mud-clast concentration, paralleled by a change from matrix-rich to matrix-poor bed types, observed on the basin floor at multiple levels in the stratigraphy, are thought to record the influence of repeated periods of incision occurring further upstream in the system. Deviation from this trend can be driven by: 1) successive periods of system waning, perhaps during channel infilling, resulting in the reverse of this trend; 2) lobe switching on the basin floor prior to significant waning of upstream channel incision upstream, resulting in the persistence of matrix-rich bed types; 3) a potential increase in the magnitude of incision during upstream channel incision.

Large-scale replacement of matrix-rich bed types by matrix-poor bed types in fan successions can be driven by: 1) waning of the system, with incision becoming reduced, or positioned further upstream (lower vs. upper Mam Tor succession); or 2) progradation and/or reduction in the availability of muddy substrate for incision, due to the development of sandier substrate, or higher frequency of incision events following progradation (Mam Tor vs. Shale Grit succession). Thus, no single control is thought to have been solely responsible for driving clay-enrichment, flow transformation, and the emplacement of matrix-rich bed types in the Edale Basin.

Thus, the occurrence of matrix-rich bed types, interpreted as HEBs, was influenced on a number of timescales by the interplay of multiple factors promoting clay-enrichment, flow transformation, and deposition on the basin floor (i.e. the nature of upstream entrainment of muddy substrate, system retrogradation and progradation, and lobe switching). Observations suggest flows are not simply characterised by a single style of flow transformation (i.e. turbulence suppression or enhancement) during downstream run-out. Flows which can be classified as being longitudinally segregated, in terms of possessing discrete rheological zones (e.g. hybrid flow sensu Haughton et al., 2003, 2009), can exhibit discrete flow characteristics depending upon the rheology of the frontal (earlier depositing) region of the flow, which can either be non-cohesive, or relatively more cohesive and turbulence-suppressed. These discrete rheological zones may develop and evolve discretely, due to differing processes of clay-enrichment and turbulence suppression. As such, models for hybrid flow (Haughton et al., 2003, 2009) and transitional flow (Baas et al. 2009, 2011; Sumner et al., 2009; Kane & Pontén, 2012), and associated flow transformation processes, need not be considered mutually exclusive, and may be applicable to the evolution of individual gravity flows during their run-out distally.

Chapter 6. Influence of flow containment and substrate entrainment upon sandy hybrid event beds containing a co-genetic, mud-clast-rich division

6.1 Introduction

Data described in Chapter 4 from the confined, uncontained Edale Basin has demonstrated that HEBs are not always localised adjacent to confining topography. Thus flow transformation to hybrid flow (*sensu lato*) can occur prior to the effects of flow confinement, where the preceding flow run-out distance was of sufficient length (Section 4.6.2, Fig. 4.21). Using Miocene-aged outcrop from the confined, contained Castagnola Basin, NW Italy (Fig. 6.1), this study builds on interpretations in Chapter 4 by documenting the character and distribution of HEBs, with respect to a downstream confining slope. In this case, however, basin physiography differed in that flows were contained (*sensu* Fig. 2.15c) and confined; case studies of HEBs in confined, contained deep-water systems have not previously been documented. Sedimentary logs were collected at a 1:10 scale at various locations across the basin from a study interval, some 250 m in stratigraphic thickness (Fig. 6.1c, d). The occurrence of thick mudstone between beds in this tabular system, was conducive to correlation of event beds across the basin (c. 5 km laterally), and thus assessment of bed type character and distribution across the study interval.

In light of earlier studies which document HEB localisation and variation in depositional character towards confining topography (Barker et al., 2008; Patacci et al., 2014), in addition to findings outlined in Chapter 4 (section 4.6), this chapter seeks to address the following lines of research:

- 1) to ascertain whether HEB distributions are similarly localised to confining topography where the basin physiography results in flow containment in addition to flow confinement;
- 2) to determine whether HEBs exhibit systematic variations in their depositional character, and if so, whether such variation is a function of increasing proximity to their downstream onlap onto the confining basin margin;
- 3) to investigate the controlling parameters upon the character of HEBs.

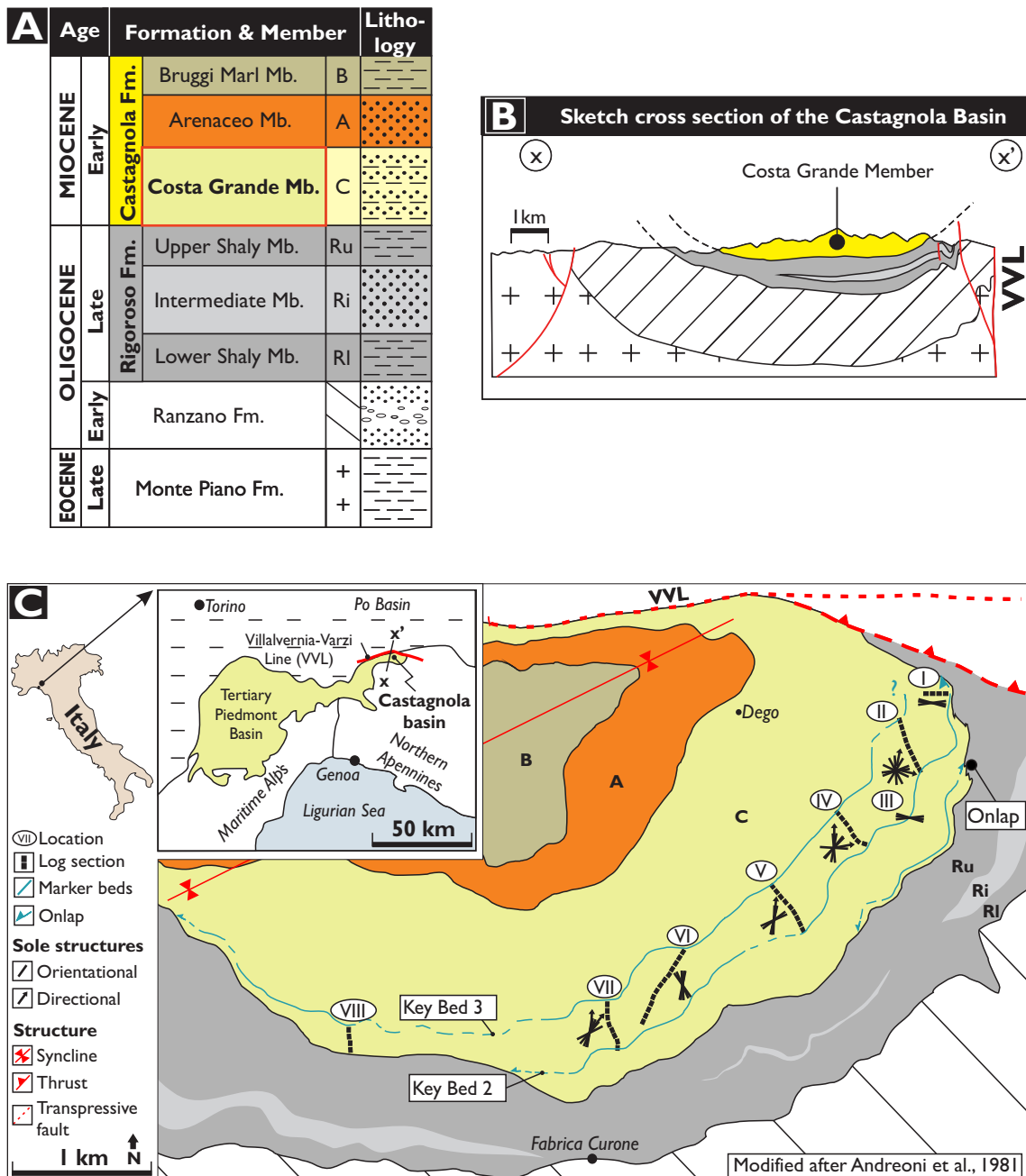


Figure 6.1 (continued overleaf). **A)** Stratigraphy of the Castagnola Basin (after Andreoni et al. 1981). **B)** Sketch cross-section of the Castagnola Basin (after Di Giulio & Galbiati 1993). **C)** Geological sketch map (redrawn and modified after Stocchi et al. 1992) of the Castagnola Basin showing the distribution of logged sections and palaeoflow with respect to confining basin margins on to which strata onlap. Inset shows the regional location of the Castagnola Basin in the eastern portion of the Tertiary Piedmont Basin of north west Italy (modified after Felletti, 2002a).

6.2 Geological background

The Tertiary Piedmont Basin of NW Italy was an episutural basin formed during Late Cretaceous - Late Eocene, Meso-Alpine collision of the European plate and the Adria microplate (Ricci Lucchi, 1986; Biella et al., 1992; Maino et al., 2013) (Fig. 6.1a-c). The eastern Tertiary Piedmont Basin contains a Late Eocene - Early Miocene deep-water turbiditic success-

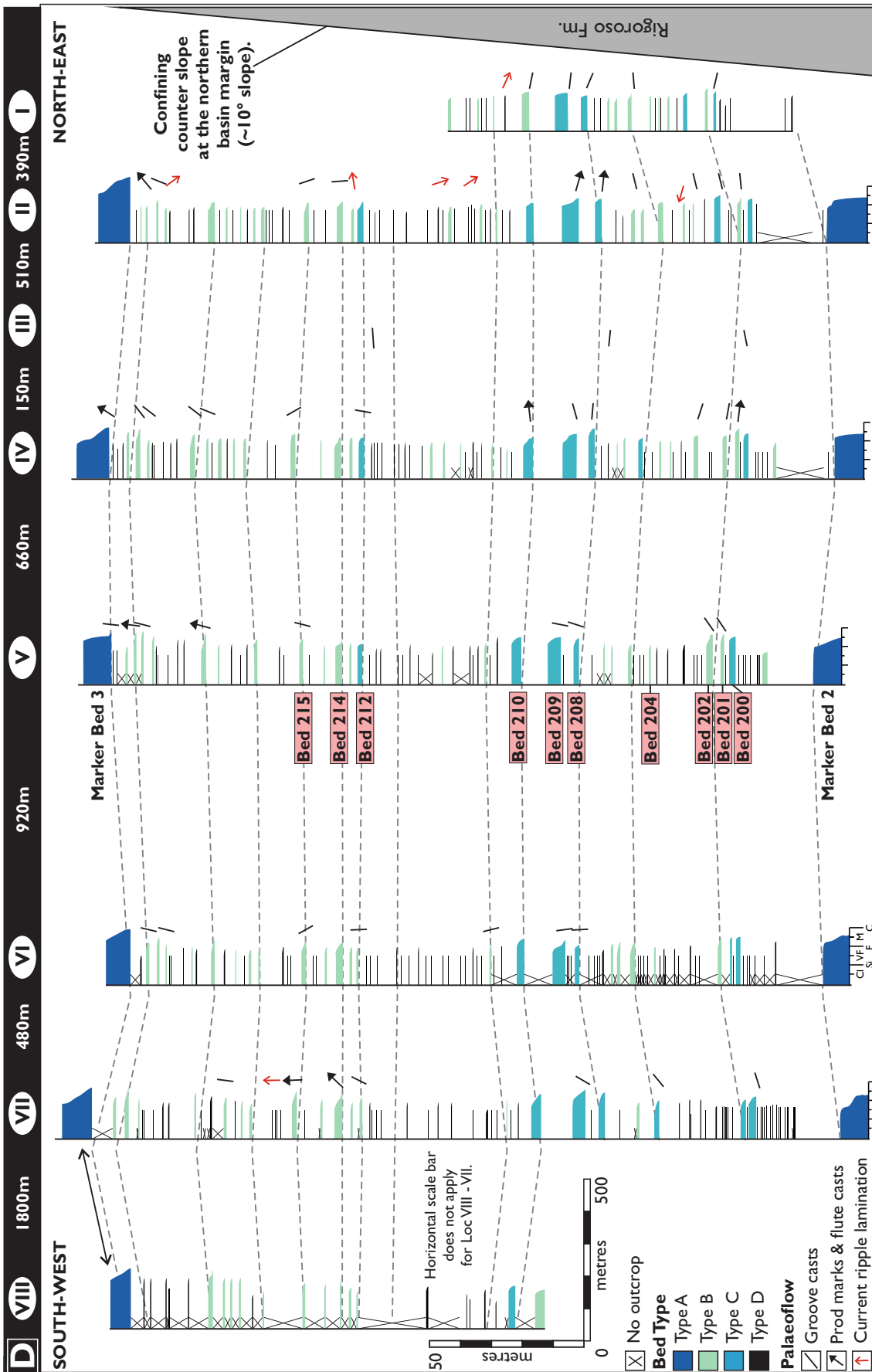


Figure 6.1 ctd. D) Correlation of logged section in the study interval and their distribution with respect to the downstream northern confining basin margin. The study interval is sheet-like and thins towards confining basin margins (south and north). Log positions are indicated on Fig. 6.1 c. Cl, clay; Si, silt; VF, very fine sand; FS, fine sand; M, medium sand; C, coarse sand.

ion (c. 3 km-thick, Fig. 6.1a). Several major unconformities, present in the lower part of the succession, record regional tectonic events and changes in basin physiography (Cavanna et al., 1989; Di Giulio & Galbiati, 1993). Chattian-Aquitainian transpressive motion along the E-W trending Villalvernia-Varzi line, located in the easternmost Tertiary Piedmont Basin, folded Oligocene strata into the asymmetric, ENE-WSE trending Castagnola sub-basin (Ibbeken, 1978; Andreoni et al., 1981; Cavanna et al., 1989; Di Giulio & Galbiati, 1993) (Fig. 6.1b, c), which is the focus of this study.

Sediment gravity currents entered the Castagnola Basin from the SW (Stocchi et al., 1992), and emplaced the c. 800 m-thick Castagnola Formation, which overlapped the underlying Rigoroso Formation (Cavanna et al., 1989; Andreoni et al., 1981; Di Giulio & Galbiati, 1993) (Fig. 6.1a-c). During emplacement of the Costa Grande Member, termination of activity on the Villalvernia-Varzi line around the Chattian-Aquitainian boundary forced a depositional change from laterally offset, stacked sand bodies, to simple sheet-like deposits (e.g. sub-units A-H and sub-unit I, respectively, of Felletti, 2002, 2004a). Sheet-like deposits were then persistent throughout the remaining depositional episode of the Costa Grande Member (Stocchi et al., 1992; Baruffini et al., 1994), including the period represented by the study interval. Southern exposures of upstream, shallower-water strata are lacking, and thus little is known of the shelf and feeder system for the Castagnola Basin. Estimates of the basin width (c. 11 km), and downstream basin length (c. 5 km) during deposition of the study interval, are constrained by the extent of deposits of the Costa Grande Member. Gravity currents emplacing the Costa Grande Member were contained (*sensu* Fig. 2.15c) within the basin, resulting in the development of thick mud caps between beds, and a lack of comparable correlative strata beyond the basin (Stocchi et al., 1992; Baruffini et al., 1994). Palaeocurrent indicators record flow reflection and deflection by the downstream counter slope of the northern basin margin (Stocchi et al., 1992; Baruffini et al., 1994; Felletti, 2002; Fig. 6.1c).

6.3 Data and methods

A c. 250 m-thick (stratigraphic thickness) interval within the turbiditic Costa Grande Member was logged using a Jacob staff at eight locations across the Castagnola sub-basin (Fig. 6.1c, d). Together, these logs form a 4.9 km-long transect orientated: 1) near-oblique (030/045-210/225°) to the palaeoflow direction of the gravity currents entering the basin (SW-NE); 2) highly oblique to the E-W striking, downstream confining northern basin margin; and 3) highly oblique to the palaeoflow direction of gravity currents which were deflected east at this margin. Correlation of individual beds to a high confidence level was aided by good exposure, the presence of several distinctly thick marker beds, and the tabular nature of the study

interval within the Costa Grande Member (Fig. 6.1d). These correlations support those documented in Stocchi et al. (1992) and Felletti (2002), and provide the framework for an assessment of bed characteristics spatially (palaeogeographically and stratigraphically), in relation to the confining northern basin margin. Where outcrop permitted, transects of beds were also made over shorter length-scales (<100 m) with the intention to characterise bed character on relatively shorter length-scales; such transects are comparable in orientation to the larger, basin-scale transects, and thus are slightly oblique to the palaeoflow of gravity flows entering the basin (SW-NE). Palaeocurrent readings (n=220) were measured from flute casts, groove and prod marks, and current-ripple laminations present within the study interval.

6.4 Results

6.4.1 Bed types of the Costa Grande Member

The studied interval of the Costa Grande Member has a simple, tabular, sheet-like architecture with the most pronounced thinning of the succession occurring in the north and south due to the nearby basin margins (Fig. 6.1d). Thinning towards the southern basin margin occurs less abruptly, and suggests that the feeder slope was inclined at a relatively lower angle compared with the northern basin margin; estimates of dip on the latter at the time of deposition are thought to be on the order of 10° (Felletti, 2002, 2004b). In the study interval, four bed types were defined, using a descriptive basis of facies type (sediment texture, composition and structures) and facies arrangement within individual beds, upon which process-based interpretations of sediment transport and deposition were made (Fig. 6.2).

6.4.1.1 Type A – Very thick, stratified mega-beds

Type A beds typically comprise non-stratified sandstone (i.e. lacking sedimentary structures), overlain by variably arranged laminated sandstone facies types (crude widely spaced [<10 mm] planar lamination (*sensu* Talling et al., 2012b, sub- and super-critical climbing-ripple laminations and subordinate sinusoidal and current ripple lamination). Both inverse and normal grading can be present within a single bed, with the former being most common lower within the bed, where thin traction carpets (S2 of Lowe, 1982) and dewatering pipes can also be present. Sole structures (groove casts and prod marks) on bed bases record palaeoflow towards the north-north-east and east, whereas ripple lamination within the bed can record more complex and opposing current directions (Fig. 6.3). Two Type A beds bound the study interval, with several instances present throughout the Costa Grande Member; they are oversized (>10 m) in terms of bed thickness compared to other bed types (Fig. 6.4). Erosion at the bed base is common, and does not appear to vary significantly across the basin (e.g. Marker Bed 3; Fig. 6.1d). Mud

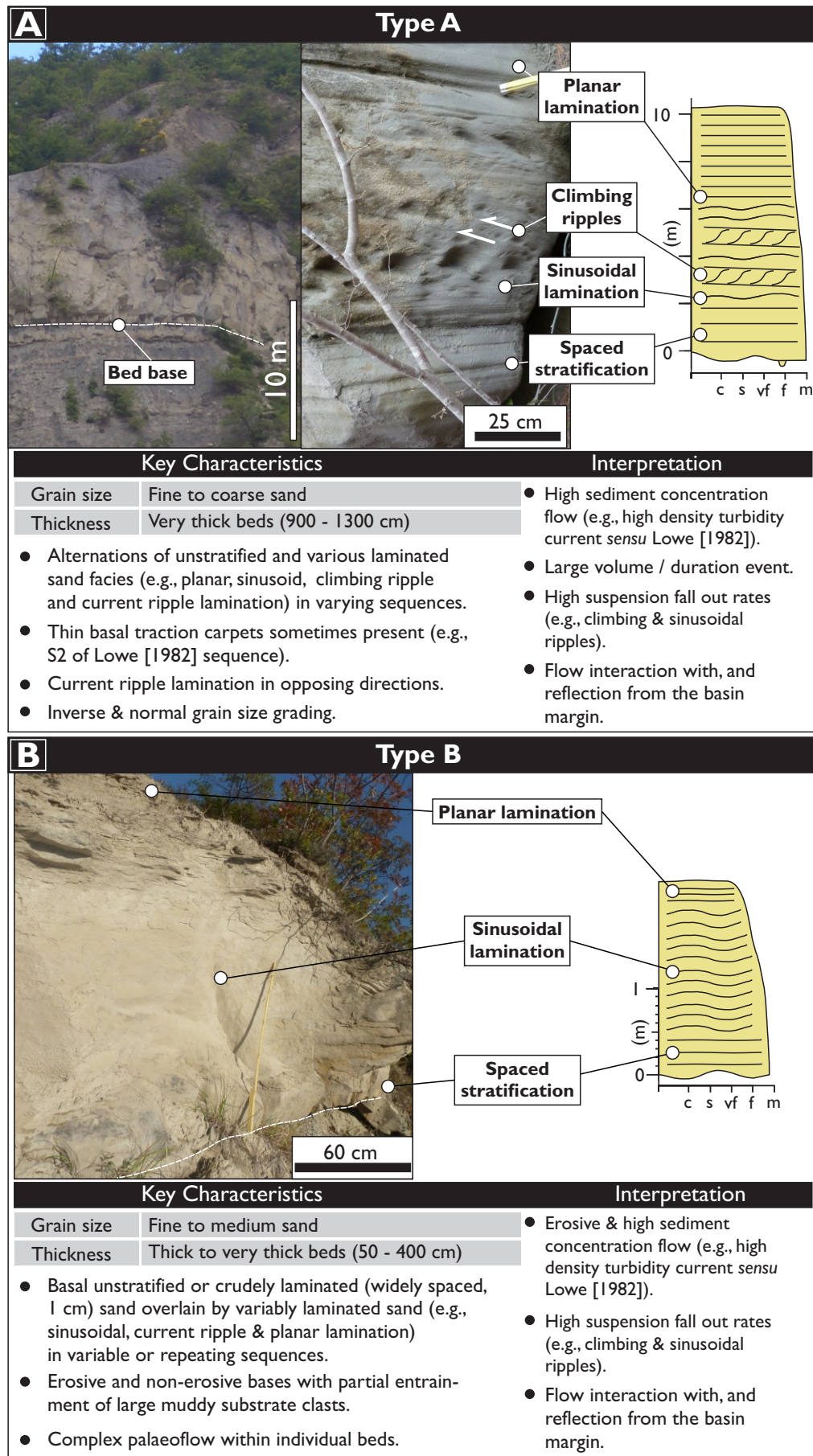


Figure 6.2 (continued overleaf). Summaries for the Types A to D beds recognised within the studied interval of the Costa Grande Member study interval.

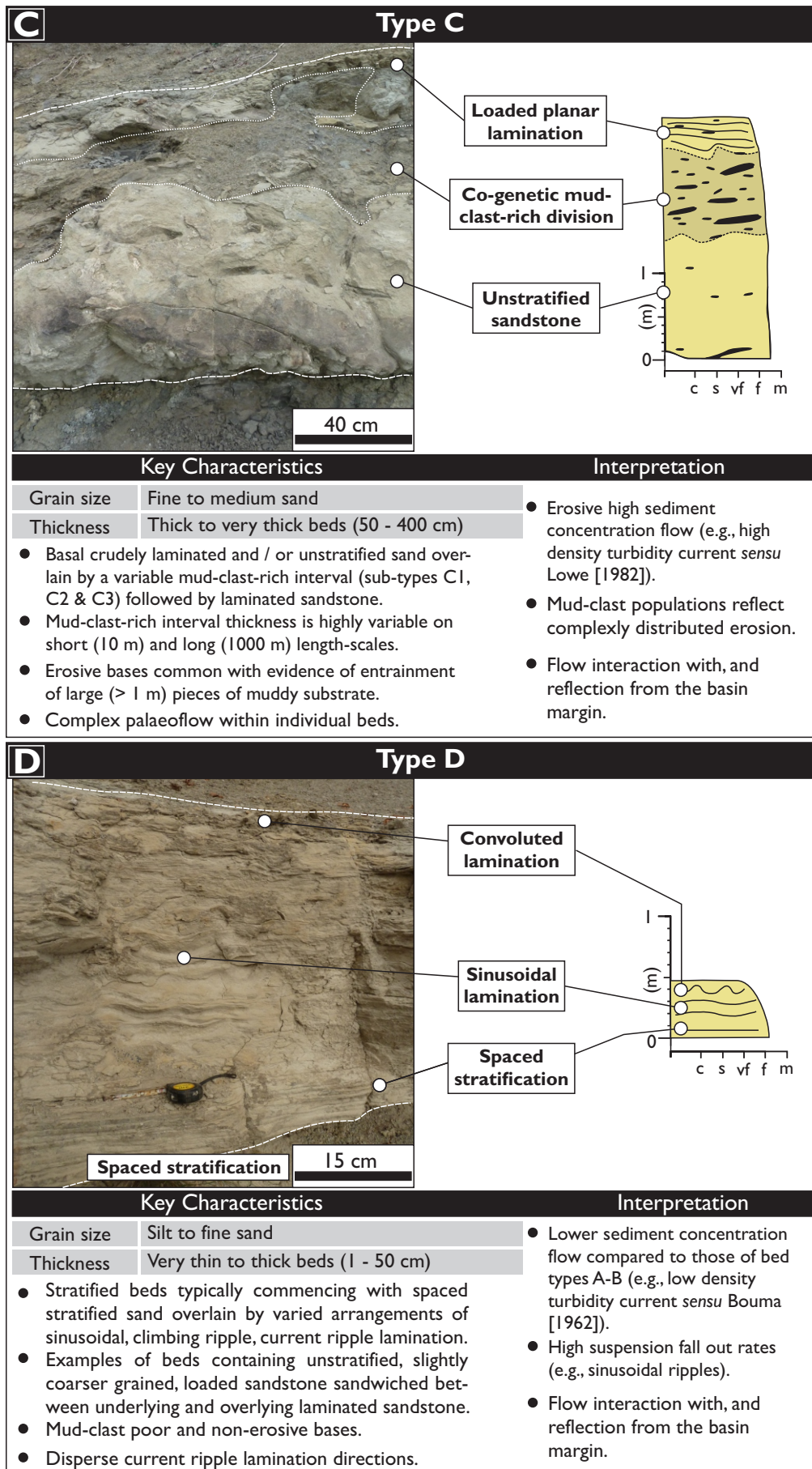


Figure 6.2 ctd.

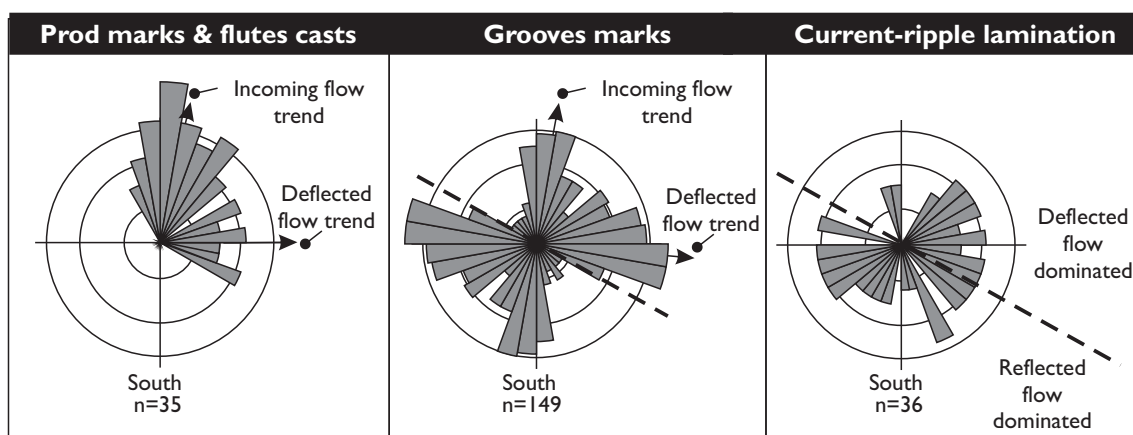


Figure 6.3. Palaeoflow data collected from different palaeoflow indicators found within the study interval. Sole structures (groove marks, prod marks and flute casts) record two distinct trends with incoming flow directed north-north-east towards the confining northern margin of the Castagnola Basin and flow which was deflected eastwards by the northern basin margin. Current-ripple lamination, representing relatively late-stage deposition after sole-structure formation, records wide-spread palaeoflow directions which are often directed at a high angle away from the confining northern basin margin. The directionality of trends documented in groove mark alignment was inferred from directional data provided by prod marks and flute casts.

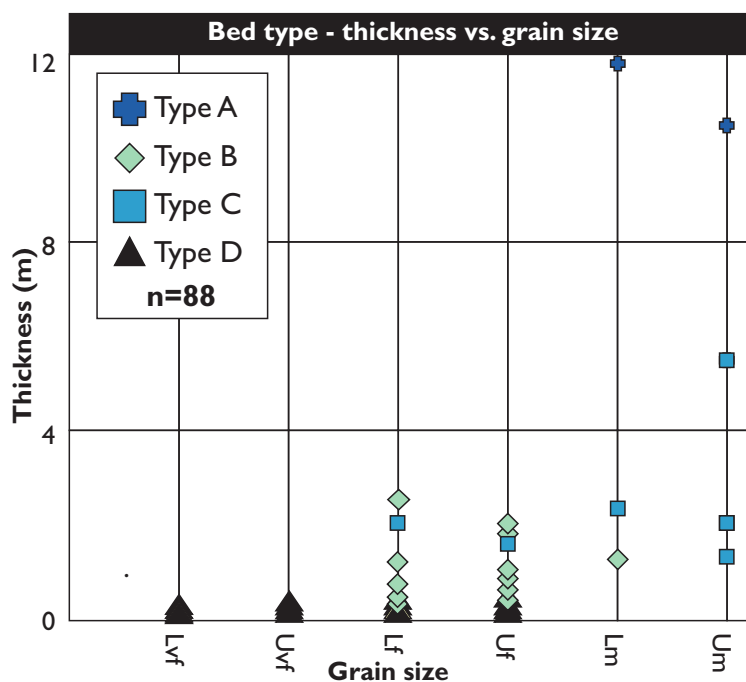


Figure 6.4. Graph depicting bed type maximum grain size versus bed thickness. Type A beds are outsized in terms of their thickness compared to other bed types whilst Type D beds are thinner bedded and finer grained. The ranges of bed thickness and grain size in Type B and C beds overlap with Type C beds being thicker and coarser grained. Wentworth grain-size classification with the following grain size abbreviations: **Lvlf**, lower very fine; **Uvlf**, upper very fine; **Lf**, lower fine; **Uf**, upper fine; **Lm**, lower medium; **Um**, upper medium.

clasts can also be present at the bed base (Fig. 6.5, Style 1), and occur as discrete horizons, or isolated clasts (Fig. 6.5, Style 1); however, mud-clast-rich (MCR) divisions (Fig. 6.5, Style 3) are lacking. Type A beds retain their character, and do not transition laterally into other bed types across the study interval (Fig. 6.1d).

Type A beds are interpreted to record deposition from flow which was initially of a high concentration, with a high rate of sediment fall-out, both of which declined during deposition

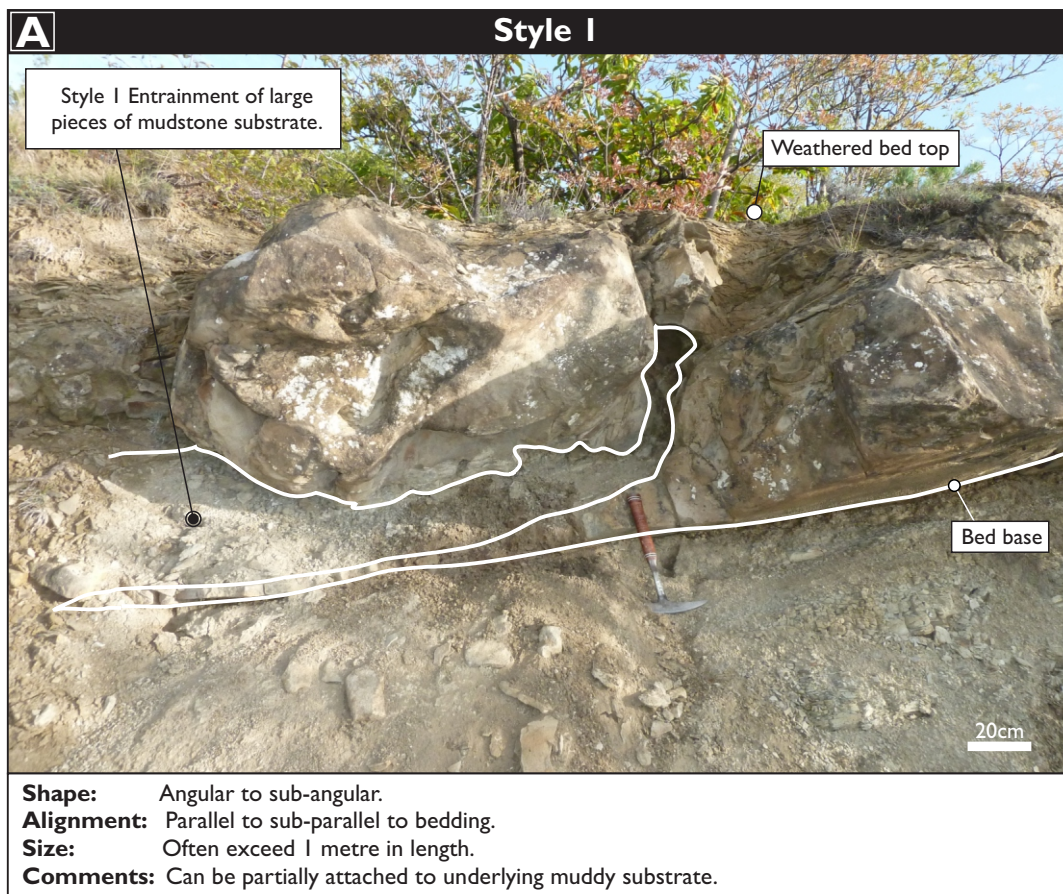


Figure 6.5 (continued overleaf). Key characteristics of the different styles of mud-clast distribution observed within deposits of the Costa Grande Member.

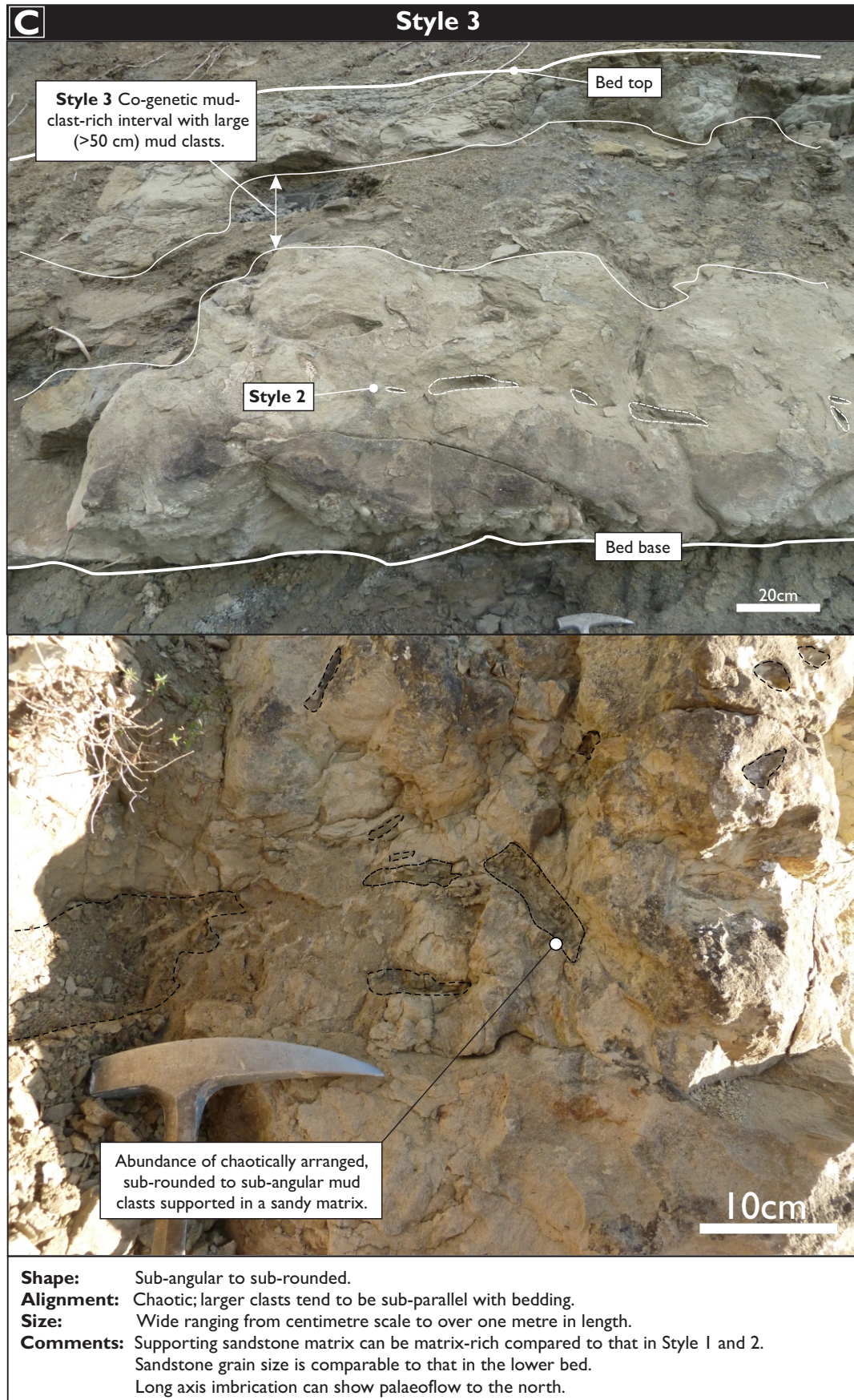


Figure 6.5. ctd.

of the bed (e.g. producing non-stratified sand, largely overlain by planar and climbing ripple lamination; Lowe, 1988; Jobe et al., 2012). The significant thickness of Type A beds may reflect a relatively greater flow duration or volume of emplaced sediment, as compared with flows depositing other bed types. Sole structures record palaeoflow in a similar direction to that observed for other bed types, and suggests all flows entered the basin from the south (Fig. 6.1d). Palaeoflow indicators recording complex (multi-directional) flow events, record the effects of flow confinement during deposition within the Castagnola Basin (Fig. 6.3; Pickering & Hiscott, 1985; McCaffrey & Kneller, 2001).

6.4.1.2 Type B – Thick to very thick, stratified, mud-clast-poor beds

Type B beds comprise thick- to very thick-bedded (0.35-2.8 m), fine- to medium-grained deposits which typically commence with non-stratified sandstone overlain by a range of laminated sandstone facies types (Fig. 6.2). Beds exhibit weak normal grading, with grading being most pronounced in the upper part of the bed; dewatering structures and convoluted lamination are also present. Sole structures on the bed base record flow towards the north-northeast and east, whereas ripple laminations higher within the same bed records more disperse palaeoflow directions, often at high angles away from the northern basin margin (Fig. 6.3). Bed bases can be sharp, planar, and apparently non-erosive, or erosive at multiple points across the basin where mud clasts are concentrated at bed bases (Fig. 6.5, Style 1), some of which are only partially detached from the underlying mudstone. Mud clasts can also occur as distinct horizons, often at the junction between non-stratified and stratified sandstone (Fig. 6.5, Style 2). Total mud clast abundance within Type B beds is less than that observed in Type C beds. Type B beds retain their depositional character laterally (Fig. 6.6, Bed 215; Fig. 6.7, Bed 214), but in rare instances can pass abruptly (<15 m) into a Type C bed character (Fig. 6.8).

Type B beds are interpreted as the depositional products of aggradation beneath an initial high-density turbulent flow (*sensu* Lowe 1982), which progressively became less concentrated with time. A high rate of suspension fall-out dominated during deposition of the bed (sinusoidal lamination, *sensu* Jobe et al., 2012; dewatered convoluted lamination). Flows were often erosive, and entrained mud clasts locally from the basin floor. However, such entrainment appears to have been less efficient than that of Type C beds, as examples of mud clasts which are still partially attached to the substrate are more common at the base of Type B beds. Palaeoflow indicators recording multiple flow directions during deposition of a single bed, demonstrate the effect of flow confinement during deposition (Pickering & Hiscott, 1985; McCaffrey & Kneller, 2001).

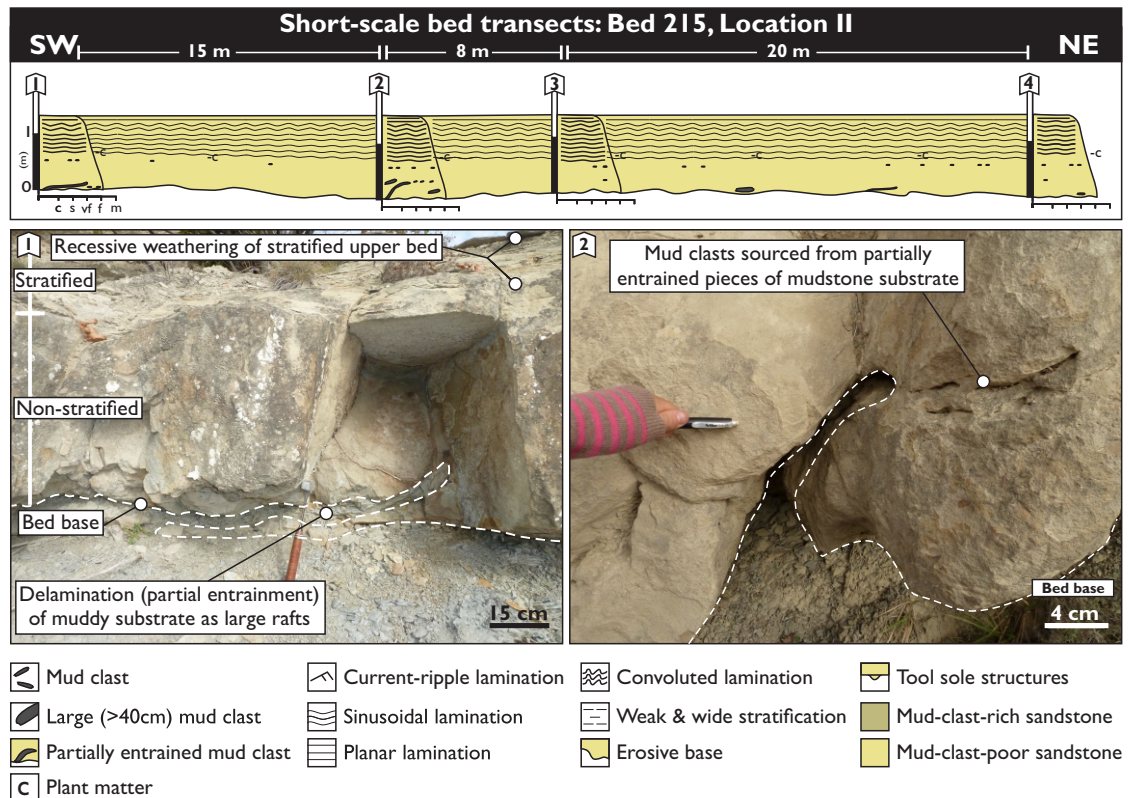


Figure 6.6. Short length-scale transect through a Type B bed at Location II. Type B beds retain their depositional character over short length-scales compared to Type C beds (Fig. 6.8 & 6.10). Partial entrainment of muddy substrate is preserved along the base of the bed.

6.4.1.3 Type C – Thick to very thick, variably stratified beds, with a co-genetic mud-clast-rich division

At the base of Type C beds, non-stratified sandstone or crude widely spaced planar laminated sandstone (*sensu* Talling et al., 2012b), in some instances containing dewatering pipes, pass upwards into an overlying MCR division (Fig. 6.5, Style 3), in turn overlain by plane-parallel and current-ripple laminated sandstone at the bed top. The thickness and grain size of Type C beds are comparable to those in the upper range of Type B beds (Fig. 6.4), and exhibit overall normal grading, which is most pronounced in the bed top. Type C bed bases are commonly erosive at multiple sites across the basin floor (Fig. 6.7, Beds 208, 210); such erosional surfaces may be associated with the entrainment of large mud clasts (c. 1 m), some of which are still partially attached to the underlying substrate (as observed in Type B beds, Fig. 6.5, Style 1). Sole structures record initial palaeoflow towards the north-northeast and east, whereas current ripple lamination, deposited higher (later) within the same bed, records a change to more disperse palaeoflow, often at high angles away from the northern confining basin margin (Fig. 6.3).

Within the MCR division, the supporting sandstone matrix is subtly more matrix(clay)-rich in places, compared to relatively mud-clast-poor sandstone observed beneath this MCR

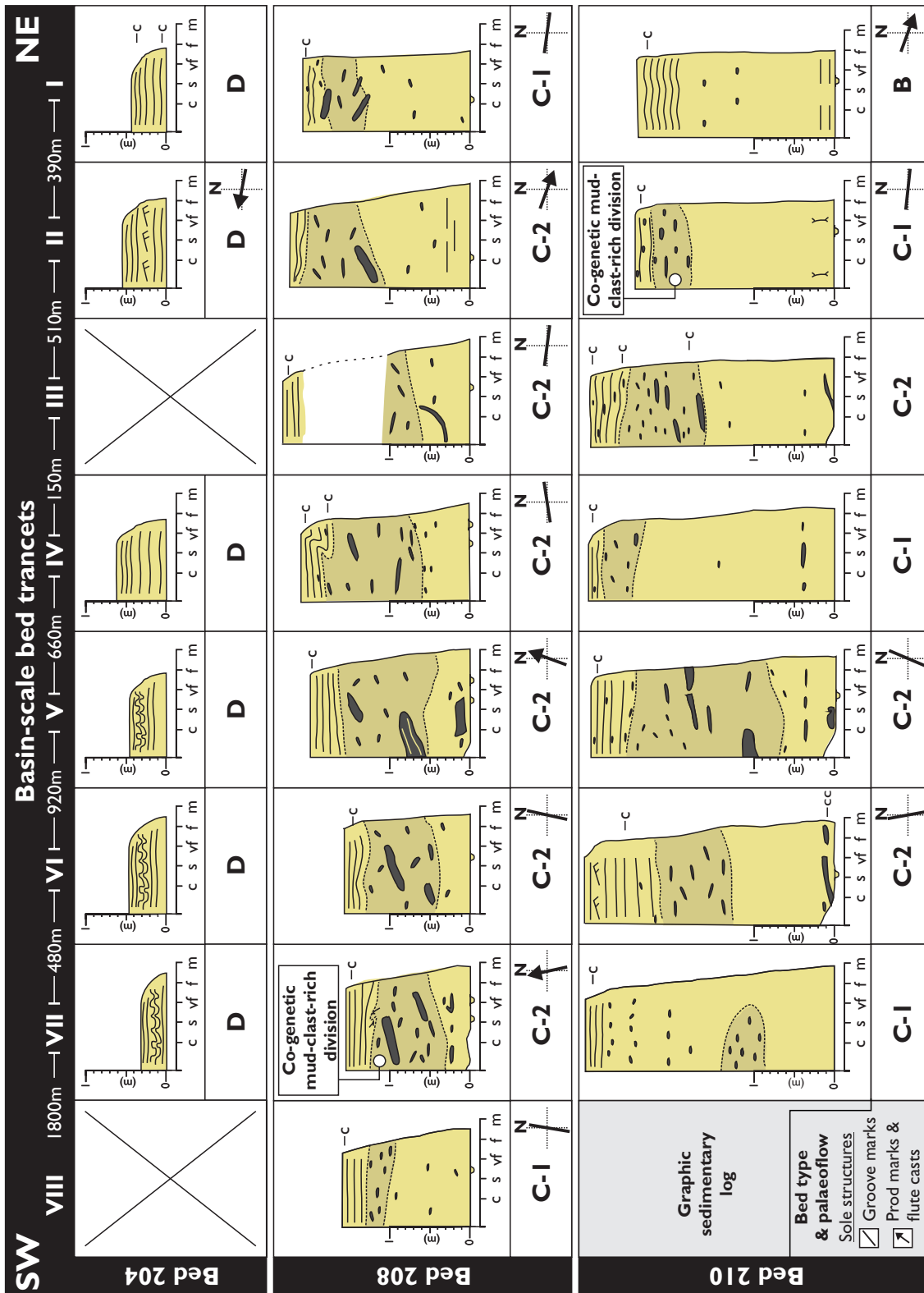
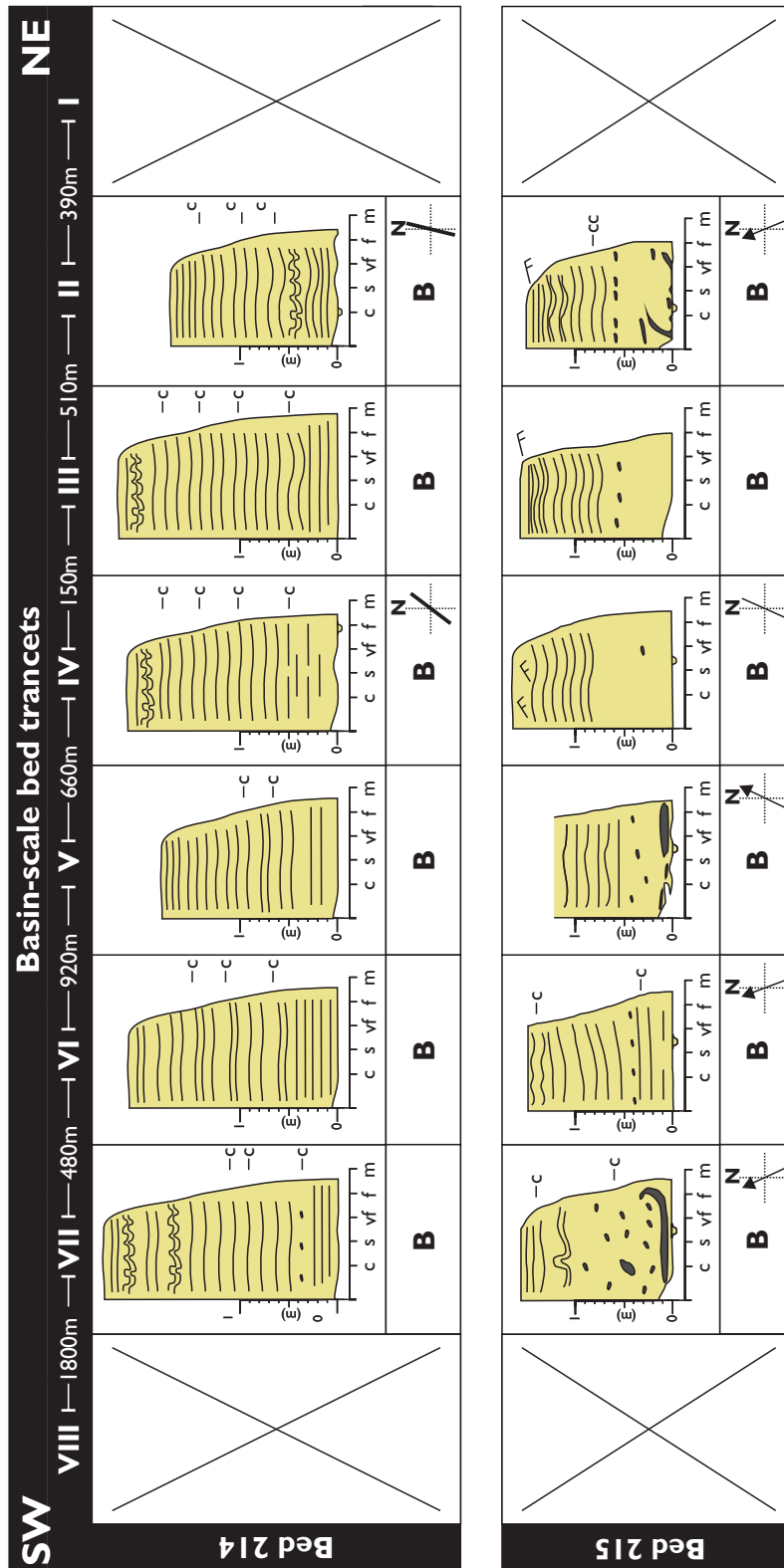


Figure 6.7 (continued overleaf). Basin-scale transects of individual bed types across the studied interval of the Costa Grande Member study interval. Type B and D beds retain their depositional character across the basin whereas Type C beds are highly variable in terms of the thickness of their co-genetic mud-clast-rich division and the size and abundance of mud clasts within this division. Co-genetic mud-clast-rich divisions are extensive across the basin (>5 km) and variation in their character is non-systematic with respect to palaeoflow direction and proximity towards the downstream confining northern basin margin. See Fig. 6.6 for key to the sedimentary graphic logs. For bed type codes A-D and descriptions see section 6.4.1.



in a lower volume of sandstone matrix (Type C2); and 3) predominantly large mud clasts, sometimes over several m in length, which can contain sand laminae (Type C3). The size of mud clasts within Type C3 beds can result in very thin sandstones being preserved at their bases and tops, such that the bed can easily be mistaken for a succession of thin-bedded strata (Fig. 6.9, Bed 200). Laterally, Type C3 beds can pass into other sub-Type C beds across the

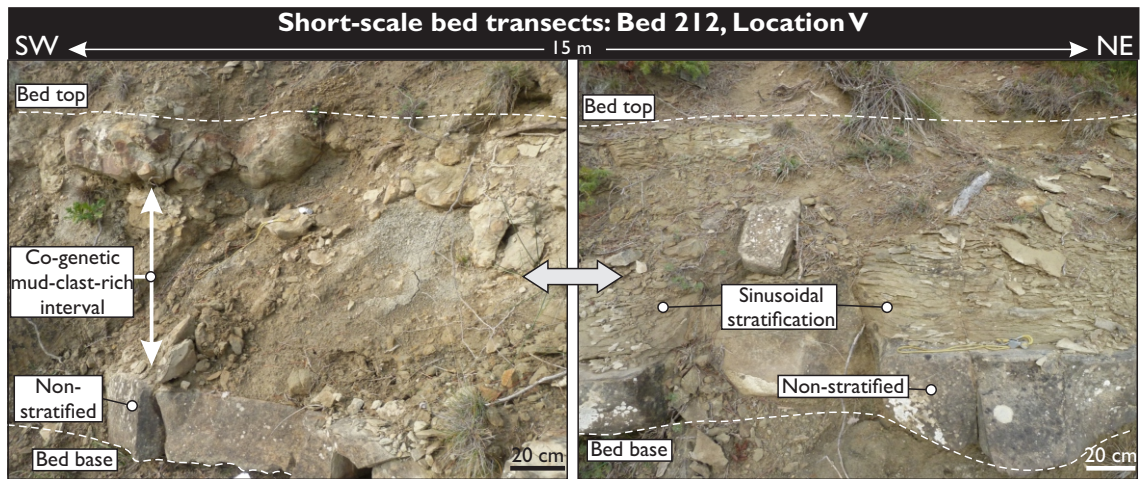


Figure 6.8. Example of a lateral transition from a Type C2 (left) to a Type B (right) bed character over 15m. Typically Type B beds retain their depositional character over outcrop (Fig. 6.6) and basin (Fig. 6.7; Bed 214) -scales whereas Type C beds are typically variable between Type C sub-types (Figs. 6.7; Bed 208, 210, 6.10).

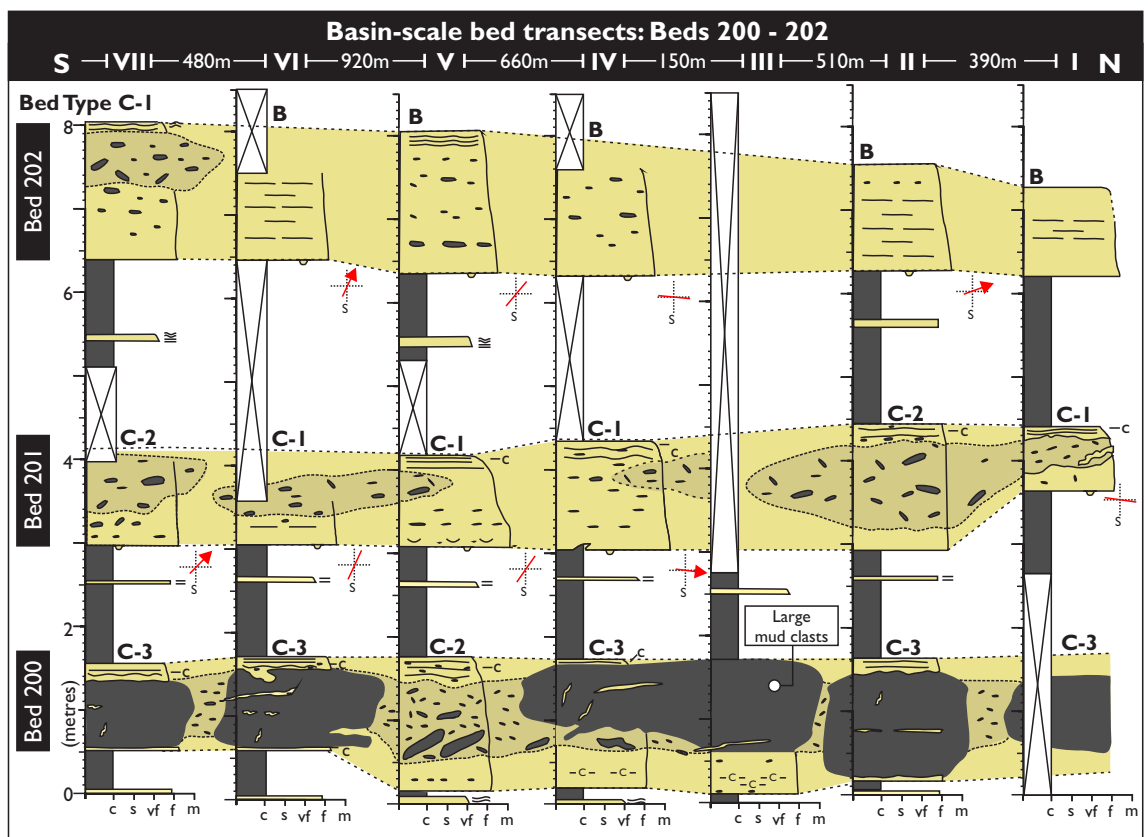


Figure 6.9. Lateral variation in the size and abundance of mud clasts results in significant variation in the character of the co-genetic mud-clast-rich division (e.g., Beds 200, 201) and overall bed character. Sub-type C3 is rare and comprises significantly large mudstone rafts (often >1 metre length) which result in the supporting sandstone matrix being sparse and irregular in shape; sub-type C3 in Bed 200 is seen to pass laterally into sub-type C2 along a single continuous outcrop (Location V) over a distance of 30 m (not shown). See Fig. 6.6 for the key to graphic logs.

basin (Fig 6.9, Bed 200), in addition to over relatively short-length scales (tens of m's) in a single outcrop; transitions of a similar scale have been documented by Hodgson (2009) in the Permian-aged Tanqua depocentre, S Africa. The sandstone matrix, which supports the mud clasts in the MCR division, is of comparable grain size to overlying and underlying relatively

mud-clast-poor sandstone in the same bed. The capping laminated sandstone, which overlies the MCR division, can display an undulose lower contact, most pronounced when occurring in Type C2 beds. Lamination in these undulose sandstones can exhibit systematic variation in lamination spacing laterally (i.e. growth lamination), recording syn-depositional loading processes (Fig. 6.10). Laterally, the character (Type C1 to C3) and thickness of MCR divisions can vary significantly (0-1.4 m-thick), and repeatedly, both on the scale of an individual outcrop (tens to hundreds of m's length; Fig. 6.10) and on the scale of the basin infill and extent of the study interval (>km-scale; Fig. 6.7). Although uncommon, lateral transition to Type B beds was observed (Fig. 6.8); however, transition into Type A and D beds was not observed.

Vertical grain size grading, and the repeated association of a relatively mud-clast-poor sandstone, a MCR division and overlying, loaded, laminated sandstone, record the co-genetic association of facies emplaced during a single flow event. Initial deposition of Type C beds was characterised by high rates of sediment fall-out from a high-concentration flow (e.g. producing non-stratified and weakly stratified sandstone at the base of the bed). Late-stage deposition of finer-grained, well-stratified sandstone, records a change to deposition beneath relatively low-concentration, dilute turbulent flow (e.g. low-density turbidity current - *sensu* Lowe, 1982). Palaeoflow indicators recording multiple flow directions during the deposition of a single bed record the effect of flow confinement during deposition. During the transition between deposition beneath higher- to lower-concentration flow (i.e. to produce basal, non-stratified sandstone, and capping stratified sandstone, respectively), a co-genetic MCR division was emplaced under flow conditions in which fluid turbulence and bed form generation remained suppressed, presumably by a high concentration of sediment and mud clasts. This distinct, often thick (<1.4 m), co-genetic MCR division is comparable to that found in HEBs described from the distal settings of deep-water systems, in relatively less topographically complex settings (Haughton et al., 2003, 2009; Hodgson, 2009; Talling, 2013), albeit the former are less matrix (clay)-rich. The origin and significance of co-genetic MCR divisions within Type C beds is discussed further below.

6.4.1.4 Type D – Very thin to thick, well-stratified beds

Type D beds are normally graded, and dominated by well-stratified sandstone (e.g. sinusoidal and supercritical climbing ripple, current ripple and planar lamination; Fig. 6.2). Dewatering and convolution are easily recognised within these well-stratified beds. Rarely, Type D beds can exhibit complex lamination, with internal truncations, or a non-stratified sandstone perched higher within the bed that is not notably coarser grained (Fig. 6.11). Type D beds are the thinnest (<0.5 m) and finest grained bed type. Bed bases are seldom erosional, and mud clasts are rare and small (<10 mm). Current ripple lamination records disperse (widespread)

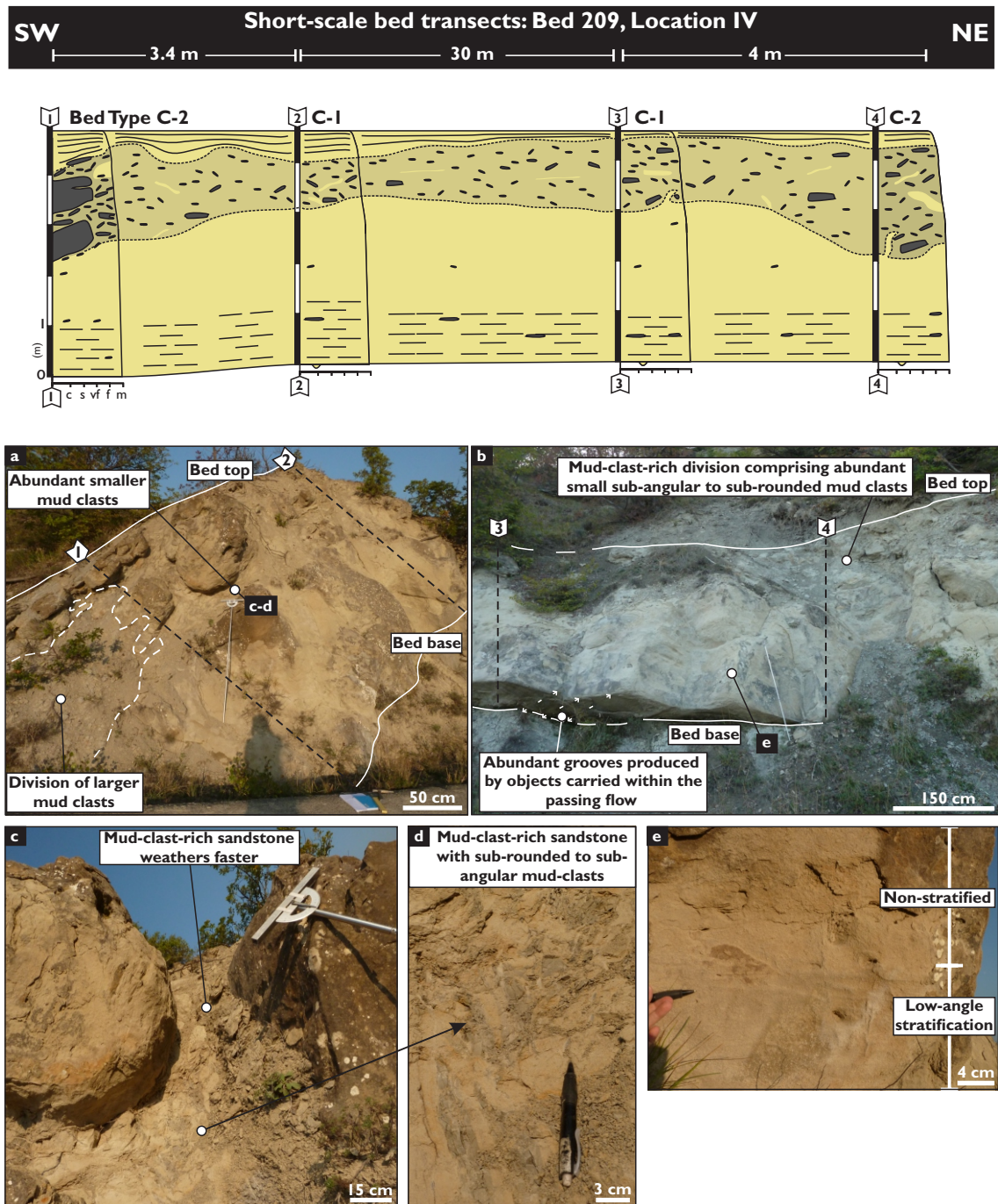


Figure 6.10. Short length-scale transect through a Type C bed at Location IV illustrating how the thickness of the co-genetic mud-clast-rich division, and the mud-clast abundance and size within, is highly variable over short length-scales. **A-B)** Bed character at log sites 1 through to 4. **C-D)** Mud-clast-rich sandstone near log position 1. **E)** Low-angle stratification and non-stratified sandstone near the base of the bed at log position 2.

palaeoflow directions, often at high angles away from the northern confining basin margin (Fig. 6.3). Type D beds retain their stratified character across the basin, and do not transition into other bed types across the studied interval.

Type D beds are interpreted to record aggradation beneath low-density turbulent flows (Bouma, 1962; Lowe, 1982), with lower sediment concentrations than those emplacing other

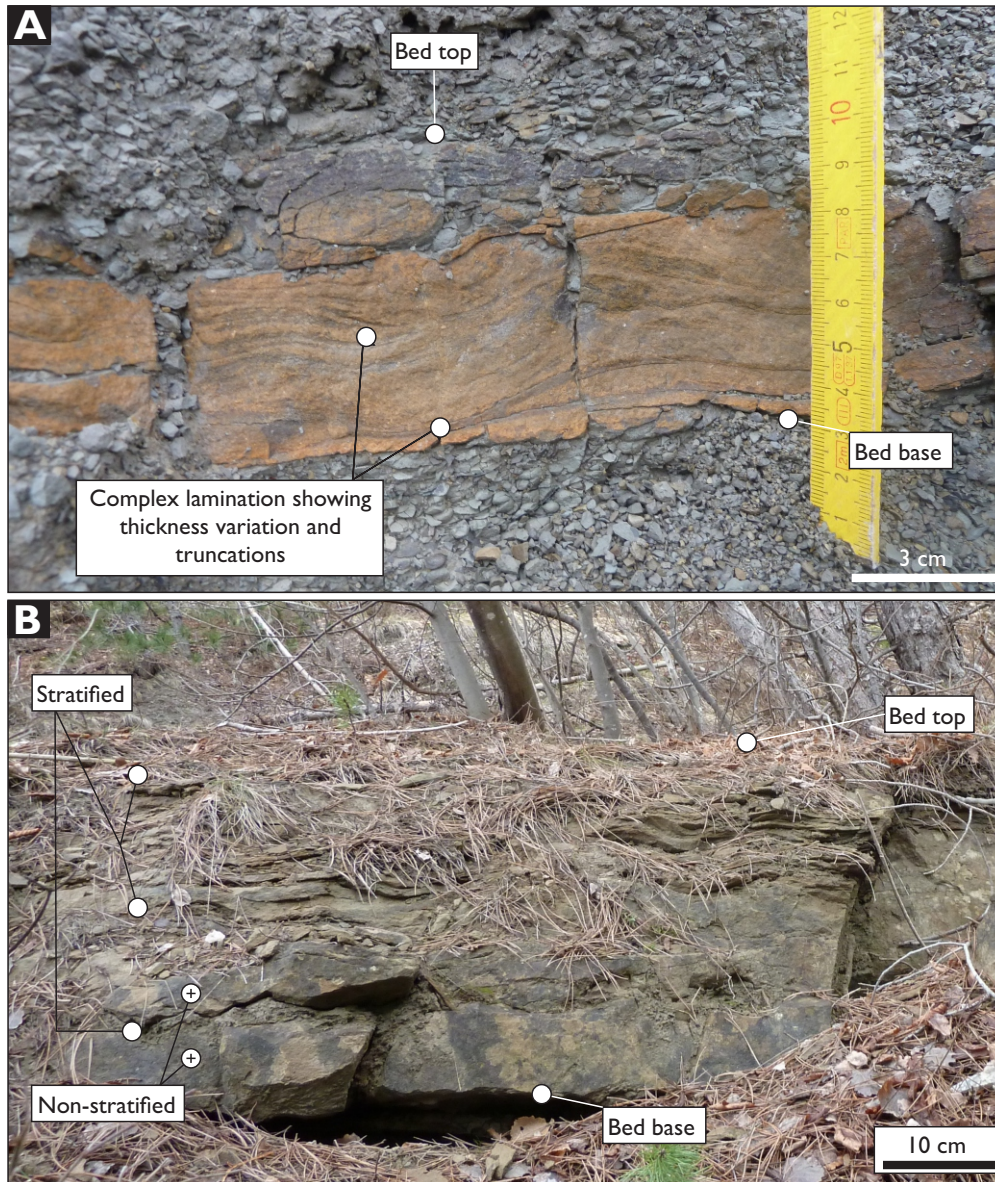


Figure 6.11. A) Type D bed with internally complex lamination with truncation of laminae. **B)** Vertically alternating stratified and non-stratified sandstone within a Type D bed dominated by sinusoidal lamination in the upper half of the bed.

bed types. However, sinusoidal- and supercritical- climbing-ripple lamination (*sensu* Jobe et al., 2012), indicate suspension fall-out rates were still relatively high. Beds containing perched non-stratified sandstones have been described adjacent to confining topography in the confined Sorbas Basin, and were interpreted to record reflection of the flow head away from the confining basin margin, and subsequent deposition above stratified sandstone that was more recently deposited from the flow body (Haughton, 1994). The origin of this facies arrangement, and development of internally truncated lamination observed periodically in Type D beds is discussed further below.

6.4.2 Evolution of palaeoflow associated with a confining basin margin

Flute and prod marks ($n=35$), current ripple lamination ($n=36$), and groove casts ($n=149$) were measured from beds within the study interval. Sole structures (e.g. flute casts, groove and prod marks) indicate that flows entered the basin from the SSW, and travelled NNE (Fig. 6.12, Loc. VII-V) towards the confining counter slope of the northern basin margin, where they were subsequently deflected (Fig. 6.12, Loc. IV-I); this change in flow direction is observed along individual beds (Fig. 6.7, Beds 208, 210). Current ripple lamination, which is present

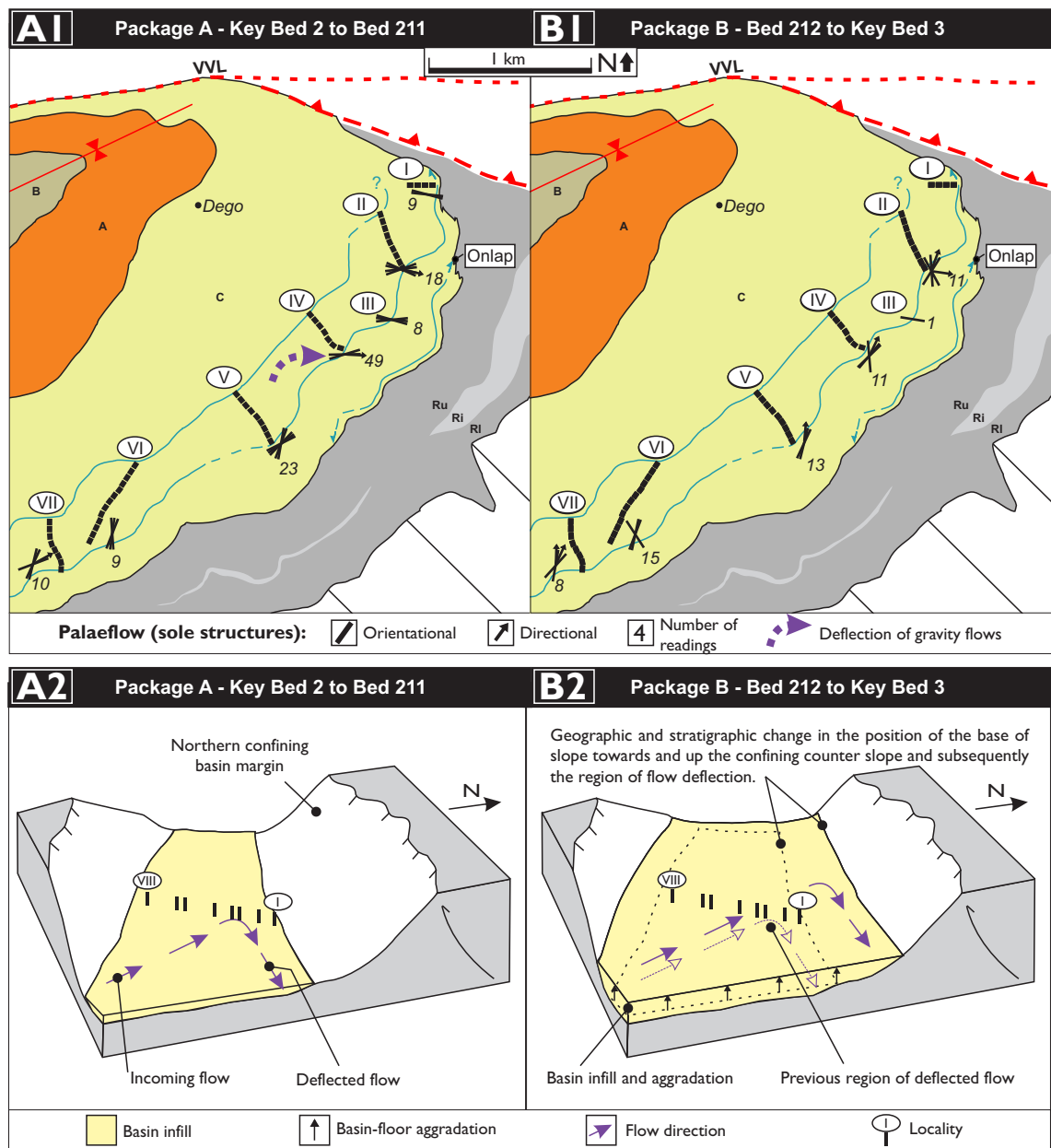


Figure 6.12. A1 & A2) Sole structures record flow deflection commencing between Locations V and IV during early deposition of the study interval whilst during later deposition of the study interval (**B1 & B2**) the zone of flow deflection is inferred to have advanced north beyond Location I. Such shift in the zone of deflection is resultant of basin-floor aggradation within a basin with inclined basin margins (sensu Kneller & McCaffrey, 1999) and does not record a change to an unconfined setting as bed thicknesses remains similar and current ripple lamination records continued reflection of flow away from the northern basin margin (Fig. 6.1d).

higher within the same bed, records palaeoflows that are more variable in direction, either parallel, or more commonly at a high angle away from the strike of the northern basin margin (Fig. 6.3). Similar observations for different types of palaeoflow indicators have been made in previous studies of the Castagnola Basin (Baruffini et al., 1994; Felletti, 2002), and in a number of confined systems (Haughton, 1994; Kneller et al., 1991; Kneller & McCaffrey, 1999; McCaffrey & Kneller, 2001; Bersezio et al., 2009; Felletti & Bersezio, 2010), as well as experimental studies (Kneller et al., 1991). These characteristics are considered to represent contrasting responses in higher and lower concentration portions of the flow (e.g. deflection and reflection, respectively) to confining topography (Kneller & McCaffrey, 1999). All flute casts and prod marks that record flow deflection near the northern confining basin margin, record flow deflection towards the east. This trend is interpreted to be as a result of oblique incidence between flows travelling north-north-east, and the east-west strike of the local northern basin margin.

Sole structures recording deflected palaeoflows near the northern basin margin are common in the lower half of the study interval (Fig. 6.1d, strata below Bed 212; Fig. 6.12, Package A), but are not identified stratigraphically higher in the study interval (Fig. 6.1d, strata above Bed 212; Fig. 6.12, Package B). The vertical loss of deflected sole structures is not considered to represent a change from confined to unconfined flow, or a different entry point of flows into the basin for the following reasons: 1) ripple laminations continue to record widespread palaeoflow away from the basin margin (Fig. 6.1d); 2) sole structures indicate that flows retained entry points from the SSW; and 3) the vertical loss of deflected sole structures does not coincide with a decrease in bed thickness, which may otherwise indicate a change to unconfined settings over a larger depositional area. This vertical change is instead interpreted as an effect of basin-floor aggradation in a basin which possessed inclined margins, with subsequent migration of the point of onlap, both towards and up the basin margins (*sensu* Kneller & McCaffrey, 1999). Thus, in a one-dimensional section, successive beds record depositional sites which became increasingly further from the basin margin, and sole-structure orientation records a change from flow that was deflected to flow that was not yet deflected by the confining topography (cf. Kneller & McCaffrey, 1999). Such migration in the point of basin-margin onlap is thought to result in the stratigraphic change in sole-structure orientation, with deflected sole structures inferred to be located farther north of the outcrop window (e.g. north of Locality II). The rapidity with which this change occurs suggests the presence of a terrace, or a reduction in gradient on the confining slope, resulting in a sudden shift in the region of onlap to the north; an uneven gradient was documented on the confining basin margin below the study interval by Felletti (2002). Considering the confinement of gravity currents within the contained Castagnola Basin, and previous research on depositional trends

adjacent to confining topography (Barker et al., 2008; Patacci et al., 2014), the following sections detail how the depositional character of beds containing a co-genetic MCR division varies across the basin, and in relation to the downstream confining slope at the northern basin margin.

6.4.3 Spatial variation of depositional character with respect to a downstream confining basin margin

Correlation of logged sections across the basin has allowed the construction of individual bed transects, orientated approximately NE-SW, slightly oblique to the palaeoflow of gravity currents entering the basin (NNE), and highly oblique to both the strike of the northern basin margin (E-W) and flow which was locally deflected towards the east (Fig. 6.7). The scale of bed transects is largely comparable to the downstream length of the basin (~5 km) at the level of the study interval, as suggested by the overall thinning of the succession at either end of the study interval. Across the basin, maximum grain size remains constant within individual beds, with only minor reductions at Location 1 close to the northern basin margin (Fig. 6.7, Beds 208, 210). Bed thickness across the basin typically remains constant (Beds 210, 214), or thickens (Beds 204, 208) prior to eventual thinning and onlap onto the northern basin margin (Beds 204–214); thickness trends show no apparent relation to bed type. A similar increase in bed thickness, and sand-to-mud ratio prior to eventual onlap onto confining topography, has been documented in other basins (Haughton, 1994, 2001; Kneller & McCaffrey, 1999), and in older strata of the Costa Grande Member (Felletti, 2002, 2004b); such characteristics are attributed to the forced flow deceleration, loss of energy, and subsequent sediment deposition due to proximity to the confining basin margin.

Beds containing a co-genetic MCR division (Type C) can be present at any location within the basin, with MCR divisions found at least 3.1 km upstream of the northern basin margin (Fig. 6.1d; Fig. 6.7, Bed 208). A MCR division can be present within an individual bed, regardless of the change in palaeoflow direction (e.g. incoming or deflected) recorded at the base of the bed (Fig. 6.7, Beds 208, 210), with the thickness of this division exhibiting no trend in relation to palaeoflow direction. Laterally, the thickness of this division is highly variable (~0.1 to 1.4 m) in a non-systematic manner, with repeated thickening and thinning occurring both on a basin-scale (Fig. 6.7), as well as on the scale of an individual outcrop (tens to hundreds of m's distance; Fig. 6.11). Furthermore, the division in Type C beds does not exhibit systematic trends in mud clast abundance, as inferred from the dominant bed sub-type at each section, nor maximum size with respect to palaeoflow direction, or proximity towards the downstream confining counter slope at the northern basin margin. Large mud clasts (>0.4 m in length) are found both adjacent to, and away from, the northern basin margin (Fig. 6.7, Bed

208, Loc. II and VII). Variation in the thickness and character of the co-genetic MCR division, and thus lateral transition between bed sub-types C1 to C3, can occur over short distances (tens of m's distance) and can be observed a number of times within a single bed (Fig. 6.7). Such variations are non-systematic with respect to palaeoflow direction, or proximity to the downstream confining northern basin margin (Fig. 6.7). Stratigraphically (vertically), there is an apparent concentration of beds containing a MCR division (Type C) at the base of the study interval; however, similar deposits are also present in abundance above the study interval.

Despite trends of reducing bed thickness and grain size adjacent to the northern basin margin, bed type, and the character of the MCR division within Type C beds, exhibits no systematic lateral or stratigraphic variation in relation to palaeoflow direction, or proximity towards the downstream counter slope at the northern basin margin. Such findings are in contrast with previous studies concerning the localised distribution of mud-clast- matrix-rich sandstone facies with respect to confining topography (Barker et al., 2008; Patacci et al., 2014). The potential causal factors driving the lack of variation in depositional character, locally adjacent and towards confining slopes within the Castagnola Basin are explored in the following section.

6.5 Discussion

6.5.1 Gravity-current confinement and containment within the Castagnola Basin

A number of sedimentological features described in section 6.4 indicate that gravity currents were both confined and contained within the Castagnola Basin. Confinement is evidenced by observations of direct bed onlap onto the basin margin, near the base, and below the study interval (Felletti, 2002), with thinning of the succession towards the basin margins (Fig. 6.1d). In contained systems, notably thick turbiditic muds commonly occur above sandstone beds (e.g. ponded muds - Pickering & Hiscott, 1985; Haughton, 1994, 2001); although differentiation between turbiditic and hemipelagic mud could not be deduced in the Castagnola Basin, thicker mudstones are consistently found above thicker sandstone beds. (Fig. 6.1d, Key Bed 2, Beds 209, 210). This relationship suggests that such beds were emplaced by larger volume events, resulting in a greater volume of turbiditic sand and mud which was contained (ponded) by the physiography of Castagnola Basin. Flow confinement processes are also demonstrated by the variation of palaeoflow along individual beds towards the basin margin, as well as variation between the base and top of the bed, indicating that flow confinement persisted during bed aggradation. Such trends in palaeoflow have been documented in a number of systems from

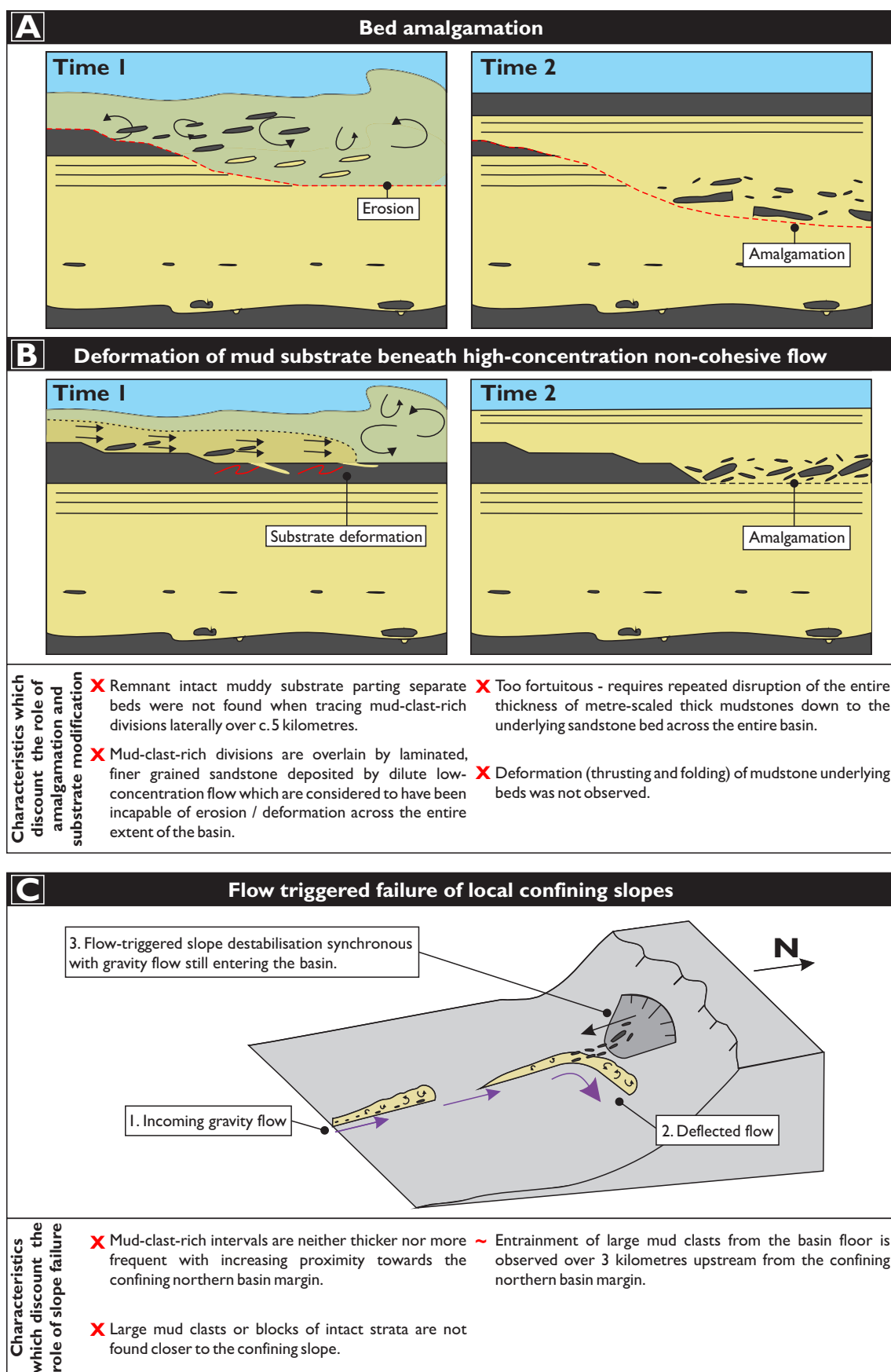


Figure 6.13. Characteristics which discount various mechanisms for the development of pseudo-HEB deposits containing a distinct mud-clast-rich division. **A)** Sandstone bed amalgamation between successive gravity currents *sensu* Walker (1966). **B)** Substrate deformation and sandstone bed amalgamation beneath high-concentration, non-cohesive flow (modified from Butler & Tavarnelli (2006). **C)** Gravity current-triggered destabilisation of muddy slopes on confining sea-floor topography (*sensu* Kneller & McCaffrey, 1999).

topographically complex settings (Pickering & Hiscott, 1985; Haughton, 1994; Kneller et al., 1991; Kneller & McCaffrey, 1999; McCaffrey & Kneller, 2001; Bersezio et al., 2009; Felletti & Bersezio, 2010).

Sedimentary features indicative of high rates of sediment fall-out during deposition (e.g. planar, sinusoidal, climbing-ripple lamination, and convoluted lamination; Lowe, 1982; Jobe et al., 2012), are commonly described where flow confinement occurs (Pickering & Hiscott, 1985; Haughton, 1994). In such settings, these features likely represent reduced flow carrying capacity (*sensu* Hiscott, 1994a), as a result of flow modification following confinement by sea-floor topography (Edwards et al., 1994; Kneller & Branney, 1995; Kneller & McCaffrey, 1999). The dominance of these styles of stratification in deposits across the study interval, and the presence of encircling-containing basin margins, suggests flows were subject to flow confinement and containment within the Castagnola Basin. Occurrences of complex facies arrangements within individual beds (e.g. perched non-stratified sandstone within stratified sandstone), in places developed in Type D beds, have previously been documented in deposits from confined systems (Pickering & Hiscott, 1985; Haughton, 1994, 2001; Sinclair, 1994). Such an arrangement has been attributed to collapse of the flow head away from confining topography, with subsequent deposition above recently deposited stratified sandstone from the flow body (e.g. “quick beds” - Haughton, 1994). Similar deposits in the Castagnola Basin are also interpreted to record individual sedimentation events, as bed amalgamation is not observed within the study interval. However, as perched, non-stratified sandstones do not coincide with significant grain size change in Type D beds, these arrangements may instead record fluctuation in local suspension fall-out rate, driven by complex flow dynamics within a confined, contained flow, following interaction with multiple basin margins (section 6.5.3), as opposed to a distinct collapse of the flow head (*sensu* Haughton 1994).

6.5.2 Origin of mud-clast-rich divisions within Type C beds

The following sections evaluate a range of feasible processes for emplacing mud-clast-rich strata encased within sandstone, to investigate the origin of the co-genetic MCR division observed within Type C beds.

6.5.2.1 Gravity-flow-driven substrate modification

Where a flow erodes (Fig 6.13a; Walker, 1966a), or shears (Fig 6.13b; Butler & Tavarnelli, 2006), the underlying muddy substrate, and penetrates down to an underlying sandstone bed, a composite deposit may result comprising a MCR division encased within overlying and underlying sandstone. In these cases, the MCR division (“ghost bedding” *sensu* Butler & Tavarnelli, 2006) should be traceable laterally into intact mudstone between the separate beds.

Neither of these processes are considered plausible formation mechanisms for MCR divisions in the Costa Grande Member, however, as they are not observed to pass laterally into intact mudstone partings (Fig. 6.7). Additionally, it is unlikely that erosion or deformation would have been capable of affecting the entire thickness of substrate mudstone, which commonly exceeds 1 m in thickness, across the entire extent of the basin. Furthermore, sandstone overlying MCR divisions tends to be finer grained and laminated, suggesting emplacement by relatively dilute, low-concentration flow, which would have been incapable of such basin-wide erosional effects; bypass of an early high-density flow whose presence went unrecorded is unlikely in the small, contained Castagnola Basin.

Experimental studies have demonstrated that non-cohesive gravity flows can enter, and flow intact, in a soft muddy substrate, where bed shear stress and flow density exceeds the cohesive strength and density of the muddy substrate (Verhagen et al., 2013; Baas et al., 2014). The experimental deposits comprised sandy deposits encasing a mud-rich layer, with significant loading at their bases, and were likened to hybrid event beds (Baas et al., 2014). However Type C beds frequently exhibit groove marks (sometimes flute casts), and lack widespread soft-sediment deformation features across the base of beds. Furthermore, beds are relatively tabular, and evidence of flow entering the substrate was not documented. As such, the lack of evidence for such intra-bed flow in the contained Castagnola Basin, where “ponded” turbiditic muds were likely to be thick and relatively soft, suggests that bed shear stress may have often been too high, and resulted in the entrainment of this material into the flow, rather than flow entering the substrate. Similar processes were observed in the relatively upstream locations of the experiments of Baas et al. (2014). High shear stresses may have been promoted by the contained nature of the Castagnola Basin, in which restricted flow expansion limited the dissipation of turbulence energy. As such, it is suggested that intra-bed flow processes are less likely to occur in contained settings, compared with confined and unconfined settings.

6.5.2.2 Interaction of gravity flows with a confining basin margin

Gravity-current-triggered destabilisation of muddy slopes on local sea-floor topography has been proposed to trigger secondary, synchronous MCR debris flows, which result in the emplacement of sandstone beds containing a distinct MCR division (McCaffrey & Kneller, 2001). MCR divisions generated in such a manner might be expected to be localised, thicker, and perhaps contain larger mud clasts locally adjacent to the slope with which the gravity currents interacted. However, MCR divisions in the Costa Grande Member are not localised to the downstream counter-slope at the northern basin margin, and exhibit no distinct trends in terms of frequency, thickness, or mud-clast size towards this confining feature (Fig. 6.13c).

Basin-margin slope instability is therefore considered unlikely, as stand-alone slumps or debris flow deposits are lacking in the Costa Grande Member (Baruffini et al., 1994; Felletti, 2002).

Case studies have highlighted the effects of confining sea-floor topography on modifying gravity currents, as inferred from laterally varying depositional character towards such confining topography (Barker et al., 2008; Patacci et al., 2014). Patacci et al. (2014) described the localised development and thickening of a MCR division within HEBs, with increasing proximity towards a confining slope; such facies development was localised to within 1 km of onlap onto the slope. They consider this facies tract to record the forced deceleration of gravity currents with a compositional and rheological complexity (arising from segregation of mud clasts to the rear of the flow), which was present prior to confinement by the slope, and which was captured by the resulting deposits locally adjacent to the slope. The localised confinement by topography, *sensu* Patacci et al. (2014), is not thought to have produced the co-genetic MCR division found in Type C beds, based on their extent across the basin (at least 3.1 km upstream of the basin margin) and the lack of systematic variation in their thickness and character towards this margin (Figs 6.1d, 6.7). Furthermore, if co-genetic MCR divisions were related to the localised effects of confining slopes, it might be expected that in a suitably located vertical succession such deposits would become less common vertically as the basin infilled, and the depositional point becomes farther from the point of onlap onto the basin margin (see section 6.4.2). However, this is not the case, and co-genetic MCR divisions are present throughout and above the studied interval of the Costa Grande Member.

6.5.2.3 Entrainment and transport of substrate-derived mud clasts

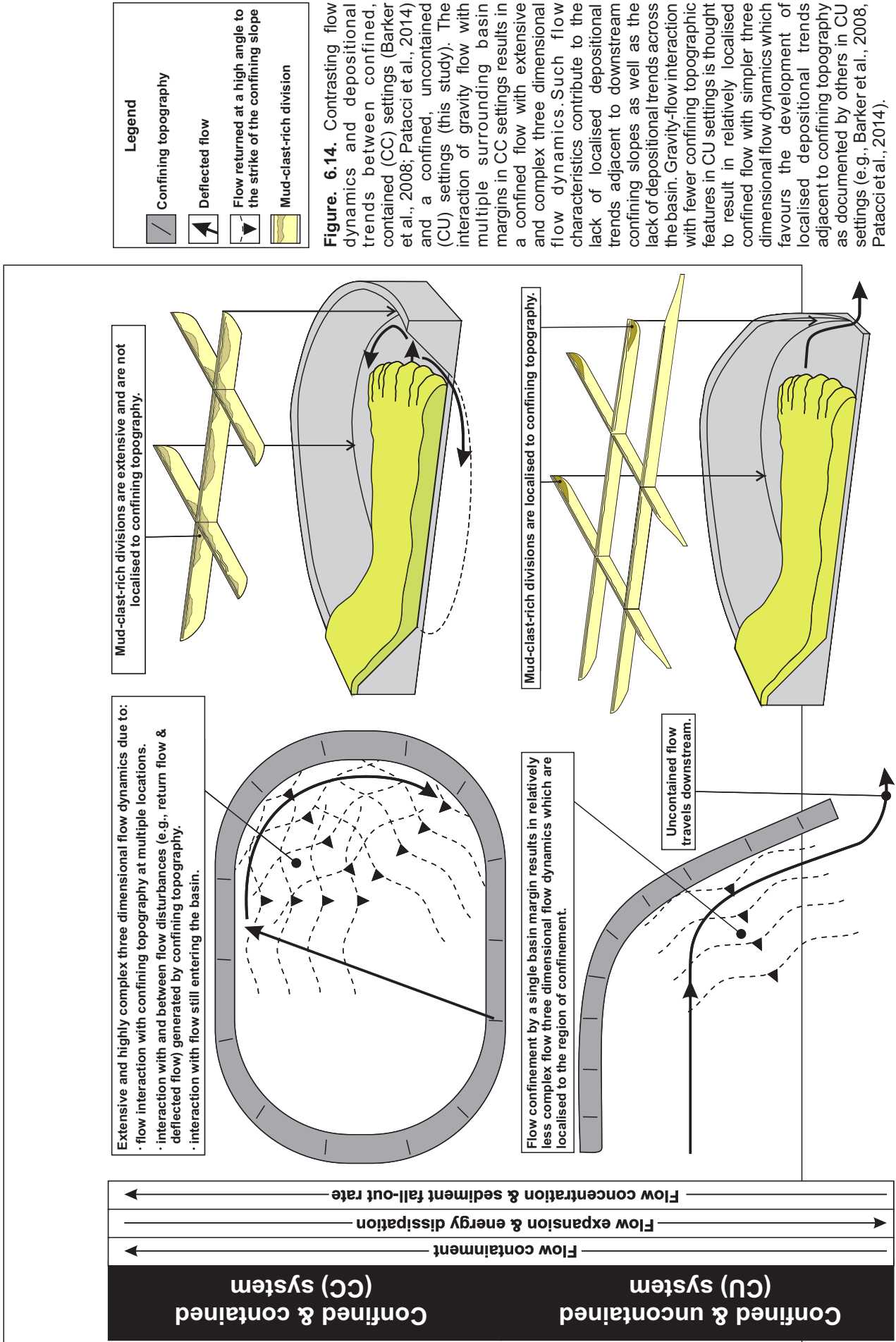
Type C beds exhibit substrate erosion and entrainment of mud clasts at multiple sites across the basin (Fig. 6.7, Bed 208, Loc. VII, V, Bed 215, Loc. VII, V, II), with relatively large mud clasts (> 1 m length), some of which maintain partial attachment to the underlying mudstone substratum (Fig. 6.5, Style I). Such entrainment, which was both voluminous and randomly distributed across the basin floor, is inferred to establish a MCR flow in which mud clasts were unevenly distributed. Such flow character, in addition to flow containment effects (section 6.5.3), is thought to have contributed to the character of the co-genetic MCR division, whose presence and thickness within Type C beds varies both significantly and non-systematically in downstream and cross-flow directions. Entrainment of muddy substrate into the flow is frequently cited as a mechanism initiating the development of hybrid flows which emplace HEBs, containing a distinctly thick co-genetic MCR division (Haughton et al., 2003, 2009; Talling et al., 2004; Amy & Talling, 2006; Davis et al., 2009; Patacci et al., 2014), comparable to that within Type C beds.

In Type C beds, mud clasts are more abundant, reach a greater maximum size (>1 m), and are concentrated into distinct, often thick (<1.4 m), co-genetic MCR divisions compared to mud clasts observed in Type A and B beds. All bed types exhibit erosive bases and partial entrainment of large pieces of muddy substrate, therefore Type C flows are likely distinct, in that they were more efficient at entraining muddy substrate, limiting mud clast diminution during transport, and supporting and concentrating mud clasts within the flow. Coarse grain sizes, and less common examples of partial substrate entrainment compared to other bed types, suggests that Type C flows may have been more efficient at entraining substrate from the basin floor. The predominance of non-stratified sandstone in the lower parts of Type C beds suggests flows were of relatively higher sediment concentration, in which fluid turbulence would have been more suppressed (Lowe, 1988), and attained lower rates of mud-clast breakup (Smith, 1972), compared to those in relatively lower concentration flows which emplaced better-stratified deposits (e.g. Type A and B beds). Although a wide range of mud-clast shapes (e.g. sub-rounded to angular) are found in Type C beds, angular examples are relatively common compared to other bed types. However, angular clasts do not directly indicate reduced clast breakup within Type C flows, as angular mud clasts can be released into the flow during the transportation and break-up of larger mud clasts (Fig. 6.6). Furthermore, the evolution of mud-clast characteristics (e.g. size and shape) is expected to be influenced by a number of factors, whose relative importance and interplay during the flow event are poorly understood. For example, mud-clast size and shape can be influenced both by the intensity of fluid turbulence and the duration of transport within the flow, both of which may act in combination or in opposition in the flow (Smith, 1972). Thus, constraining whether efficient entrainment or limited mud clast breakup was more influential in the development of co-genetic MCR divisions within Type C beds is problematic.

The elevation of the co-genetic MCR division within Type C beds, emplaced by aggradation (section 6.4.1), suggests mud clasts were retained within the flow, whilst the underlying relatively mud-clast-poor sandstone was deposited. Mud clasts may have been located in a more rearward, later depositing region of the flow perhaps following longitudinal fractionation processes during flow run-out (see Haughton et al., 2003). However, considering the recent entrainment of mud clasts and limited available flow run-out distance across the basin floor (< 5 km), such rearward segregation may have been relatively incomplete, and as such may not have been the dominant process driving the concentration of mud clasts into the co-genetic MCR divisions. Processes which provided mud-clast support within high-concentration flow (e.g. mud clast buoyancy, hindered settling and kinetic sieving) whilst deposition of much of the sand fraction occurred were likely more influential. Mud clasts can be positively buoyant where their density is lower than that of the surrounding sediment-

water mixture (Flemings et al., 2006; Talling et al., 2010). High rates of sediment fall-out typical of high-concentration flows (Lowe, 1988) can drive a significant upwards-flux of displaced fluid, which may hinder the settling of other particles (e.g. hindered settling; Davis, 1968; Druitt, 1995); mud clasts may have been preferentially supported due to their larger surface areas compared to sand grains. Displacement of mud clasts upwards through the flow can also occur in high-concentration flows as smaller sand-grade particles are more likely to fall into voids and thus settle downwards, whereas larger mud clasts settle less freely (e.g. kinetic sieving; Bridgwater, 1976; Gray & Chugunov, 2006). Similar mechanisms were proposed to provide mud-clast support in the experiments of Postma (1988), which demonstrated that mud clasts, including outsize examples, could be elevated and concentrated in a flow, and transported at a density interface between an underlying, high-concentration, low-turbulence layer and overlying, lower-concentration, more turbulent layer. With sand deposition and subsequent reduction of flow concentration beneath a critical threshold, mud-clast support mechanisms associated with higher-concentration flow would have been subdued, or removed, resulting in the deposition of a co-genetic MCR division above relatively mud-clast-poor sandstone in the same bed. Flow confinement is known to increase sediment fall-out rate (Kneller & McCaffrey, 1999); as such, a sudden increase of sediment fall-out rate, reduction of flow concentration and onset of mud-clast deposition may have resulted from the effects of both flow confinement and containment within the Castagnola Basin.

Although Type C beds record deposition beneath a high-concentration, weakly to non-turbulent, sandy flow, they are considered distinct from high-density turbidites (Lowe, 1988), which typically contain much thinner mud-clast horizons, or no such horizons. Type C beds are somewhat more comparable to HEBs, as described by Haughton et al. (2003, 2009) and Talling (2013), which also contain a distinct thick co-genetic MCR division overlying relatively mud-clast-poor sandstone within the same bed. However, Type C beds differ in that the supporting sandstone matrix within the co-genetic MCR division is not as matrix-rich as that described in these previous studies, and is thus not considered to have been deposited beneath a region of notably more cohesive (clay-rich) flow within the flow event (Haughton et al., 2003, 2009; Talling, 2013). The relatively matrix-poor nature of the matrix within Type C co-genetic MCR divisions may reflect the relatively recent entrainment, shorter flow run-out distance and limited disaggregation of mud clasts within the contained Castagnola Basin, as compared with the larger flow run-out distances achieved in the uncontained systems from which HEBs with more matrix-rich co-genetic MCR divisions have hitherto been described (Haughton et al., 2003, 2009; Amy & Talling, 2006; Davis et al., 2009; Hodgson, 2009). Thus, the term “sandy-HEB” is used herein for beds containing a thick, co-genetic MCR division, with a relatively matrix(clay)-poor sandstone matrix that may also exhibit significant, non-systematic



lateral variability in terms of its presence, thickness and character; it can pass laterally into relatively mud-clast-poor sandstone. Flows emplacing such deposits may represent the early stages of hybrid-flow development (*sensu* Haughton et al., 2003, 2009).

6.5.3 Influence of flow containment upon the character and distribution of sandy HEBs in confined deep-water systems

The lack of localised systematic trends in depositional character near to confining topography within the confined and contained (CC) Castagnola Basin is in contrast to that documented by Barker et al. (2008) and Patacci et al. (2014) in confined, uncontained (CU) settings. The following section assesses the importance of flow containment (ponding), in addition to flow confinement, in CC settings, and its potential influence upon gravity-flow dynamics and deposit character, and distribution within topographically complex settings.

6.5.3.1 Processes of flow confinement and containment

Considerable experimental work has explored the interaction of gravity currents and topography (Pantin & Leeder, 1987; Edwards et al., 1994; Kneller, 1997; Kneller & McCaffrey, 1999; Lamb et al., 2004, 2006; Toniolo et al., 2006a,b; Sequireos et al., 2009). Many have demonstrated how disturbances, characterised by downstream changes in flow velocity and thickness, are locally generated where flows are obstructed by a confining obstacle (Pantin & Leeder, 1987; Edwards et al., 1994; Kneller, 1997; Lamb et al., 2004, 2006; Toniolo et al., 2006a, b; Sequireos et al., 2009). Such topographically-induced flow non-uniformity (*sensu* Kneller & Branney, 1995) can be associated with a reduced sediment carrying capacity, and increase in sediment fall-out rate from the flow (Kneller & McCaffrey, 1999); where flow containment occurs in addition to flow confinement, such as that in the Castagnola Basin, such flow non-uniformity effects extend across the entire experimental basin (Pantin & Leeder, 1987; Kneller, 1991; Alexander & Morris, 1994; Kneller & McCaffrey, 1995; Lamb et al., 2004, 2006 Toniolo et al., 2006a, b) and likely records the effects of containment and limited flow expansion in such settings (Middleton, 1967; Scheidegger & Potter, 1971; Garcia, 1994). Similarly extensive flow non-uniformity effects and limited flow expansion are thought to occur in the Castagnola Basin based on the dominance and basin-wide extent of features associated with a high sediment fall-out rates (e.g. deposits dominated by non-stratified sandstone and/or sandstone exhibit long-wavelength, low-relief styles of stratification [crude, planar or sinusoidal stratification]).

Both experimental and outcrop studies have demonstrated how complex multi-directional flow is established where flows interact with and are confined by a single topographic feature (Kneller et al., 1991; Haughton, 1994; Kneller & McCaffrey, 1999; Amy et

al., 2004). Kneller & McCaffrey (1999) showed how confinement of a density-stratified flow can result in the reflection of the upper dilute layer at a high angle to the strike of the counter slope, whilst the basal, higher-concentration layer is deflected laterally parallel to the strike of the slope. Such palaeoflow trends, recording complex three-dimensional flow dynamics, have been documented in outcrop studies (Kneller et al., 1991; McCaffrey & Kneller, 2001) including the Castagnola Basin (this study Figs 6.3, 6.10; Felletti, 2002). Furthermore, where the incidence angle is oblique with the confining obstacle, such as in the Castagnola Basin, the flow reflected in a direction perpendicular away from the counter slope is both oblique to the deflected dense basal layer as well incoming flow still entering the basin (Fig. 6.14; Kneller et al., 1991; McCaffrey & Kneller, 2001). However, the majority of experimental studies have generally focussed upon flow interaction with a single confining slope (CU setting) and consequently largely fail to explore how the three-dimensional flow dynamics of a confined flow may evolve in CC settings. However, in the oblique-incidence experiments of Kneller et al. (1991), the reflected flow (triggered by the initial downstream confinement), travelled towards and interacted with the sidewall of the tank. Thus, in CC settings it is probable that reflected and deflected flows generated from initial interaction with a confining basin margin may further interact with one or more of the following: 1) additional surrounding basin margins (Kneller et al., 1991); 2) other flow disturbances generated at these margins, such as that observed from “sloshing” liquids in transportation vessels (Bryant & Stiassnie, 1995; Faltinsen et al., 2005); and 3) flow which continued to enter the basin (Pantin & Leeder, 1987; Edwards et al., 1994). The oblique-incidence angle with a downstream confining basin margin, and presence of encircling confining topography in the Castagnola Basin, would have favoured such complex three-dimensional flow dynamics. This, in addition to voluminous and recent entrainment of muddy substrate shortly prior to deposition, is thought to have resulted in the lack of systematic depositional trends across the basin.

Distinct sedimentary structures (e.g. biconvex-rounded-current ripples, and small-scale hummocky-type lamination with internal truncations) in the Marnosa Arenacea Formation have been interpreted as records of multi-directional flow adjacent to confining topography in deep-water CU systems (Tinterri, 2011). The lack of comparable structures recording multi-directional flow in the Castagnola Basin likely results due to the CC setting of the basin which promoted a higher sediment fall-out rate (due to limited flow expansion) and perhaps more complex multi-directional flow dynamics (due to flow interaction with multiple basin margins) compared to that occurring in CU settings. At a sufficiently high sediment fall-out, bed aggradation outpaces traction resulting in bed forms that preferentially develop low-relief, long-wavelength stratification with minimal asymmetry (Lowe, 1988; Jobe et al., 2012); such structures are poor indicators of paleoflow direction. The dominance of non-stratified

sandstone and sandstone with low-relief, long-wavelength stratification styles in Type A, B and C beds of the Castagnola Basin suggests that sediment fall-out rates were too high to allow the development of higher-relief traction sedimentary structures capable of recording multi-directional flow *sensu* Tinterri (2011). Examples of deposits with syn-depositional truncation of stratification can occur in Type D beds; these thinner-bedded and finger-grained bed types are interpreted as lower magnitude events entering the Castagnola Basin and suggest that when flow concentration and sediment fall-out rates are lower, higher relief bed forms capable of recording complex multi-directional flow could develop. Further, experiments have shown that in the presence of highly complex three-dimensional flow (such as that thought to occur in the Castagnola Basin), the lack of an established flow direction hinders the development of ripples and other high-relief asymmetrical bed forms capable of recording multi-directional flow (see Yokokawa, 1995, Yokokawa et al., 1995).

6.6 Conclusions

Gravity currents entering the Castagnola Basin were subject to deflection and reflection following their oblique incidence and interaction with a downstream confining counter slope at the northern basin margin, and were fully contained by encircling basin margins. Bed-to-bed correlations, orientated at a high angle to the strike of the downstream northern basin margin, demonstrate the distribution and depositional character of sandy HEBs (Type C beds) over short (<100 m) and relatively longer (<5 km) length-scales. Individual bed transects demonstrate that sandy HEBs are extensive (>3 km) across the basin, and display significant lateral variability in terms of the presence and thickness of a co-genetic MCR division, as well as the size and abundance of mud clasts within this division, over short (tens of m's) and longer (<1 km) length scales. Such variation is non-systematic with respect to palaeoflow direction, and with increasing proximity to confining sea-floor topography. The extensive and non-systematic variable character of sandy HEBs within the confined and contained Castagnola Basin setting is in contrast to similar deposits from confined uncontained settings, where systematic depositional trends have been locally recognised locally near to confining sea-floor topography (Barker et al., 2008; Patacci et al., 2014).

Distinct co-genetic MCR divisions, which exhibit highly variable and non-systematic lateral variation in depositional character and distribution with respect to their distance from confining topography, likely resulted from the volume, support, and uneven distribution of abundant mud clasts in high-concentration flows. Flow containment, in addition to flow confinement, is thought to establish extensive, complex, three-dimensional flow dynamics

across the basin following interaction with multiple basin margins, which perturbed the development of localised or coherent depositional trends adjacent to confining topography.

This study sheds light on the contrasts in HEB distribution and depositional trends in different topographically complex settings; specifically that HEBs are not necessarily localised adjacent to confining topography, and can vary non-systematically in their depositional character where the effects of flow containment were superimposed upon those of flow confinement. These insights highlight the importance of being able to recognise the type of confined system (e.g. contained or uncontained), and have implications for the prediction of depositional character, and thus reservoir quality distribution, in topographically complex settings.

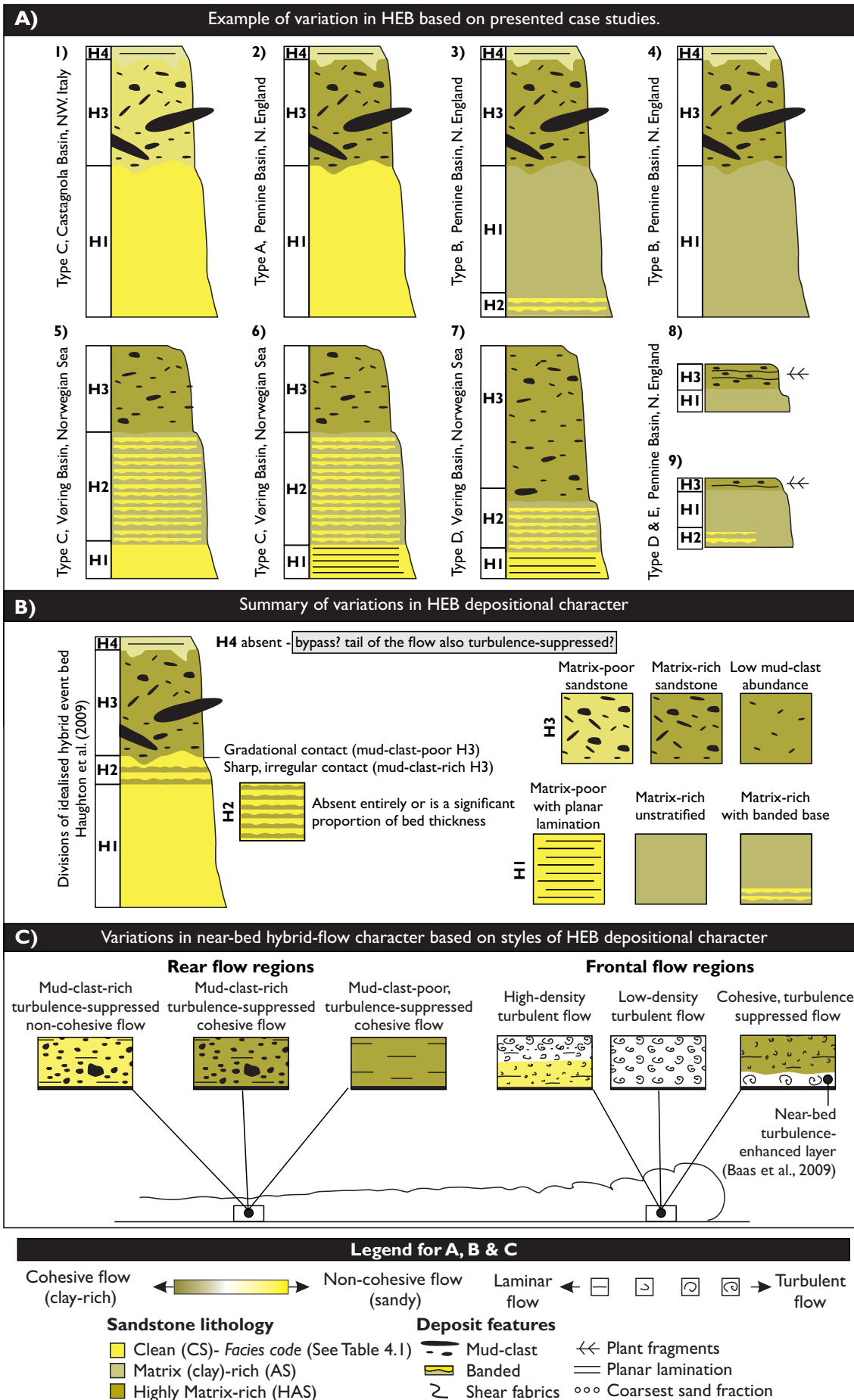


Figure 7.1. Variations in HEB depositional character and inferred variations in flow character based on insights gained from the presented case studies.

Chapter 7. Discussion, conclusions and further work

7.1 Introduction

Chapters 3 to 6 have detailed the findings of outcrop and subsurface investigations into the character and distribution of HEBs in a range of systems, affected by discrete elements of basin physiography. This chapter seeks to integrate the key findings of these case studies, in order to formulate generic insights into the nature of flow responsible for emplacing HEBs in deep-water systems, and to offer suggestions for further work to expand our understanding of these flow types and their deposits.

The findings of this research can be considered in terms of the following themes:

- 1) insights into the character and evolution of flows emplacing HEBs;
- 2) the influence of basin physiography on the former;
- 3) industrial applications (principally with respect to hydrocarbon reservoir evaluation).

7.2 Insights into the character and evolution of flows emplacing HEBs

A range of HEB deposits and inferred flow characters were documented in Chapters 3 to 6 (Figs 7.1a, 7.1b, 7.2). This spectrum suggests that a range of boundary conditions may promote and influence flows emplacing HEBs (Fig. 7.2a), such as the initial flow character, the type and consolidation state, and volume of any cohesive material eroded by the flow, the mechanisms of clay enrichment within the flow, and the effects of topography. Further, it is likely that the full range of such conditions (and their interactions) is not yet fully understood, with a more complete understanding awaiting future research (section 7.6). Previous studies have investigated the effect of varying clay concentration on the suppression of fluid turbulence (Baas et al., 2009, 2011; Sumner et al., 2009), and the ability of flows to support mud clasts (Talling et al., 2010; Talling, 2013). However, our understanding of the longitudinal distribution of rheology in these flow types, and its spatio-temporal evolution during downstream run-out, is relatively immature (i.e. Haughton et al. 2009, Kane & Pontén, 2012). The following section outlines the documented variations in HEB character, as presented in the preceding case studies, and discusses the further insights they provide in terms of the character and evolution of flows depositing HEBs.

7.2.1 Clay content of the upper “linked debrite” in matrix-poor HEBs

Sandstone in the MCR division of sandy HEBs (Fig. 7.1a, Example 1) in the Castagnola Basin is visibly cleaner (matrix-poor), compared to similar facies in other presented case studies (Fig. 7.1a, Examples 2-7). The matrix-poor character of sandstone supporting mud clasts may be an indicator of the immaturity of the linked debrite division, in which mud clasts underwent

relatively less disaggregation, due to the late entrainment and restricted flow run-out in a small, contained basin (Fig. 7.3a). [SS3] This suggests that the matrix content of the sandstone in the MCR division can be an indicator of relative proximity to the site of entrainment; however, such interpretations should be made with caution, and applied only with reference to a given depositional system due to the likely variation that can occur in initial-flow clay concentration between separate depositional systems. Thus, where HEBs are deposited relatively soon after mud-clast entrainment, the MCR division may be matrix-poor, and behave only as a baffle to hydrocarbon-fluid flow, as opposed to more distal HEBs in which matrix-rich MCR divisions act as barriers to hydrocarbon-fluid flow (Figs 3.7, 3.8). The significance of variations in HEB deposition character to the hydrocarbon industry is discussed further below (Section 7.5 and 7.6).

7.2.2 Development of stratified sandstone in the lower part of HEBs

Most commonly, HEBs exhibit matrix-poor, non-stratified sandstone in their basal divisions (Haughton et al., 2003, 2009; Hodgson, 2009; Davis et al., 2009; Patacci et al., 2014). However, HEBs from the Vøring and Pennine Basins (Chapters 3 and 4) can exhibit lamination (planar lamination, sometimes current-ripple or consolidation lamination) and banding in the lower facies of the bed (Fig. 7.1a, Examples 6, 7). The association of laminated matrix-poor sandstone with overlying matrix-rich facies (recording later deposition from a more cohesive turbulence-suppressed flow state), demonstrates preceding deposition from a turbulent suspension (*sensu stricto*), and thus the rheological heterogeneity associated with these flow types. The significance of lamination within HEBs is discussed in section 7.2.3, and banded sandstone in section 7.2.4.

7.2.3 Downstream variation of facies in the lower part of HEBs

The Vøring Basin case study is novel as it focusses on downstream variations (probability of occurrence and proportion of bed thickness) of the lower, relatively matrix-poor sandstone facies beneath the matrix-rich, non-stratified sandstone towards the top of beds. The documented downstream change from non-stratified to laminated sandstone at the base of deposits, interpreted as deposits of progressive aggradation, demonstrates how distinct rheological zones within hybrid flows can undergo discrete styles of flow evolution during downstream run-out (Figs 3.16, 7.2b). Whilst the rear of the flow evolved to become increasingly cohesive and turbulence-suppressed, more headward regions of the flow underwent a transformation from high- to low-density turbulent flow downstream, as is commonly interpreted for non-cohesive turbidity currents. This style of hybrid flow evolution has not previously been documented, and highlights the dynamic spatio-temporal transformation and evolution of such flows. Further, these observations demonstrate that an initial non-cohesive flow underwent partial cohesive-material-driven turbulence-suppression

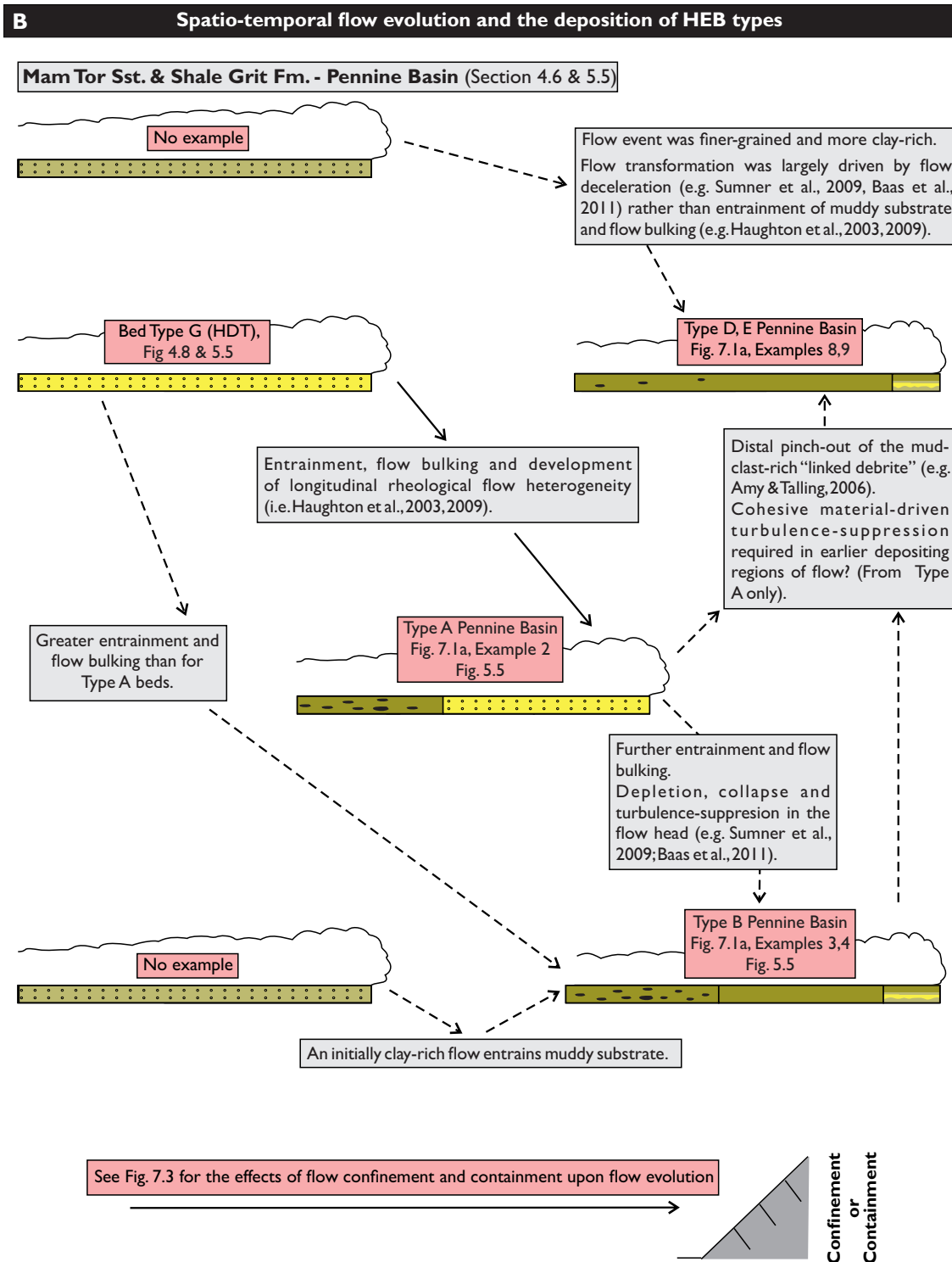


Figure 7.2b. ctd.

and flow transformation during downstream run-out. Flow evolution during downstream run-out will be influenced by the response of rheological zones to a range of boundary conditions (i.e. changes in sea-floor gradient, flow constriction or clay concentration), operating individually or in combination, and is a topic which warrants future research (Section 7.6).

7.2.4 Clay content of facies in the lower part of HEBs

Examples from the Pennine Basin demonstrate that mud-clast-rich HEBs of otherwise similar depositional character from the same system, can comprise either matrix-poor, or matrix-rich sandstone in the lower part of the bed (Fig. 7.1a, Examples 2, 4, respectively; Fig. 7.2b). These observations further highlight the range of flow characters that can occur in the frontal regions of hybrid flows and suggests that in addition to possessing a non-cohesive and variably turbulent character (Chapter 3, section 3.4.4.2), frontal regions of some hybrid flows may also be characterised by relatively cohesive, turbulence-suppressed transitional flow (*sensu* Baas et al., 2009) with succeeding rearward-flow being enriched in mud clasts (Chapter 5, section 5.4.2). As such, significant overlap may exist between flow processes associated with conceptual models of longitudinally-segregated hybrid flow (Haughton et al., 2009), and those of experimental vertically-stratified, clay-rich transitional flow types (Baas et al., 2009, 2011; Sumner et al., 2009) with regards to character and evolution of hybrid flow types. Thus, some hybrid flows may exhibit pronounced longitudinal heterogeneity in terms of flow rheology, with non-cohesive (sandy) flow passing rearward into increasingly cohesive, turbulence-suppressed, mud-clast-rich flow rearwards (i.e. “hybrid flow” - *sensu stricto* Haughton et al., 2009; Fig. 7.1a, Examples 2 and 5). Other hybrid flows may exhibit less pronounced longitudinal rheological heterogeneity, with frontal regions of the flow already being cohesive and turbulence-suppressed (Fig. 7.1a, Examples 3, 4, 8, 9, Chapter 5, section 5.4.2).

Flows undergoing cohesive-material-driven turbulence suppression, and emplacing co-genetic matrix-rich and matrix-poor sandstones are expected to be complex, in that rheological variation occurs both spatially (vertically and laterally along the flow) and temporally within the flow. Variations in the relative importance of these flow characteristics are currently poorly understood, but are likely to reflect a range of boundary conditions which influence the concentration and behaviour of cohesive material within a flow. These include variations associated with: 1) initial flow composition (e.g. Lee et al., 2013); 2) the entrainment of cohesive material (e.g. Haughton et al., 2009); 3) the timing and rate of flow depletion, which can result in the relative enrichment of cohesive material within flows (e.g. Sumner et al., 2009). This list is non-exhaustive, and a complete understanding of the range and influence of such boundary conditions is beyond the scope of this investigation, and should form a significant focus for future research (see section 7.6).

7.2.5 Position and proportion of banded sandstone facies

When documented, (Chapters 3, 4 and 5), banded sandstone repeatedly occurs beneath matrix-rich, non-stratified sandstone, a position commonly documented in other studies (Lowe & Guy, 2000; Barker et al., 2008; Davis et al., 2009; Haughton et al., 2009). However, banded sandstone occurred above matrix-poor sandstone in these previous studies compared with the

bed-basal occurrences of banded sandstone documented in the Pennine Basin (Fig. 7.1a, Examples 3, 9). Further, banded sandstone can be a significantly greater proportion of bed thickness (Fig. 7.1a, Example 5, 6, 7, Chapter 3); large proportions of banded sandstone have only previously been documented in the Cretaceous Britannia Sandstone Member, North Sea (Lowe & Guy, 2000; Barker et al., 2008)

A number of models have been proposed to account for the emplacement of banded sandstone, invoking either: 1) temporal fluctuations in the rheology of near-bed flow (Blackbourn & Thompson 2000; Lowe & Guy, 2000; Baas et al., 2005); or 2) reworking of sand, deposited earlier from the same flow, by near-bed turbulence-enhanced flow present at the base of transitional and lower transitional plug flow states, *sensu* Baas et al. (2009, 2011). Although it has not been possible to constrain the dominance of a given mechanism in the case studies presented herein, variations in the position and thickness of banded sandstone in these studies, as well as that in previous studies, offer further insight into how these mechanisms may be variably expressed. Where relatively thin intervals of banded sandstone occur at the bed base it suggests either: 1) deposition from flow temporally fluctuating in its rheology was limited and deposition from the preceding non-cohesive flow did not occur, either due to absence or bypassing of non-cohesive flow; or 2) the proportion of sandstone deposited prior to reworking was limited, or largely removed by intense reworking. When banded sandstone is positioned higher in the bed (where it typically forms a greater proportion of bed thickness), it suggests the following: 1) deposition from flow with temporally fluctuating flow rheology was relatively longer-lived, and was preceded by deposition from non-cohesive flow; or 2) a greater proportion of sandstone was deposited prior to reworking, or reworking was less intense.

Flow run-out distance and internal flow organisation have previously been suggested as possible influences on the significance of a zone of temporally fluctuating flow rheology within the flow (Haughton et al., 2009). In addition to flow run-out distance, the tendency to develop zones of temporally-fluctuating flow rheology could also reflect a number of variables, associated with the initial flow character, or entrainment of cohesive material (see section 7.6). In light of the mechanism suggested by Baas et al. (2011), as well as findings presented in the previous chapters which highlight the dynamic nature of the front regions of flows emplacing HEBs (Section 3.5.1, 4.6.1.3 and 5.4.2), a number of variables should be considered in the interpretation of banded sandstone and inferred flow character. Variation in the flow structure in terms of the character of the frontal (earliest-depositing) flow, and thus the amount and type of sandstone deposited prior to reworking and the development of banded sandstone will influence the thickness and position of banded sandstone within deposits. Furthermore, variation in the character of the later-depositing, clay-rich turbulence-suppressed flow may govern the thickness and position of banded sandstone, depending on its ability to develop and

sustain a zone of near-bed turbulence-enhanced flow (*sensu* Baas et al., 2009). For example, where clay enrichment occurs relatively rapidly (i.e. rapid entrainment, rapid flow depletion), or where clay enrichment is of a significant magnitude, flow transformation to early-stage transitional flow (with a zone of near-bed turbulence-enhanced flow) may be relatively short-lived, or may not occur at all, resulting in the absence of banded sandstone. If banded sandstone is generated beneath transitional flow (*sensu* Baas et al. 2009, 2011), then its occurrence in HEBs from the Vøring and Pennine basins suggests an overlap between conceptual models concerning longitudinally-segregated hybrid flow (Haughton et al., 2003, 2009), and observations from experimental variably clay-rich transitional flows (Baas et al., 2009, 2011; Sumner et al., 2009; Fig. 5.5). Future research should investigate the potential range of mechanisms and controlling factors which produce banded sandstones, in order to improve our understanding of the spectrum of HEB and inferred flow character.

In summary, the variations in HEB depositional character discussed above highlight the complexity of processes occurring within flows that are transitional between fully turbulent and fully cohesive flow behaviour (Figs 7.1, 7.2). Variations in the character of these flows are inferred to reflect the influence of a number of controlling factors, either singly, or in combination. A non-exhaustive list of such factors includes the following: 1) variations in the character of the initial flow); 2) variations in the types and character of processes promoting flow transformation (partially or wholly) to a more cohesive turbulence-suppressed flow state; and 3) interactions with confining or containing basin physiography (see Section 7.3, below). This research has highlighted the significance of factors 2 and 3 (Figs 7.2, 7.3); however, due to limitations in the presented datasets, the first of these factors could not be directly addressed, and warrants further research (Section 7.6).

7.3 Influence of basin physiography

In addition to variations in the type and nature of processes driving flow transformation and development of hybrid flow, this research has also highlighted the influence of basin physiography, and associated flow non-uniformity (spatial flow deceleration), upon the character and distribution of HEBs in deep-water systems (Figs 7.3, 7.4[SS4]). The insights gained from the presented case studies, as discussed in Chapters 3 to 6, are integrated in these figures with those from previous studies (sections 2.6 and 2.10) which also document the character and distribution of HEBs in either unconfined systems (Haughton et al., 2003, 2009; Hodgson, 2009; Kane & Pontén, 2012) or confined, uncontained systems (Barker et al., 2008; Davis et al., 2009; Patacci et al., 2014). Prior to the research presented herein, previous studies of confined, uncontained systems had not considered how the magnitude of

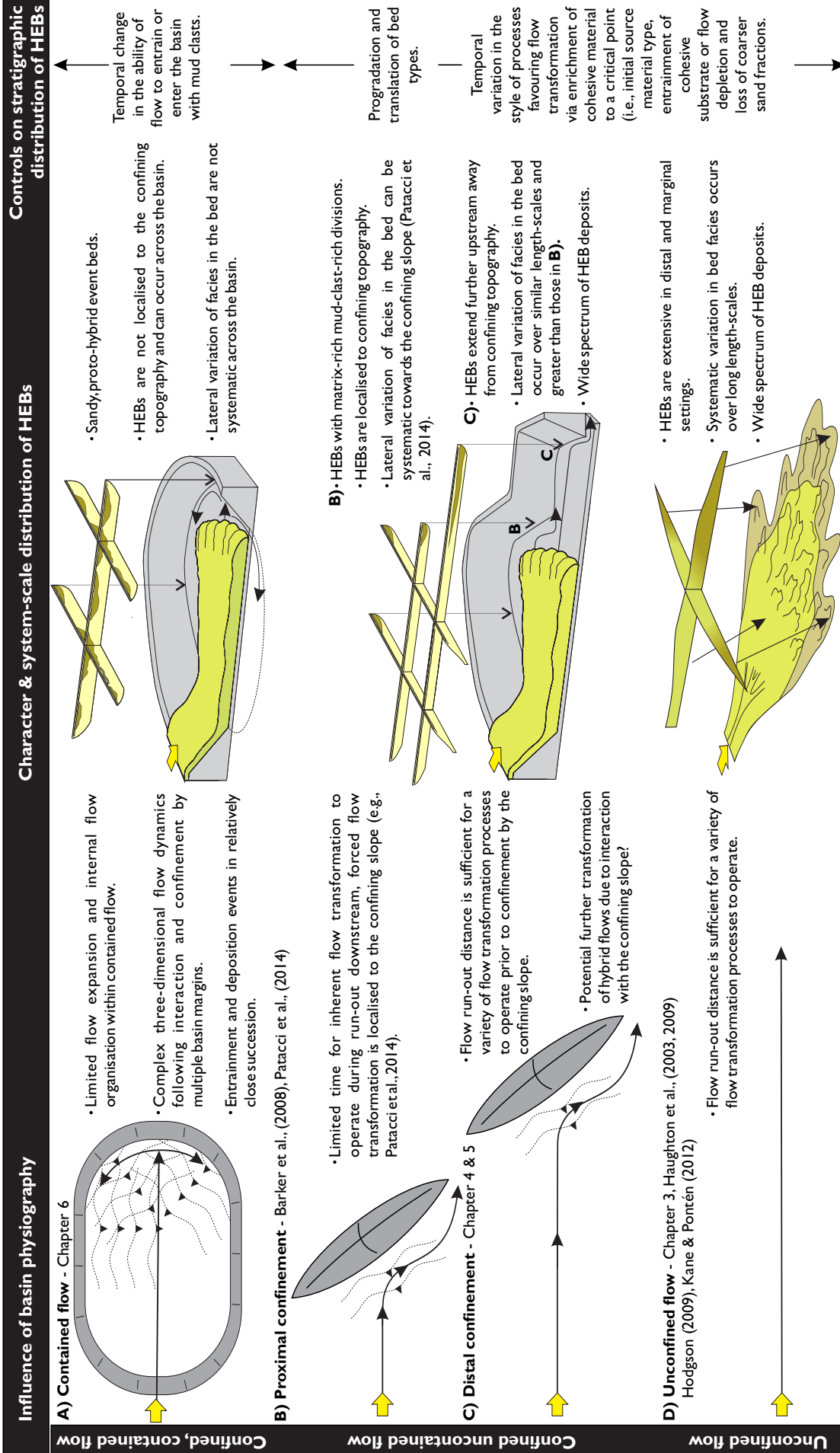


Figure 7.3. Diagram summarising the generic insights gained into the influence of basin physiography upon hybrid event bed occurrence in settings with varying confining topography.

flow run-out distance could influence the character and distribution of HEBs with respect to confining topographic obstacles of the sea-floor (Chapter 4 & 5); nor did studies of HEBs in confined, contained settings such as mini-basins exist (Chapter 6). Thus, figures 7.3 and 7.4 provide a novel framework, constrained by multiple case studies, within which to consider the character and distribution of HEBs in deep-water systems that were variably affected by sea-floor topography.

7.3.1 Influence of the timing of flow confinement

Chapter 4 outlined how the magnitude of flow run-out distance that is achieved prior to flow confinement, and thus the duration over which progressive flow transformation processes can operate, is considered to be an important factor governing the character and distribution of HEBs in confined, uncontained systems (Fig. 7.3b,c; Fig 7.4c,d). Where flows that are prone to becoming hybrid flows are confined in a relatively proximal position along the flow pathway, their flow transformation may have been relatively immature. Thus, confining topography may locally force flow transformation (cf., Barker et al., 2008; Patacci et al., 2014) and result in the development of HEBs in a region that is relatively localised (c.1km, Patacci et al., 2014) to onlap onto the topographic obstacle (Fig. 7.3b). Subsequently, the lateral transitional of a beds depositional character from turbidite to matrix-richer HEB, as well as the progressive thickening of the matrix-rich MCR sandstone within HEBs, towards the point of onlap onto the obstacle occurs over a comparably short length-scale (Fig 7.3b). As the flow run-out distance achieved prior to confinement is increased, or where inherent termination of the flow occurs (Fig 7.3c,d, respectively), flow transformation processes can operate for longer and promote the development of more extensive HEBs with variation from turbidite to HEB also occurring over relatively greater distances. Such HEBs need not be localised to confining topography cf., Barker et al., (2008) and Patacci et al., (2014) and may exhibit distributions more comparable to that documented in unconfined systems (Fig. 7.4d). The character of the flow at the time of confinement, and associated character and distribution of HEBs, are also expected to be influenced by variations in the position at which the flow transformation mechanism was initiated upstream and the rate at which such flow transformation occurs. Such factors are difficult to explore in outcrop and will likely benefit from experimental or numerical studies.

7.3.2 Influence of flow containment

Chapter 6 documents HEBs in a confined, contained system (Castagnola Basin) and further demonstrates how a variation in basin physiography (i.e., one that promotes flow containment) can prevent the development of HEBs which are localised to topographic obstacles cf. Barker et al., (2008) and Patacci et al., (2014). In the presented case study, HEBs were instead extensive across the basin and did not exhibit systematic variation in the presence of thickness

Variations in flow confinement and associated flow non-uniformity upon HEB distribution			Examples
Unconfined settings	Uniform flow	<p>Relatively steady thickness of matrix-rich sandstone facies.</p>	No examples
	Progressive radial spreading	<p>Promotes development of matrix-rich sandstone facies.</p>	Haughton et al., (2003) Kane & Pontén (2012) Cretaceous, Vøring Basin, Norwegian Sea (Chapter 3)
Confined settings (contained or uncontained)	Proximal abrupt forced deceleration	<p>“Proximally” positioned confining counter-slope</p> <p>Promotes localised development of matrix-rich sandstone.</p>	Barker et al., (2008) Patacci et al., (2014)
	Distal abrupt forced deceleration	<p>“Distally” positioned confining counter-slope</p> <p>Matrix-rich sandstone facies are not localised to the confining slope and may pinch-out prior to onlap</p>	Carboniferous, Pennine Basin, N England (Chapter 4 & 5)
	Containment	<p>Sandy HEBs extensive but highly variable across basin infill</p>	Miocene, Castagnola Basin, NW Italy (Chapter 6)
	Accumulative flow	<p>Channel margin / Diapir</p> <p>Thinning / Loss of matrix-rich sandstone. ? = Renewed erosion.</p>	Davis et al., (2009) Talling et al., (2007a)

Figure 7.4. Schematic diagram illustrating the effect of flow confinement and associated flow non-uniformity upon HEB distribution as inferred from the case studies presented in Chapters 3 to 6 and in previous case studies.

of the MCR division with increasing proximity towards their onlap onto the basin margin (Fig. 7.3a). The characteristics of these HEBs are attributed to the influence of flow containment, which is thought to have limited the degree of lateral organisation internally within the flow and thus the re-distribution of recently entrained muddy substrate (Fig. 7.3a). The degree of

lateral organisation within flows, and their subsequent deposits, are thought to be more limited in confined, contained settings compared with confined, uncontained settings due to the following factors: 1) lateral flow expansion is limited by encircling basin margins; 2) muddy-substrate entrainment and deposition of the bed occur in relatively close succession; and 3) multi-directional flow, arising from flow interaction with obstacles on the sea-floor, is expected to be more extensive across the basin (cf. Pantin & Leeder, 1987; Lamb et al., 2004, 2006) and potentially more complex due to interaction at multiple points along encircling basin margins (cf. Bryant & Stiassnie, 1995; Faltinsen et al., 2005).

As discussed in section 7.2.1, the sandstone that supports mud clasts in the MCR division of HEBs from the Castagnola Basin (Fig. 7.1a, Example 1) is visibly cleaner compared with similar facies from larger uncontained systems in which longer flow-run out distances are achieved (Fig. 7.1a, Examples 2-7). Thus, sandy proto-HEBs may be more common in settings where flows that are prone to entraining significant volumes of muddy substrate are also contained relatively soon after by containing basin physiography; such variations could influence how the MCR divisions within these beds acts as a baffle or barrier to fluid flow.

7.3.3 Implications for the stratigraphic distribution of HEBs

Based on sections 7.3.1 and 7.3.2, the range of controls on the stratigraphic distribution of HEBs in deep-water systems is expected to differ, depending on whether: 1) initial HEB deposition was forced by confining topography or not (i.e. proximal vs. distal confinement); 2) whether the systems in confined, uncontained or confined, contained; and 3) temporal variations in the mechanisms promoting flow transformation (Section 5.5.1). In settings where HEB deposition is forced by confining topography (cf. Barker et al., 2008; Patacci et al., 2012) the stratigraphic distribution of HEBs will be influenced by how long such topography remains expressed on the sea floor. Stratigraphic variations in HEB occurrence may be driven by temporal variations in the mechanisms promoting flow transformation (Section 5.5.1). In settings where HEB deposition commences prior to, or in the absence of, confining topography (Fig. 7.3c, d, respectively), the stratigraphic distribution of HEBs can be influenced by progradation and stratigraphic translation of bed types (i.e. Walther's law, Middleton, 1973; Section 3.5.4 and 5.5.1), as well as temporal variations in the mechanisms promoting flow transformation (Section 5.5.1). In contained settings dominated by system-aggradation rather than progradation, the stratigraphic distribution of HEBs may simply reflect temporal variations in the ability of successive flows to entrain, or enter the basin with mud clasts.

7.4 Applications to the hydrocarbon industry – reservoir quality and prediction

As wells are drilled in greater water depths, they are increasingly likely to encounter the distal and marginal regions of deep-water systems (e.g. Boswell et al., 2012). Thus, HEBs are likely to form an increasing proportion of the reservoir volume in future deep-water hydrocarbon prospects. Furthermore, it is known that HEBs may constitute an important component of successions which onlap confining topography (Barker et al., 2008; Patacci et al., 2014; Chapters 4, 6); the potential for stratigraphic traps associated with such settings make them attractive hydrocarbon prospects. As such, the insights gained from the presented case studies have an applied significance to the hydrocarbon industry, as discussed below:

- HEBs are not always localised in narrow regions (~1 km wide) adjacent to onlap of confining topography, as documented in previous studies (Barker et al., 2008, Patacci et al., 2014). Instead, they may be relatively extensive (>6 km) upstream of where confinement and onlap occurs. As such, their presence does not necessarily indicate proximity to confining topography; downstream variation from turbidites (dominated by matrix-poor sandstone) to HEB (dominated by more matrix-rich sandstone) may occur over relatively longer length-scales (Fig. 7.3).
- The flow run-out distance achieved, and thus duration over which processes promoting flows that emplace HEBs operate, is inferred to affect the distribution of HEBs with respect to confining topography. Slope-localised occurrences are thought to be preferentially associated with confining slopes encountered relatively early along the flow run-out pathway. In addition, variation in the relative position at which flow transformation processes were initiated and the rate at which they operate within the flow are also likely to influence the degree of flow transformation, and the extent of HEB development in relation to confining topography. Thus, later onset of transformation and slower rates of transformation are both likely to be associated with slope-localised patterns of HEB occurrence.
- Small systems developed in confined, contained settings can develop sandy HEBs with thick MCR divisions. The MCR division is not necessarily localised to the downstream confining slope, it can be extensive across the basin and exhibit significant variation in thickness which is not systematic with respect to palaeoflow direction or proximity to confining topography. Such deposits may be a significant component of basin infill. The presence of thick MCR divisions will influence hydrocarbon fluid-flow and estimates of in-place reserves in contained basins, which are often targets due to the thick accumulations of sand that can occur there (e.g. mini-basins, Gulf of Mexico).

- Although permeability is significantly reduced in matrix-rich sandstone, significant reservoir quality can remain in the form of micro-porosity; Figs 3.7, 3.8). Thus, prospects with high proportions of HEBs may perform significantly better as gas, rather than as oil reservoirs (compared to turbidite reservoirs), and may benefit from the use of hydraulic fracturing techniques.
- Existing reservoir models investigating the influence of HEBs on hydrocarbon-fluid flow (e.g. Amy et al., 2009) should be expanded to incorporate the recognised spectrum in HEB depositional character, as documented both in the presented case studies (Fig. 7.1), and in the wider literature. In particular, the potential variation of facies in the lower portion of beds, as highlighted by this research (Fig. 7.1a, Examples 2, 4, 5, 6), and thus associated reservoir quality, should be considered given that the greatest porosity and permeability values are generally found in the lower half of HEBs (Figs 3.7, 3.8; Sylvester & Lowe, 2004; Amy et al., 2009).
- The documented range of HEB deposit character, and the inferred spectrum of associated HEB flow types, suggests variations may occur in the flow run-out distance achieved, and thus the size and shape of the depositional elements they construct. As such, differences in system size, geometry, and distributions and proportions of reservoir quality are expected occur between those dominated by turbidites or by particular styles of HEB; current understanding of such potential variation is remains limited.
- Misinterpretation of deposits with a pseudo-HEB character as those deposited from flows characterised by complex rheological heterogeneity, has implications for the prediction of facies and reservoir quality distribution away from one-dimensional core data. Rare examples in the Pennine Basin suggest that a number of characteristics associated with the sandstone facies in the upper part of such deposits can be used to determine where substrate modification (*sensu* Butler & Tavarnelli 2006) has resulted in HEB-like deposits (Figs 4.19, 4.20).
- Further research into the range of boundary conditions that can promote turbulence-suppression and flow transformation (see section 7.6) will significantly benefit predictive concepts for HEB character and distribution in deep-water systems.

7.5 Main conclusions

The principal conclusions of this research are as follows:

- 1) The wide range in documented HEB depositional character, and inferred flow evolution, highlights the dynamic and complex nature of processes occurring within flows that emplace HEBs; further, it suggests that a wide range in boundary conditions influences these flows.
- 2) Discrete styles of flow transformation can modify distinct regions of the flow during overall large-scale flow transformation during downstream run-out. During a flow event, rearward regions of near-bed flow became increasingly cohesive (clay-rich) and turbulence-suppressed during run-out, and resulted in the deposition of matrix-rich unstratified sandstone in the upper part of beds. During the same flow event, headward regions of near-bed flow may undergo downstream transformation from high-concentration, turbulence-suppressed, and non-cohesive flow to low-concentration, turbulent and non-cohesive flow depositing matrix-poor unstratified and stratified sandstone facies, respectively, in the lower part of beds. Thus, variation in the depositional character of lower sandstone facies, and inferred character of earliest depositing flow (the frontal part of the flow, in the absence of significant bypass), is greater than currently suggested in the literature. Early depositing flow may consist of: 1) non-cohesive, high-concentration and non-turbulent flow (emplacing matrix-poor non-stratified sandstone); 2) non-cohesive, low-concentration and turbulent flow (emplacing matrix-poor stratified sandstone); 3) relatively cohesive, turbulence-suppressed flow (emplacing matrix-rich non-stratified sandstone) or 4) relatively cohesive, turbulence-enhanced flow (emplacing banded sandstone), potentially occurring as a near-bed zone beneath more turbulence-suppressed flow as described prior in 3. Further, variations in the evolution of frontal flow during run-out, will influence the variation of facies present in the lower part of HEBs, and are expected to be influenced by a range of boundary conditions (see section 7.6).
- 3) Confinement exerts variable influence upon HEB character and distribution depending on the flow run-out distance and the degree of flow transformation achieved prior to slope interaction. Confinement of flows at relatively proximal positions along the flow run-out pathway are thought to result in a more slope-localised occurrence of HEBs with variation from turbidite (dominated by matrix-poor sandstone) to HEB (dominated by matrix-rich sandstone) occurring over similarly short length-scales. The degree of flow transformation, and thus HEB distribution, is also expected to vary depending on the relative position at which flow transformation processes were initiated, and the rate at which they operate, with earlier-occurring or faster rates of

flow transformation resulting in HEBs that are more extensive away from downstream confining topography.

- 4) In confined settings HEBs, are not always localised and genetically linked to the confining topography as has been documented in previous studies.
- 5) The physiography of a containing basin, and subsequent flow containment, are additional factors to consider when investigating the character and distribution of HEBs in deep-water systems affected by sea-floor topography. The limited flow expansion and run-out distance in contained systems can result in the emplacement of relatively sandy HEBs with thick MCR divisions, where flows are prone to entrain significant muddy substrate. Further, these deposits are extensively distributed across the basin, and exhibit non-systematic variation in their depositional character with respect to their proximity to a downstream confining counter slope; such observations differ to those made in previous studies of HEB character and distribution in confined, but uncontained, deep-water systems.

7.6 Future work

This research has highlighted a number of lines of research for future pursuit.

A crucial strand of future research should focus on the types and distributions of cohesive material that can influence gravity flow dynamics. For example, although the effect of clay upon gravity flow dynamics has been investigated in a number of studies (Coussot, 1997; Marr et al., 2001; Baas and Best, 2002; Baas et al., 2009, 2011; Sumner et al., 2009), the potential influence of cohesive biogenic material upon gravity flow dynamics is only recently being realised (Malarkey et al., 2015). This may be significant as organisms have long been known to influence both the composition and stability of sea-floor substrate (Rhoads & Young, 1970). Furthermore, the consolidation of substrate on the sea floor may differ depending on local gradients or the recurrence time of erosive gravity flows, and thus the potential for unconsolidated muddy substrates to accumulate. The character of cohesive material(s) may determine its impact once incorporated into a sediment gravity flow, in terms of its preferential distribution in the flow, the rate at which it achieves this distribution, its potential cohesive-strength and thus where and when turbulence-suppression and flow transformation occurs in a gravity flow. Research concerning how cohesive material types and blends vary geographically (i.e. with water depth and latitude), or temporally (as ocean dynamics and biota change) may be expected to account for some of the variation observed in HEBs, and inferred flow character. It is difficult to entrain a cohesive bed beneath experimental particulate gravity flows, however in future experiments, different types of cohesive material could be injected into the near-bed flow region in a range of different flow types (i.e. turbulent and variably

transitional flow), in order to explore its influence on flow and behaviour. These different flow types could be used to infer the evolution of discrete rheological zones that develop during downstream run-out. Further research into the influence of a range of cohesive material upon flow behaviour may help to account for the variable occurrence of HEBs in deep-water systems. The lack of evidence for intra-bed flow processes (*sensu* Baas et al., 2014) in the presented case studies, suggest that many flows entrain or override their substrate. Thus, entrainment of substrate may not be the sole requirement for the deposition of HEB as HEBs are not present in all systems despite many flows and deposits showing evidence for substrate entrainment. This hints at the influence of other controlling factors such as variations in the composition of cohesive material, or variations in the timing of entrainment versus the flow character at the time of entrainment.

Further research should also consider the range of mechanisms by which cohesive material is entrained into gravity flows, and how this varies with flow character (i.e. concentration and rheology). Substrate entrainment may occur via turbulent scouring beneath relatively turbulent flow, or due to the pressure gradient associated with the passing of a range of gravity flows (Eggenhuisen et al., 2010). As such, the rate or total volume of entrained material, and subsequent downstream flow evolution, may vary depending on the mechanism; individual mechanisms may be variably limited by flow capacity (*sensu* Hiscott 1994a), and flow type (i.e. turbulent or laminar). An understanding of such mechanisms could be expected to reveal the full spectrum of documented HEB depositional character and variations in styles of downstream flow transformation.

A major challenge to experimental studies is effectively simulating the longitudinal structure (i.e. concentration, grain size, composition and associated rheology) of variably clay-rich flows, and its spatio-temporal evolution during downstream flow run-out. In order to achieve this, future experiment-based analyses should use methods *sensu* McCaffrey et al. (2003) and Baas et al., (2005), or non-intrusive monitoring approaches (Tilston et al., 2014) in longer experimental tanks. If achieved, such work should advance our ability to address questions regarding the following:

- 1) the spatio-temporal evolution of longitudinal and vertical flow structures within variably clay-rich flows;
- 2) the long-term behaviour and influence of a range of cohesive materials within a range of gravity flow types;
- 3) the response of variably clay-rich flow types in terms of downstream flow transformation to a range of boundary conditions (i.e. total volume, relative timing and

rates of flow enrichment with cohesive material, magnitude, relative timing and rate of flow depletion);

- 4) the response of variably clay-rich flows to flow non-uniformity associated with confining topography; such investigation would address the uncertainty described in Chapter 4 as to if, and how, hybrid flows undergo further flow transformation upon confinement by topography;
- 5) the current disparity between flow process associated with conceptual hybrid flow models (Haughton et al., 2003, 2009), and those suggested from experimental clay-rich transitional flows (Baas et al., 2009, 2011; Sumner et al., 2009); it seems likely that both may simultaneously occur within single gravity flow events.

In the absence of flume tanks of sufficient length which permit the development and evolution of longitudinal flow structure, experiments could simulate the response to confining topography of hybrid flows characterised by pronounced longitudinal rheological heterogeneity by conducting separate runs with distinct flow character, considered analogous to the rheological divisions associated with hybrid flow. Such investigations could reveal the potential range of facies proportions, and deposit geometries, that can occur where HEBs onlap and pinch-out onto confining topography. Numerical modelling of variably clay-rich sediment gravity flows is in its relative infancy and is expected to offer insight into the complex relationships between parameters associated with these flow types where laboratory experimental set-ups may be limited.

Reference list

- Aitkenhead, N.** (2002) British Regional Geology: the Pennines and adjacent areas. British Geological Survey.
- Al Ja'Aidi, O.S., McCaffrey, W.D. & Kneller, B.C.** (2004) Factors influencing the deposit geometry of experimental turbidity currents: implications for sand-body architecture in confined basins. *Geological Society of London, Special Publications*, **222**, 45-58.
- Alexander, J. & Morris, S.** (1994) Observations on Experimental, Non channelized High-Concentration Turbidity Currents and Variations in Deposits around Obstacles. *Journal of Sedimentary Research*, **64**, 899-909.
- Allen, J.R.L.** (1960) The Mam Tor Sandstones: a turbidite facies of the Namurian deltas of Derbyshire, England. *Journal of Sedimentary Research*, **30**, 193-208.
- Allen, J.R.L.** (1970) Physical processes of sedimentation. George Allen & Unwin Ltd, London. 248pp.
- Allen, J.R.L.** (1984a) Parallel lamination developed from upper-strage plane beds: a model based on the larger coherent structures of the turbulent boundary layer. *Sedimentary Geology*, **39**, 227-242.
- Allen, J.R.L.** (1985) Principles of Physical Sedimentology. George Allen & Unwin Ltd, London. 272pp.
- Allen, J.R.L.** (1991) The Bouma A division and the possible duration of turbidity currents. *Journal of Sedimentary Research*, **61**, 291-295.
- Altinaker, M.S., Graf, W.H. & Hopfinger, E.J.** (1996) Flow structure in turbidity currents. *Journal of Hydraulic Research*, **34**, 713-718.
- Amy, L.A. & Talling, P.J.** (2006) Anatomy of turbidites and linked debrites based on long distance (120 x 30 km) bed correlation, Marnoso Arenacea Formation, Northern Apennines, Italy. *Sedimentology*, **53**, 161-212.
- Amy, L.A., McCaffrey, W.D. & Kneller, B.C.** (2004) The influence of a lateral basin-slope on the depositional patterns of natural and experimental turbidity currents. In: *Deep-Water Sedimentation in the Alpine Basin of SE France* (Eds. P. Joseph & A. Lomas). *Geological Society of London, Special Publications*, **221**, 311-330.
- Amy, L.A., Peachey, S.A., Gardiner, A.A. & Talling, P.J.** (2009) Prediction of hydrocarbon recovery from turbidite sandstones with linked-debrite facies: Numerical flow-simulation studies. *Marine and Petroleum Geology*, **26**, 2032-2043.
- Andreoni, G., Galbiati, B., Maccabruni, A. & Vercesi, P.L.** (1981) Stratigrafia e paleogeografia dei depositi oligocenici sup. – miocenici inf. nell'estremità orientale del bacino ligure-piemontese. *Rivista Italiana di Paleontologia e Stratigrafia*, **87**, 245-282.
- Arnott, R.W.C. & Hand, B.M.** (1989) Bedforms, primary structures and grain fabric in the presence of suspended sediment rain. *Journal of Sedimentary Research*, **59**, 1062-1069.
- Baas, J.H.** (2002) EZ-ROSE: a computer program for equal-area circular histograms and statistical analysis of two-dimensional vectorial data. *Computer & Geosciences*, **26**, 153-166.

- Baas, J.H. & Best, J.L.** (2002) Turbulence modulation in clay-rich sediment-laden flows and some implications for sediment deposition. *Journal of Sedimentary Research*, **72**, 336-340.
- Baas, J.H. & Best, J.L.** (2008) The dynamics of turbulent, transitional and laminar clay-laden flow over a fixed current ripple. *Sedimentology*, **55**, 635-666.
- Baas, J.H., Best, J.L. & Peakall, J.** (2011) Depositional processes, bed form development and hybrid bed formation in rapidly decelerated cohesive (mud-sand) sediment flows. *Sedimentology*, **58**, 1953-1987.
- Baas, J.H., Best, J.L., Peakall, J. & Wang, M.** (2009) A phase diagram for turbulent, transitional and laminar clay suspension flows. *Journal of Sedimentary Research*, **79**, 162-183.
- Baas, J.H., Hailwood, E.A., McCaffrey, W.D., Kay, M. & Jones, R.** (2007) Directional petrological characterisation of deep-marine sandstones using grain fabric and permeability anisotropy: methodologies, theory, application and suggestions for integration. *Earth Science Reviews*, **82**, 101-142.
- Baas, J.H., Manica, R., Puhl, E., Verhagen, I. & O.Borges, A.L.** (2014) Processes and products of turbidity currents entering soft muddy substrates. *Geology*, **42**, 371-374.
- Baas, J.H., McCaffrey, W.D., Haughton, P.D.W. & Choux, C.** (2005) Coupling between suspended sediment distribution and turbulence structure in a laboratory turbidity current. *Journal of Geophysical Research, Oceans*, **110**, 1-22.
- Bagnold, R.A.** (1962) Auto-suspension of transported sediment; turbidity currents. *Proceedings of the Royal Society of London, Series A, Mathematical and Physical Sciences*, 315-319.
- Bagnold, R.A.** (1966) An approach to the sediment transport problem from general physics. *The Physics of Sediment Transport by Wind and Water: A Collection of Hallmark Papers by R.A. Bagnold*, 231-291.
- Barker, S.P., Haughton, P.D.W., McCaffrey, W.D., Archer, S.G. & Hakes, B.** (2008) Development of rheological heterogeneity in clay-rich high-density turbidity currents: Aptian Britannia Sandstone Member, UK continental shelf. *Journal of Sedimentary Research*, **78**, 45-68.
- Baruffini, L., Cavalli, C. & Papani, L.** (1994) Detailed stratal correlation and stacking patterns of the Gremiasco and lower Castagnola turbidite systems, Tertiary Piedmont Basin, northwestern Italy. In: *15th Annual Research Conference Submarine Fans and Turbidite Systems* (Eds. P. Weimer, A.H. Bouma & B.F. Perkins). *Society of Economic Palaeontologists and Mineralogists, Gulf Coast Section*, 9-21.
- Beard, D.C. & Weyl, P.K.** (1973) Influence of texture on porosity and permeability of unconsolidated sand. *American Association of Petroleum Geologists Bulletin*, **57**, 349-369.
- Beaubouef, R.T., Abreu, V. & Van Wagoner, J.C.** (2003) Basin 4 of the Brazos-Trinity slope system, western Gulf of Mexico: The terminal portion of a late Pleistocene lowstand systems tract. In: *Shelf margin deltas and linked down slope petroleum systems: Global significance and future exploration potential* (Eds. H.R. Roberts, N.C. Rosen, R.F. Fillon & J.B. Anderson). *Proceedings of the 23rd Annual Research Conference, Gulf Coast Section Society of Economic Palaeontologists and Mineralogists Foundation*, 45-66.

- Bersezio R., Felletti, F., Riva R. & Micucci L.** (2009) Bed thickness and facies trends of turbiditic sandstone bodies: Unravelling the effects of basin confinement, depositional processes and modes of sediment supply. In: *External Controls on Deep-Water Depositional Systems* (Eds. B. Kneller, O.J. Martinsen & B. McCaffrey). *Society of Economic Palaeontologists and Mineralogists Special Publication*, **92**, 303-321.
- Best, J. & Bridge, J.** (1992) The morphology and dynamics of low amplitude bed-waves upon upper stage plane beds and the preservation of planar laminae. *Sedimentology*, **39**, 737-752.
- Biella, G.C., Clari, P., De Franco, R., Gelati, R., Ghibaudo, G., Gnaccolini, M., Lanza, R., Polino, R., Ricci, B. & Rossi, P.M.** (1992) Geometrie crostali al nodo Alpi/Appennino: conseguenze sull'evoluzione cinematica dei bacini neogenici. 76 Congresso Societa. Geologica. Italian., Abstracts, 192-195.
- Blackbourn, G.A. & Thomson, M.E.** (2000) Britannia Field, UK North Sea: petrographic constraints on Lower Cretaceous provenance, facies and the origin of slurry-flow deposits. *Petroleum Geoscience*, **6**, 329-343.
- Boswell, R., Frye, M., Shelander, D., Shedd, W., McConnel, D.R. & Cook, A.** (2012) Architecture of gas-hydrate-bearing sands from Walker Ridge 313, Green Canyon 995 and Alaminos Canyon, 21: Northern dewater Gulf of Mexico. *Marine and Petroleum Geology*, **34**, 134-149.
- Bouma, A.H.** (1962) *Sedimentology of Some Flysch Deposits: A Graphic Approach to Facies Interpretations*. Elsevier, Amsterdam, 168 pp.
- Bradley, D. & Hanson, L.** (1998) Paleoslope analysis of slump folds in the Devonian flysch of Maine. *Journal of Geology*, **106**, 305-318.
- Branney, M.J. & Kokelaar, B.P.** (2002) Pyroclastic density currents and the sedimentation of ignimbrites. *Geological Society of London Memoirs*, **27**, 143 pp.
- Bridgwater, J.** (1976) Fundamental powder mixing mechanisms. *Powder Technology*, **15**, 215-236.
- Bristow, C.S.** (1993) Sedimentology of the Rough Rock: a Carboniferous braided river sheet sandstone in northern England. *Geological Society of London, Special Publications*, **75**, 291-304.
- Brunt, R.L., McCaffrey, W.D. & Kneller, B.C.** (2004) Experimental modelling of the spatial distribution of grain size developed in a fill-and-spill mini-basin setting. *Journal of Sedimentary Research*, **74**, 438-446.
- Bryant, P.J. & Stiassnie, M.** (1995) Water waves in a deep square basin. *Journal of Fluid Mechanics*, **302**, 65-90.
- Buckee, C., Kneller, B. & Peakall, J.** (2001) Turbulence structure in steady solute-driven gravity currents. In: *Particulate Gravity Currents* (Eds. W.D. McCaffrey, B. Kneller & J. Peakall). *Special Publication of the International Association of Sedimentologists*, **31**, 173-188.
- Butler, R.W.H. & Tavarnelli, E.** (2006) The structure and kinematics of substrate entrainment into high-concentration sandy turbidites: a field example from the Gorgoglione 'flysch' of southern Italy. *Sedimentology*, **53**, 655-670.

- Carter, R.M.** (1975) A discussion and classification of subaqueous mass-transport with particular application to grain-flow, slurry-flow and fluxoturbidites. *Earth Science Reviews*, **11**, 145-177.
- Cavanna, F., Di Giulio, A., Galbiati, B., Mosna, S., Perotti, C.R. & Pieri, M.** (1989) Carta geologica dell'estremità orientale del Bacino Terziario Ligure Piemontese. *Atti Ticinensi di Scienze della Terra*, **32**.
- Choux, C.M. & Druitt, T.H.** (2002) Analogue study of particle segregation in pyroclastic density currents, with implications for the emplacement mechanisms of large ignimbrites. *Sedimentology*, **49**, 907-928.
- Choux, C.M., Baas, J.H., McCaffrey, W.D. & Haughton, P.D.W.** (2005) Comparison of spatio-temporal evolution of experimental particulate gravity flows at two different initial concentrations, based on velocity, grain size and density data. *Sedimentary Geology* **179**, 49-69.
- Choux, C.M., Druitt, T.H. & Thomas, N.** (2004) Stratification and particle segregation in flowing polydisperse suspensions, with applications to the transport and sedimentation of pyroclastic density currents. *Journal of Volcanology and Geothermal Research*, **138**, 223-241.
- Clark, I.R. & Cartwright, J.A.** (2009) Interactions between submarine channel systems and deformation in deep-water fold belts: examples from the Levant Basin, Eastern Mediterranean sea. *Marine and Petroleum Geology*, **26**, 1465-1482.
- Clark, J.D. & Pickering, K.T.** (1996) *Submarine Channels: Process and Architecture*. Vallis Press, London, 231 pp.
- Collinson, J.D.** (1968) Deltaic sedimentation units in the Upper Carboniferous of northern England. *Sedimentology*, **10**, 233-254.
- Collinson, J.D.** (1969) The sedimentology of the Grindslow Shales and the Kinderscout Grit: a deltaic complex in the Namurian of northern England. *Journal of Sedimentary Research*, **39**, 194-221.
- Collinson, J.D.** (1970) Deep channels, massive beds and turbidity current genesis in the Central Pennine Basin. *Proceeding of the Yorkshire Geological Society*, **37**, 495-519.
- Collinson, J.D.** (1988) Controls on Namurian sedimentation in Central Province Basin of northern England. In: *Sedimentation in a Synorogenic Basin Complex: the Upper Carboniferous of Northwestern Europe* (Eds. B.B. Besley & G. Kelling). Blackie, Glasgow, 85-101.
- Coussot, P.** (1997) Mudflow rheology and dynamics: Delft Hydraulics, *International Association for Hydraulic Research Monograph*, 270 pp.
- Davies, C.** (2012) Investigation into the origin and significance of hybrid event beds in mixed sand-mud deep-sea fan systems. Unpublished PhD Thesis, University Of Leeds, 323 pp.
- Davis, C., Haughton, P.D.W., McCaffrey, W.D., Scott, E., Hogg, N. & Kitching, D.** (2009) Character and distribution of hybrid sediment gravity flow deposits from the outer Forties Fan, Palaeocene Central North Sea, UKCS. *Marine and Petroleum Geology*, **26**, 1919-1939.
- Davies, R.** (1968) The experimental study of the differential settling of particles in suspension at high concentrations. *Powder Technology*, **2**, 43-51.

- Davies, S.J.** (2008) The record of Carboniferous sea-level change in low-latitude sedimentary successions from Britain and Ireland during the onset of the late Paleozoic ice age. *Geological Society of America Special Papers*, **441**, 187-204.
- Debacker, T.N., Dumon, M. & Matthys, A.** (2009) Interpreting fold and fault geometries from within the lateral to oblique parts of slumps; a case study from the Anglo-Brabant Deformation Belt (Belgium). *Journal of Structural Geology*, **31**, 1525-1539.
- Del Pino Sanchez, A.** (2006) The kinematic significance of small-scale remobilisation fabrics in deep-water sediments: implications for facies architecture in slope-adjacent settings. Unpublished PhD Thesis, University Of Leeds, 251 pp.
- Di Giulio, A. & Galbiati, B.** (1993) Escursione nell'estremità orientale del Bacino Terziario Piemontese. Interazione tettonica-eustatismo nella sedimentazione di un bacino tardo-post orogenico. 3 Convegno del Gruppo Informale di Sedimentologia del CNR.
- Dorrell, R.M., Darby, S.E., Peakall, J., Sumner, E.J., Parsons, D.R. & Wynn, R.B.** (2013) Super elevation and overspill control secondary flow dynamics in submarine channels. *Journal of Geophysical Research*, **118**, 3895-3915.
- Druitt, T.H.** (1995) Settling behaviour of concentrated dispersions and some volcanological applications. *Journal of Volcanology and Geothermal Research*, **65**, 27-39.
- Druitt, T.H.** (1998) Pyroclastic density currents. In: *The Physics of Explosive Volcanic Eruptions* (Eds. J.S. Gilbert & R.S.J. Sparks). *Geological Society of London Special Publications*, **145**, 145-182.
- Dzulynski, S. & Sanders, J.E.** (1962) Current marks on firm mud bottoms. *Transactions Of The Connecticut Academy Of Arts And Sciences*, **42**, 58-96.
- Edwards, D.A., Leeder, M.R., Best, J.L. & Pantin, H.M.** (1994) On experimental reflected density currents and the interpretation of certain turbidites. *Sedimentology*, **41**, 437-461.
- Eggenhuisen, J.T., McCaffrey, W.D., Houghton, P.D. & Butler, R.W.H.** (2010) Small-scale spatial variability in turbidity-current flow controlled by roughness resulting from substrate erosion; field evidence for a feedback mechanism. *Sedimentology*, **80**, 129-136.
- Eggenhuisen, J.T., McCaffrey, W.D., Houghton, P.D. & Butler, R.W.H.** (2011) Shallow erosion beneath turbidity currents and its impact on the architectural development of turbidite sheet systems. *Sedimentology*, **58**, 936-959.
- Ehrenberg, S.N.** (1997) Influence of depositional sand quality and diagenesis on porosity and permeability: examples from Brent Group reservoirs, northern North Sea. *Journal of Sedimentary Research*, **67**, 197-211.
- Einsele, G., Chough, S.K. & Shiki, T.** (1996) Depositional events and their records - an introduction. *Sedimentary Geology*, **104**, 1-9.
- Elmore, R.D., Pilkey, O.H., Clearey, W.J. & Curran, H.A.** (1979) The Black Shale turbidites, Hatteras Abyssal Plain, western Atlantic Ocean. *Geological Society of America Bulletin*, **90**, 1165-1176.

- Embley, R.W.** (1976) New evidence for the occurrence of debris flow deposits in the deep sea. *Geology*, **4**, 371-374.
- Færseth, R. & Lien, T.** (2002) Cretaceous evolution in the Norwegian Sea – a period characterised by tectonic quiescence. *Marine and Petroleum Geology*, **19**, 1005-1027.
- Faltinsen, O.M., Rognebakke, O.F. & Timokha, A.N.** (2005) Classification of three-dimensional nonlinear sloshing in a square-base tank with finite depth. *Journal of Fluids and Structures*, **20**, 81-103.
- Felletti, F.** (2002) Complex bedding geometries and facies associations of the turbiditic fill of a confined basin in a transpressive setting (Castagnola Fm., Tertiary Piedmont Basin, NW Italy). *Sedimentology*, **49**, 645-667.
- Felletti, F.** (2004a) Statistical modelling and validation of correlation in turbidites: an example from the Tertiary Piedmont Basin (Castagnola Fm., Northern Italy). *Marine and Petroleum Geology*, **21**, 23-39.
- Felletti, F.** (2004b) Spatial variability of Hurst statistics in the Castagnola Formation, Tertiary Piedmont Basin, NW Italy: discrimination of sub-environments in a confined turbidite system. *Geological Society of London Special Publications*, **222**, 285-305.
- Felletti F. & Bersezio R.** (2010) Quantification of the degree of confinement of a turbidite-filled basin: a statistical approach based on bed thickness distribution. *Marine and Petroleum Geology*, **27**, 515–532.
- Figueiredo, J.J., Hodgson, D.M., Flint, S.S. & Kavanagh, J.P.** (2013) Architecture of a channel complex formed and filled during long-term degradation and entrenchment on the upper submarine slope, Unit F, Fort Brown Fm., SW Karoo Basin, South Africa. *Marine and Petroleum Geology*, **41**, 104-116.
- Fisher, R.V.** (1983) Flow transformations in sediment gravity flows. *Geology*, **11**, 273-274.
- Fisher, R.V.** (1990) Transport and deposition of a pyroclastic surge across an area of high relief: the 18 May 1980 eruption of Mount St. Helens, Washington. *Geological Society of America Bulletin*, **102**, 1038-1054.
- Flemings, P.B., Behrmann, J.H. & John, C.M.** (2006) Gulf of Mexico Hydrogeology. *Proceedings of the International Ocean Drilling Program*, **308**, College Station, Texas, USA.
- Folk, R.L. & Ward, W.C.** (1957) Brazos River bar: a study in the significance of grain size parameters. *Journal of Sedimentary Research*, **21**, 3-26.
- Fonneland, H.C., Lien, T., Martinsen, O. J., Pedersen, R.B. & Kosler, J.** (2004) Detrital zircon ages: a key to understanding deposition of deep marine sandstones in the Norwegian Sea. *Sedimentary Geology*, **164**, 147-159.
- Fonnesu, M., Haughton, P., Felletti, F. & McCaffrey, W.D.** (2015) Short-length scale variability of hybrid event beds and its applied significance. *Marine & Petroleum Geology*.

- Fraser, A.J. & Gawthorpe, R.L.** (2003) An atlas of Carboniferous basin evolution in Northern England. *Geological Society of London, Memoirs*, **28**, 79 pp.
- Garcia, M.H.** (1993) Hydraulic jumps in sediment-driven bottom currents. *Journal of Hydraulic Engineering*, **119**, 1094-1117.
- Garcia, M.** (1994) Depositional Turbidity Currents Laden with Poorly Sorted Sediment. *Journal of Hydraulic Engineering*, **120**, 1240-1263.
- Garcia, M. & Parker, G.** (1993) Experiments on the entrainment of sediment into suspension by dense bottom current. *Journal of Geophysical Research*, **98**, 4793-4807.
- Gardner, M.H., Borer, J.M., Melick, J.J., Mavilla, N., Dechesne, M. & Wagerle, R.N.** (2003) Stratigraphic process-response model for submarine channels and related features from studies of Permian Brushy Canyon outcrops, West Texas. *Marine and Petroleum Geology*, **20**, 757-787.
- Gee, M.J.R. & Gawthorpe, R.L.** (2006) Submarine channels controlled by salt tectonics: examples from 3D seismic data offshore Angola. *Marine and Petroleum Geology*, **23**, 443-458.
- Giles, K.A. & Lawton, T.F.** (2002) Halokinetic sequence stratigraphy adjacent to the El Papalote diapir, northeastern Mexico. *American Association of Petroleum Geologists Bulletin*, **86**, 823-840.
- Gilligan, A.** (1920) The petrography of the Millstone Grit of Yorkshire. *Geological Society of London Quarterly Journal*, **75**, 251-294.
- Gladstone, C., Phillips, J.C. & Sparks, R.S.J.** (1998) Experiments on bidisperse, constant-volume gravity currents: propagation and sediment deposition. *Sedimentology*, **4**, 833-844.
- Grando, G. & McClay, K.** (2004) Structural evolution of the Frampton growth fold system, Atwater Valley-Southern Green Canyon area, deep water Gulf of Mexico. *Marine and Petroleum Geology*, **21**, 889-910.
- Gray, J. & Chugunov, V.A.** (2006) Particle-size segregation and diffusive remixing in shallow granular avalanches. *Journal of Fluid Mechanics*, **569**, 365-398.
- Gutteridge, P.** (1991) Aspects of Dinantian sedimentation in the Edale Basin, north Derbyshire. *Geological Journal*, **26**, 245-269.
- Hallsworth, C.R., Morton, A.C., Claoué-Long, J. & Fanning, C.M.** (2000) Carboniferous sand provenance in the Pennine Basin, UK: constraints from heavy mineral and detrital zircon age data. *Sedimentary Geology*, **137**, 147-185.
- Hampson, G.J.** (1997) A sequence stratigraphic model for deposition of the Lower Kinderscout Delta, an Upper Carboniferous turbidite-fronted delta. *Proceedings of the Yorkshire Geological Society*, **51**, 273-296.
- Hampson, G.J., Davies, S.J., Elliott, T., Flint, S.S. & Stollhofen, H.** (1999) Incised valley fill sandstone bodies in Upper Carboniferous fluvio-deltaic strata: recognition and reservoir characterization of Southern North Sea analogues. *Geological Society of London, Petroleum Geology Conference Series*, **5**, 771-788.

- Hampton, M.A.** (1972) The role of subaqueous debris flow in generating turbidity currents. *Journal of Sedimentary Research*, **42**, 775-793.
- Hampton, M.A.** (1975) Competence of fine-grained debris flows. *Journal of Sedimentary Petrology*, **45**, 834-844.
- Hand, B.M.** (1997) Inverse grading resulting from coarse-sediment transport lag. *Journal of Sedimentary Research*, **67**, 124-129.
- Haughton, P.D.W.** (1994) Deposits of Deflected and Pondered Turbidity Currents, Sorbas Basin, Southeast Spain. *Journal of Sedimentary Research*, **64**, 233-246.
- Haughton, P.D.W.** (2001) Contained turbidites used to track sea bed deformation and basin migration, Sorbas Basin, south-east Spain. *Basin Research*, **13**, 117-139.
- Haughton, P.D.W., Barker, S.P. & McCaffrey, W.D.** (2003) 'Linked' debrites in sand-rich turbidite systems - origin and significance. *Sedimentology*, **50**, 459-482.
- Haughton, P.D.W., Davis, C., McCaffrey, W.D. & Barker, S.** (2009) Hybrid sediment gravity flow deposits - Classification, origin and significance. *Marine and Petroleum Geology*, **26**, 1900-1918.
- Haughton, P.D.W., Davis, C., McCaffrey, W.D. & Barker, S.** (2010) Reply to Comment by R. Higgs on "Hybrid sediment gravity flows – classification, origin and significance. *Marine and Petroleum Geology*, **27**, 2066-2069.
- Heald, M.T. & Larese, R.E.** (1974) Influence of coatings on quartz cementation. *Journal of Sedimentary Research*, **44**, 1269-1274.
- Heezen, B.C. & Erwing, M.** (1952) Turbidity currents and submarine slumps, and the 1929 Grand Banks earthquake. *American Journal of Science*, **250**, 849-873.
- Higgs, R.** (2010) Comments on "Hybrid sedimentary gravity flows – classification, origin and significance" from Haughton, P., Davis C., McCaffrey, W. & Barker, S. *Marine and Petroleum Geology*, **27**, 2062-2065.
- Hiscott, R.N.** (1994a) Loss of Capacity, Not Competence, as the Fundamental Process Governing Deposition from Turbidity Currents. *Journal of Sedimentary Research*, **64**, 209-214.
- Hiscott, R.N.** (1994b) Traction-carpet stratification in turbidites-fact or fiction? *Journal of Sedimentary Research*, **64**, 204-208.
- Hodgson, D.M.** (2009) Distribution and origin of hybrid beds in sand-rich submarine fans of the Tanqua depocentre, Karoo Basin, South Africa. *Marine and Petroleum Geology*, **26**, 1940-1956.
- Hubbard, S.M., Covault, J.A., Fildani, A. & Romans, B.W.** (2014) Sediment transfer and deposition in slope channels: Deciphering the record of enigmatic deep-sea processes from outcrop. *Geological Society of America Bulletin*, **126**, 857-871.
- Hubert, J.F.** (1964) Textural evidence for deposition of many western North Atlantic deep-sea sands by ocean-bottom currents rather than turbidity currents. *Geology*, **72**, 757-785.

- Hurst, A. & Cronin, B.T.** (2001) The origin of consolidation laminae and dish structures in some deep-water sandstones. *Journal of Sedimentary Research*, **71**, 136-143.
- Hurst, A. & Nadeau, P.H.** (1995) Clay micro-porosity in reservoir sandstones: an application of quantitative electron microscopy in petrophysical evaluation. *AAPG Bulletin*, **79**, 563-573.
- Hurst, A., Verstralen, I., Cronin, B. & Hartley, A.** (2000) Sand-rich fairways in deep-water clastic reservoirs: genetic units, capturing uncertainty, and a new approach to reservoir modelling. *American Association of Petroleum Geologists Bulletin*, **83**, 1096-1118.
- Ibbeken, H.** (1978) The Nivione structure: contemporaneous tectonics and sedimentation between the Ligurian and Tuscan Orogenies. Inter-Union Commission on Geodynamics, Scientific Report, **38**, 274-275.
- Imran, J., Parker, G. & Pirmez, C.** (1999) A non-linear model of flow in meandering submarine and subaerial channels. *Journal of Fluid Mechanics*, **400**, 295-331.
- Iverson, R.M. & Vallance, J.W.** (2001) New views of granular mass flows. *Geology*, **29**, 115-118.
- Iverson, R.M., Logan, M., LaHusen, R.G. & Berti, M.** (2010) The perfect debris flow? Aggregated results from 28 large-scale experiments. *Journal of Geophysical Research*, **115**, F03005.
- Jackson, C.A. & Johnson, H.D.** (2009) Sustained turbidity currents and their interaction with debris-related topography; Labuan Island, offshore NW Borneo, Malaysia. *Sedimentary Geology*, **219**, 77-96.
- Janocko, M., Cartigny, M.B.J., Nemeč, W. & Hansen, E.W.M.** (2013) Turbidity current hydraulics and sediment deposition in erodible sinuous channels: Laboratory experiments and numerical simulations. *Marine and Petroleum Geology*, **41**, 222-249.
- Jobe, Z.R., Lowe, D.R. & Morris, W.R.** (2012) Climbing-ripple successions in turbidite systems: depositional environments, sedimentation rates and accumulation times. *Sedimentology* **59**, 867-898.
- Johansson, M. and Stow, D.A.V.** (1995) A classification scheme for shale clasts in deep water sandstones. In: *Characterization of Deep Marine Clastic Systems* (Eds. A.J. Hartley & D.J. Prosser). *Geological Society of London Special Publication*, **94**, 221-224.
- Johnson, A.M.** (1970) *Physical Processes in Geology*. Freeman Cooper, San Francisco, 577 pp.
- Johnson, M.R.** (1994) Thin section grain size analysis revisited. *Sedimentology*, **41**, 985-999.
- Jones, C.M.** (1980) Deltaic sedimentation in the Roaches Grit and associated sediments (Namurian R2b) in the South-West Pennines. *Proceedings of the Yorkshire Geological Society*, **43**, 39-67
- Kane, I.A.**, (2010c) Development and flow structures of sand injectites: The Hind Sandstone Member injectite complex, Carboniferous, UK. *Marine and Petroleum Geology*, **27**, 1200-1215.
- Kane, I.A. & Pontén, A.S.M.** (2012) Submarine transitional flow deposits in the Paleogene Gulf of Mexico. *Geology*, **40**, 1119-1122.

- Kane, I.A., Catterall, V., McCaffrey, W.D. & Martinsen, O.J.** (2010b) Submarine channel response to intrabasinal tectonics: The influence of lateral tilt. *American Association of Petroleum Geologists Bulletin*, **94**, 189-219.
- Kane, I.A., McCaffrey, W.D. & Martinsen, O.J.** (2009) Autogenic vs. Allogenic controls on Megafault Formation. *Journal of Sedimentary Research*, **79**, 643-651.
- Kane, I.A., McCaffrey, W.D. & Peakall, J.** (2010a) On the origin of palaeocurrent complexity in deep marine channel-levees. *Journal of Sedimentary Research*, **80**, 54-66.
- Kendrick, J.W.** (2000) Turbidite reservoir architecture in the Northern Gulf of Mexico deep-water: insights from the development of Auger, Tahoe, and Ram/Powell Fields. In: *Deep-Water Reservoirs of the World* (Eds. P. Weimer, R.M. Slatt, J. Coleman, N.C. Rosen, H. Nelson, A.H. Bouma, M.J. Stytzen & D.T. Lawrence) *Gulf Coast Section Society of Economic Palaeontologists and Mineralogists Foundation, 20th Annual Research Conference*, 450-468.
- Kittilsen, J.E., Olsen, R.R., Marten, R.F., Hansen, E.K. & Hollingsworth, R.R.** (1999) The first deep-water well in Norway and its implications for the Upper Cretaceous Play, Vøring Basin. *Petroleum Geology Conference Series*, **5**, 275-280.
- Khripounoff, A., Vangriesheim, A., Babonneau, N., Crassous, P., Dennielou, B., & Savoye, B.** (2003) Direct observation of intense turbidity current activity in the Zaire submarine valley at 4000 m water depth. *Marine Geology*, **194**, 151-158.
- Kneller, B.C.** (1995) Beyond the turbidite paradigm; physical models for deposition of turbidites and their implications for reservoir prediction. In: *Characterisation of Deep Marine Clastic Systems* (Eds. A.J. Hartley & D.J. Prosser). *Geological Society of London Special Publication*, **94**, 31-49
- Kneller, B.C.** (2003) The influence of flow parameters on turbidite slope channel architecture. *Marine and Petroleum Geology*, **20**, 901-910.
- Kneller, B.C. & Branney, M.J.** (1995) Sustained High-Density Turbidity Currents and the Deposition of Thick Massive Sands. *Sedimentology* **42**, 607-616.
- Kneller, B.C. & Buckee, C.** (2000) The structure and fluid mechanics of turbidity currents: a review of some recent studies and their geological implications. *Sedimentology*, **47**, 62-94.
- Kneller, B.C. & McCaffrey, W.D.** (1995) Modelling the effects of salt-induced topography on deposition from turbidity currents. *Society of Economic Palaeontologists and Mineralogists, Gulf Coast Section*, 137-145.
- Kneller, B.C. & McCaffrey, W.D.** (1999) Depositional effects of flow non-uniformity and stratification within turbidity currents approaching a bounding slope: Deflection, reflection, and facies variation. *Journal of Sedimentary Research*, **69**, 980-991.
- Kneller, B.C. & McCaffrey, W.D.** (2003) The interpretation of vertical sequences in turbidite beds: The influence of longitudinal flow structure. *Journal of Sedimentary Research*, **73**, 706-713.
- Kneller, B.C., Bennett, S.J. & McCaffrey, W.D.** (1997) Velocity and turbulence structure of density currents and internal solitary waves: potential sediment transport and the formation of wave ripples in deep water. *Sedimentary Geology*, **112**, 235-250.

- Kneller, B.C., Bennett, S.J. & McCaffrey, W.D.** (1999) Velocity structure, turbulence and fluid stresses in experimental gravity currents. *Journal of Geophysical Research, Oceans*, **104**, 5281-5291.
- Kneller, B.C., Edwards, D., McCaffrey, W.D. & Moore, R.** (1991) Oblique Reflection of Turbidity Currents. *Geology*, **19**, 250-252.
- Kuenen, P.H.** (1952) Estimated size of the Grand Banks turbidity current. *American Journal of Science*, **250**, 874-884.
- Kuenen, P.H.** (1966) Experimental Turbidite Lamination in a Circular Flume. *Journal of Geology*, **74**, 523-545.
- Kuenen, P.H. & Menard, H.W.** (1952) Turbidity currents, graded and non-graded deposits. *Journal of Sedimentary Petrology*, **22**, 83-96.
- Lamb, M.P., Hickson, T., Marr, J.G., Sheets, B., Paola, C. & Parker, G.** (2004) Surging versus continuous turbidity currents: Flow dynamics and deposits in an experimental intraslope minibasin. *Journal of Sedimentary Research*, **74**, 148-155.
- Lamb, M.P., Toniolo, H. & Parker, G.** (2006) Trapping of sustained turbidity currents by intraslope minibasins. *Sedimentology*, **53**, 147-160.
- Laval, A., Cremer, M., Beghin, P. & Ravenne, C.** (1988) Density surges: two-dimensional experiments. *Sedimentology*, **35**, 73-84.
- Lee, A.G.** (1988) Carboniferous basin configuration of central and northern England modelled using gravity data. *Sedimentation in a Synorogenic Basin Complex: the Upper Carboniferous of Northwest Europe*, Blackie, Glasgow, 69-84.
- Lee, S.H., Jung, W.Y., Bahk, J.J., Gardner, J.M., Kim, J.K. & Lee, S.H.** (2013) Depositional features of co-genetic turbidite–debrite beds and possible mechanisms for their formation in distal lobated bodies beyond the base-of-slope, Ulleung Basin, East Sea (Japan Sea). *Marine Geology*, **346**, 124-140.
- Leeder, M.R.** (1982) Upper Palaeozoic basins of the British Isles—Caledonide inheritance versus Hercynian plate margin processes. *Journal of the Geological Society of London*, **139**, 479-491.
- Leeder, M.R. & McMahon, A.H.** (1988) Upper Carboniferous (Silesian) basin subsidence in northern Britain. *Sedimentation in a Synorogenic Basin Complex: the Upper Carboniferous of Northwest Europe*. Blackie, Glasgow, 43-52.
- Lien, T., Midtbø, R.E. & Martinsen, O.J.** (2006) Depositional facies and reservoir quality of deep-marine sandstones in the Norwegian Sea. *Norwegian Journal of Geology*, **86**, 71-92.
- Long, R.R.** (1955) Some aspects of the flow of stratified fluids. III. Continuous density gradients. *Tellus*, **7**, 341-357.
- Lovell, J.P.B. & Stow, D.A.V.** (1981) Identification of ancient sandy contourites, *Geology*, **9**, 347-349.
- Lowe, D.R.** (1975) Water escape structures in coarse-grained sediments: *Sedimentology*, **46**, 157-204.

- Lowe, D.R.** (1982) Sediment Gravity Flows; II, Depositional Models with Special Reference to the Deposits of High-Density Turbidity Currents. *Journal of Sedimentary Research*, **52**, 279-298.
- Lowe, D.R.** (1988) Suspended-load fallout rate as an independent variable in the analysis of current structures. *Sedimentology*, **35**, 765-776.
- Lowe, D.R. & Guy, M.** (2000) Slurry-flow deposits in the Britannia Formation (lower Cretaceous), North Sea: A new perspective on the turbidity current and debris flow problem. *Sedimentology*, **47**, 31-70.
- Lowe, D.R. & LoPiccolo, R.D.** (1974) The characteristics and origins of dish and pillar structures. *Journal of Sedimentary Research*, **44**, 484-501.
- Lowe, D.R., Guy, M. & Palfrey, A.** (2003) Facies of slurry-flow deposits, Britannia Formation (Lower Cretaceous), North Sea: implications for flow evolution and deposit geometry. *Sedimentology*, **50**, 45-80.
- Lundin, E.R. & Doré, A.G.** (1997) A tectonic model for the Norwegian passive margin with implications for the NE Atlantic: Early Cretaceous to break-up, *Journal of the Geological Society of London*, **154**, 545-550.
- MacQuaker, J.H.S. & Taylor, K.G.** (1996) A sequence-stratigraphic interpretation of a mudstone dominated succession: the Lower Jurassic Cleveland Ironstone Formation, UK, *Journal of the Geological Society of London*, **153**, 759-770.
- Magalhaes, P. & Tinterri, R.** (2010) Stratigraphy and depositional setting of slurry and contained (reflected) beds in the Marnoso-arenacea Formation (Langhian-Serravallian) Northern Apennines, Italy. *Sedimentology*, **57**, 1685-1720.
- Malarkey, J., Baas, J.H., Hope, J.A., Aspden, R.J., Parsons, D.R., Peakall, J., Patterson, D.M., Schindler, R.J., Ye, L., Lichtman, I.D., Bass, S.J. Davies, A.G., Manning, A.J., & Thorner, P.D.,** (2015) The pervasive role of biological cohesive in bedform development. *Nature Communications*, **6**, Article 6257.
- Maino, M., Decarlis, A., Felletti, F. & Seno, S.** (2013) Tectono-sedimentary evolution of the Tertiary Piedmont Basin (NW Italy) within the Oligo-Miocene central Mediterranean geodynamics. *Tectonics*, **32**, 593-619.
- Major, J.J.** (1997) Depositional processes in large-scale debris-flow experiments, *Geology*, **105**, 345-366.
- Marjanac, T.** (1990) Reflected sediment gravity flows and their deposits in flysch of Middle Dalmatia, Yugoslavia. *Sedimentology*, **37**, 921-929.
- Marr, J.G., Harff, P.A., Shanmugam, G. & Parker, G.** (2001) Experiments on subaqueous sandy gravity flows: The role of clay and water content in flow dynamics and depositional structures: *Geological Society of America Bulletin*, **113**, 1377-1386.
- Martinsen, O.J.** (1990) Fluvial, inertia-dominated deltaic deposition in the Namurian (Carboniferous) of northern England. *Sedimentology*, **37**, 1099-1113.

- Martinsen, O.J.** (1993) Namurian (late Carboniferous) depositional systems of the Craven–Askrigg area, northern England: implications for sequence stratigraphic models. *Sequence Stratigraphy and Facies Associations. International Association of Sedimentologists, Special Publication*, **18**, 247-281.
- Martinsen, O.J., Collinson, J.D. & Holdsworth, B.K.** (1995) Millstone Grit Cyclicity Revisited, II: Sequence Stratigraphy and Sedimentary Responses to Changes of Relative Sea-Level. *Sedimentary Facies Analysis: A Tribute to the Research and Teaching of Harold G. Reading*, 305-327.
- Masson, D.G., Huggett, Q.J. & Brunsten, D.** (1993) The surface texture of the Saharan Debris Flow deposit and some speculation on submarine debris flow processes. *Sedimentology*, **40**, 583-598.
- Mayall, M., Lonergan, L., Bowman, A., James, S., Mills, K., Primmer, T. & Skeene, R.** (2010) The response of turbidite slope channels to growth-induced seabed topography. *American Association of Petroleum Geologists Bulletin*, **94**, 1011-1030.
- Maynard, J.R. & Leeder, M.R.** (1992) On the periodicity and magnitude of Late Carboniferous glacio-eustatic sea-level changes. *Journal of the Geological Society of London*, **149**, 303-311.
- McCabe, P.J.** (1977) Deep distributary channels and giant bedforms in the Upper Carboniferous of the Central Pennines, northern England. *Sedimentology*, **24**, 271-290.
- McCaffrey, W.D. & Kneller, B.C.** (2001) Process controls on the development of stratigraphic trap potential on the margins of confined turbidite systems and aids to reservoir evaluation. *American Association of Petroleum Geologists Bulletin*, **85**, 971-988.
- McCaffrey, W.D., Choux, C.M., Baas, J.H. & Haughton, P.D.W.** (2003) Spatio-temporal evolution of velocity structure, concentration and grain size stratification within experimental particulate gravity currents. *Marine and Petroleum Geology*, **20**, 851-860.
- McCave, I.N. & Jones, K.P.N.** (1988) Deposition of ungraded muds from high-density non-turbulent turbidity currents. *Nature*, **364**, 136-138.
- McClung, D. & Schaerer, P.** (1993) *The Avalanche Handbook*. Seattle, W.A, The Mountaineers.
- McGee, D.T., Bilinski, P.W., Gary, P.S., Pfeiffer, D.S. & Sheiman, J.L.** (1994) Models and reservoir geometries of Auger field, deep-water Gulf of Mexico. In: *Submarine fans and turbidite systems – Sequence stratigraphy, reservoir architecture and production characteristics* (Eds. P. Weimer, A.H. Bouma & B.F. Perkins). *Gulf Coast Section Society of Economic Palaeontologists and Mineralogists, 15th Annual Research Conference*, 245-256.
- Middleton, G.V.** (1967) Experiments on density and turbidity currents: III. Deposition of sediment. *Canadian Journal of Earth Sciences*, **4**, 475-505.
- Middleton, G.V.** (1970) Experimental studies related to problems of flysch sedimentation. In: *Flysch Sedimentology in North America* (Ed. J. Lajoie). *Geological Association of Canada, Special Paper*, **7**, 253-272.
- Middleton, G.V.** (1973) Johannes Walther's Law of the Correlation of Facies. *Geological Society of American Bulletin*, **84**, 979-988.

- Middleton, G.V.** (1993) Sediment deposition from turbidity currents. *Annual Review of Earth and Planetary Sciences*, **21**, 89-94.
- Middleton, G.V. & Hampton, M.A.** (1973) Sediment gravity flows: mechanics of flow and deposition. In: *Turbidites and deep water sedimentation* (Eds. G.V. Middleton & A.H. Bouma). *Pacific Section Society of Economic Palaeontologists and Mineralogists Short Course Notes*, **1**, 1-38.
- Middleton, G.V. & Hampton, M.A.** (1976) Subaqueous sediment transport and deposition by sediment gravity flows. In: *Marine sediment transport and environmental management* (Eds. D.J. Stanley & D.J.P. Swift). Wiley, New York, 197-218.
- Middleton, G.V. & Southard, J.B.** (1984) Mechanics of sediment movement. *Society of Economic Palaeontologists and Mineralogists Short Course Notes*, **3**, pp. 401.
- Miller, T.P. & Smith, R.L.** (1977) Spectacular mobility of ash flows around Aniakchak and Fisher calderas, Alaska. *Geology*, **5**, 173-176.
- Miyata, T.** (1990) Slump strain indicative of paleoslope in the Cretaceous Izumi sedimentary basin along Median tectonic line, southwest Japan. *Geology*, **18**, 392-394.
- Mohrig, D. & Marr, J.G.** (2003) Constraining the efficiency of turbidity current generation from submarine debris flows and slides using laboratory experiments. *Marine and Petroleum Geology*, **20**, 883-899.
- Mohrig, D., Whipple, K.X., Hondzo, M., Ellis, C. & Parker, G.** (1998) Hydroplaning of subaqueous debris flows. *Geological Society of American Bulletin*, **110**, 387-394.
- Morton, A.C. & Whitham, A.G.** (2002) The Millstone Grit of northern England: a response to tectonic evolution of a northern sourceland. *Proceedings of the Yorkshire Geological Society*, **54**, 47-56.
- Morton, A.C., Whitham, A.G., Fanning, C.M. & Claoue-Long, J.** (2005) The role of East Greenland as a source of sediment to the Voring Basin during the Late Cretaceous. *Norwegian Petroleum Society Special Publications*, **12**, 83-110.
- Moscardelli, L. & Wood, L.** (2008) New classification system for mass transport complexes in offshore Trinidad. *Basin Research*, **20**, 73-98.
- Moscardelli, L., Wood, L. & Mann, P.** (2006) Mass-transport complexes and associated processes in the offshore area of Trinidad and Venezuela. *American Association of Petroleum Geologists Bulletin*, **90**, 1059-1088.
- Mulder, T. & Alexander, J.** (2001) The physical character of subaqueous sedimentary density flows and their deposits. *Sedimentology*, **48**, 269-299.
- Mulder, T., Savoye, B. & Syvitski, J.P.M.** (1997) Numerical modeling of a mid-sized gravity flow: the 1979 Nice turbidity current (dynamics, processes, sediment budget and seafloor impact). *Sedimentology*, **44**, 305-326.
- Mutti, E.** (1979) Turbidites et cones sous-marins profonds. *Sédimentation détritique (fluviale, littorale et marine)*, **1**, 353-419.

- Mutti, E.** (1992) Turbidite Sandstones. Istituto di Geologia Università di Parma, 275 pp.
- Mutti, E. & Normark, W.R.** (1987) Comparing examples of modern and ancient turbidite systems: problems and concepts. In: *Marine clastic sedimentology: concepts and case studies* (Eds. J.K. Leggett & G.G. Zuffa). London, Graham and Troutman, 1-38.
- Naylor, M.A.** (1980) The origin of inverse grading in muddy debris flow deposits - a review. *Journal of Sedimentary Research*, **50**, 1111-1116.
- Nelson, C.H., Twichell, D.C., Schwab, W.C., Lee, H.J. & Kenyon, N.H.** (1992) Upper Pleistocene turbidite sand beds and chaotic silt beds in the channelized, distal, outer-fan lobes of the Mississippi fan. *Geology*, **20**, 693-696.
- Normark, W.R.** (1978) Fan valleys, channels, and depositional lobes on modern submarine fans: characters for recognition of sandy turbidite environments. *American Association of Petroleum Geologists Bulletin*, **6**, 912-928
- Normark, W.R. & Piper, D.J.W.** (1991) Initiations processes and flow evolution of turbidity currents; implications for the depositional record. In: *From Shoreline to Abyss; Contributions in Marine Geology in Honour of Francis Parker Shepard* (Ed. R.H. Osborne). *Society of Economic Paleontologists and Mineralogists Special Publications*, **46**, 207-230.
- Normark, W.R., Posamentier, H. & Mutti, E.** (1993) Turbidite Systems – State of the Art and Future Directions: *Reviews of Geophysics*, **31**, 91-116.
- Pantin, H.M. & Leeder, M.R.** (1987) Reverse Flow in Turbidity Currents - the Role of Internal Solitons. *Sedimentology*, **34**, 1143-1155.
- Parsons, J.D. & Garcia, M.H.** (1998) Similarity of gravity current fronts. *Physics of Fluids*, **10**, 3209-3213.
- Patacci, M., Haughton, P.D.W. & McCaffrey, W.D.** (2014) Rheological Complexity in Sediment Gravity Flows Forced to Decelerate against a Confining Slope, Braux, SE France. *Journal of Sedimentary Research*, **84**, 270-277.
- Patacci, M., Haughton, P.D.W. & McCaffrey, W.D.** (2015) Flow behaviour of ponded turbidity currents. *Journal of Sedimentary Research*, accepted (Feb, 2015) and awaiting volume information.
- Peakall, J., McCaffrey, W.D. & Kneller, B.C.** (2000) A process model for the evolution, morphology and architecture of meandering submarine channels. *Journal of Sedimentary Research*, **70**, 434-448.
- Pettingill, H.S.** (1998) World Turbidites – 2, Lessons learned from 43 turbidite giant fields. *Oil and Gas Journal*, **96**, 93-95.
- Pickering, K.T. & Corregidor, J.** (2000) 3D reservoir scale study of Eocene confined submarine fans, south central Spanish Pyrenees. In: *Deep Water Reservoirs of the World* (Eds. P. Weimer, R.M. Slatt, J. Coleman, N.C. Rosen, H. Nelson, A.H. Bouma, M.J. Stytzen & D.T. Lawrence) *Gulf Coast Section Society of Economic Palaeontologists and Mineralogists Foundation, 20th Annual Research Conference*, 776-781.

- Pickering, K.T. & Hiscott, R.N.** (1985) Contained (Reflected) Turbidity Currents from the Middle Ordovician Cloridorme Formation, Quebec, Canada - an Alternative to the Antidune Hypothesis. *Sedimentology* **32**, 373-394.
- Pickering, K.T., Hiscott, R.N. & Hein, F.J.** (1989) Deep Marine Environments: Clastic Sedimentation and Tectonics. Unwin Hyman, London, 416 pp.
- Piper, D.J.W., Farre, J.A. & Shor, A.N.** (1985) Late Quaternary slumps and debris flows on the Scotian Slope. *Geological Society of America Bulletin*, **96**, 1508-1517.
- Piper, D.J.W., Hiscott, R.N. & Normark, W.R.** (1999) Outcrop-scale acoustic facies analysis and latest Quaternary development of Hueneme and Dune submarine fans, offshore California. *Sedimentology*, **46**, 47-78.
- Porten, K.W., Kane, I.A., Warchoř, M., Southern, S.J. & Hadler-Jacobsen, F.** Depositional reservoir quality of deep-marine sandstones: a process-based approach. Submitted to the *Journal of Sedimentary Research*, April, 2015.
- Postma, G., Nemec, W. & Kleinspehn, K.L.** (1988) Large Floating Clasts in Turbidites - a Mechanism for Their Emplacement. *Sedimentary Geology*, **58**, 47-61.
- Prather, B.E.** (2003) Controls on reservoir distribution, architecture and stratigraphic trapping in slope settings. *Marine and Petroleum Geology*, **20**, 529-545.
- Prather, B.E., Booth, J.R., Steffens, G.S. and Craig, P.A.** (1998) Classification, lithological calibration and stratigraphic succession of seismic facies from intraslope basins, deep water gulf of Mexico, USA. *American Association of Petroleum Geologists Bulletin*, **82**, 701-728.
- Pringle, J.K., Westerman, A.R., Clark, J.D., Drinkwater, N.J. & Gardiner, A.R.** (2004) 3D high-resolution digital models of outcrop analogue study sites to constrain reservoir model uncertainty: an example from Alport Castles, Derbyshire, UK. *Petroleum Geoscience*, **10**, 343-352.
- Pritchard, D. & Gladstone, C.** (2009) Reversing buoyancy in turbidity currents: developing a hypothesis for flow transformation and for deposit facies and architecture. *Marine and Petroleum Geology*, **26**, 1997-2010.
- Puigdefàbregas, C., Gjelberg, J. & Vaksdal, M.** (2004) The Grès d'Annot in the Annot syncline: outer basin-margin onlap and associated soft-sediment deformation. *Geological Society of London Special Publications*, **221**, 367-388.
- Reading, H.G.** (1964) A review of the factors affecting the sedimentation of the Millstone Grit (Namurian) in the Central Pennines. In: *Deltaic and Shallow Marine deposits* (Ed. L.M.J.U. van Straaten). *Developments in Sedimentology*, **1**, 340-346.
- Rhoads, D.C. & Young, D.K.** (1970) The influence of deposit-feeding organisms on sediment stability and community trophic structure. *Journal of Marine research*, **28**, 150-178.
- Ricci Lucchi, F.R.** (1986) The Oligocene to Recent foreland basins of the northern Apennines. In: *Foreland basins* (Eds. P.A. Allen & P. Homewood). *International Association of Sedimentologists Special Publication*, **8**, 105-139.

- Ricci Lucchi, F.R. & Valmori, E.** (1980) Basin-wide turbidites in a Miocene, over-supplied deep-sea plain: a geometrical analysis. *Sedimentology*, **27**, 241-270.
- Riis, F.** (1996) Quantification of Cenozoic vertical movements on Scandinavia by correlation of morphological surfaces with offshore data. *Global and Planetary Changes*, **12**, 331-357.
- Roberts, A.M., Lundin E.R. & Kuszniir, N.J.** (1997) Subsidence of the Voring Basin and the influence of the Atlantic continental margin. *Journal of the Geological Society of London*, **154**, 551-557.
- Romans, B.W., Hubbard, S.M. & Graham, S.A.** (2009) Stratigraphic evolution of an outcropping continental slope system, Tres Pasos Formation at Cerro Divisadero, Chile. *Sedimentology*, **56**, 737-764.
- Rouse, H.** (1939) Laws of transportation of Sediment by Streams : Suspended Load. Reporter's discussion of topic 8(b), Sedimentation Division, Soil Conservation Service, U.S. Department of Agriculture, 7 pp.
- Sanders, J.E.** (1965) Primary sedimentary structures formed by turbidity currents and related re-sedimentation mechanisms. In: *Primary Sedimentary Structures and Their Hydrodynamic Interpretation* (Ed. G.V. Middleton). *Society of Economic Palaeontologists and Mineralogists Special Publication*, **12**, 192-219.
- Sanford, L.P.** (2008) Modelling a dynamically varying mixed sediment bed with erosion, deposition, bioturbation, consolidation and armoring. *Computers & Geosciences*, **34**, 1263-1283.
- Satur, N., Hurst, A., Cronin, B.T., Kelling, G. & Gürbüz, K.** (2000) Sand body geometry in a sand-rich, deep-water clastic system, Miocene Cingöz Formation of southern Turkey. *Marine and Petroleum Geology*, **17**, 239-252.
- Scheidegger, A.E. & Potter, P.E.** (1971) Down current decline of grain size and thickness of a single turbidite bed: a semi-quantitative analysis. *Sedimentology*, **17**, 41-49.
- Schwab, W.C., Lee, H.J., Twichell, D.C., Locat, J., Nelson, C.H., McArthur, W.G. & Kenyon, N.H.** (1996) Sediment mass-flow processes on a depositional lobe, outer Mississippi Fan. *Journal of Sedimentary Research*, **66**, 716-927.
- Sequeiros, O.E., Cantelli, A., Viparelli, E., White, J.D.L., Garcia, M.H. & Parker, G.** (2009) Modelling turbidity currents with nonuniform sediment and reverse buoyancy. *Water Resources Research*, **45**, 1-28.
- Sinclair, C.G.** (1962) The limit deposit-velocity of heterogeneous suspensions. *Proceedings of Symposium on interaction between fluid and particles*, A68-A76.
- Sinclair, H.D.** (1994) The Influence of Lateral Basinal Slopes on Turbidite Sedimentation in the Annot Sandstones of Se France. *Journal of Sedimentary Research*, **64**, 42-54.
- Sinclair, H.D.** (2000) Delta-fed turbidites infilling topographically complex basins: a new depositional model for the Annot Sandstones, SE France. *Journal of Sedimentary Research*, **70**, 504-519.
- Sinclair, H.D. & Tomasso, M.** (2002) Depositional evolution of confined turbidite basins. *Journal of Sedimentary Research*, **72**, 451-456.

- Skogseid, J. & Eldholm, O.** (1989) Voring Continental Margin: Seismic interpretation, stratigraphy and vertical movements. In: *Proceedings of the Ocean Drilling Program, Scientific Results* (Eds. O. Eldholm, J. Thiede & E. Taylor). *Ocean Drilling Program*, **104**, 993-1030.
- Smith, N.D.** (1972) Flume experiments on the durability of mud clasts. *Journal of Sedimentary Research*, **42**, 378-383.
- Smith, R.A.** (1955) Experiments on the flow of sand-water slurries in horizontal pipes. *Chemistry & Industry*, **18**, 501-504.
- Smith, R.A.** (2004) Silled sub-basins to connected tortuous corridors: sediment distribution systems on topographically complex sub-aqueous slopes. In: *Confined Turbidite Systems* (Eds. S.A. Lomas & P. Joseph). *Geological Society of London Special Publications*, **222**, 23-43.
- Sohn, Y.K., Kim, S.B., Hwang, I.G., Bahk, J.J., Choe, M.Y. & Chough, S.K.** (1997) Characteristics and depositional processes of large-scale gravely Gilbert-type forests in the Miocene Doumsan fan delta, Pohang Basin, SE Korea. *Journal of Sedimentary Research*, **67**, 130-141.
- Southern, S.J., Patacci, M., Felletti, F. & McCaffrey, W.D.M.** (2015) Influence of flow containment and substrate entrainment upon sandy hybrid event beds containing a co-genetic mud-clast-rich division. *Sedimentary Geology*, **321**, 105-122.
- Stanley, D.J.** (1982) Welded slump-graded sand couplets: evidence for slide generated turbidity currents: *Geo-Marine Letters*, **2**, 149-155.
- Stacey, M.W. & Bowen, A.J.** (1988) The vertical structure of turbidity currents and a necessary condition for self-maintenance. *Journal of Geophysical Research*, **93**, 3543-3553.
- Stevenson, C.J., Talling, P.J., Masson, D.G., Sumner, E.J., Frenz, M. & Wynn, R.B.** (2014) The spatial and temporal distribution of grain-size breaks in turbidites. *Sedimentology*, **61**, 1120-1156.
- Stevenson, I.P. & Gaunt, G.D.** (1971) *Geology of the country around Chapel en le Frith* (Vol. 99). Stationery Office Books (TSO).
- Stocchi, S., Cavalli, C. & Baruffini, L.** (1992) The Guaso (south-central Pyrenees), Gremiasco and Castagnola (eastern sector of Tertiary Piedmont basin) turbidite deposits: Geometry and detailed correlation pattern. *Atti Ticinensi di Scienze della Terra*, **35**, 153-177.
- Stow, D.A.V. & Mayall, M.** (2000) Deep-water sedimentary systems: New models for the 21st century. *Marine And Petroleum Geology*, **17**, 125-135.
- Stow, D.A.V., Reading, H.G. & Collinson, J.D.** (1996) Deep seas. In: *Sedimentary Environments: Processes, Facies and Stratigraphy* (Ed. H.G. Reading). Blackwell Science, Oxford, 395-453.
- Strachan, L.J.** (2008) Flow transformations in slumps: a case study from the Waitemata Basin, New Zealand. *Sedimentology*, **55**, 1311-1332.
- Sumner, E.J., Amy, L. & Talling, P.** (2008) Deposit structure and processes of sand deposition from decelerating sediment suspensions: *Journal of Sedimentary Research*, **78**, 529-547.

- Sumner, E.J., Talling, P.J. & Amy, L.A.** (2009) Deposits of flows transitional between turbidity current and debris flow: *Geology*, **37**, 991-994.
- Sumner, E.J., Talling, P.J., Amy, L.A., Wynn, R.B., Stevenson, C.J. & Frenz, M.** (2012) Facies architecture of individual basin-plain turbidites: Comparison with existing models and implications for flow processes. *Sedimentology*, **59**, 1850-1887.
- Surlyk, F.** (1990) Timing, style and sedimentary evolution of Late Palaeozoic-Mesozoic extensional basins of East Greenland. *Geological Society of London Special Publications*, **55**, 107-125.
- Sylvester, Z. & Lowe, D.R.** (2004) Textural trends in turbidites and slurry beds from the Oligocene flysch of the East Carpathians, Romania. *Sedimentology*, **51**, 945-972.
- Talling, P.J.** (2013) Hybrid submarine flows comprising turbidity current and cohesive debris flow: Deposits, theoretical and experimental analyses, and generalized models. *Geosphere*, **9**, 460-488.
- Talling, P.J., Amy, L.A., Wynn, R.B., Peakall, J. & Robinson, M.** (2004) Beds comprising debrite sandwiched within co-genetic turbidite: origin and widespread occurrence in distal depositional environments. *Sedimentology*, **51**, 163-194.
- Talling, P.J., Wynn, R.B., Masson, D.G., Frenz, M., Cronin, B.T., Schiebel, R., Akhmetzhanov, A.M., Dallmeier-Tiessen, S., Benetti, S., Weaver, P.P.E., Georgiopoulou, A., Zühlsdorff, C. & Amy, L.A.** (2007a) Onset of submarine debris flow deposition far from original giant landslide. *Nature*, **450**, 541-544.
- Talling, P.J., Amy, L.A., Wynn, R.B., Blackbourn, G. & Gibson, O.** (2007b) Evolution of turbidity currents deduced from extensive thin turbidites: Marnoso Arenacea Formation (Miocene), Italian Apennines. *Journal of Sedimentary Research*, **77**, 172-196.
- Talling, P.J., Malgesini, G., Sumner, E.J., Amy L.A., Felletti, F., Blackbourn, G., Nutt, C., Wilcox, C., Harding, I.C. & Khan, S.** (2012a) Planform geometry, stacking pattern, and extra-basinal origin of low-strength and intermediate-strength cohesive debris flow deposits in the Marnoso-arenacea Formation. *Geosphere*, **8**, 1-24.
- Talling, P.J., Masson, D.G., Sumner, E.J. & Malgesini, G.** (2012b) Subaqueous sediment density flows: Depositional processes and deposit types. *Sedimentology*, **59**, 1937-2003
- Talling, P.J., Wynn, R.B., Schmidt, D.N., Rixton, R., Sumner, E. & Amy, L.** (2010) How Did Thin Submarine Debris Flows Carry Boulder-Sized Intraclasts for Remarkable Distances across Low Gradients to the Far Reaches of the Mississippi Fan? *Journal of Sedimentary Research*, **80**, 829-851.
- Terlaky, V. & Arnott, R.W.C.** (2014) Matrix-rich and associated matrix-poor sandstones: Avulsion splays in slope and basin-floor strata. *Sedimentology*, **61**, 1175-1197.
- Tilston, M., Arnott, B., Rennie, C. & Long, B.** (2014) Grain size controls on the internal structure of sediment gravity currents and their implications for depositional properties; a novel application of CT imagery. *American Association of Petroleum Geologist Annual Concentration abstract 2014, Houston, Texas.*

- Tinterri, R.** (2011) Combined flow sedimentary structures and the genetic link between sigmoidal and hummocky cross-stratification. *GeoActa (Bologna)*, **10**, 1-43.
- Tinterri, R. & Magalhaes, P.M.** (2011) Synsedimentary structural control on foredeep turbidites: An example from Miocene Marnoso-arenacea Formation, Northern Apennines, Italy. *Marine and Petroleum Geology*, **28**, 629-657.
- Toniolo, H., Lamb, M. & Parker, G.** (2006a) Depositional turbidity currents in diapiric minibasins on the continental slope: Formulation and theory. *Journal of Sedimentary Research*, **76**, 783-797.
- Toniolo, H., Parker, G., Voller, V. & Beaubouef, R.T.** (2006b). Depositional turbidity currents in diapiric minibasins on the continental slope: Formulation and theory. *Journal of Sedimentary Research*, **76**, 798-818.
- Twichell, D.C., Schwab, W.C. & Kenyon, N.H.** (1995) Geometry of sandy deposits at the distal edge of the Mississippi Fan, Gulf of Mexico. In: *Atlas of Deep Water Environments: Architectural style in turbidite systems* (Eds. K.T. Pickering, R.N. Hiscott, N.H. Kenyon, F. Ricci-Lucchi & R.D.A. Smith). Chapman & Hall, London, 282-286.
- Van Vliet, A.** (1978) Early Tertiary deepwater fans of Guipuzcoa, northern Spain. In: *Sedimentation in submarine canyons, fans and trenches* (Eds. D.J. Stanley & G. Kelling). London, Dowden, Hutchinson and Ross, Inc., 190-109.
- Verhagen, I.T.E., Baas, J.H., Jacinto, R.S., McCaffrey, W.D. & Davies, A.G.** (2013) A first classification scheme of flow-bed interactions for clay-laden density currents and soft substrates. *Ocean Dynamics*, **63**, 385-397.
- Vinnels, J.S., Butler, R.W.H., McCaffrey, W.D. & Lickorish, H.W.** (2010) Sediment Distribution and Architecture Around a Bathymetrically Complex Basin: An example from the Eastern Champsaur Basin, SE France. *Journal of Sedimentary Research*, **80**, 216-235.
- Vrolijk, P.J. & Southard, J.B.** (1997) Experiments on Rapid Deposition of Sand from High-velocity Flows, *Geoscience Canada*, **24**, 45-54.
- Walker, R.G.** (1966a) Shale Grit and Grindslow Shales - Transition from Turbidite to Shallow Water Sediments in Upper Carboniferous of Northern England. *Journal of Sedimentary Research*, **36**, 90-114.
- Walker, R.G.** (1966b) Deep channels in turbidite-bearing formations. *American Association of Petroleum Geologists Bulletin*, **50**, 1899-1917.
- Walker, R.G.** (1967) Turbidite sedimentary structures and their relationship to proximal and distal depositional environments. *Journal of Sedimentary Research*, **37**, 25-43.
- Walker, R.G.** (1978) Deep-water sandstone facies and ancient submarine fans: models for exploration for stratigraphic traps. *American Association of Petroleum Geologists Bulletin*, **62**, 932-966.
- Waters, C.**, British Geological Society, personal communication, November, 2013.

- Waters, C.N. & Condon, D.J.** (2012) Nature and timing of Late Mississippian to Mid-Pennsylvanian glacioeustatic sea-level changes of the Pennine Basin, UK. *Journal of the Geological Society of London*, **169**, 37-51.
- Waters, C.N., Waters, R.A., Barclay, W.J. & Davies, J.R.** (2009) A lithostratigraphical framework for the Carboniferous successions of southern Great Britain (Onshore) *British Geological Survey Research Report*, RR/09/01.
- Winker, C.D.** (1996) High-resolution seismic stratigraphy of a Late Pleistocene submarine fan ponded by salt-withdrawal mini-basins on the Gulf of Mexico Continental Slope. *Offshore Technology Conference Proceedings*, **OTC 8024**, 619-628.
- Wolfenden, E.B.** (1958) Paleocology of the Carboniferous reef complex and shelf limestones in northwest Derbyshire, England. *Geological Society of America Bulletin*, **69**, 871-898.
- Wood, A. & Smith, A.J.** (1958) The sedimentation and sedimentary history of the Aberystwyth Grits (Upper Llandoveryan). *Quarterly Journal of the Geological Society*, **114**, 163-195.
- Wynn, R.B., Kenyon, N.H., Masson, D.G., Stow, D.A.V. & Weaver, P.P.E.** (2002a) Characterization and recognition of deep-water channel-lobe transition zones. *American Association of Petroleum Geologists Bulletin*, **86**, 1441-1462.
- Wynn, R.B., Weaver, P.P., Masson, D.G. & Stow, D.A.** (2002b) Turbidite depositional architecture across three interconnected deep-water basins on the north-west African margin. *Sedimentology*, **49**, 669-695.
- Xu, J.P., Noble, M.A. & Rosenfield, L.K.** (2004) In-situ measurement of velocity structure within turbidity currents. *Geophysical Research Letters*, **31**, L09311.
- Yokokawa, M.** (1995) Combined-flow ripples: genetic experiments and applications for geologic records. *Memoirs of the Faculty of Science Kyushu University Series D, Earth and Planetary Sciences*, **29**, 1-38.
- Yokokawa, M., Masuda, F. & Endo, N.** (1995) Sand particle movement on migrating combined-flow ripples. *Journal of Sedimentary Research*, **65**, 40-44.
- Zeng, J., Lowe, D.R., Prior, D.B., Wiseman, W.J. Jr. & Bornhold, B.D.** (1991) Flow properties of turbidity currents in Bute Inlet, British Columbia. *Sedimentology*, **38**, 975-996.

Appendix

A.1 - Mud-clast orientations, Hope Quarry, Pennine Basin.

Tables summarising mud-clast orientations as measured from two beds (Type B beds) from the lower Mam Tor Sandstones exposed at Hope Quarry. Data are presented in Fig. 4.18.

Direction of the elevated end of elongate mud clasts
and direction of the axial plane of folded mud clasts

Summary of data

8.5m, Hope Quarry log		30.9m, Hope Quarry log		Direction	1st bed	2nd bed	All clast	Frequency	Percentage
12	196	6	178	0	0	2	2		
24	196	8	182	10	1	0	1		
42	204	26	186	20	1	1	2		
56	208	42	188	30	0	0	0		
58	216	46	192	40	1	3	4		
62	218	48	192	50	2	0	2		
74	224	62	194	60	1	2	3		
74	226	68	198	70	2	3	5		
82	234	72	206	80	3	2	5	24	19
86	238	74	206	90	2	3	5		
88	242	78	212	100	2	2	4		
94	246	82	214	110	3	3	6		
98	248	84	218	120	2	2	4		
102	254	92	226	130	1	4	5		
108	266	96	244	140	3	3	6		
112	268	96	248	150	3	3	6		
116	272	106	254	160	3	4	7		
118	282	108	268	170	3	2	5	48	36
120	288	112	274	180	2	3	5		
126	292	114	278	190	5	4	9		
134	294	116	286	200	2	2	4		
144	296	126	292	210	3	3	6		
146	296	128	296	220	2	1	3		
146	306	134	304	230	2	0	2		
152	316	136	326	240	3	2	5		
156	328	136	328	250	1	1	2		
158	352	138	338	260	2	1	3	39	29
162		142	344	270	1	2	3		
166		146	356	280	2	1	3		
166		146		290	3	2	5		
172		152		300	1	1	2		
176		158		310	1	0	1		
178		158		320	1	2	3		
182		162		330	0	1	1		
184		164		340	0	1	1		
192		168		350	1	1	2	21	16
192		168							
194		172							

A.2 - Digital disc

The disc enclosed on the inside of the back cover of this thesis contains the following:

A 2.1 – Facies and bed type data, lower sandstone body, intra-Springar Sandstone, NW Vøring Basin

Excel file (A.1.1 Voring_facies_bed.xlsx) containing facies and bed data (types, proportions and thicknesses) used in Figs 3.11, 3.12, 3.14 of this thesis.

A 2.2 – Point count data collected from thin-sections, Well 4 (Gro 2) and Well 5 (Gro 1), lower sandstone body, intra-Springar Sandstone, NW Vøring Basin

The enclosed disc provides excel files (Gro_2_grain_size_measurements; Gro1_2_point_count_data_SJS.xlsx) containing grain size and composition data collected by point counting thin-sections taken from core from Well 5 (6604/10-1), NW Vøring Basin, Norwegian Sea. A total of 46 photographs, taken randomly of the thin section, are also provided and formed the basis of grain size measurements. This data was used to construct the vertical profile illustrating variations in texture and composition within Type C and D beds in Chapter 3 (Figs 3.7 & 3.8).

Comments on methodology:

Using a microscope and point counter, a total of 300 points along linear transects were used to note down the composition of constituent material in the thin-section. A total of 300 grains were measured along their axis to reliably determine grain size distributions. To avoid bias, measurements were collected by capturing an image of an area of the thin-section randomly. All grains were then measured within this region, regardless of size and of dewatering features; as a result these measurements will better reflect porosity and permeability values determined from plugs. If 300 grains were not available in an image and another one was acquired. The following equations from Folk and Ward (1975) were used to determine the textural characteristics:

Mean grain size

$$(\phi_{84} + \phi_{50} + \phi_{16}) / 3 \quad \phi = \text{phi}$$

Median grain size

$$\phi_{50}$$

Sorting: Inclusive graphic standard deviation

$$((\phi_{84} - \phi_{16}) / 4) + ((\phi_{95} - \phi_{5}) / 6.6)$$

Skewness : Inclusive graphic skewness

Value shows if the distribution is symmetric or asymmetric and shifted towards a coarse or fine fraction.

$$((\phi_{84th} + \phi_{16th} - 2 * \phi_{50th}) / (2 * (\phi_{84th} - \phi_{16th}))) + ((\phi_{95th} + \phi_{5th} - 2 * \phi_{50th}) / (2 * (\phi_{95th} - \phi_{5th})))$$

Kurtosis

Value shows if the distribution is bell shaped, very flat or very peaked. Comparison of sorting in the tails of the distribution versus the centre or peak of the distribution.

$$(\phi_{95th} - \phi_{5th}) / (2.44 * (\phi_{75th} - \phi_{25th}))$$

A 2.3 – Publications

The digital disc contains manuscripts which have been published or submitted to the review processes. These include:

Porten, K.W, Kane, I.A., Warchoł, M. & Southern, S.J. (submitted) Depositional reservoir quality of deep-marine sandstones: a sedimentological process-based approach – an examples from the Springar Formation, NWVøring Basin, Norwegian Sea. *Journal of Sedimentary Research*.

Southern, S.J., Mountney, N.P. & Pringle, J.K. (2014) The Carboniferous Southern Pennine Basin. *Geology Today*, **30**, 71-78.

Southern, S.J., Patacci, M., Felletti, F. & McCaffrey, W.D.M. (2015) Influence of flow containment and substrate entrainment upon sandy hybrid event beds containing a co-genetic mud-clast-rich division. *Sedimentary Geology*, **321**, 105-122.

Southern, S.J., Kane, I.A., Warchoł, M. & Porten, K.W. (submitted) Hybrid event beds dominated by transitional facies types: character, distribution and significance in the Maastrichtian Springar Formation, NWVøring Basin, Norwegian Sea. *Sedimentology*

A.3 - Determination of the distance at which beds occur from their point of onlap onto an inclined basin margin.

The absolute distance of beds way from their point of onlap onto the confining basin margin (**Z**) had to be determined with mapping techniques as exposures where beds are directly observed to onlap the basin margin are lacking. Further, due to the structural dip of bedding and their relation to an inclined basin margin, calculations had to correct for the apparent dip of bedding along these transects orientated perpendicular to the strike of the confining basin margin. The following outlines the steps that were taken to determine the distance (**Z**):

Using structural data from the carbonate-cored confining basin margin (Wolfenden, 1958; Stevenson & Gaunt, 1971), structure contours were constructed in order to reconstruct and project the counter-slope of the basin margin into the sub-surface.

Using the topographic height of the bed, and corresponding structure contour of the confining basin margin, the horizontal distance (**D**) at which beds occur from their onlap onto the confining basin margin was determined. This distance was measured along a transect orientated perpendicular to the average strike of the confining basin margin in the vicinity of Hope Quarry, referred to as the onlap transect herein.

The apparent dip of bedding (**Bda**) along the onlap transect was determined in order to account for the discrepancy of orientation between this onlap transect and the dip direction of bedding.

Calculation of apparent dip

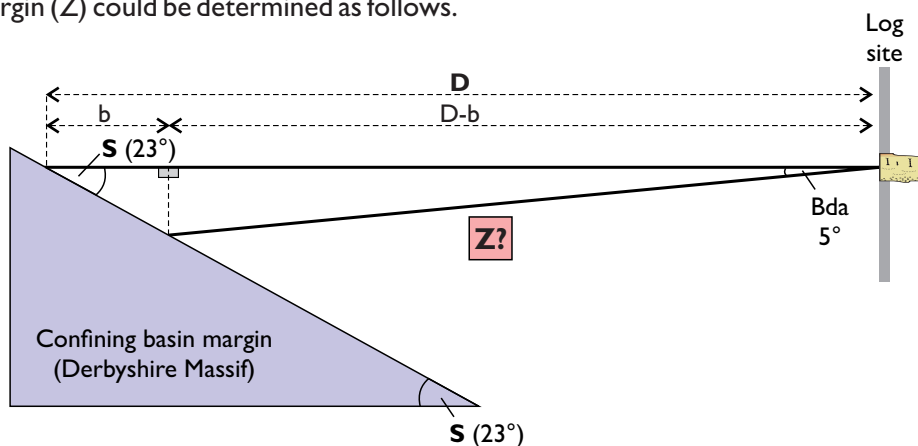
$$\tan Bda = \tan Bd \times (\sin A)$$

Bda - apparent dip of bedding.

Bd - true measured dip of bedding (5° south).

A - difference between the bearing of the onlap transect and strike of bedding

Using **Bda** and **D**, with respect to the dip of the confining basin margin (approximately, 23° in the vicinity of Hope Quarry), the absolute distance of strata away from their onlap onto the confining basin margin (**Z**) could be determined as follows.



S - Dip of the confining slope (~ 23° north).

D - Apparent (plan view) distance between the bed and the corresponding structure contour of the confining margin.

Bda - Apparent dip of bedding.

Z - Absolute distance between the bed and the confining margin.

$$b = \frac{D}{\left(\frac{\tan S}{\tan Bda} + 1\right)}$$

$$Z = \frac{D-b}{\cos Bda}$$